EUR 7879 EN

BENCHMARK

Reference Data on Post Irradiation Analysis of Light Water Reactor Fuel Samples

A review of 12 years experience, results obtained and their characterisation

S. Guardini and G. Guzzi

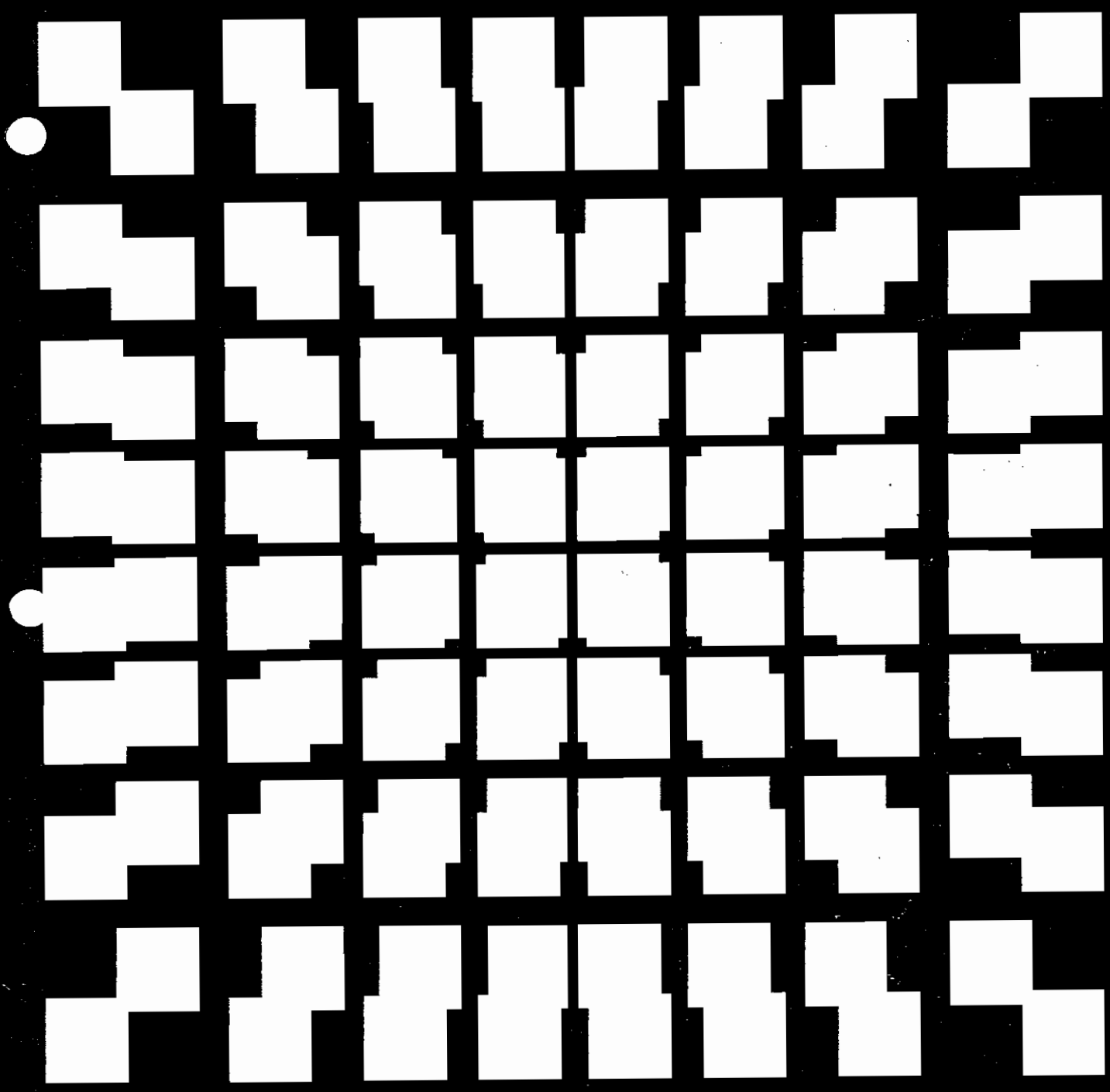

COMMISSION OF THE EUROPEAN COMMUNITIES JOINT RESEARCH CENTRE ISPRA ESTABLISHMENT

Published by the
COMMISSION OF THE EUROPEAN COMMUNITIES

Directorate-General
Scientific and Technical Information
and Information Management

Bâtiment Jean Monnet
LUXEMBOURG

EUR 7879 EN

A bibliographical slip can be found at the end of this volume

Design: P. De Hoe, J. Wells
Printed in Italy by: Arte Stampa, Varese

Foreword

This report collects and illustrates the work performed over the past 12 years at the Joint Research Centre of the Commission of the European Communities (JRC) in the field of post-irradiation examinations (PIE) on Light Water Reactors (LWR) fuels.

Early experiments on Garigliano and Trino Vercellese fuel were performed within the framework of research contracts established between Euratom, the Ente Nazionale per l'Energia Elettrica (ENEL) and FIAT.

The contracts were registered as :

Euratom - ENEL 071-66-6-TEEI-RD (1966)
Euratom - ENEL 092-66-6-TEEI (1966)
Euratom - FIAT 098-66-6-TEEI-RD (1966)

The main objective of these contracts was the measurement of isotopic composition and burnup on selected irradiated fuel samples with a view to obtaining experimental data for use in verifying the accuracy of calculation methods developed both by ENEL and FIAT Nucleare.

Another objective was to carry out metallographic analyses on UO_2 fuel and on stainless steel cladding.
From 1973 onwards this activity has been included in the JRC research programme : Technical assistance to power plant operators, under the heading: Benchmark experiments. Within this new framework two cooperation agreements have been established between Euratom, Kernkraftwerk RWE-Bayernwerk GmbH (KRB), Kernkraftwerk Obrigheim GmbH (KWO) and Kraftwerk Union AG (KWU) with the aim of carrying out post-irradiation analyses on selected fuel samples irradiated in the Gundremmingen and Obrigheim reactors.

These contracts were registered as :

Euratom - KRB-KWU 150-75 PIPGD (1975)
Euratom - KWO-KWU 139-75 PIPGD (1975)

From 1977, the Benchmark experiments' activity has been included with similar objectives in the Fissile material control programme.

Some of the work presented in this report has been performed within the framework of other activities of the JRC. In particular, the burnup calculation was largely carried out within the Nuclear waste management programme, within the framework of the activity Assessment of nuclear transmutation of actinides.

Contributors to this work :

A. Ariemma[1], R. Bannella[1], P. Barbero, G. Bidoglio, J. Biteau, L. Bramati[1], G. Buscaglia, A.M. Bresesti, M. Bresesti, A. Caldiroli, C. Cerutti, R. Chevalier, G. Cottone, A. Cricchio, D. D'Adamo, F. Daniele, R. De Meester, R. Dierckx, A. Drago, R. Ernstberger, S. Facchetti, R. Facelli, A. Federico, A. Frigo, M. Galliani[1], E. Ghezzi, P. Hansen, L. Lezzoli, R. Klersy, L. Koch, W. Konrad, L. Mammarella, F. Mannone, A. Marell, J.P. Meerschmann, M. Paoletti-Gualandi[1], A. Peil, P. Peroni[1], R. Pietra, A. Pollicini, K.H. Schrader, A. Schürenkämper, P.R. Trincherini, H. Tsuruta[2], H. Ullah[3], R. Wellum, B. Zaffiro[1].

The authors wish to thank the following organizations whose collaboration in providing irradiated fuel or interpretation tools made possible the realization of the activity reported in this paper :

Comitato Nazionale Energia Nucleare (CNEN)* Italy .
Ente Nazionale Energia Elettrica (ENEL) Italy
FIAT Nucleare, Italy
Kernkraftwerk Obrigheim GmbH (KWO) F.R. Germany
Kernkraftwerk KWE-Bayernwerk GmbH (KRB) F.R. Germany
Kraftwerk-Union AG (KWU) F.R. Germany

The authors wish also to acknowledge the evaluation work of analytical data performed by B.G.R. Smith and L. Tondinelli (CNEN, Italy) and the helpful criticisms and profitable discussions had with M. Cuypers and M. Hage.

(1) Ente Nazionale Energia Elettrica, Italy
(2) Japan Atomic Energy Research Institute
(3) Pakistan Atomic Energy Commission

(*) now ENEA, Comitato Nazionale per la Ricerca e per lo Sviluppo dell'Energia Nucleare e delle Energie Alternative

Contents

Introduction

I. Technical Description of the Activity 11

1. General Remarks 13

2. The Garigliano Reactor 15

1. The A-106 Assembly (Garigliano I) 16
- Gamma scanning of the rods 18
2. The SA-13 Assembly (Garigliano II) 20
- Gamma scanning of the rod 20

3. The Trino Vercellese Reactor 24

1. The 509-049, 509-032 and 509-104 Assemblies (Trino I) 26
- Dismantling of the fuel assemblies and visual examination of the fuel rods 29
- Metallography of the fuel 29
- Gamma scanning of the rods 30
2. The 509-069 Assembly (Trino II) 33
- Metallurgical examination 34
  - Optical inspection 34
  - Metrological examination 35
  - Metallographic examination 36
- Gamma scanning of the rods 38

4. The Obrigheim Reactor 39

1. The BE 124 and BE 210 Assemblies 40
- Gamma scanning of the rods 42

5. The Gundremmingen Reactor 49

1. The B 23 and C 16 Assemblies 45
- Gamma scanning of the rods 46

6. Destructive Analysis of the Samples 49

1. Radiochemical procedures 50
- Sample dissolution 51
- Uranium and plutonium purification 53
- Neodynium and americium purification 54
2. Preparation and measurement of alpha-sources 55
3. Gamma spectrometry 57
4. Mass spectrometry 62

II. Characterization of the Data 71

1. General Remarks 73

2. Discussion of Uncertainties 74

1. Step A: Evaluation of uncertainties from preliminary treatments 75
- Uncertainties in sample cutting 76
- Uncertainties in chemical treatment 77

2. Step B: Evaluation of analytical uncertainties from mass alpha- and gamma spectrometry ____ 77
- Uncertainty in raw data ____ 77
- Differentiation of formulae for transmission factors and evaluation of final analytical uncertainty ____ 81
3. Step C: Evaluation of the overall uncertainty ____ 92
4. Step D: Comparison with Karlsruhe data ____ 93
5. Conclusions ____ 101

3. Description and Use of the Inverse Code Theory ____ 105
1. General theory ____ 106
2. Application ____ 108

4. Isotopic Correlations ____ 113
1. Data consistency check ____ 114
2. Physical parameters investigation ____ 116
• spectrum ____ 116
• burnup ____ 118
• initial enrichment ____ 125
• correlation involving Pu and/or U isotopes ____ 125

5. Comparison with Calculated Values ____ 126
1. LASER results ____ 127
2. RIBOT results ____ 128

III. Benchmark Results and Conclusions ____ 135

1. Results ____ 137
1. Garigliano BWR (Garigliano I and II) ____ 139
2. Trino Vercellese PWR (Trino I and II) ____ 145
3. Obrigheim PWR ____ 149
4. Gundremmingen BWR ____ 155

2. Conclusions ____ 158

References ____ 159

Introduction

The aim of this report is to review the results obtained within the framework of the Benchmark activity (BM), to indicate the field of application for these results, and to provide general information that will make them simple and straightforward to use.

The Benchmark activity was a destructive assay (DA) carried out in cooperation with various European nuclear power plant utilities on irradiated LWR fuel elements.

The irradiated assemblies were dismantled, some fuel pins were selected and pellets, representative of both unperturbed and perturbed reactor core regions were cut from them after γ- scanning. The pellets were then dissolved and submitted to α, γ and mass spectrometry in order to determine fission-product and heavy-element buildup, isotopic ratios and burnup. The aim of this activity was to prepare a set of clean reference data from which many users would profit.

So maximum attention was paid to the characterization, quality and traceability of the data. As the next sections will show, many different tools were used to check the analytical data and to characterize them, and much complementary information was distributed through ad hoc reports[1,2] in order to make recalculation and proper use of the data possible.

The principal users of the Benchmark data bank should be :

- Reactor operators, for the assessment of nuclear codes and collapsed cross-section sets
- Nuclear waste operators, for the evaluation of discharge isotope vectors
- Safeguards authorities, for the assessment of inspection tools as non-destructive assay (NDA) techniques or isotopic correlation techniques (ICT), etc.

Reactor physics uses

The problem of preparing suitable reactor operation codes and cross-section sets is somewhat complicated by several factors :

- the definition of local spectrum conditions and spatial drifts is certainly one of the most complex problems linked with the core description, especially in boiling water reactors where radial and axial moderation variations are very difficult to model;
- the collapsing of cross-section sets is an equally cumbersome and problematic activity, which has to be performed by means of complicated and/or simplified but approximated computational tools. The results obtained in this process have to be continuously monitored by comparison with measurement data from post-irradiation experiments (PIE's)[3,4];
- variation of the spectrum and consequently of the effective cross-section with burnup further complicates the situation. This variation has to be described in the model used and checked again on the experimental results;

- exact knowledge of the initial fuel composition is frequently lacking, but some tools can be developed to derive it from isotopic discharge data.

Waste analysis uses

The calculation of isotopic evolution for the management of radioactive waste (production and burning of higher actinides) is carried out mainly with the aid of simplified methods which frequently contain very rough approximations : several authors[5,6] recommend that the results should be checked with more sophisticated codes and that higher actinide cross-section sets should be assessed mainly through comparison with the post-irradiation analysis of spent fuel.

Safeguards uses

As far as the safeguards of nuclear materials is concerned the main purpose of the activity was to produce reference burnup and buildup measurement data that would be useful, and sometimes even necessary, for the assessment of safeguards tools. With this in mind, two main items of interest to safeguards will be considered.

NDA-DA techniques and isotopic correlation technique

NDA-DA techniques

Non-destructive techniques for the determination of the burnup and the cooling time of spent fuel assemblies will have to be developed before efficient safeguards can be applied. So far, the most advanced technique employed for a non-destructive determination of burnup is gamma-spectrometry based on the measurement of activity ratios of some fission products such as $^{134}Cs/^{137}Cs$ or $^{154}Eu/^{137}Cs$ [7,8,9,10,11,12].

The disadvantages of this technique reside mainly in the high uncertainty due to γ ray shielding, fission product mobility in the fuel rod and reactor history dependence.
The destructive measurement of fission products was not only currently used in our work as a consistency check of our data, but also as a contribution to the assessment of the NDA techniques based on fission product detection.
Another method which is now under examination is the non-destructive determination of burnup through the detection of the passive neutron emission of spent fuels[13,14]. Irradiated fuel emits neutrons from (α,n) reactions in oxide and from spontaneous fission of the even plutonium isotopes. This technique offers several advantages over γ spectrometry as pointed out in ref.13 .

a. Higher penetration power of neutrons permits inner fueld rods to be measured.

b. More simple instrumentation allows fuel elements to be investigated with higher flexibility.

Some problems and difficulties still exist in the assessment of the passive neutron counting technique: passive neutron emission is to some extent influenced by the irradiation history, and could also be influenced by the neutron spectrum in the reactor[15,16].
Well-characterized data are therefore necessary in order to assess this neutron detection technique mainly for ^{242}Cm and ^{244}Cm buildup. These two isotopes are in fact responsible for the total passive neutron emission at relatively short cooling times.

Isotopic correlation technique

The importance of isotopic correlation technique in the present fuel cycle was stressed in the symposium already referred to in refs. 10, 17, 18, 19.
The technique has an important field of application in reactor physics and plays a fundamental role in the future of safeguards. It can be assessed only through a series of tests on reliable reference experimental data. New and reliable correlations, or checks on the existing ones, must be developed in two steps :

- Correlations between heavy isotopes and/or fission products can be assessed by means of suitable simplified reactor physics algorithms. As shown in ref. 20 a selective use of isotopic correlations must be made,

according to the effect to be detected.

- The isotopic correlations stated must be checked in data banks which contain high quality reference data. The measurement uncertainty must be low and precisely known, and the experimental data obtained must belong to fuel samples possessing irradiation-histories and spectral conditions which are both very well-documented and traceable.

To fulfil the afore mentioned requirements the analytical data obtained were carefully characterized and checked by means of different methods :

- detailed random and systematic error investigation through interlaboratory comparisons (Section II.2); some samples from each batch were measured in parallel in Ispra and Karlsruhe JRC laboratories;
- extensive use of ICT (Section II.4). It is obvious that the isotopic correlations are a tool which can be improved by analytical data production, but, conversely they can be used to check the consistency of analytical data.
- comparison with calculated values (Section II.5) : two burnup codes were used to recalculate the data, the one-dimension transport code LASER and the zero-dimension diffusion code RIBOT-5A.

The structure of the present report is as follows: in Section I the BM activity is described in detail; characteristics of the reactors and fuel assemblies examined are given, and the technical aspects of the chemical and analytical processes are discussed.

In Section II all the techniques used to certify the analytical data are presented, together with a discussion of evaluated random and systematic uncertainties. A comparison with the calculated values and the interpretation with ICT is also presented in this section.

Section III presents the results. In practice the complete sets of results referring to all JRC measurements are given here for the sake of the completeness and consistency of this final report. Certain details or restricted information, which could not be given here, can be found in literature[1.2.21.22.23.24.25.26].

I. Technical Description of the Activity

1. General Remarks

The number of U-fed light water reactors already in existence in Europe when the BM activity was started, together with the number of LWRs planned for the coming decades, suggested directing this study towards spent fuel assemblies unloaded from LWRs. Many parameters would have been worthy of investigation. First of all the reactor type and consequently both boiling and pressurized water reactors (BWR and PWR) were studied. Inside this broad subdivision, parameters such as axial and radial spectrum shifts, spectrum perturbations and void effects have been investigated. The activity covered many years, so that different generations of LWR reactors were investigated, making it possible to analyse the effects of variations in gross parameters such as cladding materials (inox and zircaloy) overall moderating ratios, axial void distribution, specific power, etc.

In Table I.1 the various reactors investigated are listed together with the burnup of the samples analysed from various

TABLE I.1. Reactors and samples investigated in the framework of the BENCH MARK ACTIVITY

Reactor	Identification	Fuel Assembly	^{235}U wt% Initial Enrichment	Number of Samples	GWD/MTU Sample Burnup Range
Garigliano (BWR)	Garigliano I	A-106	1.60	5	9.8-14.5
			2.10	13	8.9-12.7
	Garigliano II	SA-13	2.41	8	4.2- 8.6
Trino Vercellese (PWR)	Trino I	509-049	2.719	14	8.2-15.3
		509-032	3.13	8	7.2-17.7
		509-104	3.897	4	3.4-11.9
	Trino II	509-069	3.13	23	19.1-26.6
Obrigheim (PWR)		BE 124	3.00	19	15.6-36.3
		BE 210	2.83	8	24.2-37.5
Gundremmingen (BWR)		B 23	2.53	9	21.2-27.4
		C 16	2.53	7	14.4-20.3
TOTAL NUMBER OF SAMPLES				118	

fuel elements, which covered a wide range from 3,400 to 37,500 MWD/MTU.

The structure of this chapter will be as follows:

a) a detailed description of the reactors and fuel elements from which samples have been taken, will be given;

b) a description of the activities carried out for the preliminary inspection of pins and pellets will also be presented. These activities consisted mainly in whole pins gamma-scanning, optical inspections and, in some cases metallurgical examinations. Only the gamma-scanning was always carried out for all the selected pins, as a support in the choice of the pellets to be cut. As far as the optical and metallurgical examinations are concerned, they were widely carried out only in the first measurement campaigns, conducted under the heading "Technical Assistance to Power Plant Operators". In the last campaigns on fuel samples of GUNDREMMINGEN, OBRIGHEIM and GARIGLIANO IInd charge the metallurgical examinations have been conducted only partially and the results obtained will not be presented here;

c) after the descriptions of gamma scanning and visual and metallurgical inspections, this chapter will deal with the sampling plans of the pellets chosen from each fuel element, the chemical treatments performed on the samples and the analytical procedures (alpha, gamma and mass-spectrometry) carried out;

d) the elaboration of the raw data obtained, leading to the elaborated data (burnup, heavy isotope buildup, fission product ratios, etc.) are also presented at the end of the chapter.

2. The Garigliano Reactor

The GARIGLIANO nuclear power plant /27/ operated by the Italian Electricity Board Ente Nazionale per l'Energia Elettrica (ENEL), is equipped with a boiling water reactor rated at 506 MW(th).

The General Electric Corporation is the designer of the nuclear power plant. The reactor was critical by June 1963 and reached its full operation power in May 1964. The reactor core consisted of 208 square fuel assemblies (Figure I. 1) each containing 69 rods with an initial enrichment of 2.1 wt% ^{235}U and 12 corner rods with an initial enrichment of 1.6 wt% ^{235}U. 89 cruciform control rods (absorbing material B_4C) completed the reactor core. The total initial weight of uranium in the core was about 45.5 metric tons. A description of the reactor core characteristics during the

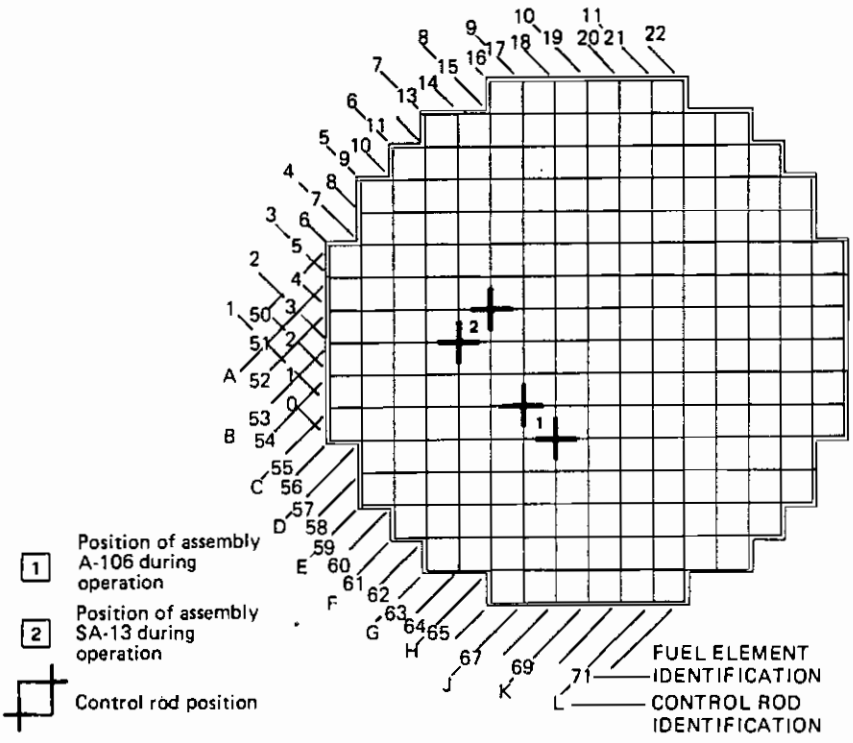

Fig. I.1. Schematic core map of the Garigliano reactor

first irradiation cycle is summarised in Table I.2. Two assemblies were selected for post-irradiation examinations: the A-106 was unloaded after the first cycle of operation, and the SA-13 recharge fuel element extracted after the second cycle.

TABLE I.2. Garigliano reactor core main characteristics

Moderation and cooling:		
Coolant pressure	181.26	kg/cm^2
Coolant average temperature	285	°C
Coolant saturation density	0.74	g/cm^3
Core average power density	20.3	KW/l (11.0 KW/KgU)
Core:		
Equivalent diameter	291.084	cm
Number of square fuel assemblies	208	
Fuel assembly pitch	17.892	cm
Initial enrichments (wt% ^{235}U)	2.1 - 1.6	
Total UO_2 weight	51,609	kg
Total U weight	45,492	kg
Number of control rods	89	

1. The A-106 Assembly (Garigliano I)

At the end of the first irradiation cycle (10th April 1964 - 7th May 1967) the fuel assembly A-106 was selected for post-irradiation examination. During cycle 1 the assembly occupied position 62-07 adjacent to the control rods F4 and G4 (Fig. I.1) and suffered a 218 day shut-down. The cycle therefore had to be subdivided into two parts A and B. The stainless steel sheath used in cycle 1A was replaced by a Zircaloy sheath in cycle 1B. Assembly A-106 was composed of 81 rods arranged in a 9x9 array. Each of the eighty-one rods consisted of four segments containing pellets of low enriched ceramic uranium oxide and sheathed in Zircaloy-2. The main geometrical dimensions of the element and of the adjacent cruciform control rods are given in Fig. I.2. The four segments of each rod were separated by zirconium connectors supporting the stainless steel grid, thus the fuel assembly was divided into four axial zones. All the pellets adjacent to the connectors had a lower enrichment in ^{235}U (1.6%) and in addition the peripheral rods contained also erbium oxide (Er_2O_3) which acted as a neutron poison to flatten flux-peaking in the grid area. The axial position of the fission chambers for the measurement of the in-core neutron flux was at about mid-height of each fuel segment. Table I.3 gives the main characteristics of the fuel element and of the adjacent control rod.
The calculated average burnup reached by the assembly was 9,458 MWD/MTU. At the level at which the samples were cut (1620 mm from the bottom of the stack) a burnup of 10,470 MWD/MTU was calculated by ENEL with the three-dimensional FLARE code /28/. The irradiation history of the fuel element

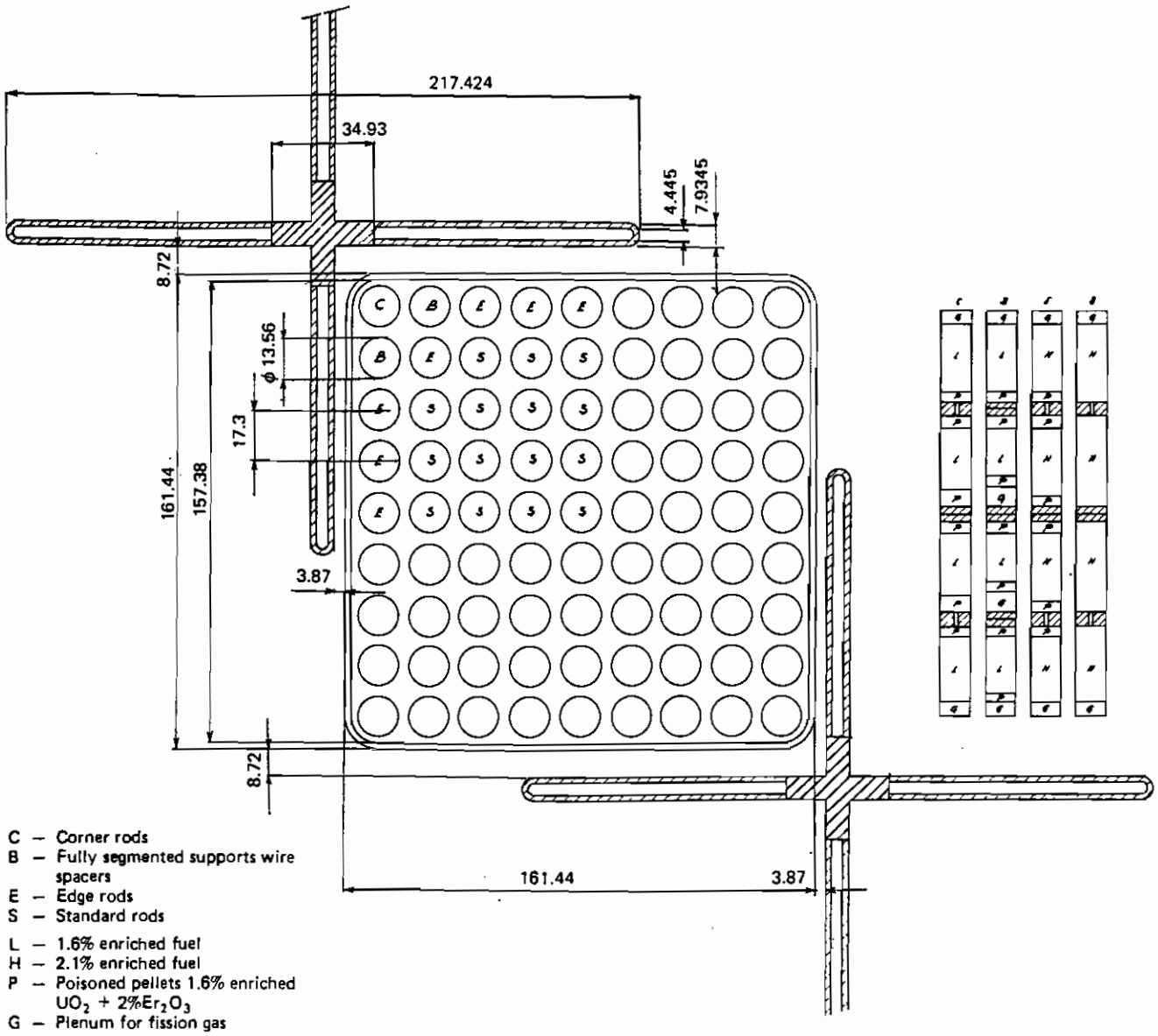

Fig. I.2. Horizontal cross-section of the Garigliano reactor fuel assembly (All dimensions are given in mm)

TABLE I.3. Garigliano fuel assembly (A-106) and control rod main characteristics

Square fuel assembly:		
Rod array	9x9	
Number of fuel rods	81	
Rod pitch	1.730	cm
Side of square fuel section	16.144	cm
Active length	267.72	cm
UO_2 weight	240.12	kg
Channel material:		
– Cycle 1A: SS AISI 304 (thickness: 0.152 cm)		
– Cycle 1B. ZRY 2 (thickness: 0.203 cm)		
Fuel pellet:		
UO_2 density (linear)	11.4	g/cm
Diameter	1.191	cm
Clad-pellet clearance	0.0063	cm
Fuel cladding:		
Outside diameter	1.356	cm
Inside diameter	1.2036	cm
Wall thickness	0.0762	cm
Material	ZRY 2	
Control rod (cruciform):		
Absorbing material	B_4C powder (density 1.8 g/cm^3) in 80 tubes	
Absorber length	273.68	cm
Cladding material	SS AISI 304	

TABLE I.4. Irradiation history of the A-106 fuel assembly

Cycle of Operation	Periods	Days	Assembly Burnup increment at measurement level MWD/MTU
FIRST CYCLE PERIOD 1 A	10.04.64 30.08.64	174	2,200
	01.09.64 03.11.64	34	–
	04.11.64 24.09.65	324	4,330
SHUT DOWN	25.09.65 27.04.66	218	–
FIRST CYCLE PERIOD 1 B	28.04.66 20.10.66	174	1,940
	21.10.66 07.05.67	197	2,000

A-106 is given in Table I.4. The bundle was dismantled in the GARIGLIANO fuel pool for testing during the 1967 shutdown.

Gamma scanning of the rods

The selection of the samples to be subjected to post irradiation examinations was as usual performed with the aid of gamma-scanning measurements. This choice was made in order to make possible the determination of the radial distribution of the burnup and of the heavy isotope content. The axial gamma scanning was carried out along the whole length of some fuel pins before cutting the samples for destructive analyses. For this purpose a continuously advancing system was used to move the rod horizontally in front of a collimator. The activity of the following isotopes was recorded

Isotopes	Half-Life (Years)	Gamma Energy (KeV)
$^{106}Ru \xrightarrow{} ^{106}Rh$	1.008	512
^{137}Cs	30.6	661.62
$^{144}Ce \xrightarrow{} ^{144}Pr$	0.778	2186

A Ge(Li) crystal (3.97 cm^3, FWHM 3.2 kev at 1.33 Mev) was employed, connected through a pre-amplifier-linear amplifier system, to a RIDL 400 channel analyser. Figure I.3 gives the normalized activity profiles of $^{106}Ru \rightarrow ^{106}Rh$, ^{137}Cs and $^{144}Ce \rightarrow ^{144}Pr$ for rod E5. After the axial gamma scanning was completed, pellet-size samples (10 mm thickness) were cut from 18 rods at only one level corresponding to 1620 mm from the bottom of the stack. The main point of this was to investigate radial effects. Figure I.4 shows the location of the rods selected for the analyses and the cutting position of the samples. In Table I.5 the rods selected for examination are listed.

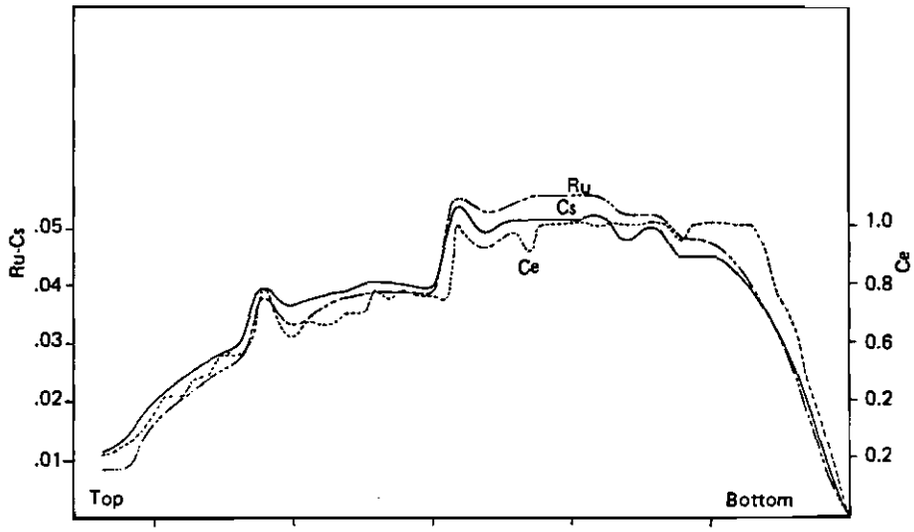

Fig. I.3. Axial activity distribution of Ru(512), Cs(662) and Ce(2186) peaks in rod E-5. (Peaks due to the presence of the Zr connection are visible).

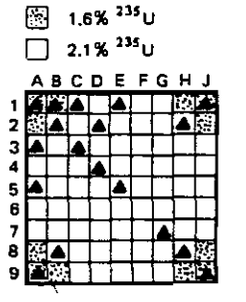

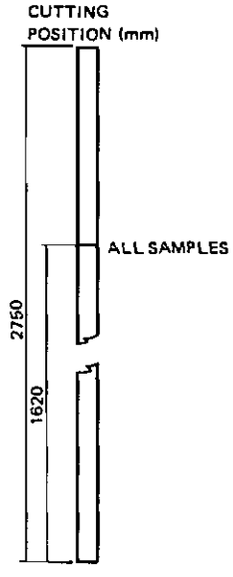

Fig. I.4. Location of selected fuel rods and cutting position of samples from Garigliano A-106 assembly

TABLE I.5. Garigliano I: selected fuel samples

Assembly (Location)	Average Burnup Range MWD/MTU	Initial Enrichment wt% ^{235}U	Rod Number	Axial Location
A-106 (62-07)	9,800-14,500	1.6	A1 A9	1 1
			J1 J9	1 1
			B1	1
	8,900-12,700	2.1	A3 A5	1 1
			B2 B8	1 1
			C1 C3	1 1
			D2 D4	1 1
			E1 E5.	1 1
			G7	1
			H2 H8	1 1

2. The SA-13 Assembly (Garigliano II)

At the end of the second irradiation cycle (10th October 1968 - 13th June 1970) the recharge fuel assembly SA-13 zircaloy-2 sheathed, was selected for post-irradiation analyses, with the aim, this time, of studying axial effects (only one rod was chosen and pellets sampled at different levels as will be shown in the following). During cycle 2 the assembly was irradiated in position 57-08 adjacent to the cruciform control rods D4 and D5 (see Fig. I.1). SA-13 consisted of 64 rods arranged in a 8x8 array. 52 rods had an initial enrichment of 2.41 wt% ^{235}U and 12 corner rods had initial reduced enrichment of 1.83 wt% ^{235}U. All recharge fuel elements were fully interchangeable with those of the first core. Two end plates connected with 8 peripheral fuel rods (tie rods) formed the frame of the assembly. Five equidistant grids also ensured the correct positioning of the rods. The main characteristics of the fuel assembly are reported in Table I.6. A schematic view of the SA-13 recharge fuel element is given in Fig. I.5 together with the adjacent control rods D4 and D5. The average burnup reached by the assembly was evaluated at 19,300 MWD/MTU. The average burnup of the rod E6 chosen for destructive analyses was evaluated at 6,950 MWD/MTU.

Gamma scanning of the rods

Rod E6 of assembly SA-13 was chosen for destructive analyses Axial gamma scanning was carried out on four segments of that rod

The whole gamma activity with energies ranging from 80 to 2,500 Kev was measured with a coaxial type Ge(Li) detector (FWHM of 2.6 Kev at 1.33 Mev) connected to an INTERTECHNIQUE Plurimat 20 processor. A collimator mounted in the concrete wall of the cell with an aperture of 0.5 mm height and 20 mm width was used. The vertical displacement unit, obtained by a stepping motor controlled by the Plurimat processor, was

TABLE I.6. Garigliano recharge fuel assembly (SA-13) and control rod main characteristics.

Square fuel assembly:		
Rod array	8x8	
Number of fuel rods	64	
Rod pitch	1.93	cm
Side of square fuel section	16.144	cm
Active length	271.8	cm
Standard rod enrichment (wt% ^{235}U)	2.41	
Corner rod enrichment (wt% ^{235}U)	1.83	
UO_2 weight	231.51	kg
Channel material	ZRY 2	(inside dimension 157.38 cm)
Fuel pellet:		
UO_2 density (linear)	13.37	g/cm
Diameter	1.290	cm
Clad-pellet clearance	0.014	cm
Fuel cladding:		
Outside diameter	1.506	cm
Inside diameter	1.318	cm
Wall thickness	0.094	cm
Material	ZRY 2	
Control rod:		
See Table I.3		

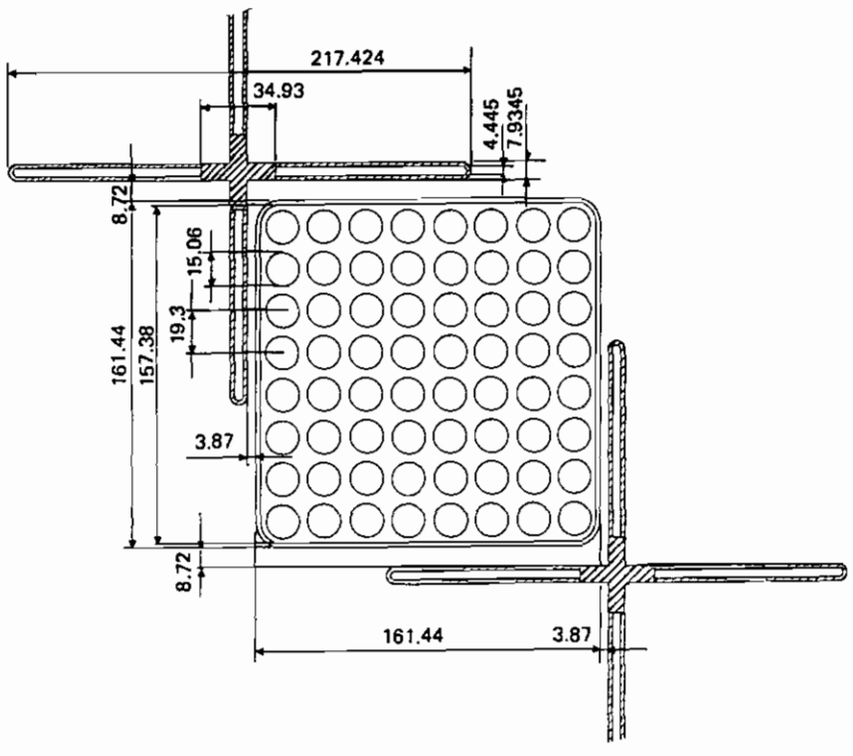

Fig. I.5. Horizontal cross-section of the Garigliano reactor SA-13 recharge fuel assembly (All dimensions are given in mm)

GARIGLIANO E6/1

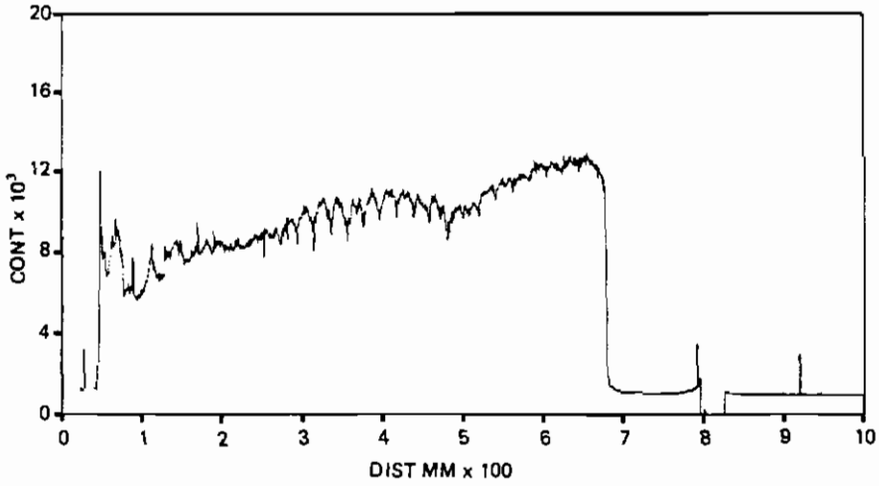

GARIGLIANO E6/2

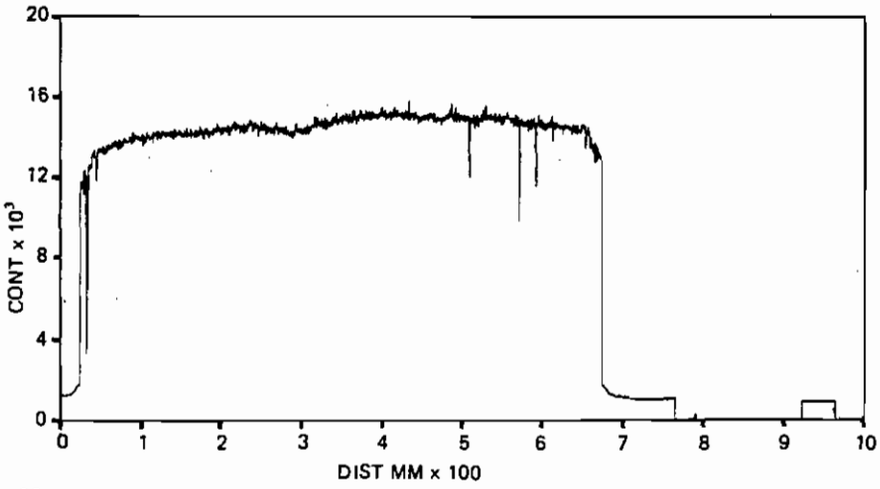

GARIGLIANO E6/3

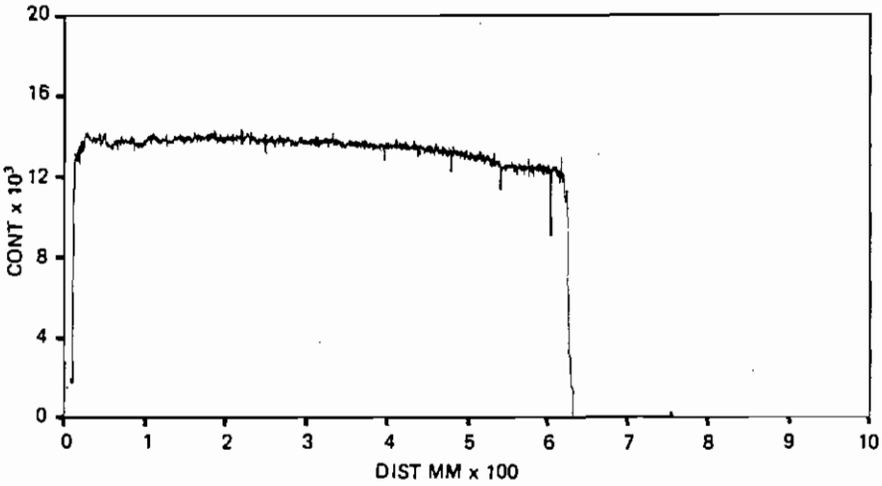

GARIGLIANO E6/4

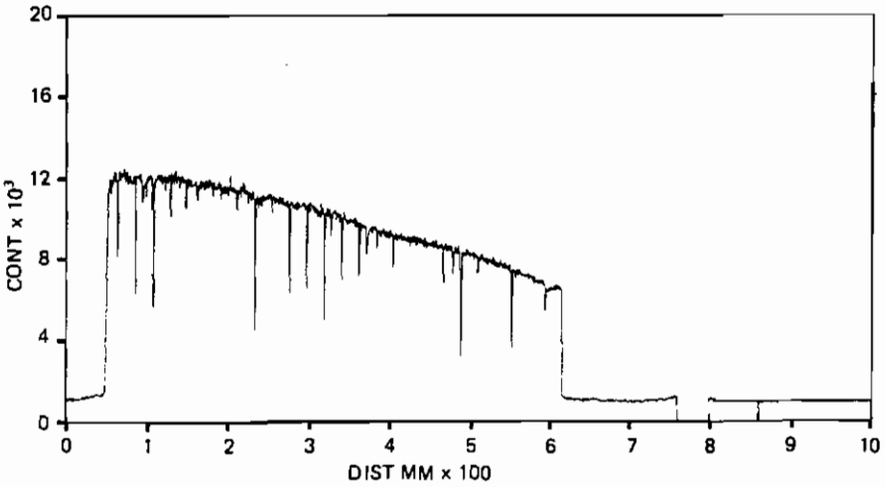

Fig. I.6.

0.5 mm. Figure I.6 shows the results obtained. Figure I.7 shows the sample cutting levels. Denser sampling was performed at the extremities of the rod, where the burnup variation was higher. The samples selected for examination are listed in Table I.7.

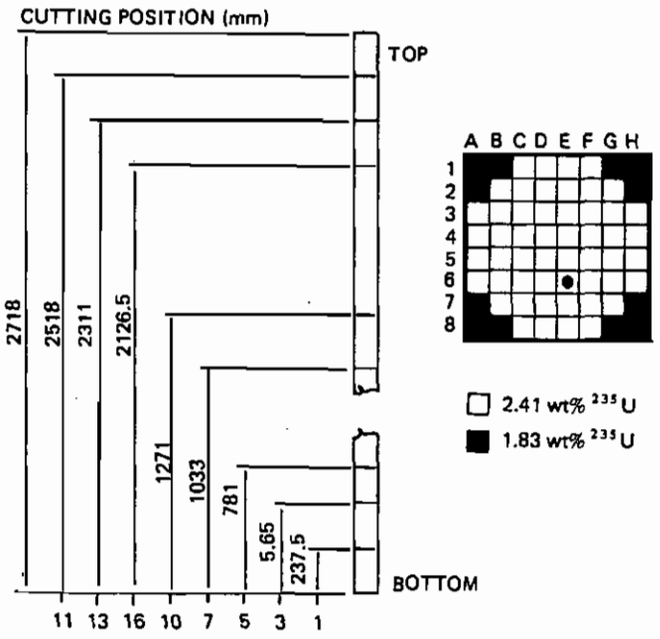

Fig. I.7. Location of selected fuel rod and cutting position of samples from Garigliano SA-13 assembly

TABLE I.7. Garigliano II; selected fuel samples

Assembly (Location)	Average Burnup Range MWD/MTU	Initial Enrichment wt% ^{235}U	Rod Number	Axial Locations
SA-13 (57-08)	4,200-8,600	2.41	E6	1-3-5-7 10-16-13-11

3. The Trino Vercellese Reactor

The TRINO VERCELLESE nuclear power plant /29/ operated by ENEL, is equipped with a pressurized water reactor rated at 825 MW(th). Westinghouse Electric Corp. is the designer and manufacturer of the nuclear steam generating plant, fuel included. The reactor was first brought to criticality in June 1964. The reactor core for cycle 1 was composed of 120 square fuel assemblies, divided into three radial zones of 40 assemblies each (initial enrichments 2.719, 3.13, 3.897 wt% ^{235}U) and 52 cruciform assemblies (initial enrichment 2.719 wt% ^{235}U). 28 cruciform fuel assemblies were connected as "fuel bearing followers" to 28 cruciform control rod, 24 were permanently in the core. Each cruciform fuel assembly contained 26 fuel rods. The control rods were composed of 32 absorber rods containing Ag, In and Cd in the ratio 80 : 15 : 5. The cladding material for both the fuel and the absorber was stainless steel. The total initial weight of uranium in the core was about 39.9 metric tons. The core was operated with a chemical shim of boric acid dissolved in the coolant. The main reactor characteristics are presented in Table I.8. The post-

TABLE I.8. Trino-Vercellese reactor main characteristics

	1st Cycle		2nd Cycle	
Moderation and cooling:				
Coolant pressure	140	kg/cm^2	140	kg/cm^2
Coolant average temperature	278	°C	269	°C
Coolant density	0.765	g/cm^3	0.782	g/cm^3
Core average power density	64.6 (21.0 KW/KgU)	KW/l	69.9 (22.8 KW/kgU)	KW/l
Core:				
Equivalent diameter	249.9	cm	240.0	cm
Number of square fuel assemblies	120		112	
Number of cruciform assemblies	52		52	
Initial enrichment (wt% ^{235}U):				
— Square assemblies	2.719-3.13-3.897		2.719-3.13-3.897	
— Cruciform assemblies	2.719		2.179	
Number of reload assemblies			40	
Reload assemblies enrichment (wt% ^{235}U)			3.897	
Total UO_2 weight	44,634	kg	41,939	kg
Total U weight	39,873	kg	36,968	kg
Number of control rods	28		28	

irradiation analyses were originally performed on fuel irradiated during the first cycle of reactor operation (23rd October 1964 - 28th April 1977). Three assemblies were selected for this TRINO I campaign: 509-049, 509-032 and 509-104. During this cycle, two extended shutdowns occurred, so the cycle can be considered to be divided into three periods summarized in Table I.9. Following the second cycle (20th May 1970 - 9th July 1971) the 509-069 assembly was selected for further post-irradiation examinations (TRINO II campaign). A schematic map of the reactor core, indicating the position of the selected fuel assemblies during the first and the second irradiation cycles, is given in Fig. I.8. The irradiation history of the four selected assemblies is also given in Table I.9. In Table I.10 the burn-up increment of each sample has been calculated for each irra-

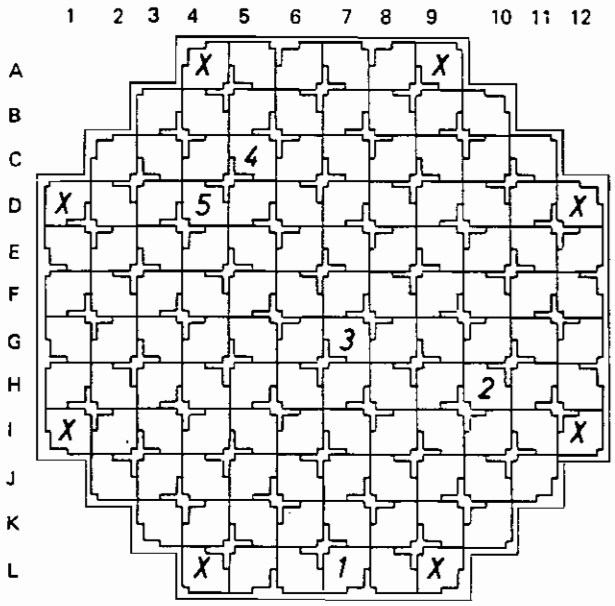

X Dummy assemblies (second cycle only)
1 Position of assembly 509-104 during the first cycle
2 Position of assembly 509-032 during the first cycle
3 Position of assembly 509-049 during the first cycle
4 Position of assembly 509-069 during the first cycle
5 Position of assembly 509-069 during second cycle

Fig. I.8. Schematic core map of the Trino Vercellese reactor

TABLE I.9. Irradiation history of the fuel assemblies of Trino Vercellese reactor

Cycle of Operation	Periods	Days	Core Burnup increment MWD/MTU	Position within the Core			
				509-049	509-032	509-104	509-069
FIRST	23.10.64 05.06.65	226	2,200	G-7	H-10	L-7	C-5
	06.06.65 30.08.65	86	–				
	31.08.65 20.05.66	263	4,050				
	21.05.66 10.07.66	51	–				
	11.07.66 28.04.67	292	5,050				
SHUT DOWN	29.04.67 19.05.70	1117	–	UNLOADED			
SECOND	20.05.70 09.07.71	416	8,155				D-4

TABLE I.10. Trino Vercellese burnup increments

Fuel Element	Initial Enrichment 235U wt %	Sample	First Cycle		Second Cycle		Burnup MWD/MTU
			F_1	ΔBU_1	F_2	ΔBU_2	
509-049	2.719	L5 1	.69	7,800			7,800
		4 □	1.27	14,300			14,300
		9	.93	10,500			10,500
		J8 1	.76	8,600			8,600
		4	1.33	15,000			15,000
		7	1.35	15,300			15,300
		9	.98	11,100			11,100
		A1 1	.78	8,800			8,800
		7	1.43	16,200			16,200
		9	1.04	11,800			11,800
509-032	3 130	E11 1	.66	7,500			7,500
		4 □	1.35	15,200			15,200
		7 □	1.40	15,800			15,800
		9	1.03	11,600			11,600
		H9 4	1.47	16,600			16,600
		7	1.51	17,100			17,100
		9	1.11	12,500			12,500
		Q15 7	1.62	18,300			18,300
509-104	3.897	M11 7 □	1.08	12,200			12,200
		A12 1	.30	3,400			3,400
		7	.65	7,400			7,400
509-069	3.130	E5 4 □	1.35	15,300	1.03	8,400	23,700
		7 □	1.41	15,900	1.07	8,900	24,700
		9	1.10	12,400	.84	6,900	19,300
		L5 4 □	1.37	15,500	1.04	8,500	24,000
		7 □	1.38	15,600	1.05	8,700	24,300
		E11 1	.74	8,400	.56	4,500	12,900
		2 □	1.20	13,600	.91	7,400	21,000
		4 □	1.35	15,200	1.02	8,400	23,600
		5 □	1.38	15,600	1.05	8,600	24,200
		7 □	1.40	15,800	1.06	8,700	24,500
		8 □	1.36	15,400	1.03	8,400	23,800
		9	1.15	13,000	.87	7,100	20,100
		L11 4 □	1.37	15,500	1.04	8,500	24,000
		7 □	1.40	15,800	1.06	8,700	24,500
		A1 1	.87	9,800	.66	5,400	15,200
		7	1.58	17,800	1.21	10,000	27,800
		J9 4	1.41	15,900	1.08	8,900	24,800
		7	1.45	16,400	1.10	9,000	25,400

□ Samples irradiated in asymptotic positions

diation cycle. This calculation has been done by multiplying the corresponding reactor burnup increments or power levels by the factor F_1 (for the first cycle) and by the factor F_2 (for the second cycle), which take into account the assembly burnup increase and the rod position factors.

1. The 509-049,509-032 and 509-104 Assemblies (Trino I)

At the end of the first cycle, in addition to the 40 assemblies of the inner core region (enrichment 2.719 wt%), some assemblies of the intermediate and outer regions (enrichments 3.13 and 3.897 wt%) were also unloaded from the reactor for reprocessing. Thus assemblies of three different enrichments were available for post-irradiation examinations. The main data relative to the fuel assemblies and the control rod are presented in Table I.11.

The criteria for selection of assemblies, rods and samples have been the following:

- wide range of initial enrichment (2.719, 3.13 and 3.897 wt% ^{235}U);
- wide range of burnup values (3,400 to 17,700 MWD/MTU for the single samples);
- different assembly location within the core (centre, intermediate, periphery, near to and far from control rods, etc.);
- different rod location within the assemblies (corner rods, rods near the central water hole provided for in-core instrumentation thimble, rods from unperturbed positions) corresponding to different neutron spectra;
- different axial location of samples along the rods in order to obtain axial profiles of burnup and isotopic composition. A total of 8 rods and 21 samples were selected. The rods and samples selected for examination are listed in Table I.12

TABLE I.11. Trino Vercellese fuel assemblies and control rod main characteristics

Square fuel assembly:		
Rod array	15x15	
Number of fuel rods	208	
Rod pitch	1.303	cm
Side of square fuel section	20.0	cm
Active length	264.9	cm
UO_2 weight	353.81	kg
Channel material	SS AISI 304	
Cruciform fuel assembly:		
Number of fuel rods	26	
Rod pitch	1.390	cm
Rod outer diameter	1.092	cm
Active length	240.3	cm
UO_2 weight	44.0	kg
Channel material	SS AISI 304	(thickness: 0.073 cm)
Fuel pellet:		
UO_2 density (linear)	6.6	g/cm
Diameter	0.890	cm
Clad-pellet clearance	0.0114	cm
Fuel cladding:		
Outside diameter	0.9786	cm
Inside diameter	0.9010	cm
Wall thickness	0.0388	cm
Material	SS AISI 304	
Control rod:		
Absorbing material	Ag, In, Cd	
Absorber length	269.2	cm
Cladding material	SS AISI 304	

TABLE I.12. TRINO I: selected fuel samples

Assembly (Location)	Average Burnup Range MWD/MTU	Initial Enrichment wt% ^{235}U	Rod Number	Axial Locations
509-049 (G-7)	8,200-15,300	2.719	L5	1-4-9
			J8	1-4-7-9
			A1	1-7-9
509-032 (H-10)	7,200-17,700	3.130	E11	1-4-7-9
			H9	4-7-9
			Q15	7
509-104 (L-7)	3,400-11,900	3.897	M11	7
			A12	1-7

and in Fig. I.9, where the cutting positions are indicated schematically.

A square fuel assembly consisted of a 15x15 array of fuel rods. Some of the peripheral fuel rods were omitted to provide slots for the passage of the control rod blades. The central rod was also omitted. The number of fuel rods per assembly is therefore 208. The fuel rods were kept in place by ten spacer grids welded to the perforated steel can which surrounds the fuel bundle. The horizontal cross section of a typical fuel assembly is presented in Fig. I.10 together with a cruciform fuel assembly.

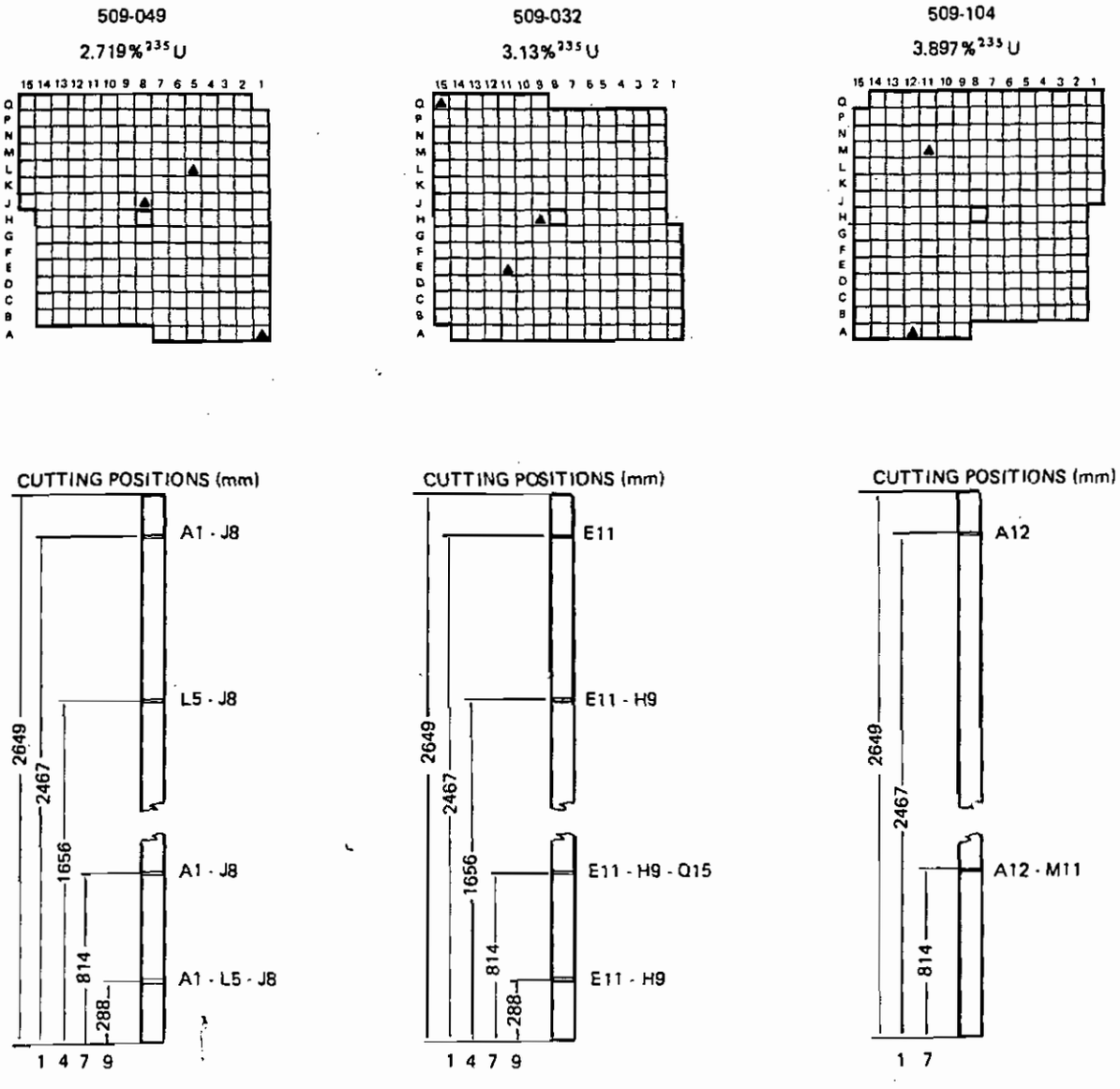

Fig. I.9. Location of selected fuel rods and cutting positions of samples from Trino Vercellese reactor - first core (TRINO I)

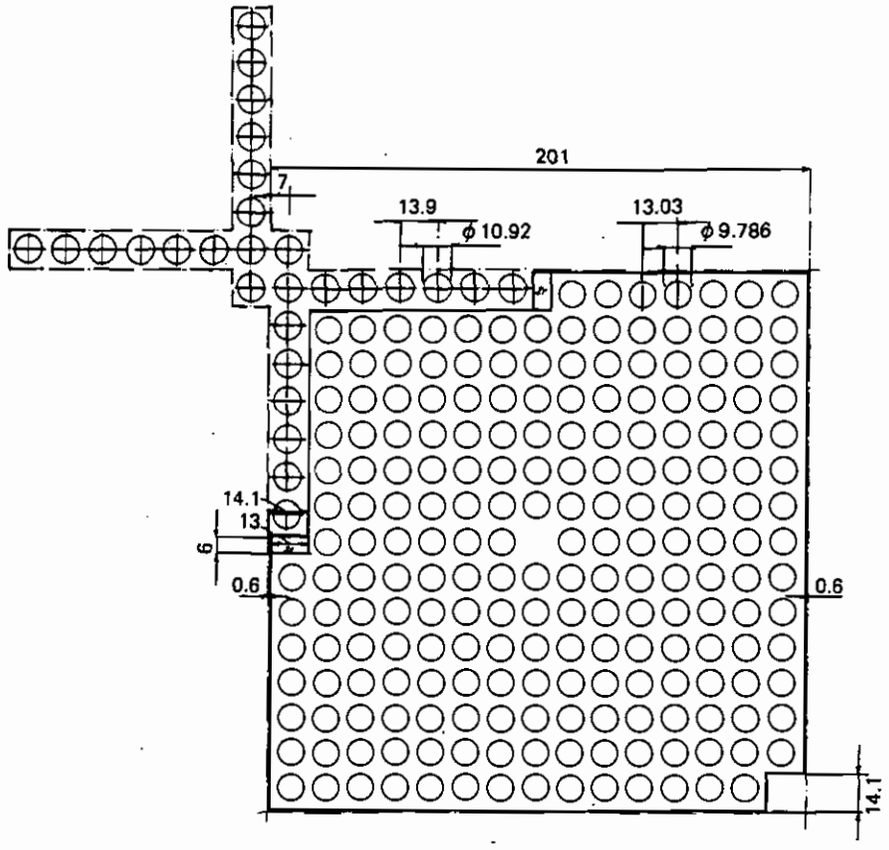

Fig. I.10. Horizontal cross-section of the Trino Vercellese reactor fuel assembly (All dimensions are given in mm)

Dismantling of the fuel assemblies and visual examination of the fuel rods

The dismantling of the fuel assemblies and the extraction of the selected fuel rods were done at Ispra in the water pool of the ESSOR reactor. The operation was performed by means of a special device designed by ENEL /30/ (see Fig. I.11). The fuel rods were then transferred to the main examination cell of the "Atelier Demantellement Elements Combustibles" (ADECO). Each rod was fixed to a sliding support, in front of the lead windows of the cell, and examined visually very carefully by means of a high magnification monocular periscope, a Questar telescope and a special binocular. Pictures were then taken by means of a SINAR camera equipped with a 500 mm focal length lens. Results of the examination can be found in /22/ in more details but in conclusion the visual and optical examination of the fuel showed only a few small defects on the cans. After examination, the fuel rods were cut into three parts using an abrasive disk cutting machine and then sent to the metallurgical hot laboratory.

Metallography of the fuel

The main purpose of the metallographic analysis was (besides

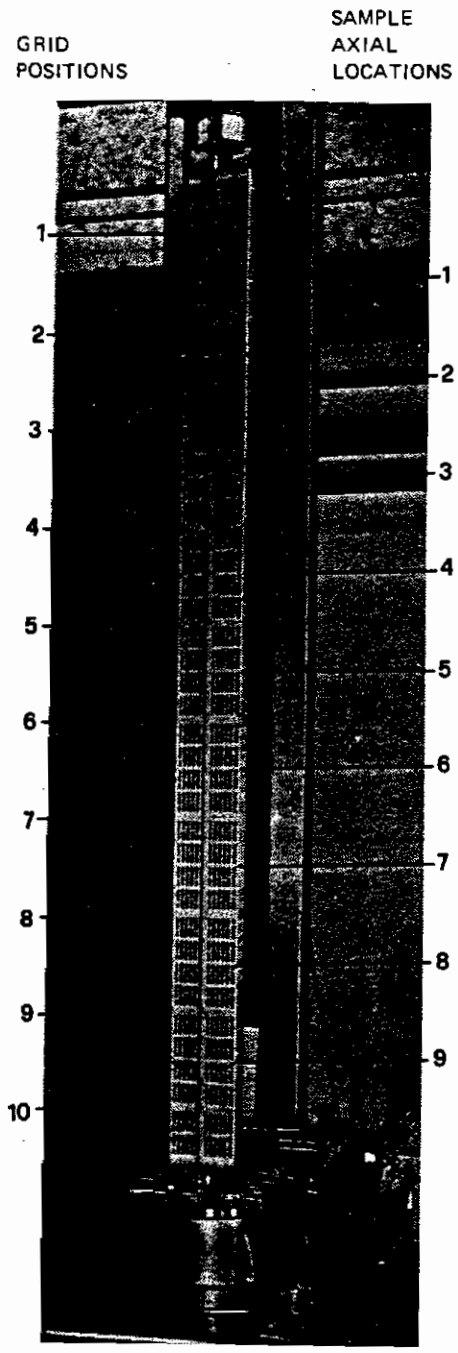

Fig. I.11. Fuel assembly showing positions of grids and axial locations of samples examined

clearing up the extent of the defects observed on the surface of the fuel rods) to inspect the UO_2 fuel. Rod A12 with the lowest burnup and rod E11 with a higher burnup have been analysed. Figures I. 12 and I. 13 present cross sections of these two rods showing cracks typical of the fuel examined. Figures I. 14 and I. 15 are micrographs of the fuel. In both cases there is no significant difference between the microstructure observed in the center and in the external zone of the fuel. Furthermore, there was no significant difference between the two fuel rods. Summarizing: the microscopic examination of the fuel led us to conclude that, apart from the cracking in the fuel, there was no particular modification in the microstructure which could be attributed to temperature or irradiation. This confirmed the results of temperature calculations /31, 32/ on the fuel, which predicted a maximum of about 1500°C. For this temperature no change of the microstructure of the fuel could be expected.

Gamma scanning of the rods

The gamma scanning equipment consisted of a mechanism installed inside a hot cell, a collimator system mounted in the concrete wall of the cell and the multi-channel analyser installed outside the hot cell. An electronic control unit allowed measurements to be run automatically following a preselected program for the displacement of the fuel rod and counting time. During counting the rod rotated, but its vertical axis remained fixed. The collimator had an aperture of 0. 5 mm height and 20 mm width. A NaI crystal and a Ge(Li) detector were used, with a 400 channel analyser. The maximum length of a fuel rod which could be mounted on the mechanical scanning system was 130 cm. The 3 m long fuel rods therefore had to be cut into three parts which have been analysed separately. The distribution of the total gamma activity in the energy range from 50 KeV to 2500 KeV was measured using the NaI crystal in steps of 0. 5 mm in the axial direction. Due to the rotation of the rod, mean values of the different sections were obtained. Figure I. 16 shows a typical result of the measured activity distribution of a part of a fuel rod, where a number of equidistant well-pronounced minima are visible due to the interfaces between fuel pellets. Figure I. 17 shows the results for one of the fuel rods examined. The three parts of the rods, measured separately, are reassembled in the figure. Evidently, the decrease in activity near the cuts is caused by the picture rearrangement and is not due to a local decrease of the concentration of fission products. The points of the rods where

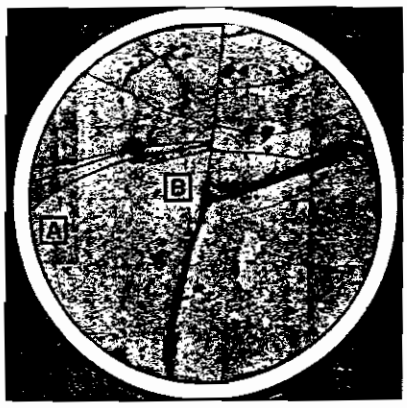

Fig. I.12. Cross section of the fuel rod A-12 (low burnup) x 12

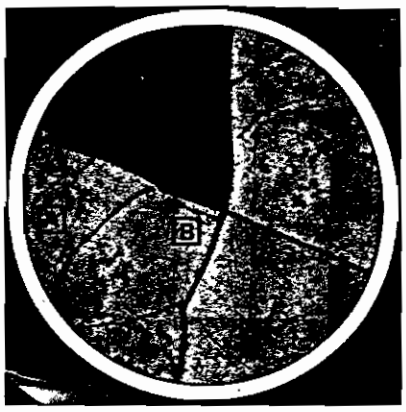

Fig. I.13. Cross section of the fuel rod E-11 (high burnup) x 12

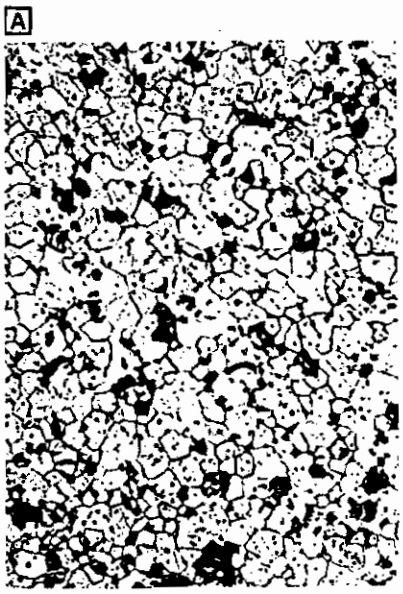

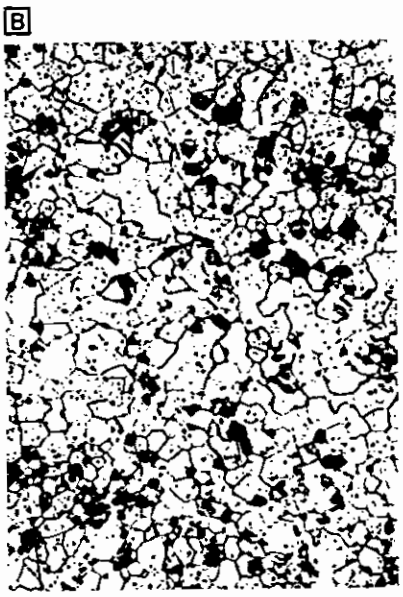

Fig. I.14. Microstructure of the fuel x 360

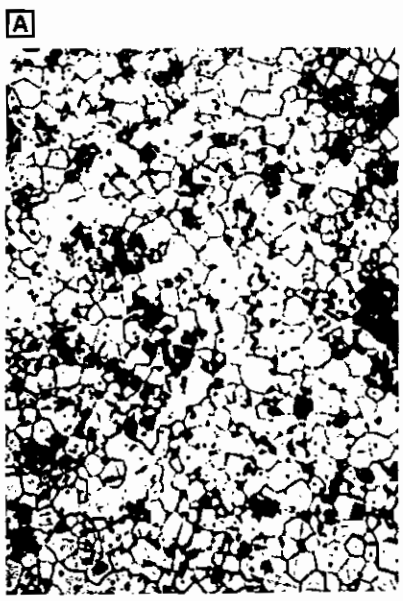

Fig. I.15. Microstructure of the fuel. x 360

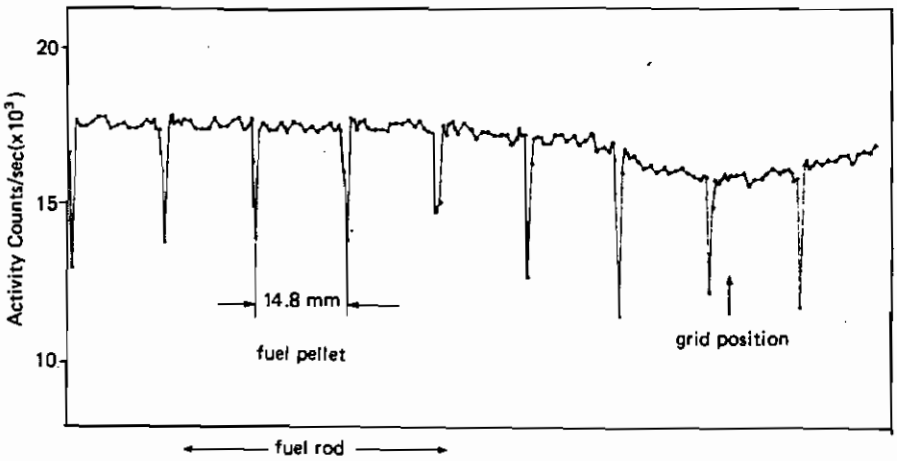

Fig. I.16. Total gamma-activity, part of rod 15 (509-049 fuel assembly)

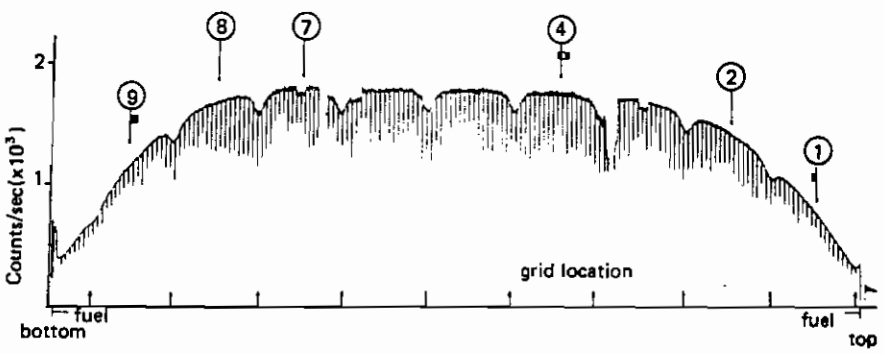

Fig. I.17. Total gamma activity: Assembly 509-049, rod L5

gamma spectrometry has been carried out (1, 2, 4, 7, 8, 9) (see also Fig. I.11) are indicated as well as the location of fuel samples cut off for the destructive analysis.

The following conclusions may be drawn from the results we have obtained:

- all the fuel rods show well-pronounced minima of activity due to the interface of different fuel pellets. This indicates that no metallurgical interaction between the different pellets occurred during irradiation and confirms the metallographic examination of the fuel;
- all fuel rods showed a decrease in activity near the grid positions corresponding to a real decrease in the burnup due to the flux depression caused by the displacement of water by the grids;
- corner fuel rods A1 (509-049 fuel assembly) and Q15 (509-032 fuel assembly) showed flux depressions due to the mechanical structure of the fuel box.

2. The 509-069 Assembly (Trino II)

At the end of the first irradiation cycle the reactor core was reduced by replacing 8 fuel assemblies with 8 dummy assemblies. The second irradiation cycle was consequently run under different conditions. It was then decided to select a further assembly for post-irradiation examinations to be performed at the end of the cycle. The fuel assembly 509-069 was selected. It had an initail enrichment of 3.13 wt% ^{235}U and reached an average burnup of 21,700 MWD/MTU. The irradiation history and the characteristics of the fuel assembly are shown in Tables I.9 and I.11. Figure I.18 and Table I.13 show the locations in the assembly of the fuel rods selected for the measurements and the axial locations from which the fuel samples were taken for the analysis of burnup and isotopic composition. A total of 7 rods and 18 samples were selected for examination. Rod Q15 was only used for gamma scanning purposes. Most of the fuel sections were taken from the asymptotic spectrum region at different axial locations, in order to obtain axial profiles and wide ranges of burnup and isotopic compositions.

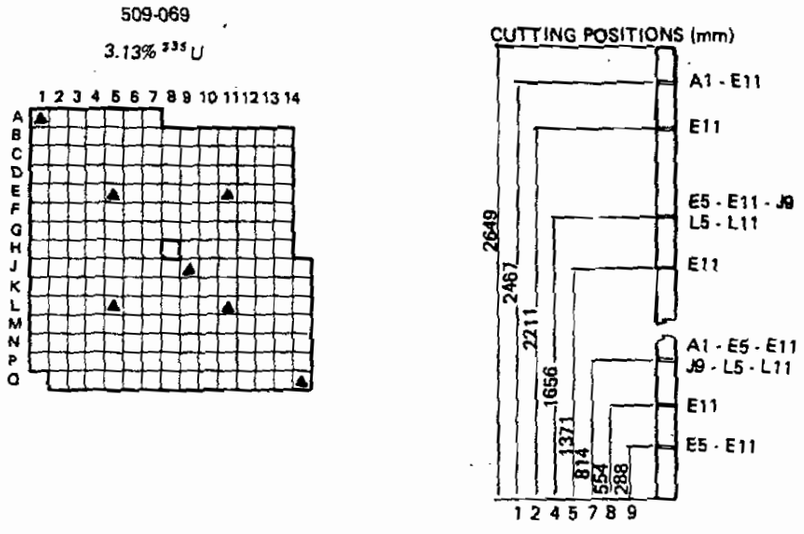

Fig. I.18. Location of selected fuel rods and cutting positions of samples from Trino Vercellese reactor - second core (TRINO II)

TABLE I.13. TRINO II: selected fuel samples

Assembly (Location)	Average Burnup Range MWD/MTU	Initial Enrichment wt% ^{235}U	Rod Number	Axial Locations
509-069 (C-5) 1) (D-4) 2)	19,100-26,600	3.13	E5	4-7-9
			L5	4-7
			E11	1-2-4-5-7-8-9
			L11	4-7
1) 1st cycle			A1	1-7
2) 2nd cycle			J9	4-7

Metallurgical examination

The dismantling of the fuel assembly No. 509-069 and the removal of the seven selected fuel rods were also done in the water pool of the ESSOR reactor. The operation was performed by means of the special device designed by ENEL, and already used for the other TRINO I assemblies. Following removal from the fuel element and storage in a basket, the fuel rods were transferred to the main examination cell of the ADECO laboratory. After a visual examination and a gross total gamma scanning, the fuel rods were cut into three pieces of about 80 cm each and transferred to the "Laboratoire Moyenne Activité" (LMA). In the ADECO and LMA laboratories the following examinations were carried out: optical inspection, metrology, mechanical tests on the fuel cladding and metallography.

Optical inspection

In the ADECO laboratory each rod was examined visually using the equipment already described. The mode of presentation of the rods in front of the lead window of the cell was modified in order to obtain within a single picture the total expanded surface of the rods. A special device, called a "Periphotograph", using reflecting mirrors, was placed in the cell in order to obtain three exposures of the fuel rod on the same picture. This principle is schematically presented in Fig. I. 19. The visual and photographic examinations of the external surface of the rods, performed in the ADECO and LMA laboratories, have shown the presence of black longitudinal scars which correspond to the spring positions. The presence of bright circumferential scars and points of fretting corrosion at the contact of the spring with the can were also observed. On the other hand,

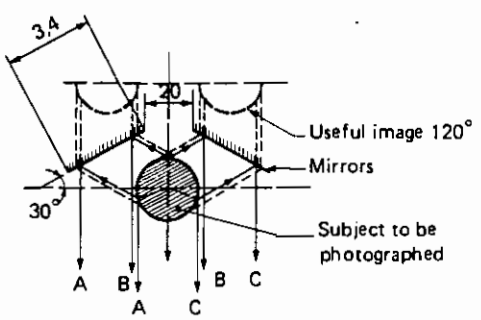

PROJECTION OF THE IMAGE

unity of measure: mm

Fig. I.19. Principle of the "Periphotograph" device

there was no evidence of external chemical corrosion of the cladding. Optical inspection of the internal cladding surface and of the fuel pellets was carried out in the LMA laboratory. Sections 7-8 cm long were cut out at different axial positions on the pins. These sections were then cut longitudinally in order to remove a cladding section. The inner surface of the removed cladding and the corresponding fuel pellet surfaces were examined under a periscope and photographed. The inner surface of the cladding can be considered as a photographic image of the fuel surface, showing clear traces of pellet-pellet interactions and pellet cracks. Figure I.20 presents an image of an inner cladding surface. Finally, it has been observed that a large percentage of pellets were broken and brittle. The brittleness of the fuel becomes evident when it is pushed out of the cladding. Using an optical metrological bench the length of a number of pellets from the L11 pin was determined.

Fig. I.20. Inner surface of cladding

Metrological examination

Sections of pins having a length of about 80 cm have been mounted on a special metrological bench allowing the linear diameter profile or the continuous spiral diameter profile to be recorded at the same time as the axial profile of the pin. Figures I.21 and I.22 present the linear diameter profiles of the three sections of the J9 pin, determined along the orthogonal planes of symmetry, the plane 0^{o} and 90^{o}. In Fig. I.23 the same three sections of the J9 pin are presented as continuous spiral diameter profiles, while Fig. I.24 shows the central part of Fig. I.23 with two different scale amplifications. In the middle of Fig. I.24 can be observed the deviation of the pin axis from the ideal line 0. The analysis of the diameter variation showed that all the pins considered have suffered a cladding diameter contraction. The diameter contraction is

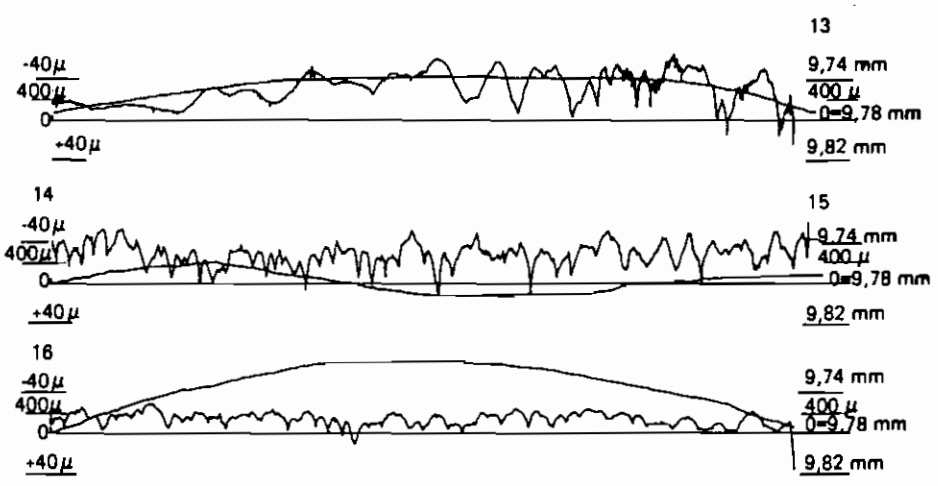

Fig. I.21. Linear diameter profile of the three sections of J9 pin in the 0^{o} plane and the relative axis profile

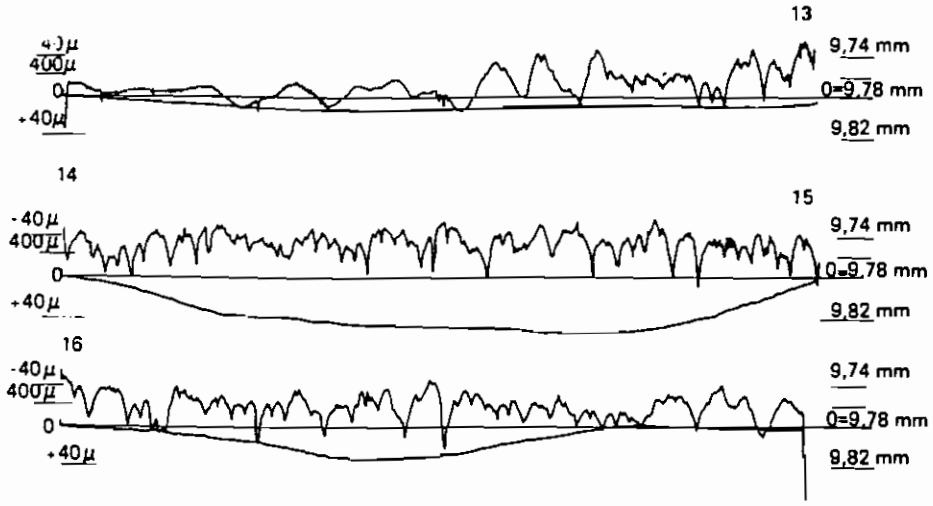

Fig. I.22. Linear diameter profile of the three sections of J9 pin in the 90° plane and the relative axis profile

Fig. I.23. Continuous spiral diameter profile of the three J9 sections

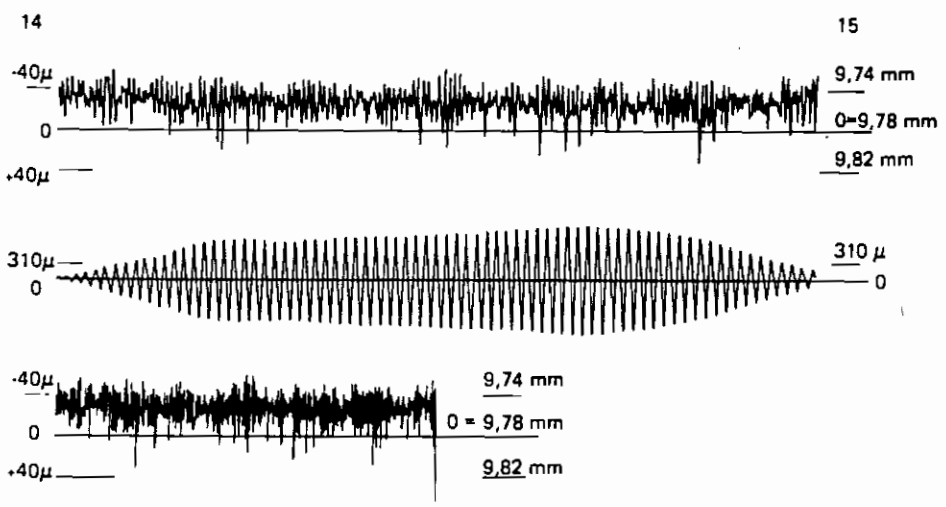

Fig. I.24. The continuous spiral diameter profile of the central section of J9 pin on two different scales

very small, the maximum contraction value being about 60 μm and the mean diameter value being about 30 μm smaller than the nominal original value.

Metallographic examination

Samples from pins L11 and E5 have been prepared for metallographic examination. The samples were cut from the central and lower regions of the pin. The fuel showed the presence of a

large number of cracks crossing the pellet volume as can be seen in Fig. I.25. The fuel material in the central region appeared denser than that at the periphery. Once the grain structure is brought out by chemical etching, one can see a grain size variation moving from the centre to the pellet periphery. In the central region the grains were large and closely packed, whereas towards the periphery the grain size decreased and the packing was looser. Such a change of structure along the diameter of the pellet is shown in Fig. I.26.

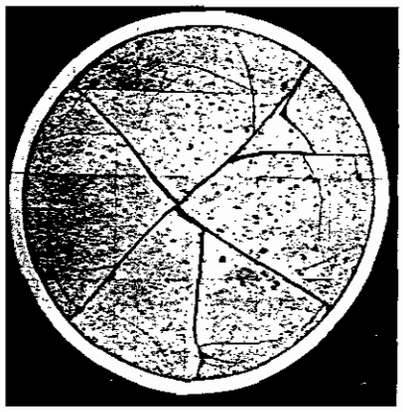

Fig. I.25. Cross section of the fuel rod L11 (x 18) (central part)

a) periphery of the pellet

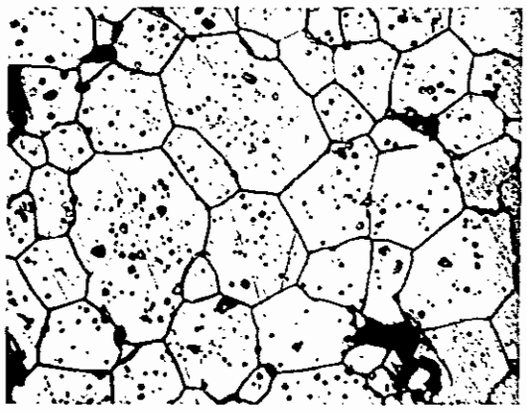

b) 1/8 of radius from periphery

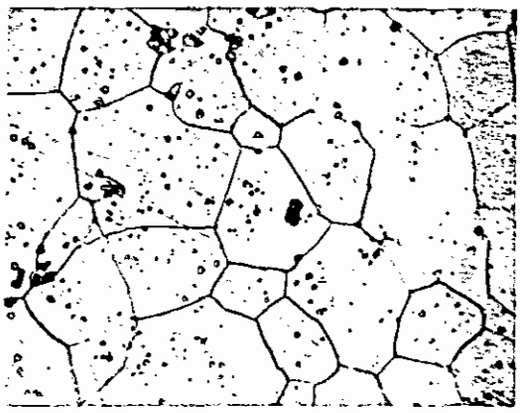

c) 1.4 of radius from periphery

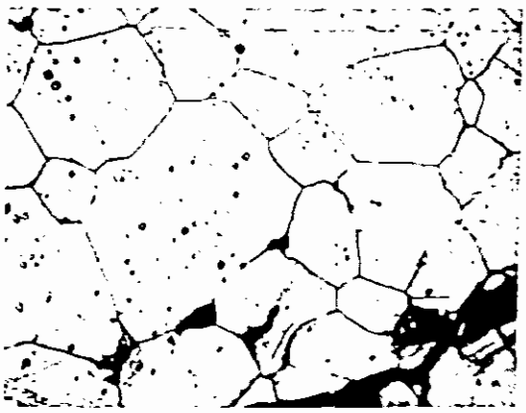

d) center of the pellet

Fig. I.26. Microstructure of the fuel at different radial positions

Gamma scanning of the rods

A gross total gamma scanning of four fuel rods was performed in the ADECO laboratory before cutting. The equipment used (a NaI(Tl) crystal placed in front of a lead collimator) was the same as that described for the TRINO I campaign. The rods were moved axially by a stepping motor. Steps of 0.2 mm each were set up but measurements were taken at 4 step (0.8 mm) intervals only. After examination the fuel rods were cut into three sections of about 80 cm (using an abrasive disk cutting machine) and transferred to the metallurgical section of LMA for further investigations. The gamma scanning measurements of the seven rods were carried out at the LMA laboratory, using the apparatus which was already described. Gamma rays with an energy of between 80 KeV and 2500 KeV were detected with a Ge(Li) crystal in combination with a collimator having an aperture of 0.5 mm height and 20 mm width. The vertical displacement unit obtained by the stepping motor was 0.5 mm. One example of the results obtained is given in Fig. I.27 where the total gamma activity of rod E5 is presented. From the measurements of the total gamma activity, the fuel pellet length and grid location can be seen for all the measured rods.

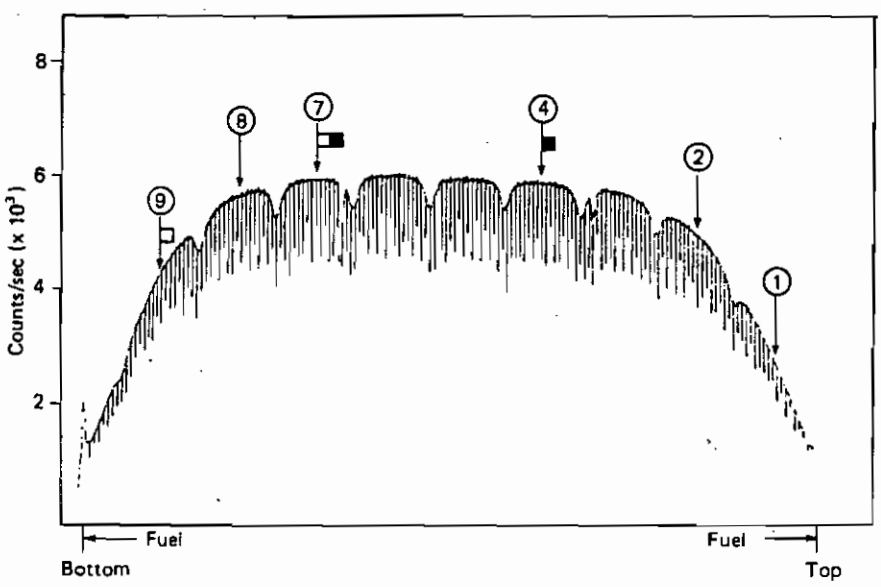

Fig. I.27. Total gamma activity rod E5

4. The Obrigheim Reactor

The OBRIGHEIM nuclear power plant /33, 34/ operated by Kernkraftwerk Obrigheim GmbH (KWO) is equipped with a pressurized water reactor rated at 350 MW(e). The reactor went critical in September 1968 and began commercial operation in March 1969. The core consisted of 121 square fuel assemblies in a 14 x 14 array, composed of 180 rods plus 16 guide tubes for control rod (absorbing material Ag-In-Cd) insertion. Initially,

TABLE I.14. Obrigheim reactor core main characteristics

Moderation and cooling:		
Coolant pressure	147.8	kg/cm^2
Inlet temperature	283	°C
Outlet temperature	313	°C
Core:		
Number of square fuel assembly	121	
Initial enrichment (wt% ^{235}U)	2.5-2.8-3.1	
Total UO_2 weight	39,930	kg
Total U weight	35,200	kg
Number of control rod clusters	32	

TABLE I.15. Irradiation history of the core and of the fuel assemblies of Obrigheim reactor

Cycle of Operation	Periods	Days (*)	Burnup Increments (MWD/MTU)				
			Core	Fuel Elements			
				BE 124	Position	BE 210	Position
SECOND	30.09.70 12.08.71	258	8,275	6,600	G-1		
SHUT-DOWN	13.08.71 29.09.71	48					
THIRD	30.09.71 07.09.72	295	9,194			9,900	D-11
SHUT DOWN	08.09.72 04.10.72	27					
FOURTH	05.10.72 01.09.73	283	9,718	12,000	D-7	11,400	J-5
SHUT-DOWN	02.09.73 24.09.73	23					
FIFTH	25.09.73 16.08.74	229	9,579	10,400	D-4	8,800	G-3

(*) Full power days only

it was divided into three zones of different enrichment, i.e. 3.1 2.8 and 2.5 wt% ^{235}U. The total weight of the uranium in the core was 35.2 metric tons. The main characteristics of the reactor are given in Table I.14. At the end of the fifth cycle of operation, two fuel assemblies were selected for post-irradiation examination:

- fuel element BE124, the irradiation of which started on 30th September 1970 and finished on 16th August 1974;
- fuel element BE210, the irradiation of which started on 30th September 1971 and finished on 16th August 1974.

The irradiation histories of the core and of the fuel assemblies are reported in Table I.15. A schematic map of the reactor core indicating the positions of the selected fuel assemblies during the various irradiation cycles is given in Fig. I.28. The horizontal cross section of a typical fuel assembly is presented in Fig. I.29.

1. The BE 124 and BE 210 Assemblies

The fuel assembly BE124 was irradiated during the second, the fourth and the fifth cycle of operation in positions G-1, D-7 and D-4, respectively and reached an average burnup of 29,000 MWD/MTU. The fuel assembly BE210 was irradiated during the third, fourth and fifth cycle of operation in positions D-11, J-5 and G-3, respectively and reached an average burnup of 30,100 MWD/MTU.

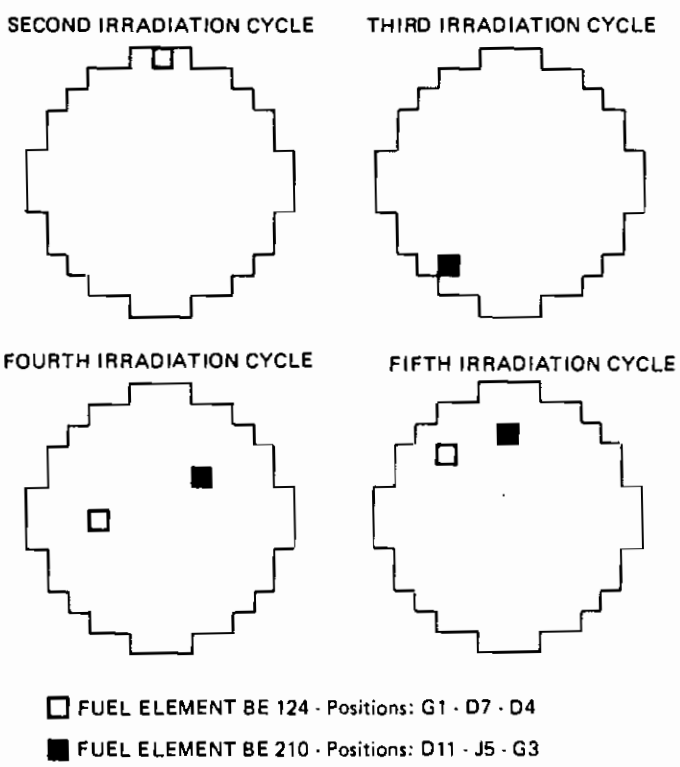

Fig. I.28. Schematic core maps of the Obrigheim reactor during different irradiation cycles. The position of the elements Be124 and Be210 are indicated.

BE124 had an initial enrichment of 3.0 wt% ^{235}U and BE210 an initial enrichment of 2.63 wt% ^{235}U. Both assemblies were cladded in Zircaloy-4. The main information relative to the fuel assemblies and the control rod is reported in Table I.16.

A total of six fuel rods and 23 samples were chosen for post-irradiation examination: four rods belonging to fuel element BE 124 and two to BE 210. The rods and samples selected are

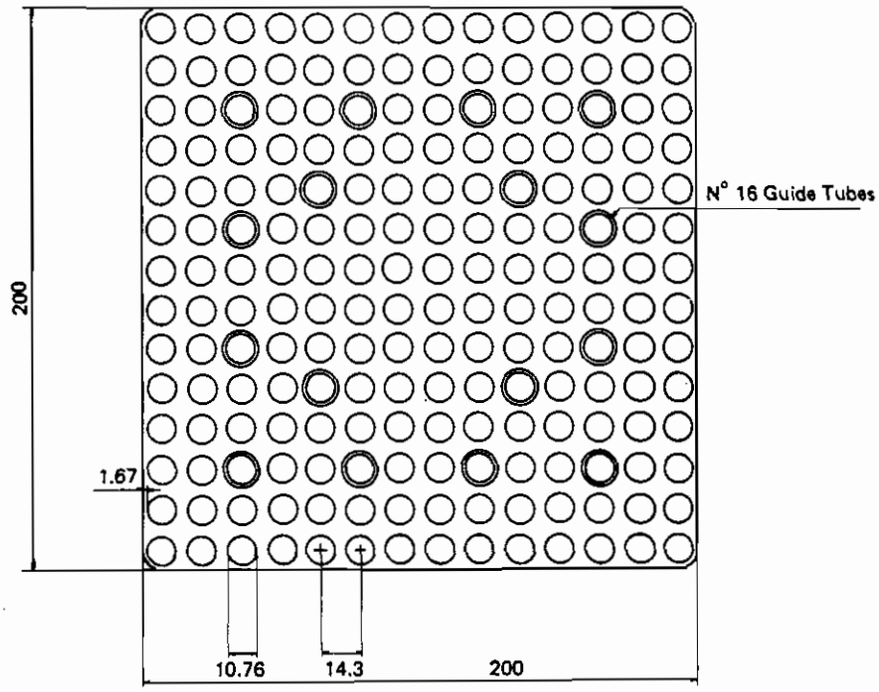

Fig. I.29. Horizontal cross section of the fuel assembly. (All dimensions are given in mm).

TABLE I.16. Obrigheim fuel assemblies and control rod main characteristics

Square fuel assembly.		
Rod array	14x14	
Number of fuel rods	180	
Rod pitch	1.43	cm
Side of square fuel section	20.0	cm
Active length	295.6	cm
UO_2 weight	221.83	kg
Channel material	ZRY 4	
Fuel pellet:		
UO_2 density (linear):		
– BE124 fuel assembly	6.68	g/cm
– BE210 fuel assembly	6.52	g/cm
Diameter	0.904	cm
Clad-pellet clearance	0.0139	cm
UO_2 density (linear):		
– BE124 fuel assembly	6.68	g/cm
– BE210 fuel assembly	6.52	g/cm
Diameter	0.904	cm
Clad-pellet clearance	0.0139	cm
Fuel cladding:		
Outside diameter	1.076	cm
Inside diameter	0.9318	cm
Wall thickness	0.0721	cm
Material	ZRY 4	
Control rod:		
Absorbing material	Ag, In, Cd	
Cladding material	SS	

reported in Table I.17. Figure I.30 shows the location of the fuel rods selected and their cutting positions.

Gamma scanning of the rods

A gross total gamma scanning of the fuel rods was carried out in the ADECO laboratory before they were cut. The equipment consisted of a Ge(Li) detector having a FWHM of 2.3 KeV at 1.33 MeV of ^{60}Co, connected to an INTER-TECHNIQUE Plurimat Multi 8 processor.
A lead collimator with an aperture of 0.5x10x283 mm was used. The rods are moved axially by a stepping motor: measurements have been done every 0.4 mm.

TABLE I.17. Obrigheim: selected fuel samples

Assembly (Location)	Average Burnup Range MWD/MTU	Initial Enrichment wt% ^{235}U	Rod Number	Axial Locations
BE 124	15,600-36,300	3.00	D1	1-2-3
(G1 2nd cycle)			E3	1-2-3-4-5
(D7 4th cycle)			G7	1-2-3-4-5
(D4 5th cycle)			M14	1-3-4
BE 210 (D11 3rd cycle) (J5 4th cycle) (G3 5th cycle)	24,200-37,500	2.83	G14	3(1)-4(1) 5(1)-5(2)
			K14	1-3(1)-4(1)

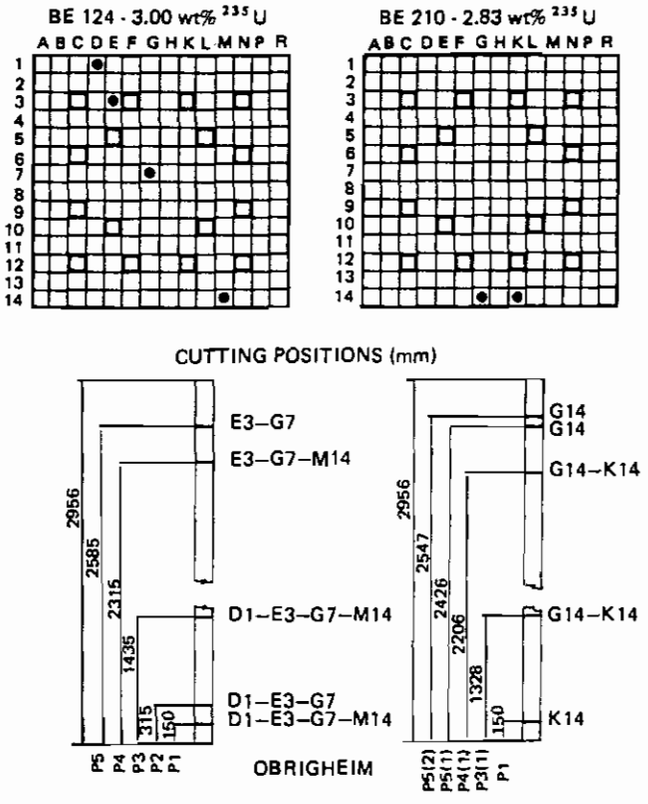

Fig. I.30. Cutting positions of the fuel samples selected for analyses

From the distribution curve of gamma activity obtained, it was possible to determine the length of the rods and the cutting levels, with a precision given by the scanning step (0.4 mm). Figure I.31 shows the results for rod G7 of the BE 124 fuel element. In the same figure the cutting positions are also indicated by arrows.

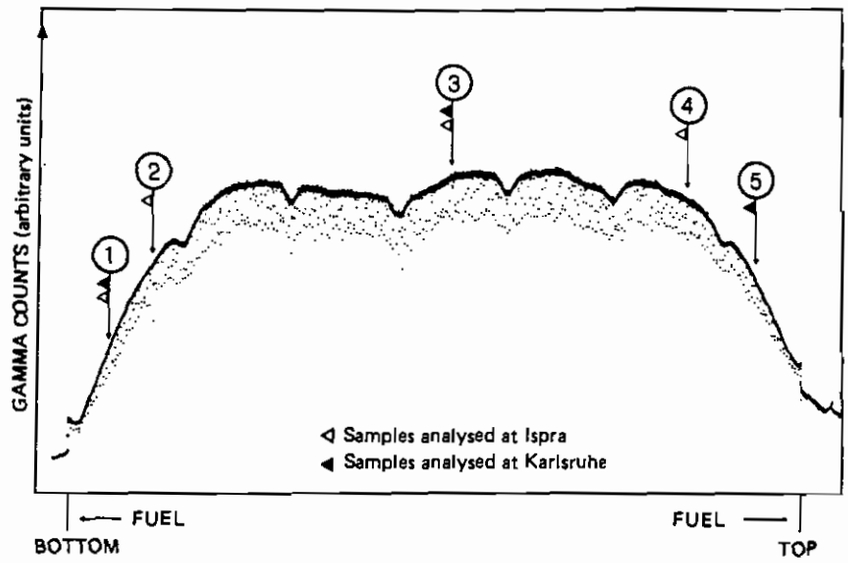

Fig. I.31. Total gamma activity. Be124 rod G7.

5. The Gundremmingen Reactor

The GUNDREMMINGEN Nuclear Power plant /35/, operated by Kernkraftwerk RWE-Bayernwerk GmbH (KRB) is equipped with a dual cycle boiling water reactor rated at 250 MW(e). The reactor was first brought to criticality on August 1966 and to commercial operation on April 1967. The reactor core is composed of 368 square fuel assemblies in a 6x6 array and of 89 cruciform control rods (absorbing material B_4C. The total weight of the uranium in the core was 46.7 metric tons.

The main characteristics of the reactor are reported in Table I.18.

At the end of the fifth cycle of operation two fuel assemblies were chosen for examination:

- fuel element B23 the irradiation of which was started on the 25th of August 1969 and terminated on the 5th of March 1973,
- fuel element C16 the irradiation of which was started on the 25th of July 1970 and terminated on the 5th of March 1973.

Figure I.32 presents the schematic map of the core with an indication of the position of assemblies B23 and C16 during the various irradiation cycles.

TABLE I.18. Gundremmingen reactor core characteristics

Moderation and cooling:		
Coolant pressure	70.35	kg/cm^2
Inlet temperature	266	°C
Outlet temperature	286	°C
Core:		
Equivalent diameter	274.8	cm
Number of square fuel assembly	368	
Total UO_2 weight	52,982	kg
Total U weight	46,703	kg
Number of control rods	89	

1. The B 23 and C 16 Assemblies

The fuel assemblies B23 and C16 selected for post-irradiation analyses consisted of 29 rods with initial enrichment of 2.53 wt% ^{235}U, and 7 rods with initial enrichment of 1.87 wt% ^{235}U.
B23 was irradiated during the second, third, fourth and fifth cycles in positions 65-07, adjacent to control rod H4 and 66-07 adjacent to control rod J4 and reached an average burnup of 22,600 MWD/MTU.
C16 was irradiated during the third, fourth and fifth cycles of operation in positions 67-16 adjacent to control rod J9 and 61-12 adjacent to control rod F7 and reached an average burn-up of 17,100 MWD/MTU.
The main characteristics of a typical fuel assembly and the control rod are reported in Table I.19. (A cross-section of the assembly, together with an adjacent control rod is shown in Fig. I.33.)
A total of 10 fuel rods (6 belonging to the B23 assembly and 4 to the C16 assembly) were selected for post-irradiation examinations. Table I.20 reviews the rods and samples chosen for analysis. The irradiation histories of the fuel elements are given in Table I.21.

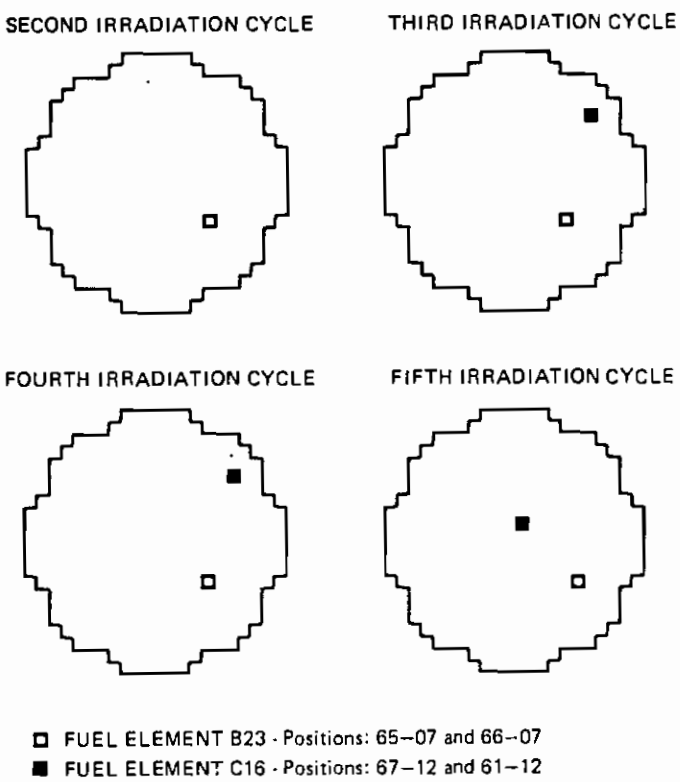

Fig. I.32. Schematic core maps of the Gundremmingen reactor during different irradiation cycles. The position of the elements B23 and C16 is indicated

TABLE I.19. Gundremmingen fuel assemblies and control rod main characteristics

Square fuel assembly:		
Rod array	6x6	
Number of fuel rods	36	
Rod pitch	1.78	cm
Side of square fuel section	11.352	cm
Active length	330.2	cm
UO_2 weight	144.0	kg
Channel material	ZRY 4	
Fuel pellet:		
UO_2 density (linear)	12.36	g/cm
Diameter	1.224	cm
Clad-pellet clearance	0.0137	cm
Fuel cladding:		
Outside diameter	1.428	cm
Inside diameter	1.250	cm
Wall thickness	0.089	cm
Material	ZRY 2	
Control rod (cruciform):		
Absorbing material	B_4C powder	
Absorber length	325.0	cm
Cladding material	SS 304	

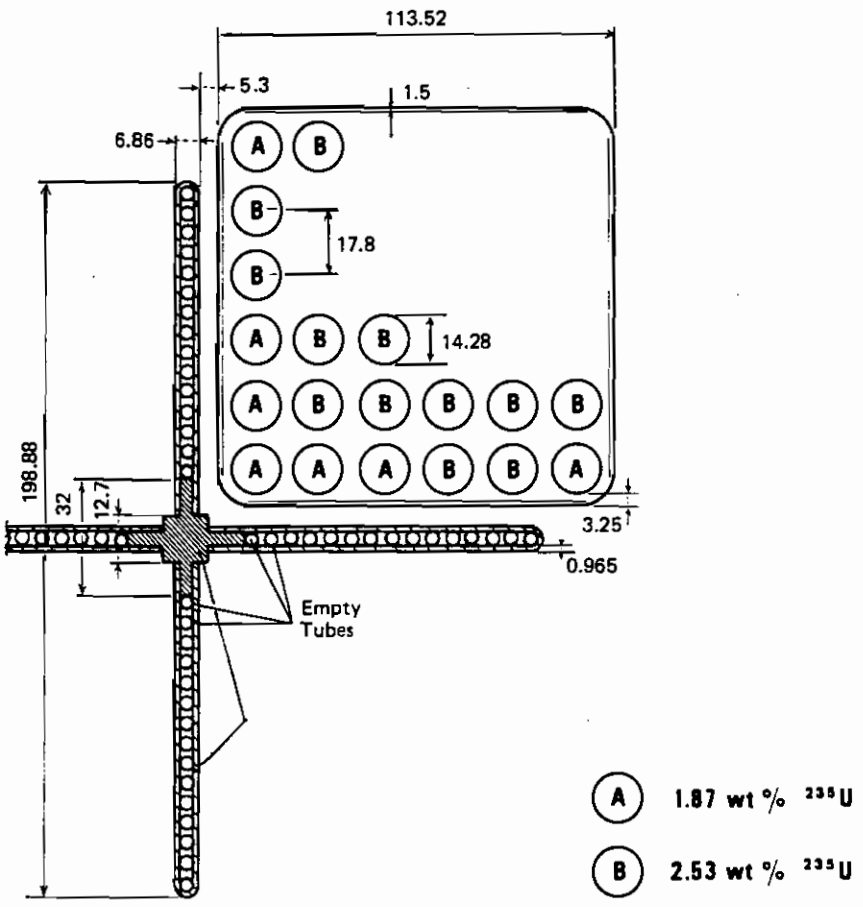

Fig. I.33. Cross section of the Gundremmingen assembly (All dimensions are given in mm)

Gamma scanning of the rods

Gamma-spectrometric measurements were carried out on the fuel rods with a coaxial type Ge(Li) detector having an FWHM of 2.6 KeV at 1.33 MeV, connected to an INTERTECHNIQUE Plurimat 20 processor. All the fuel pins were cut at 2680 mm from the bottom, in the steam-water zone, where an average

TABLE I.20. Gundremmingen: selected fuel samples

Assembly (Location)	Average burnup range (MWD/MTU)	Initial enrichment wt % ^{235}U	Rod number	Axial Location
B23 (65-07)	21,200-27,400	2.53	A1	1-2
			B3	1
			B4	1
(66-07) 5th cycle			C5	1
			E3	1
			E5	1
C16 (67-16)	14,400-20,300	2.53	A1	1-2
			B3	1
(61-12) 5th cycle			C5	1
			E5	1

TABLE I.21. Irradiation history of the fuel assemblies of the Gundremmingen reactor

Cycle of operation	Periods	Days	Core burnup increment (MWD/MTU)	
			Fuel element B23	Fuel element C16
SECOND	25.08.69 30.05.70	279	5,839	
SHUT DOWN	31.05.70 24.07.70	56	–	
THIRD	25.07.70 12.06.71	323	6,131	5,959
SHUT DOWN	13.06.71 15.07.71	33	–	–
FOURTH	16.07.71 30.04.72	290	5,483	5,083
SHUT DOWN	01.05.72 30.06.72	61	–	–
FIFTH	01.07.72 05.05.73	309	5,174	6,026

void fraction of about 50% was evaluated. Only rod A1 was also cut at 440 mm from the bottom, in the water phase. The two different cutting levels of rod A1 are indicated in this work as:

A1 (1) the sample cut at 440 mm level,

A1 (2) the sample cut at 2680 mm level.

Figures I. 34 shows the results obtained by the gamma scanning of rod C5 of the B23 fuel element. Figure I. 35 shows the location of the fuel pins selected and their cutting position.

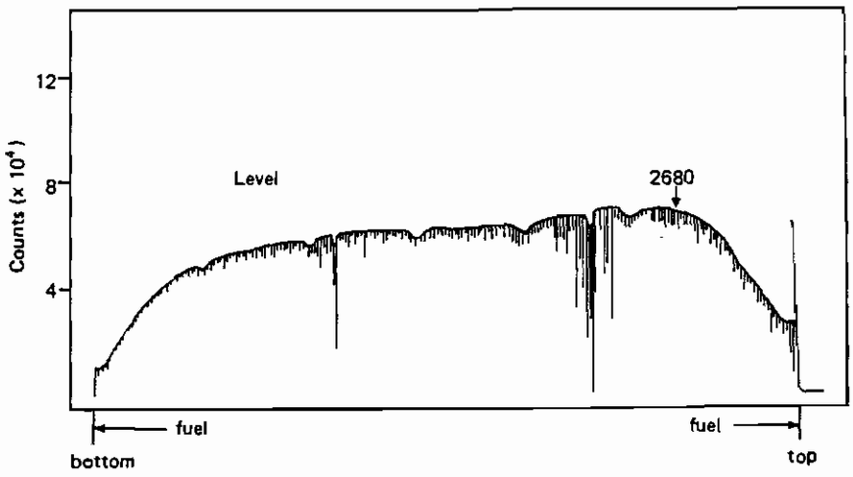

Fig. I.34. Gamma scanning of the rod C5 (B23 fuel element)

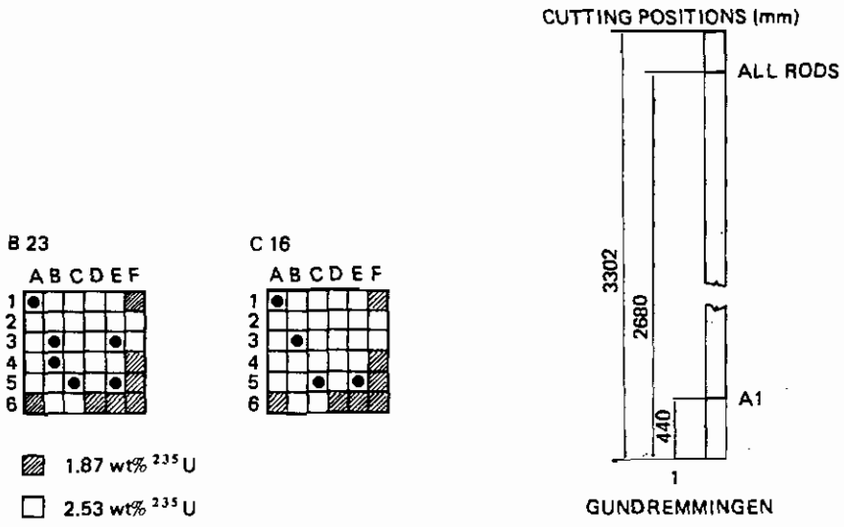

Fig. I.35. Cutting positions of the fuel samples selected for analyses

6. Destructive Analysis of the Samples

After the non-destructive tests on the fuel rods and the selection of the cutting levels performed with the aid of gamma scanning, pellet-size samples (10 mm thickness) were cut in the hot cells of the LMA Laboratory (Ispra) and of the Transuranium Institute (Karlsruhe). Three fuel samples were always cut for each chosen position, two for destructive analyses and one to be kept in reserve. Pairs of adjacent pellets were analysed in the Ispra and Karlsruhe laboratories in order to check the accuracy of the experimental data.

Table I. 22 gives the distribution of samples to the Ispra and Karlsruhe laboratories. Destructive analyses were performed according to the diagram presented in Fig. I. 36. The fuel samples selected for analyses were dissolved in 8M HNO_3 in hot cells. Small aliquots of the solution, which can be handled without heavy shieldings, were then transferred to glove-boxes for preparation of alpha and gamma sources and for radiochemical processes.

TABLE I.22. Distribution of samples to the Ispra and Karlsruhe laboratories

Reactor	Fuel Element	Total Samples Cut	Samples analysed	
			Ispra	Karlsruhe
GARIGLIANO (BWR)	A-106	18	–	10
	SA-13	8	8	–
TRINO VERCELLESE (PWR)	509-049	14	8	6 (4)
	509-032	8	7	1
	509-104	4	3	1 (1)
	509-069	23	13	10 (5)
OBRIGHEIM (PWR)	BE124	19	11	8 (3)
	BE210	8	6	2 (1)
GUNDREMMINGEN (BWR)	B23	9	6	3 (2)
	C16	7	4	3 (2)
	TOTAL	118	66	52 (18)

Number of check samples is indicated within brackets

1. Radiochemical procedures

The purpose of radiochemical processes was to obtain from the original fuel solutions purified samples of uranium, plutonium, americium and neodymium to be analysed by alpha and mass spectrometry. As shown in Fig. I.36 some stages of purification processes were carried out after an isotopic dilution step, i.e. the addition of tracers of suitably chosen isotopes. The purpose of the alpha and mass spectrometry measurements was to determine the abundance of heavy isotopes formed during irradiation inside the fuel assembly. In the earliest post-irradiation analytical campaigns (GARIGLIANO I, TRINO I and TRINO II /21, 22, 23/, uranium, plutonium, americium and neodymium were individually purified of interfering material. Later on, radiochemical techniques capable of purifying both uranium - plutonium and neodymium-americium in the same steps were developed. This chapter describes only these last procedures. The earlier approaches can be found described in detail also in Ref. 25, 36, 37.

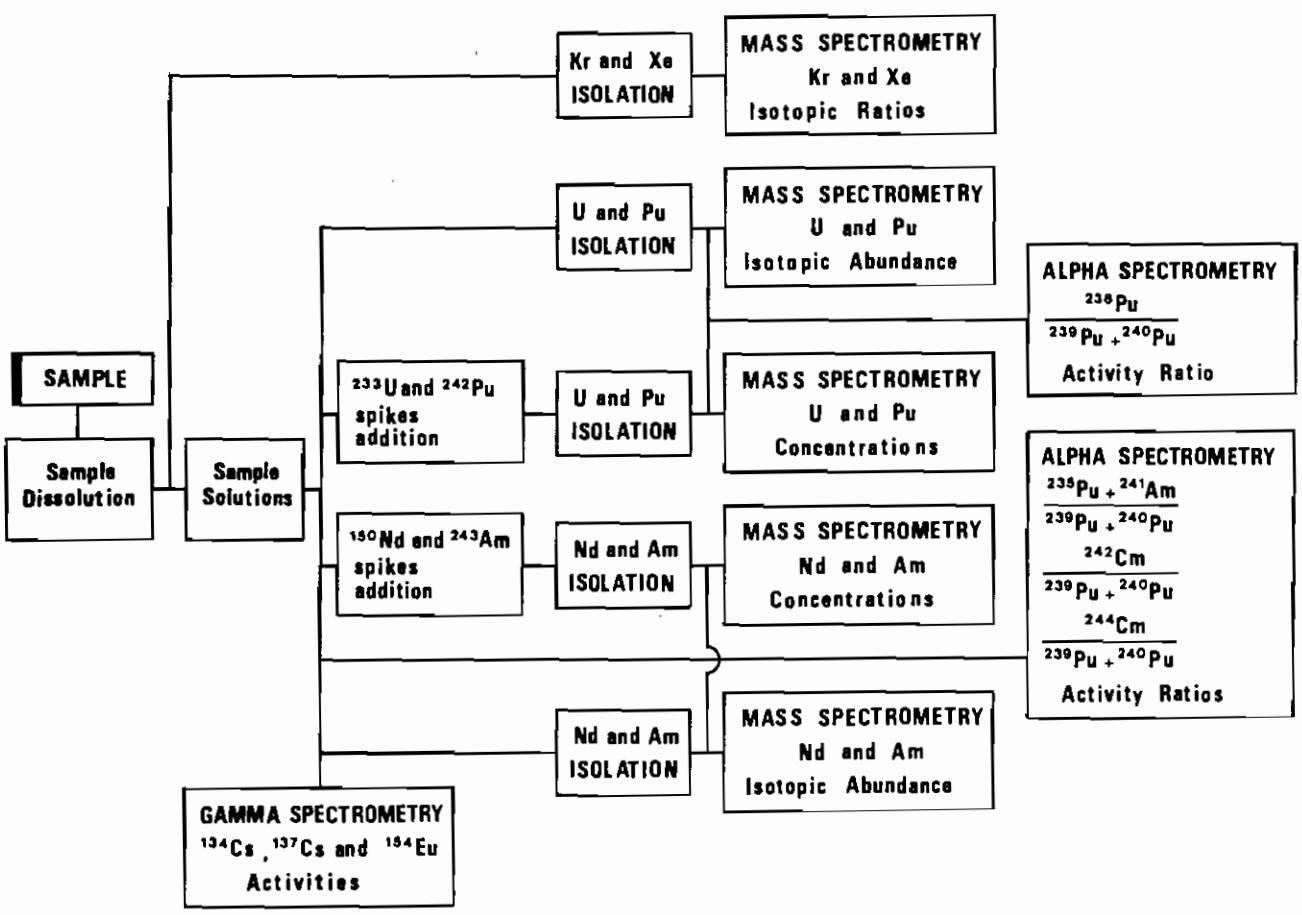

Fig. I.36. Destructive analysis scheme

Sample dissolution

The Karlsruhe Laboratory used a dissolution procedure /21/ which allowed the collection of Xe and Kr fission gases for the mass spectrometry measurements of their isotopic ratios. The procedure can be schematized as follows:

i) the weighed sample W_1 is brought into the dissolution flask (C) and the apparatus cleaned by flushing with helium (A);

ii) the collection flask (F) is evacuated to 1 Torr;

iii) 100 ml of concentrated HNO_3 are transferred into C and heated to boiling;

iv) the fission gases are transferred by a helium stream to (F). In order to avoid losses due to leakage no excess pressure is allowed to build up in the apparatus;

v) after complete dissolution of the sample, the fission gases are forced through the washing bottles (G) ($KMnO_4$ solution, $NaHSO_3$-NaOH, $CaCl_2$, CuO furnace, $Mg(ClO_4)_2$ + natronasbestos furnace with titanium sponge) with helium into absorption tubes (H) which are then cooled by liquid nitrogen. The speed of dissolution is about 12 mg/min. cm^2;

vi) the sample is separated from helium by adsorption on molecular sieves. The Xe and Kr isotopes are determined by mass spectrometry;

vii) the sample solution is transferred into a weighing bottle and the weight W_2 of the solution determined;

viii) the undissolved ring of cladding from the fuel element is dried and the weight W_3 determined;

ix) an aliquot of solution is diluted to about 0.2 mg/g and the dilution factor determined.

The weight of the dissolved sample W is calculated: $W = W_1 - W_3$.
The concentration of sample solution C is: $C = W/W_2$.
The apparatus used is shown in Fig. 1.37.
At Ispra Laboratory the dissolution procedure /22/ was the following:

i) a cladded fuel cross section of about 10-11 g UO_2 is brought into the dissolution flask (C) containing 200 - 220 ml of a solution composed by 7M HNO_3 and 15 gr/l $Cs\,NO_3$;

ii) the solution is heated to boiling and maintained for about 1.5 h until complete dissolution of the UO_2;

iii) nitrous vapours developed during the reaction are partially absorbed in traps (A) and (B) containing about 150 ml of 2M Na_2SO_3 solution;

iv) after cooling by the (D) system an aliquot of solution is diluted 1 : 1 by volume (the weight is not calculated) with 7M HNO_3. This aliquot is used for all subsamples needed for the different analyses.

The dissolution apparatus located in a hot cell is shown schematically in Fig. I. 38. For each dissolved fuel pellet, three spiked and three unspiked aliquots were purified for subsequent mass spectrometry analyses. The third sample was held in reserve in case of any lack of agreement in the results from the mass spectrometry of the first two.

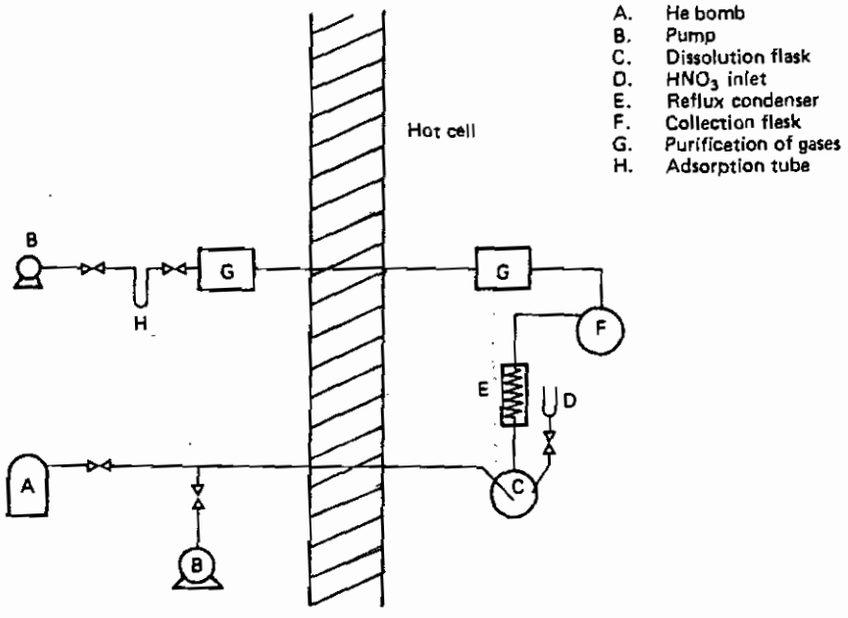

Fig. I.37. Apparatus for sample dissolution and fission gas collection used in Karlsruhe laboratory

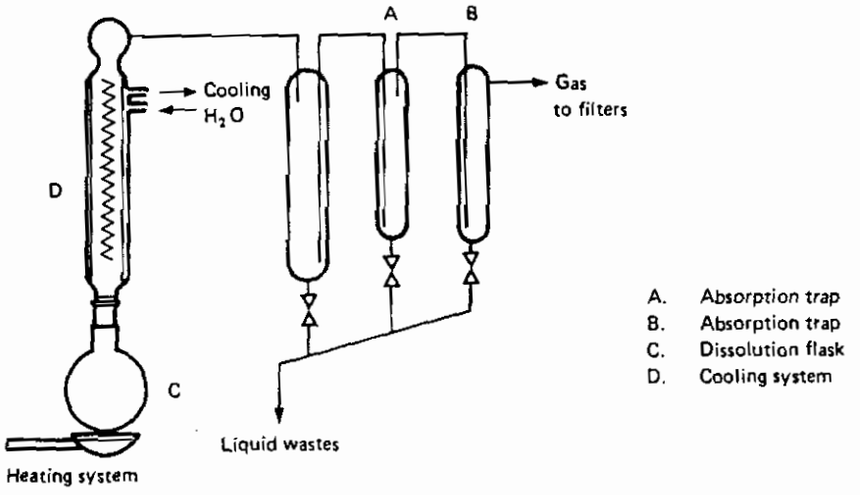

Fig. I.38. Apparatus for sample dissolution used in Ispra laboratory

Uranium and plutonium purification

Sample solutions both spiked by addition of ^{233}U and ^{242}Pu pure isotope and unspiked, were subjected to the radiochemical purification procedure shown in Fig. I. 39. Known aliquots of the diluted sample solution, containing about 10 µg U and 1 µg Pu and the spiking solution-if required - containing about 5 µg of ^{233}U and 0. 25 µg of ^{242}Pu, were mixed and evaporated to dryness in order to ensure the depolymerization of Pu and to allow the conditioning of the solution to 0. 5 M nitric acid. After addition of 0. 5 M nitric acid, the plutonium was reduced to the trivalent state by hydroxylamine hydrochloride at 80°C for 10 minutes and then oxidized to the tetravalent

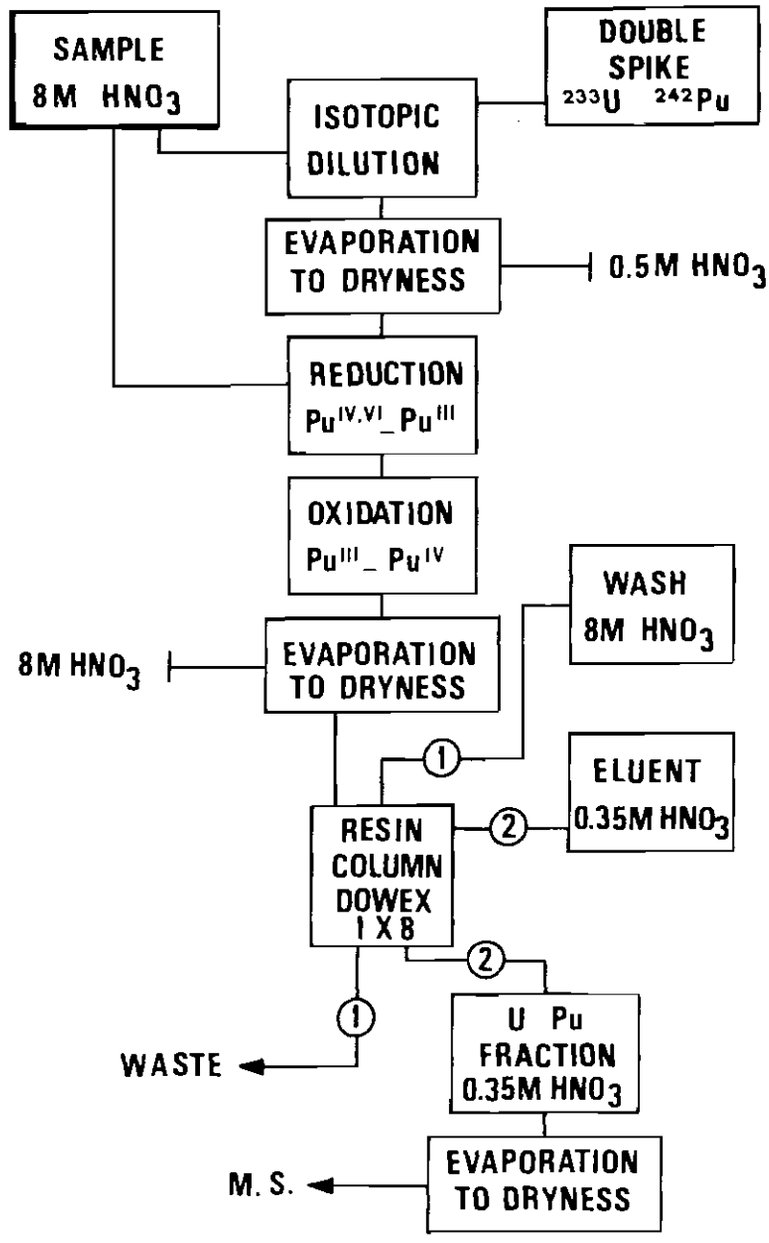

Fig. I.39. Uranium and plutonium purification scheme

state by sodium nitrite. This redox treatment was made in order to have Pu in an extractable form and to promote its isotopic exchange. The solution in 8M HNO_3 was then passed through a DOWEX-1 ion-exchange column (0.5 g, x8, 200-400 mesh). The first fraction containing fission products was discarded; most of the uranium was removed with 8M HNO_3 and a mixed uranium-plutonium fraction washed off with 0.35 M HNO_3. After drying, the residue was dissolved in 1 M HNO_3 for mass spectrometry.

Neodymium and americium purification

Spiked and unspiked sample solutions were subjected to the purification procedure shown in Fig. I.40:

. after the addition of ^{150}Nd and ^{243}Am spikes - if re-

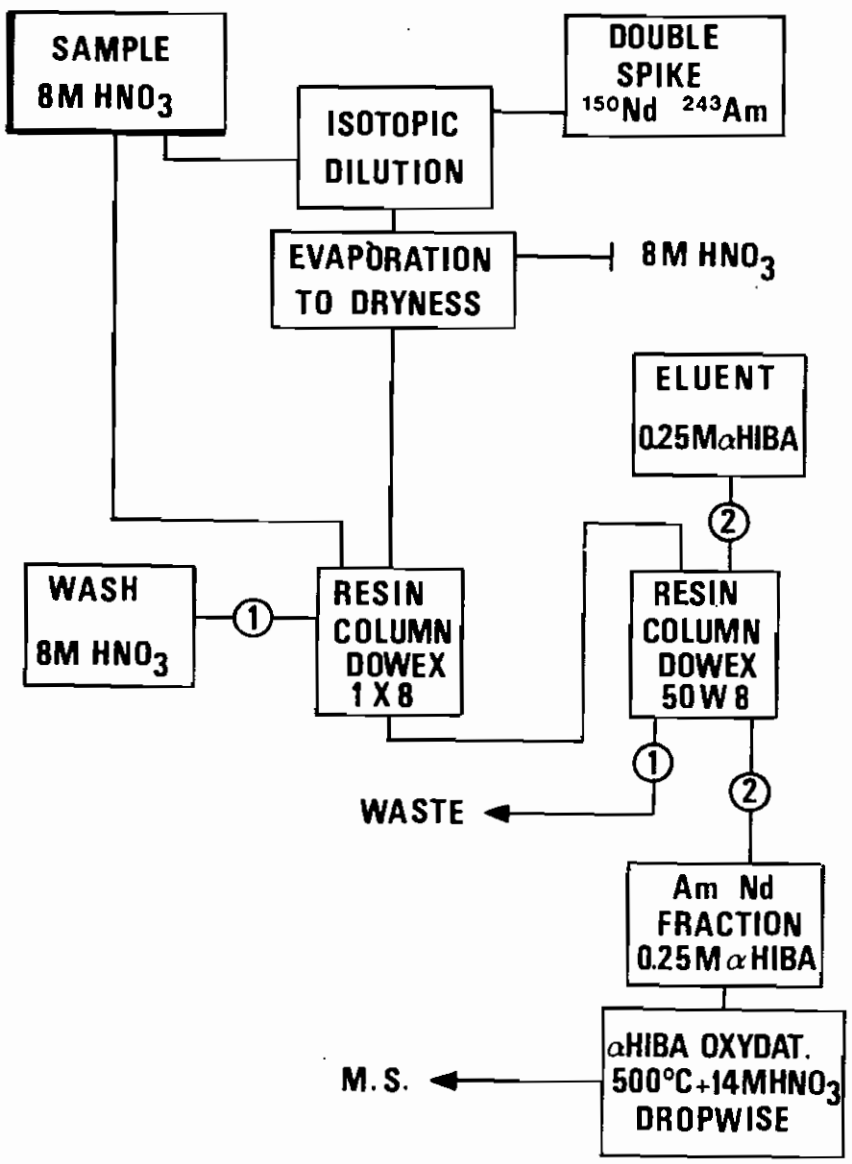

Fig. I.40. Neodynium and americium purification scheme

quired - the solutions were conditioned as for the uranium-plutonium purification and passed through a DOWEX-1 column in 8M HNO_3; the first fraction, containing both fission products and neodymium and americium, was collected and dried;

- the residue was dissolved in 0.05M HCl and the rare earths and americium absorbed on a DOWEX-50 cation column (0.3 g, x8, 200-400 mesh). After washing with 0.05M HCl, the neodymium was iluted with 0.05M α-isobutyric acid at pH 4.6;
- the elution was monitored by an alpha counter, by which means the fraction containing americium could be observed and kept and the next fraction, containing neodymium, could also be preserved;
- the Am and Nd fractions were evaporated in the presence of 14M HNO_3 to eliminate traces of organic material and the residue taken up in 1M HNO_3 for mass spectrometry.

2. Preparation and measurement of alpha-sources

Without any chemical treatment, aliquots of fuel solution were prepared for α-spectrometry according to the following procedures:

- ISPRA: samples containing about 0.01 mg of uranium were dropped onto tantalum counting plates and dried. The plates were then counted by means of a silicon semiconductor detector connected to a LABEN 70I minicomputer for data storage and processing. Recently /25, 26/ a 150 mm^2 surface barrier semiconductor detector with FWHM of 22 KeV at 5.5 MeV of ^{241}Am has been used connected to a SILENA System 27 processor;
- KARLSRUHE: samples of 6-10 μl were dried on stainless steel planchets and then heated to dull red heat to remove volatile salts and organic material. α-spectra were obtained by using a silicon semiconductor detector connected to a FRIESEKE & HOEPFNER multichannel analyser which in turn was connected to a PDP 11 computer for spectra pocessing.

Since the alpha decay energies partly overlap only the activity ratios were measured from the untreated solutions:

$$\frac{^{238}Pu + ^{241}Am}{^{239}Pu + ^{240}Pu}; \quad \frac{^{242}Cm}{^{239}Pu + ^{240}Pu}; \quad \frac{^{244}Cm}{^{239}Pu + ^{240}Pu}$$

Similar procedures were applied for aliquots of the purified solution taken up from the uranium-plutonium fraction in

which the activity ratios:

$$\frac{^{238}Pu}{^{239}Pu + ^{240}Pu}; \quad \frac{^{236}Pu}{^{239}Pu + ^{240}Pu}$$

were measured.

The alpha energies are given in Table I.23.

TABLE I.23. Alpha energies of Pu, Am and Cm isotopes

Isotope	Half-Life (years)	Alpha Energies (MeV)	Percentage Absolute Abundance
^{236}Pu	2.85	5.721 5.768	31 69
^{238}Pu	87.8	5.460 5.501	28 72
^{239}Pu	2.41×10^4	5.143 5.157	11 88
^{240}Pu	6.55×10^3	5.128 5.168	24 76
^{241}Am	432	5.440 5.499	13 85
^{242}Cm	0.466	6.066 6.110	26 74
^{244}Cm	18.11	5.759 5.801	23 77

The difficulty encountered in alpha spectrometry measurement involved mainly the background subtraction procedure. This aspect will not be dealt with in detail here, because several reports describe all the technical details of an inter-laboratory experiment for the evaluation of α-spectra /38, 39, 40, 41/. One of the main conclusions of this exercise was that the "effect of peak overlapping on the accuracy of evaluation is clearly confirmed by the range of the results from the different laboratories. This range decreases with decreasing ^{238}Pu content". However, at very low ^{238}Pu contents one

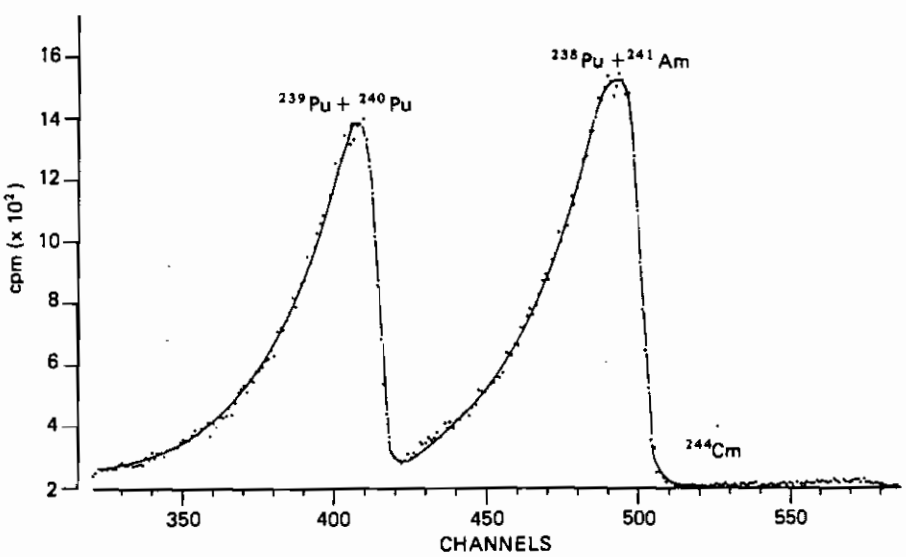

Fig. I.41. GARIGLIANO II

is obliged to prepare more concentrated solutions which results in a degraded spectrum.

Two typical spectra at low and high burnup are shown in Figs. I.41 and I.42, from samples of GARIGLIANO (8, 325 MWD/MTU) and OBRIGHEIM (27, 710 MWD/MTU), respectively.

These points will be raised again in Section II where the experimental uncertainties will be analysed.

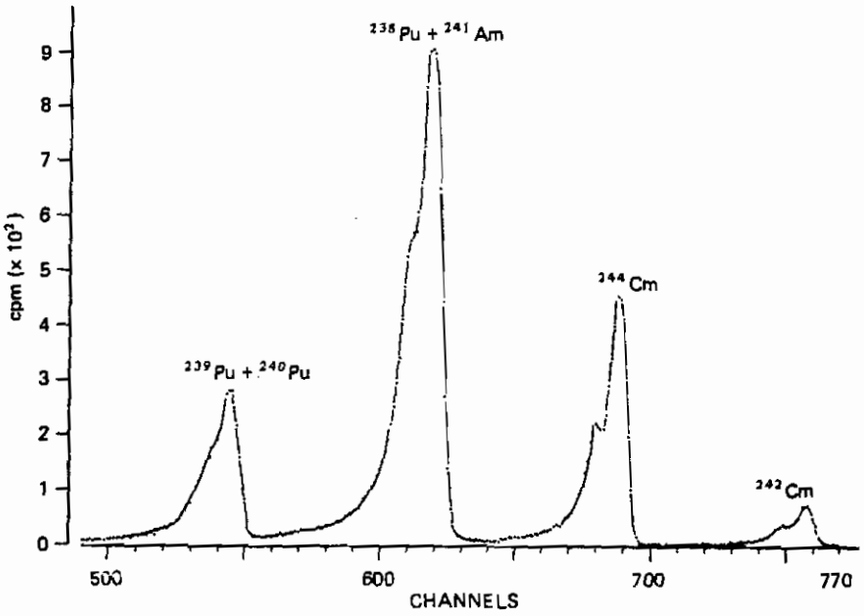

Fig. I.42. OBRIGHEIM

3. Gamma spectrometry

Gamma spectrometry measurements were carried out both on entire fuel pellets to determine ^{137}Cs activity and on aliquots of sufficiently diluted fuel solutions to determine the activities of ^{134}Cs, ^{137}Cs and ^{154}Eu.

For some reactor assemblies a few other fission product isotopes such as ^{106}Ru and ^{144}Ce were also measured. The aim of the non-destructive and/or destructive fission product measurements was the evaluation of the burnup of the fuel samples and the assessment of the isotopic correlation technique.

The isotopes and gamma lines selected for destructive measurements were those indicated in the following Table.

Isotope	Half-Life (years)	Gamma Energy (KeV)	Percentage Gamma Ray Absolute Abundance
^{134}Cs	2.05	795.8 + 802.0	94.1
^{137}Cs	30.1	661.6	86.4
^{154}Eu	8.6	1274.3	34.7
$^{106}Ru \xrightarrow{106} Rh$	1.007	511.9	20.5
$^{144}Ce \xrightarrow{144} Pr$	0.78	134.0 2185.8	0.73

Pellets:

Gamma measurements on fuel pellets were usually performed by the use of coaxial type Ge(Li) detectors, having a FWHM of about 2.6 KeV at the 1.33 MeV peak of ^{60}Co. Detectors were connected to the INTERTECHNIQUE Plurimat 20 processor. A typical gamma-ray spectrum obtained for a TRINO fuel pellet is given in Fig. I.43.

Due to the low intensity of the $^{144}Ce \rightarrow {}^{144}Pr$ peak at 2186 KeV, the use of a NaI(Tl) crystal was sometimes necessary.

The errors on the areas of the gamma peaks range from 1.5% to 2% for ^{137}Cs, 2.5% for ^{134}Cs and 3.0% for $^{106}Ru \rightarrow {}^{106}Rh$.

The ^{137}Cs activity values measured on the pellets, and reported at the end of the reactor operation have been converted to burnup by means of a calibration curve obtained using the burnup values derived from destructive ^{148}Nd determination (see ref. 22, 23, 24, 25, 26).

A deeper study was carried out for the TRINO VERCELLESE 509-049, 509-032 and 509-104 fuel assemblies.

For these assemblies, gross gamma scanning and metallographic examinations had indicated that there was no significant migration of fission products. Therefore the observed activity could be considered proportional to the concentration of the corresponding isotopes.

A statistical analysis was carried out to compare the values from the gamma scanning measurements with the values obtained by destructive tests. A direct comparison of the burnup determination with ^{137}Cs activity measurement was thus

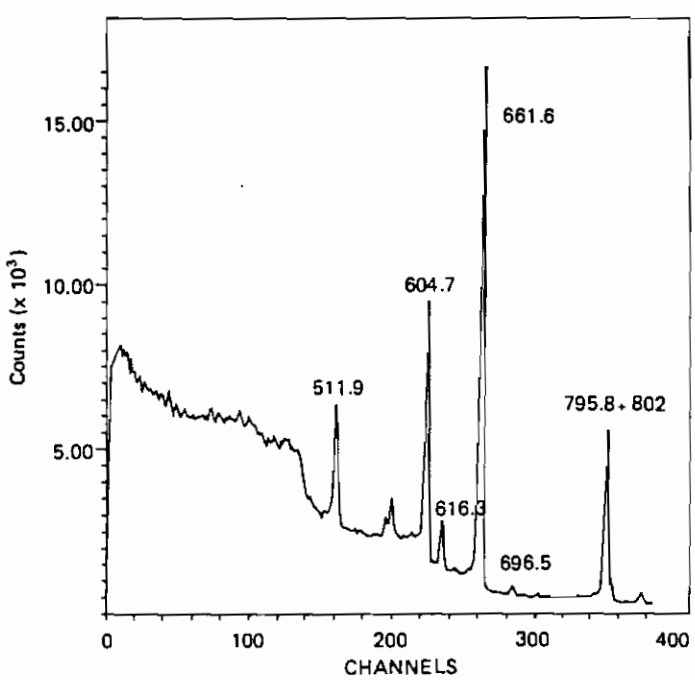

Fig. I.43. Ge(Li) gamma spectrum of fission products from a fuel pellet

possible. The results and the conclusion of this experiment can be found in detail in Ref. 22.

Solutions:

The measurements of gamma activities on fuel solutions were performed by the use of different coaxial type Ge(Li) detectors with FWHM ranging from 2.0 KeV to 3.5 KeV at 1.33 MeV of ^{60}Co.

Different multichannel analysers or processors were used such as a LABEN 2048 channel analyser, a LABEN 70 minicomputer and a SILENA System 27 for data acquisition and processing.

A typical gamma-ray spectrum obtained from a dissolved fuel sample from the TRINO reactor is shown in Fig. 1.44.

The absolute activity of the selected isotopes was determined by comparison with reference gamma sources supplied both by IAEA, Vienna, and the Radiochemical Center, Amersham.

From the uranium concentration determined in the solutions by isotopic dilution mass spectrometry it was possible to calculate the specific activity of the selected isotopes expressed in dis. $sec^{-1} g^{-1}$ final uranium.

Statistical errors evaluated in the determination of the specific activity of the five selected isotopes were 1.2% for $^{144}Ce \rightarrow {}^{144}Pr$, 1.4% for $^{106}Ru \rightarrow {}^{106}Pr$, 1.1% - 1.5% for ^{134}Cs, 1.5% - 1.6% for ^{137}Cs and 5.0% for ^{154}Eu.

The results obtained at the Ispra and Karlsruhe laboratories for the different reactor fuel sample solutions are presented in Tables I.24 to I.29.

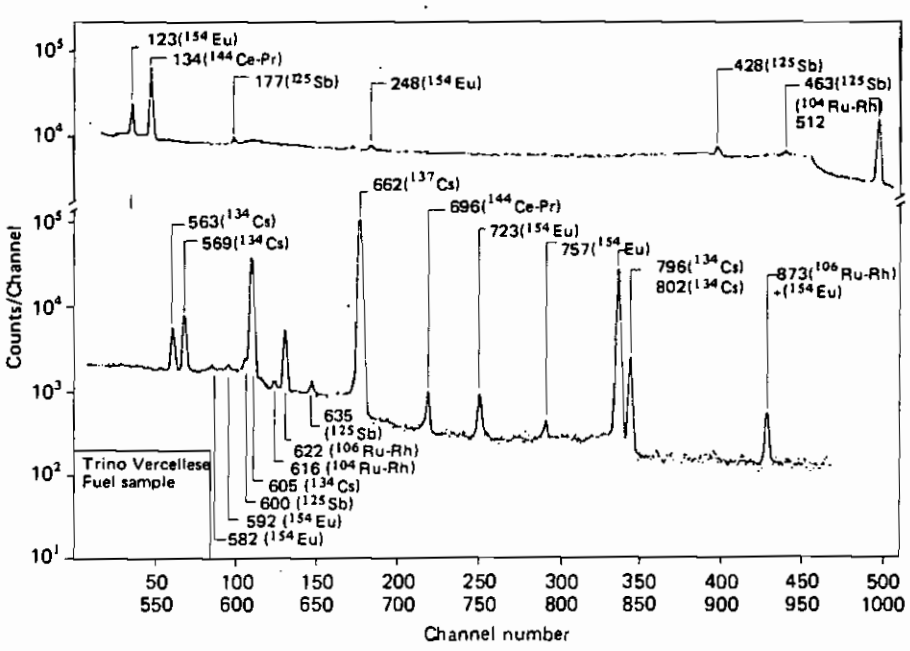

Fig. I.44. Gamma spectrum of fission products from a dissolved fuel sample

TABLE I.24. GARIGLIANO I: specific activity of the fuel sample solutions at the reactor shutdown (dps/g of final U)

Fuel Element	Sample	^{134}Cs ($\times 10^{-8}$)	^{137}Cs ($\times 10^{-9}$)	^{106}Ru ($\times 10^{-9}$)	^{144}Ce ($\times 10^{-10}$)
A-106 INITIAL ENRICHMENT 1.6 wt% 235U	A1	6.068	1.221	5.402	1.077
	9	12.691	1.588	7.511	1.269
	B1	6.919	1.11	4.662	1.006
	J1	7.585	1.487	6.167	1.269
	9	13.024	1.624	7.548	1.325
A-106 INITIAL ENRICHMENT 2.1 wt% 235U	A3	7.067	1.203	4.107	1.139
	5	7.77	1.243	4.403	1.095
	B2	6.882	1.158	3.848	1.051
	8	8.954	1.391	4.995	1.169
	C1	7.511	12.136	4.366	1.065
	3	6.031	1.043	3.774	0.962
	D2	6.346	1.080	3.774	0.969
	4	5.920	1.021	3.626	0.928
	E1	7.881	1.214	5.069	1.099
	5	6.068	1.021	3.552	0.906
	G7	7.215	1.169	4.514	1.058
	H2	8.806	1.328	4.810	1.132
	8	9.324	1.402	4.773	1.184

Measurements performed at Karlsruhe

TABLE I.25. GARIGLIANO II: specific activity of the fuel sample solution at the reactor shutdown (dps/g of final U)

Fuel Element	Sample	^{134}Cs ($\times 10^{-9}$)	^{137}Cs ($\times 10^{-9}$)
SA-13 INITIAL ENRICHMENT 2.41 wt% 235U	E6 1	1.513	0.449
	3	3.59	0.836
	5	5.346	1.042
	7	4.871	0.997
	10	5.131	1.121
	16	4.999	1.113
	13	3.695	0.92
	11	1.993	0.666

Measurements performed at Ispra

TABLE I.26. TRINO I; specific activity of the fuel sample solutions at the reactor shutdown (dps/g of final U)

Fuel Element	Sample	^{134}Cs ($\times 10^{-9}$)	^{137}Cs ($\times 10^{-9}$)	^{106}Ru ($\times 10^{-9}$)	^{144}Ce ($\times 10^{-10}$)
509-049 INITIAL ENRICHMENT 2.719 wt% 235U	L5 1	0.507	0.947	3.848	1.587
	4	1.580	1.732	8.214	2.475
	9	0.855	1.276	5.513	1.965
	J8 1	0.585	1.010	4.144	1.687
	4	1.698	1.798	8.769	2.549
	A1 1	0.610	1.080	4.514	1.794
	7	1.913	1.987	9.842	2.731
	9	1.062	1.450	6.549	2.257
509-032 INITIAL ENRICHMENT 3.13 wt% 235U	E11 1	0.455	0.899	3.119	1.621
	4	1.765	1.876	8.029	2.716
	7	1.868	1.912	8.584	2.660
	9	1.021	1.369	5.486	2.098
	H9 7	2.105	2.017	6.364	2.375
	9	1.128	1.491	6.364	2.375
	Q15 7	2.253	2.183	9.250	3.067
509-104 INITIAL ENRICHMENT 3.897 wt% 235U	M11 7	1.029	1.469	5.291	2.179
	M12 1	0.082	0.444	1.091	0.881
	7	0.031	0.895	2.342	1.428

TABLE I.27. TRINO II: specific activity of the fuel sample solutions at the reactor shutdown (dps/g of final U)

Fuel Element	Sample		Laboratory	^{134}Cs ($\times 10^{-9}$)	^{137}Cs ($\times 10^{-9}$)	^{154}Eu ($\times 10^{-8}$)
509-069 INITIAL ENRICHMENT 3.13 wt% ^{235}U	E5	4	Ispra	2.939	2.788	1.765
		7	Ispra	3.054	2.909	1.919
		7	Karlsruhe		2.909	
		9	Ispra	1.965	2.248	1.149
	L5	4	Ispra	2.939	2.821	1.768
		7	Ispra	3.005	2.862	1.849
	E11	1	Ispra	0.941	1.486	0.517
		2	Ispra	2.312	2.418	1.398
		2	Karlsruhe		2.495	
		4	Ispra	2.914	2.775	1.779
		4	Karlsruhe		2.821	
		5	Ispra	3.030	2.864	1.568
		7	Ispra	2.987	2.818	1.650
		7	Karlsruhe	2.987	2.955	
		8	Karlsruhe		2.797	
		9	Karlsruhe		2.355	
	L11	4	Karlsruhe		2.825	
		7	Ispra	3.048	2.881	1.718
		7	Karlsruhe		2.889	
	A1	1	Ispra	1.248	1.765	0.568
		7	Karlsruhe		3.261	
	J9	4	Ispra	3.132	2.927	1.686
		7	Karlsruhe		2.982	

TABLE I.28. OBRIGHEIM: specific activity of the fuel sample solutions at reactor shutdown. (dps/g of final U)

Fuel Element	Sample		^{134}Cs ($\times 10^{-9}$)	^{137}Cs ($\times 10^{-9}$)	^{154}Eu ($\times 10^{-8}$)
BE 124 INITIAL ENRICHMENT 3.00 wt% ^{235}U	D1	P2	4.287	3.308	1.916
		P3	6.512	4.097	2.652
	E3	P1	2.115	2.372	0.779
		P3	6.926	4.361	2.555
		P4	5.468	3.774	2.147
		P5	3.084	2.751	1.186
	G7	P1	1.714	2.053	0.547
		P2	3.749	3.041	1.653
		P3	5.940	3.871	2.481
		P4	4.752	3.356	1.999
	M14	P3	5.068	3.539	2.102
BE 210 INITIAL ENRICHMENT 2.83 wt% ^{235}U	G14	P3(1)	7.597	4.665	2.743
		P4(1)	6.842	4.376	2.609
		P5(1)	5.091	3.758	2.079
		P5(2)	3.244	2.968	1.338
	K14	P1	3.236	2.782	1.364
		P3(1)	7.353	4.438	2.909

Measurements performed at Ispra

TABLE I.29. GUNDREMMINGEN: specific activity of the fuel sample solutions at reactor shutdown (dps/g of final U).

Fuel Element	Sample	Laboratory	^{134}Cs ($\times 10^{-9}$)	^{137}Cs ($\times 10^{-9}$)	^{154}Eu ($\times 10^{-8}$)
B 23 INITIAL ENRICHMENT 2.53 wt% ^{235}U	A1 1	Ispra	3.49	3.66	1.79
	A1 2	Ispra	3.28	2.89	1.80
	B3	Ispra	2,57	2.61	1.55
		Karlsruhe		2.67	
	B4	Ispra	2.94	2.70	1.49
	C5	Karlsruhe		3.07	
	E3	Ispra	3.00	2.75	1.53
	E5	Ispra	3.25	3.08	1.61
		Karlsruhe		3.24	
C 16 INITIAL ENRICHMENT 2.53 wt% ^{235}U	A1 1	Ispra	2.26	2.55	0.89
	A1 2	Ispra	2.85	2.69	1.09
	B3	Ispra	1.45	1.83	0.75
		Karlsruhe		1.91	
	C5	Karlsruhe		2.20	
	E5	Ispra	1.63	1.92	0.84
		Karlsruhe		2.32	

4. Mass spectrometry

The instruments employed at Karlsruhe for the measurement of the isotopic ratios were CH-5 Varian MAT, mass spectrometers. One was equipped with an automatic sample changer and has already been described /21/, while the other was a standard model. The data were handled by an automatic system comprising a PDP-11 as data collector connected to an IBM-370 for data storage and for calculating results.

Uranium and plutonium were measured as metal ions using the two-filament technique. An amount containing as maximum 100 µg Pu as determined by α-counting was dried on the evaporation filament for the purpose of mass spectrometry.

Neodymium was measured as MeO^+ ion from a single filament on the CH-5 mass spectrometer. Corrections in this case were made for contributions due to ^{18}O and also from background neodymium which was estimated from the level of ^{142}Nd found. During the analysis checks were made for Sm and Ce which interfere in the Nd measurement.

The determination of Xe and Kr fission gas isotopic ratios was also carried out by means of a CH-4 type, Varian MAT mass spectrometer, at the Karlsruhe laboratory. As these results are not further treated for burnup and buildup eva-

luations, they are given in this chapter and presented in Tables I. 30 to I. 34 for the different reactor fuel samples analysed.

The average standard deviations of the measurements were the following:

$^{83}Kr/^{86}Kr$	0.3%	$^{131}Xe/^{134}Xe$	0.2%
$^{84}Kr/^{86}Kr$	0.2%	$^{132}Xe/^{134}Xe$	0.2%
$^{85}Kr/^{86}Kr$	0.3%	$^{136}Xe/^{134}Xe$	0.2%

At the Ispra laboratory a Varian MAT type CH-4 spectrometer with thermal ionisation double filament sources was used first. Then a Micromass VG 30 B mass spectrometer was used, equipped with thermal ionisation triple filament sources and connected to a PDP-8 computer for data treatment. The isotope composition and the concentration of americium was also determined in a few cases at Ispra by mass spectrometry.

The ^{233}U, ^{242}Pu, ^{150}Nd and ^{243}Am spikes were calibrated against NBS and CBNM Geel standards. The mass discrimination factors for these elements were determined for each machine also using NBS standards.

Further details of the methods employed are given in references 22, 23, 24, 36, 37.

TABLE I.30. GARIGLIANO I: Kr and Xe isotopic ratios

Fuel Element	Sample		Krypton			Xenon		
			83/86	84/86	85/86	131/134	132/134	136/134
A-106 INITIAL ENRICHMENT 1.6 wt% ^{235}U	A	1	0.263	0.576	0.118	0.354	0.668	1.431
		9	0.245	0.590	0.114	0.339	0.682	1.517
	B	1	0.269	0.592	0.116	0.351	0.665	1.423
	J	1	0.257	0.596	0.116	0.342	0.682	1.481
		9	0.248	0.597	0.118	0.337	0.686	1.538
A-106 INITIAL ENRICHMENT 2.1 wt% ^{235}U	A	3	0.263	0.567	0.115	0.349	0.650	1.371
		5						
	B	2	0.268	0.570	0.117	0.351	0.655	1.358
		8	0.256	0.571	0.114	0.343	0.661	1.413
	C	1	0.264	0.567	0.111	0.349	0.653	1.368
		3	0.271	0.569	0.119	0.349	0.652	1.304
	D	2	0.270	0.568	0.110	0.349	0.652	1.327
		4	0.270	0.565	0.118	0.349	0.679	1.294
	E	1	0.265	0.573	0.112	0.348	0.657	1.364
		5	0.263	0.568	0.115	0.346	0.655	1.367
	G	7	0.270	0.570	0.118	0.349	0.659	1.349
	H	22	0.260	0.568	0.114	0.342	0.661	1.398
		8	0.262	0.586	0.119	0.347	0.667	1.404

TABLE I.31. TRINO I: Kr and Xe isotopic ratios

Fuel Element	Sample	Krypton			Xenon		
		83/86	84/86	85/86	131/134	132/134	136/134
509-049 INITIAL ENRICHMENT 2.719% U-235	L5 1						
	4	0.257	0.564	0.095	0.328	0.662	1.406
	9	0.267	0.566	0.108	0.341	0.639	1.351
	J8 1						
	4						
	7	0.255	0.563	0.104	0.329	0.666	1.429
	9	0.261	0.556	0.106	0.342	0.639	1.366
	A1 1	0.267	0.548	0.108	0.352	0.617	1.295
	7	0.255	0.572	0.105	0.324	0.666	1.448
	9						
509-032 INITIAL ENRICHMENT 3.13 wt% U-235	E11 1						
	4						
	7						
	9						
	H9 4	0.255	0.565	0.106	0.325	0.666	1.403
	7						
	9						
	Q15 7						
509-104 INITIAL ENRICHMENT 3.897 wt% U-235	M11 7	0.266	0.552	0.105	0.339	0.633	1.280
	A12 1						
	7						

TABLE I.32. TRINO II: Kr and Xe isotopic ratios

Fuel Element	Sample	Krypton		Xenon		
		83/86	84/86	131/134	132/134	136/134
509-069 INITIAL ENRICHMENT 3.13 wt % U-235	E5 4					
	7	0.246	0.588	0.296	0.700	1.411
	9					
	L5 4					
	7					
	E11 1					
	2	0.252	0.578	0.311	0.694	1.362
	4	0.259	0.595	0.306	0.709	1.392
	5					
	7	0.246	0.588	0.300	0.709	1.399
	8	0.248	0.586	0.305	0.708	1.383
	9	0.253	0.575	0.319	0.684	1.340
	L11 4	0.248	0.588	0.300	0.707	1.388
	7	0.246	0.587	0.301	0.711	1.396
	A1 1					
	7	0.237	0.593	0.293	0.718	1.440
	J9 4					
	7	0.244	0.591	0.300	0.713	1.406

TABLE I.33. OBRIGHEIM: Kr and Xe isotopic ratios

Fuel Element	Sample		Krypton			Xenon		
			83/86	84/86	85/86	131/134	132/134	136/134
INITIAL ENRICHMENT 3.00 wt % U-235	D1	P1	0.134	0.305	0.055	0.335	0.685	1.412
		P2						
		P3						
	E3	P1						
		P2	0.233	0.613	0.100	0.306	0.734	1.520
		P3						
		P4	0.231	0.611	0.105	0.296	0.625	1.518
		P5						
	G7	P1	0.255	0.573	0.104	0.333	0.656	1.400
		P2						
		P3	0.229	0.613	0.104	0.294	0.757	1.534
		P4						
		P5	0.245	0.602	0.107	0.304	0.723	1.487
	M14	P1	0.257	0.567	0.106	0.339	0.649	1.375
		P3						
		P4	0.241	0.594	0.105	0.303	0.700	1.491
INITIAL ENRICHMENT 2.83 wt % U-235	G14	P3(1)	0.212	0.631	0.104	0.275	0.761	1.585
		P4(1)						
		P5(1)						
		P5(2)						
	K14	P1						
		P3(1)						
		P4(1)	0.241	0.594	0.105	0.303	0.700	1.491

TABLE I.34. GUNDREMMINGEN: Kr and Xe isotopic ratios

Fuel Element	Sample		Krypton			Xenon		
			83/86	84/86	85/86	131/134	132/134	136/134
B 23 INITIAL ENRICHMENT 2.53 wt % U-235	A1	1						
		2						
	B	3	0.245	0.589	0.107	0.303	0.698	1.424
		4						
	C	5	0.239	0.594	0.106	0.306	0.714	1.443
	E	3						
		5	0.258	0.681	0.121	0.294	0.711	1.510
C 16 INITIAL ENRICHMENT 2.53 wt % U-235	A1	1						
		2						
	B	3	0.256	0.571	0.111	0.335	0.675	1.363
	C	5	0.254	0.573	0.111	0.327	0.666	1.404
	E	5	0.249	0.581	0.112	0.328	0.675	1.450

Isotopic dilution analysis

The isotopic dilution technique was used for the mass spectrometric analysis in order to determine the isotopic concentration. This technique is briefly described below.
Let A be the isotope, the quantity of which has to be determined, and I the known quantity of the spike isotope which

has been added to the sample to be analysed. After separation of the element from the sample (the separation yield need not be known), the isotopic ratio A/I is measured. The quantity of isotope A = $\frac{A}{I}$ I.

Frequently, however, the sample already contains some amount of I_p of the spike isotope and it may be that some A_i of the isotope A to be determined is already in the spike. Therefore the isotopic ratio R in the sample ($A/I_p = R_p$) and in the indicator ($A_i/1 = R_i$) has to be determined.

The mixture of the spike solution and the sample consequently contains the quantity of the spike isotope $I_m = I_p + I$ and the quantity of the isotope to be determined $A_m = A_i + A$.

The isotopic ratio in the mixture, $R_m = A_m/I_m$ follows from considerations of R_p and R_i.

$$R_m = \frac{A + I\,R_i}{A/R_p + I} \qquad A = I\,\frac{R_m - R_i}{1 - R_m/R_p}$$

This means that also in this case only isotopic ratios have to be determined:

A more general relationship among isotopic ratios of sample spike and mixed solutions has been suggested by R.K. Webster /42/ for the calculation of the concentration of one element in the sample solution. This relationship takes into consideration all isotope ratios of that element determined by mass spectrometry in the sample, spike and mixture solutions. The concentration C_R of the element is given by:

$$C_R = \frac{W_S}{W_R}\,C_S\,\frac{R'_R - R_M}{R_M R_S - 1}\cdot\frac{\sum_{i=1}^{n} M_i R_i}{\sum_{i=1}^{n} M_i R'_i}$$

where:

W_S weight of spike solution

W_R weight of sample solution

C_S concentration of spike isotope (y) in the spike solution

R'_R, R_M, R_S isotope abundance ratio $R(\frac{x}{y})$, measured in spike, mixed and sample solutions respectively

$\sum_{i=1}^{n} M_i R_i$, $\sum_{i=1}^{n} M_i R'_i$ sum of isotopic ratios measured in the sample and the spike solutions. (M_i atomic weights of the isotopes)

In most isotopic analyses only the isotopic concentration of the most abundant single isotope is determined. The concentration of the other isotopes in the sample follows from the corresponding isotopic ratio.

Mass spectrometry measurements of heavy isotopes in general lead to the determination of the following isotopic ratios:

. for U unspiked solutions:

$^{234}U/^{238}U$, $^{235}U/^{238}U$, $^{236}U/^{238}U$

. for Pu unspiked solutions:

$^{240}Pu/^{239}Pu$, $^{241}Pu/^{239}Pu$, $^{242}Pu/^{239}Pu$

. for Nd unspiked solutions:

$^{142}Nd/^{148}Nd$, $^{143}Nd/^{148}Nd$, $^{144}Nd/^{148}Nd$,
$^{145}Nd/^{148}Nd$, $^{146}Nd/^{148}Nd$, $^{150}Nd/^{148}Nd$

. for Am unspiked solutions:

$^{242}Am/^{241}Am$, $^{243}Am/^{241}Am$

In the spiked solutions used for the concentration determination by isotope dilution, the following isotopic ratios are measured:

$^{238}U/^{233}U$, $^{239}Pu/^{242}Pu$, $^{148}Nd/^{150}Nd$ and $^{241}Am/^{243}Am$.

The raw data were then used to calculate the buildup and the burnup both from ^{148}Nd and from ^{137}Cs.
In order to derive the buildup and depletion of different isotopes, each heavy isotope N_i was related to the total heavy isotopes ΣN_i^o before irradiation, i.e. to all initial uranium atoms, using the following equation:

$$\frac{N_i}{\Sigma N_i^o} = \frac{R_i}{\Sigma R_i + \Sigma \Delta} \qquad /1/$$

with:

R_i = the ratio of each isotope in atoms, to the post-irradiation atoms of ^{238}U (i = ^{235}U, ^{236}U, ^{238}U, ^{238}Pu, ^{239}Pu, ^{240}Pu, ^{241}Pu, ^{242}Pu, ^{241}Am, ^{242}Am, ^{243}Am, ^{242}Cm, ^{244}Cm)

$\Sigma \Delta$ = the ratio of fissioned nuclides in atoms to the post-irradiation atoms of ^{238}U, obtained from ^{148}Nd or ^{137}Cs analyses, i.e.

atoms $\frac{^{148}Nd}{^{238}U} / Y \ (^{148}Nd)$ or

atoms $\frac{^{137}Cs}{^{238}U} / Y \ (^{137}Cs)$

The burnup (B) is first derived in terms of percentage of fissioned atoms referred to the initial heavy atoms, F_T, which is given by the following relationship:

$$F_T = \frac{R/Y}{\Sigma R_i + R/Y} \qquad /2/$$

with:

R = the ratio between ^{148}Nd or ^{137}Cs atoms (formed during the irradiation) and ^{238}U atoms present at the end of the irradiation

Y = the average fission yield of ^{148}Nd or ^{137}Cs

ΣR_i = the sum of the ratio of all uranium, plutonium, americium and curium atoms to the ^{238}U atoms at the end of the irradiation.

Before applying equation /2/ it was necessary to introduce some corrections to take into account:

a) the ^{148}Nd burn out by neutron capture

b) the ^{148}Nd buildup by $^{147}Nd\ (n,\gamma)\ ^{148}Nd$ reaction

c) the ^{137}Cs decay during the irradiation.

The correction factor for a) was given by the following equation:

$$C_1 = 1 + 0.012 \times D_{25}$$

where:

0.012 is the ratio $\sigma_a\ ^{148}Nd/\sigma_a\ ^{235}U$

$D_{25} = \frac{W_o - W}{W_o}$ W_o and W being the initial and final uranium enrichments

The correction factor for b) was derived from a work by Maeck et al. /43/ in which the activation cross-section of ^{147}Nd is evaluated as

$$\sigma_c^{147} = 440 \pm 150\ b$$

The correction factors applied are a function of the different burnup levels of the samples and of the different neutron fluxes in the reactor.

The correction factor for c) was given by the equation:

$$C_3 = \frac{\lambda(137Cs) \cdot \sum_{i=1}^{n} T_i}{\sum_{i=1}^{n} (1 - e^{-\lambda(137Cs) \cdot T_i}) \cdot e^{-\lambda(^{137}Cs)t_i}}$$

where:

T_i represents the time of irradiation for any i-th period

t_i represents the time of decay from any i-th period to the end of the irradiation

The correction factors introduced in the calculation of burn-up are given in the following Table:

Correction Factors	Reactors			
	Garigliano	Trino Vercellese	Obrigheim	Gundremmingen
a)	1.006 – 1.008		1.005 – 1.010	
b)	1.010 – 1.020		1.010 – 1.015	
c)	I° Cycle 1.036 II° Cycle 1.022	I° Cycle 1.0286 II° Cycle 1.083	B23 1.041 C16 1.035	BE124 1.041 BE210 1.033

a) ^{148}Nd burn out by neutron capture

b) ^{148}Nd buildup by $^{147}Nd\ (n, \gamma)\ ^{148}Nd$ reaction

c) ^{137}Cs decay during irradiation

II. Characterization of the Data

1. General Remarks

As already said in the introduction, the main scope of the Bench Mark activity was to provide a set of data of wide application to different fields, but with the characteristic of being highly qualified data. For this reason the greatest effort in all campaigns has been put into the discussion and elaboration of the data. Great attention was paid to the identification and reduction of random and systematic errors, to the recalculation of the data by means of burn-up codes and to checking the data with ICT. One particular activity concerned the setting up of an inverse code (THEORY), which, starting from experimental details, can evaluate cross-section ratios by means of data fitting.
The topics in this chapter will be:

1) evaluation of typical overall errors;
2) description and use of the inverse code THEORY;
3) ICT;
4) comparison with calculated values.

All these checks, together with the traceability given to the data by the diffusion of irradiation characteristics, should qualify the data for the aims and the purposes of a wide range of users.

2. Discussion of Uncertainties

The problem of determining the measurement uncertainty presents different aspects: first one must evaluate the uncertainties in the raw data from all possible sources. Then it is necessary to evaluate the contribution of these uncertainties to elaborated data (buildup, burnup, etc.) determining the overall precision of the measurements. And finally the possible bias of the elaborated data should be investigated by having a paired analysis of couples of results in parallel with other laboratories. The logical scheme followed in the analysis of the experimental error to encompass the above requirements is shown in Fig. II.1, where four steps are considered and indicated by A through D. In fact, the evaluation of the typical uncertainty connected with the determination of burnup and buildup of heavy elements in spent LWR fuel assemblies is quite complex since it involves several laboratories and various treatments. So the first aim of the analysis (step A in Fig. II.1) was to identify and evaluate any possible error sources already existing before the analytical measurements.

Step B deals with actual analytical measurement uncertainties (α, γ and mass-spectrometry).

Step C consists in a combination of the above uncertainties to give the final global error.

Step D concerns the interlaboratory comparison, through a paired analysis of couples of pellets cut at the same nominal position in the rod and analysed in parallel by the two JRC laboratories of Ispra and Karlsruhe.

In addition the functional dependence of uncertainties upon the burnup level has been investigated, determining the error values for 4 different burnups.

Before going into detail on the assessment of the uncertainties, a remark should be made: throughout this chapter the

errors and discrepancies are generally quoted as percentages with two decimal figures. This frequently makes poor physical sense, but has been adopted for two reasons:

- first, because most of the figures derive from mathematical treatment (e.g. curve fitting);
- second, because in certain cases a rounding to one decimal figure would have led to an error or a discrepancy of zero which has even less physical sense.

So for reasons of homogeneity, two decimal figures are given for all values presented.

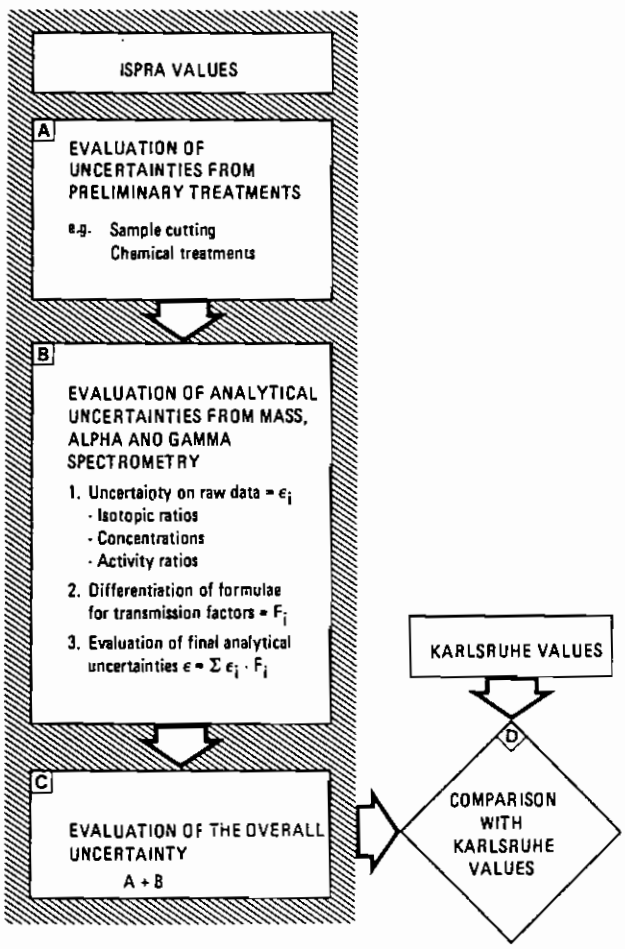

Fig. II.1. Scheme adopted for evaluation of the uncertainties

1. Step A: Evaluation of uncertainties from preliminary treatments

The possible error sources before the measurements were identified in sample cutting and chemical treatment.

Uncertainties in sample cutting

The uncertainty in the cutting position has been evaluated to $\pm$ 2 mm (standard deviation) which corresponds to about 0.5% in the burnup value (the burnup variation is around 0.3% mm^{-1} in the upper and lower fuel sections). Similar error levels are estimated for U and Pu axial distribution. More difficult is the evaluation of the uncertainty introduced by the loss of fuel material during the cutting (a non-homogeneous loss in the radial sense could alter the Pu/U ratio due to the radial complex Pu formation distribution). Qualitative and quantitative methods (optical and photographic inspections and weighing) were normally applied to minimize losses, but the possibility of small uncontrolled losses remains.

An approximate evaluation of the uncertainty deriving from the material loss from the pellets has been carried out starting from reasonable conservative hypotheses.

First, the assumption has been made of a loss of 5% of material in the pellet, a loss which has been concentrated subsequently in five concentric regions of the rod (see Fig. II.2). The Pu/U distribution has been evaluated by means of the LASER burnup code /44/ in the cell geometry of TRINO VERCELLESE PWR for a burnup of 30 GWD/MTU and is shown in Fig. II.3. The parameter Pu/U has been chosen

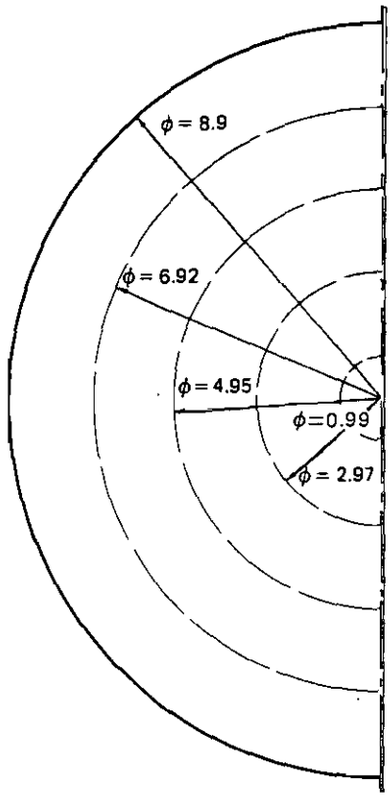

Fig. II.2. LASER TRINO II: Schematic representation of the rod (dimensions are in mm)

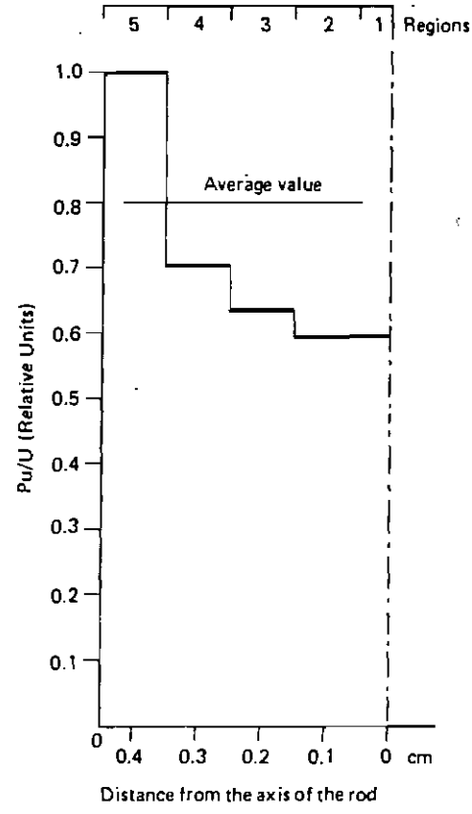

Fig. II.3. LASER TRINO II: Relative spatial distribution of Pu/U mass ratio in the asymptotic rod

as being more sensitive than others to the concentrated loss of material. The burnup is certainly much less sensitive, since it is evaluated from ^{137}Cs or from ^{148}Nd, which, being fission products, are distributed quite flatly in the pin. The effect of 5% material loss concentrated in the different regions (with regard to the unperturbed situation) was of the order of $\pm$ 1.5%.

Then we assumed that an uncertainty of about 0.7% (standard deviation) on Pu/U should be a reasonable estimate for a casual loss of 5% owing to the fact that a concentrated loss in the outer or inner zone of the pellet has a low probability of occurrence and can be easily detected.

Care must be taken, however, with the cutting of pellets since a loss greater than 5% would lead to an error able to modify substantially the overall quoted uncertainty.

A second exercise was performed assuming a concentrated loss of 2.5% which would be more likely to occur and would be more difficult to detect. It would also have the effect of modifying the results by about 0.7%.

An average uncertainty of 0.5% was then evaluated as the most probable value to be transmitted to the final results, (see Tables II.9, II.10, II.11) as a consequence of a maximum loss of 2.5% not completely concentrated in the outer or innermost regions.

Uncertainties in chemical treatment

The high quality of the methods used and the care taken with their application together ensure that the chemical treatment leads only to negligible errors. Such phenomena as physico-chemical modification of the samples (e.g. ageing) were avoided. Because the possible uncertainties introduced by chemical treatment were of a relative nature, they had low transfer factors on the final results.

2. Step B: Evaluation of analytical uncertainties from mass alpha- and gamma- spectrometry

This paragraph deals with the accurate error analysis performed in the various laboratories involved in the measurements, for an assessment of analytical uncertainty.

Uncertainty on raw data

The first point (B.1 in Fig. II.1) consisted in the evaluation of the uncertainties in the raw and measured data. We have

grouped the raw data into three categories: isotopic ratios, element concentrations and fission yields.

The uncertainty as to the isotopic ratios has been evaluated by fitting experimental errors quoted in the various measurement campaigns. These errors were given in terms of instrumental reproducibility combined with repetitive analysis on the same pellet. This procedure is described in Figs. II. 4 - II. 7, in which typical fittings of experimental errors are illustrated. Figure II. 4 gives the fitting vs burnup of the declared JRC errors for most mass spectrometric measurements of the isotopic ratio $^{235}U/^{238}U$. The points are representative of all the JRC analytical campaigns. Each point represents the error in the measured parameter, as deduced from repetitive measurements of the same filament and frequently from 3–4 different filaments of the same sample (single pellet solution). It thus represents a total variability within one laboratory, not a pellet to pellet (sample to sample) variability.

The increase in uncertainty regarding $^{235}U/^{238}U$ with burnup is coherent with the decrease of the signal (^{235}U content). Figure II. 5 gives the corresponding fit of the declared uncertainties on the isotopic ratio $^{242}Pu/^{239}Pu$.

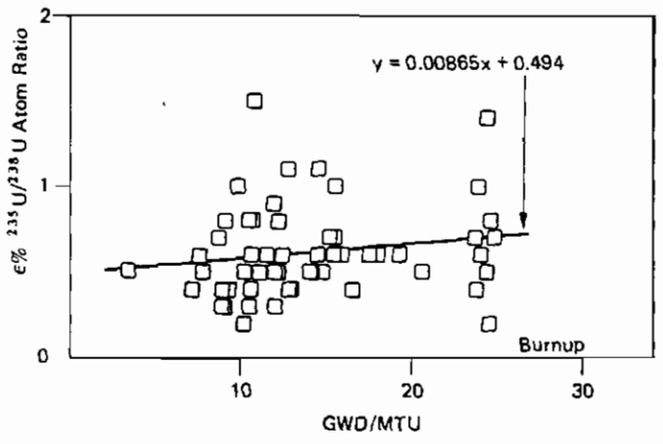

Fig. II.4. Linear fitting of the $^{235}U/^{238}U$ errors against burnup

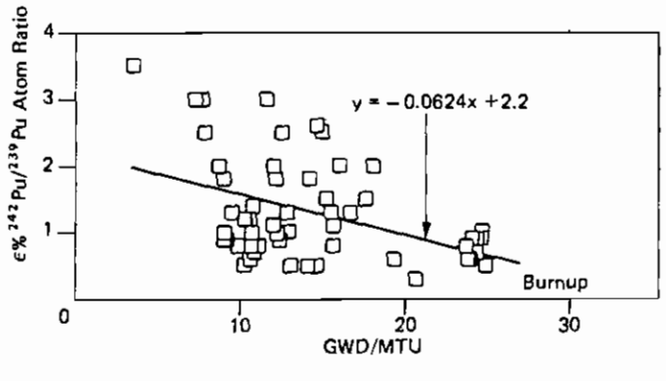

Fig. II.5. Linear fitting of the $^{242}Pu/^{239}Pu$ errors against burnup

The fit correctly decreases with burnup, due to the signal increase of ^{242}Pu isotope. For the α activity ratios the situation is slightly different as can be seen from Figs. II. 6 and II. 7. In fact, the errors do not in practice decrease with the burnup and this is due to the opposing influences of the two factors affecting the measurements already pointed out in section 1. 6. At low burnup the weak signal makes highly concentrated sources necessary, with

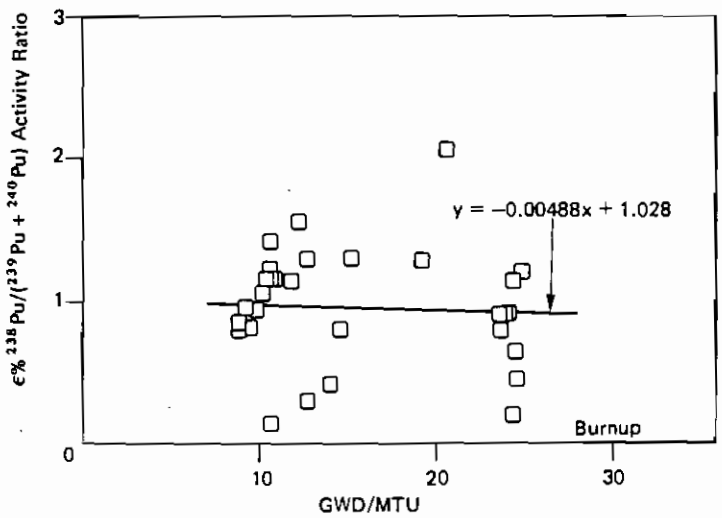

Fig. II.6. Linear fitting of the $^{238}Pu/(^{239}Pu + ^{240}Pu)$ errors against burnup

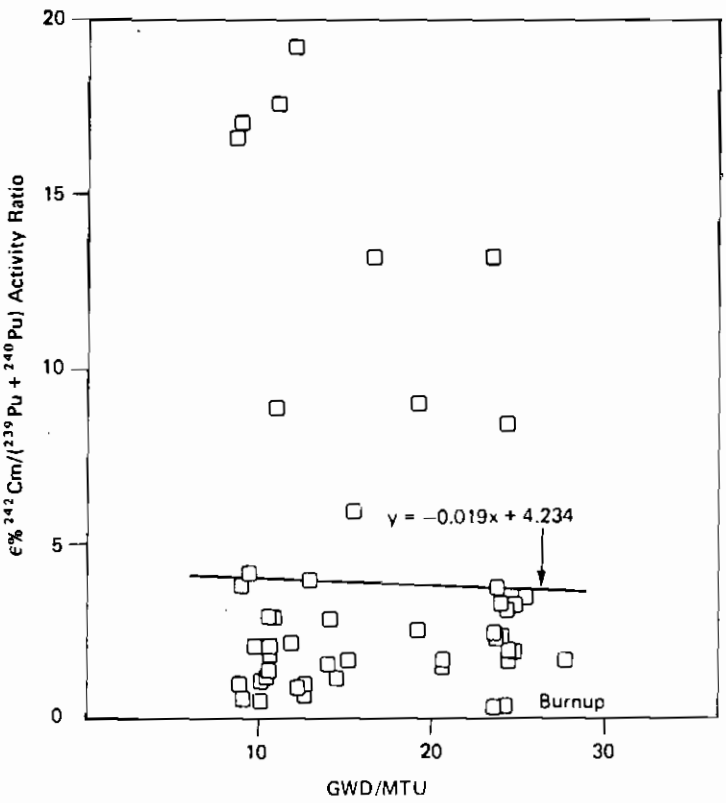

Fig. II.7. Linear fitting of the $^{242}Cm/(^{239}Pu + ^{240}Pu)$ errors against burnup

the consequent degrading of the spectrum. At high burnup, mainly for ^{238}Pu, peak tail corrections become important and systematic error components due to the background subtraction procedure, can have a very strong influence on the overall uncertainty /38/.

The error on raw data of the two ratios has been considered constant also in view of the large spread of experimental error data points (see Figs. II. 6 and II. 7). This point will be taken up again when the systematic error is discussed.

The evaluated uncertainties for the raw parameters: "isotopic ratios and alpha activity ratios", are given in Table II. 1 at four different burnup levels.

It is perhaps worthwhile mentioning now the fact that the above procedure, followed for the assessment of raw data uncertainties vs burnup, is not completely rigorous for various reasons: firstly, the dispersion of the points is sometimes extensive and the fitting with a straight line can become problematic; secondly, the buildup of nuclides or their percent content is not a straight line (see section II. 5) so their error dependence should also at a first order approximation be represented by higher curves.

Finally, in certain cases, (α measurement for instance) the error dependence is complex, having different functional dependence on burnup at different burnup levels. So it cannot be described by only one analytical expression in the whole burnup range.

It is thus evident that a straight line is only roughly representative of the more complex curves which should be employed.

TABLE II.1. Evaluated percentage uncertainties for measured raw parameters

Parameter	Burnup (MWD/MTU)			
	7694	10932	19039	24637
$^{235}U/^{238}U$	056	0.59	0.66	0.71
$^{236}U/^{238}U$	1.64	1.57	1.38	1.24
$^{240}Pu/^{239}Pu$	0.41	0.42	0.45	0.48
$^{241}Pu/^{239}Pu$	0.65	0.64	0.60	0.58
$^{242}Pu/^{239}Pu$	1.70	1.52	1.01	0.67
$^{242}Cm/(^{239}Pu + ^{240}Pu)$	4.00	4.00	4.00	4.00
$^{244}Cm/(^{239}Pu + ^{240}Pu)$	8.51	7.43	4.47	2.42
$(^{238}Pu + ^{241}Am)/(^{239}Pu + ^{240}Pu)$	0.81	1.02	1.58	1.97
$^{238}Pu/(^{239}Pu + ^{240}Pu)$	1.00	1.00	1.00	1.00
Pu concentration	0.65	0.65	0.65	0.65
U concentration	0.58	0.58	0.58	0.58
Nd concentration	0.60	0.60	0.60	0.60
$^{148}Nd/^{238}U$	1.00	1.00	1.00	1.00
initial ^{235}U wt%	0.60	0.60	0.60	0.60
fission yield (^{148}Nd)	1.00	1.00	1.00	1.00

To a first approximation, however, we have considered this model as sufficiently adequate to describe the error variation.

In Table II.1 the error values for the concentration of Pu, U and Nd are also given. The above uncertainty values have been evaluated by differentiating the Webster formula which is repeated here for completeness.

$$C_R = \frac{W_S}{W_R} C_S \frac{R'_R - R_M}{R_M R_S - 1} \cdot \frac{\sum_{i=1}^{n} M_i R_i}{\sum_{i=1}^{n} M_i R'_i}$$

The meaning of the symbols and the errors evaluated for the different parameters are shown in Table II.2.

The results of the analysis of uncertainties on the measurement of Pu, U and Nd concentration (Table II.1) showed that the error values were practically constant with the burnup. This was due to the fact that the dominant uncertainties are represented by the declared error on spike concentration (C_S) and by the error on the measured isotope abundance ratio (R_M) which were constant with the burnup.

For completeness in Table II.1 are also presented the uncertainty values assigned to the ratio $^{148}Nd/^{238}U$, to the initial ^{235}U enrichment and to the fission yield of ^{148}Nd /45/.

Differentiation of formulae for transmission factors and evaluation of final analytical uncertainty

The error source having now been identified and assessed, the various uncertainties of raw data have to be inserted in the formulae leading to the burnup and buildup values.

TABLE II.2. Percentage errors evaluated for the Webster's formula parameters

Symbol	Significance	ε % Pu	ε % U	ε % Nd
W_S	Weight of the spike solution	0.05	0.05	0.05
W_R	Weight of the sample solution	0.05	0.05	0.05
C_S	Spike concentration	0.28	0.30	0.28
R'_R	Isotope ratio in the spike solution	0.17	0.10	0.09
R_M	Isotope ratio in the mixture solution	0.30	0.30	0.30
R_S	Isotope ratio in the sample solution	0.10	0.02	0.08
$\Sigma M_i R_i$	Sum of the isotopic ratios in the sample solution	0.17	0.15	0.08
$\Sigma M_i R'_i$	Sum of the isotopic ratios in the spike solution	0.12	0.15	0.06
C_R	Concentration of the element in the solution	0.65	0.58	0.60

With this aim the relationships giving the different final parameters have been differentiated (3.2 in Fig. II.1) expressing the overall relative uncertainties as a function of the uncertainty of the original parameters and their transmission factor (B.3 in Fig. II.1). Supposing a parameter P function of various original raw data R_j

$$P = f(R_j)$$

The general form of the overall evaluated analytical uncertainty was the following:

$$\epsilon_p^2 = \sum_{j=1}^{n} \left(F_j \cdot \frac{dR_j}{R_j}\right)^2 = \sum_{j=1}^{n} (F_j \cdot \epsilon_j)^2$$

with:

j = index for different original raw data R (mass spectrometry, isotope ratios, activity ratios, etc.)

$\frac{dR_j}{R_j} = \epsilon_j$ = relative uncertainty evaluated for the individual parameters

F_j = transmission factors of the uncertainty

Some typical examples are given in the following paragraphs of how the analytical uncertainty on some parameters has been evaluated at different burnups starting from the errors on the raw data just shown in Table II.1.

It must be pointed out for the sake of clarity that the formulae for ϵ^2 reported in Tables II.3 to II.6 are, as previously mentioned, simplified expressions for easier understanding. In

TABLE II.3. Evaluation of the analytical uncertainty on the burnup. (Percentage of fissioned atoms referred to the initial heavy atoms)

$$\text{Burnup } (F_T\,\%) = \frac{\frac{^{148}Nd}{^{238}U}\,\frac{1}{Y}}{\sum_{i=1}^{n} r_i + \frac{^{148}Nd}{^{238}U}\,\frac{1}{Y}}$$

Schematic equation:

$$F_T = \frac{A\,\frac{1}{Y}}{S + A\,\frac{1}{Y}}$$

Percentage error:

$$\epsilon^2 = \left\{F(A)\frac{dA}{A}\right\}^2 + \left\{F(Y)\frac{dY}{Y}\right\}^2 + \left\{F(S)\frac{dS}{S}\right\}^2$$

Error transmission factors against burnup (MWD/MTU) and experimental uncertainties on F_T

BURNUP MWD/MTU	F (A)	$\frac{dA}{A}$	F (Y)	$\frac{dY}{Y}$	F (S)	$\frac{dS}{S}$	Total ϵ %
7694	1.01	1.00	1.01	1.00	0.99	0.014	1.41
10932	1.01	1.00	1.01	1.00	0.99	0.013	1.41
19039	1.02	1.00	1.02	1.00	0.98	0.013	1.42
24637	1.03	1.00	1.03	1.00	0.97	0.013	1.43

the error calculations, however, the complete expressions were used. This also explains why the errors in the simple parameter (dA/A, dB/B, etc.) do not always correspond to the uncertainty reported in Table II. 1. In fact they are not necessarily the same parameters, but frequently A, B, etc. are a combination of different raw (measured) data.
In Table II. 3 the evaluation of the analytical uncertainty on the burnup is derived from the following simplified expression:

$$\epsilon^2 = \{F(A)\frac{dA}{A}\}^2 + \{F(Y)\frac{dY}{Y}\}^2 + \{F(S)\frac{dS}{S}\}^2$$

which was deduced from the more complete derivation of the analytical expression for the burnup:

$\frac{dA}{A}$ is the relative uncertainty linked with $\frac{^{148}Nd}{^{238}U}$ atom ratio

$\frac{dY}{Y}$ is the relative uncertainty linked with ^{148}Nd fission yield

$\frac{dS}{S}$ is the relative uncertainty linked with $\sum_{i=1}^{n} r_i \ (r_i = \frac{^{i}Isotope}{^{238}U})$

The above error values are given in Table II.3 for different burnups. The analytical expressions of the corresponding transmission factors are also given and their absolute values quoted for different burnups.
It is obvious how the uncertainty on the measure of $\frac{^{148}Nd}{^{238}U}$ ratio and on the fission yield have the same "weight" on the final error. It is consequently unreasonable to improve the precision of the measurement of concentrations before having a more precise determination of the fission yield.
The burnup dependence of the burnup analytical uncertainty is very weak (Fig. II. 8) and is essentially due to a small increase in the transmission factors. The uncertainty can be considered constant around 1.4%.

A second example is the uncertainty in the determination of ^{236}U buildup. The error expression is again split into two terms (Table II. 4) but it is evident that the only significant contribution comes from the determination of the $^{236}U/^{238}U$ ratio in the sample.
The burnup dependence of the ^{236}U content is more marked (see Fig. II. 9) due simply to the increasing signal-to-background ratio (^{236}U content).

The third example concerns an important parameter, i.e. ^{235}U depletion. The analytical expression from raw data

is given in Table II.5 together with the simplified derivation of the analytical error expressed in three terms, which are linked respectively to a knowledge of:

W5 = the initial enrichment in ^{235}U (weight%)

U5 = the measured final $^{235}U/^{238}U$ ratio

Z = a correction factor for heavy isotope burnout

The original error dW5/W5 was considered constant at 0.6% (the initial enrichment was measured by the shipper: we adopted the typical mass spectrometry error value), while the error dU5/U5 (derived by fitting experimental points as previously outlined) slowly increased with the burnup, following the decreasing signal from ^{235}U (Fig.II.4). Nevertheless the marked decrease of the transmission factors of both dW5/W5 and dU5/U5 determine the trend

TABLE II.4 Evaluation of the analytical uncertainty of the ^{236}U buildup. (Atoms % of initial heavy atoms)

$$^{236}U \text{ buildup} = \frac{^{236}U}{^{238}U} \frac{100}{\sum_{i=1}^{n} r_i + \frac{^{148}Nd}{^{238}U} \frac{1}{Y}}$$

Schematic equation:

$$^{236}U_B = U6 \cdot Z$$

Percentage error:

$$\epsilon^2 = \left\{F(U6)\frac{dU6}{U6}\right\}^2 + \left\{F(Z)\frac{dZ}{Z}\right\}^2$$

Error transmission factors against burnup (MWD/MTU) and experimental uncertainties on ^{236}U buildup

BURNUP MWD/MTU	F (U6)	$\frac{dU6}{U6}$	F (Z)	$\frac{dZ}{Z}$	Total ϵ %
7694	1.00	1.64	1.00	0.018	1.64
10932	1.00	1.57	1.00	0.021	1.57
19039	1.00	1.38	1.00	0.031	1.38
24637	1.00	1.24	1.00	0.038	1.24

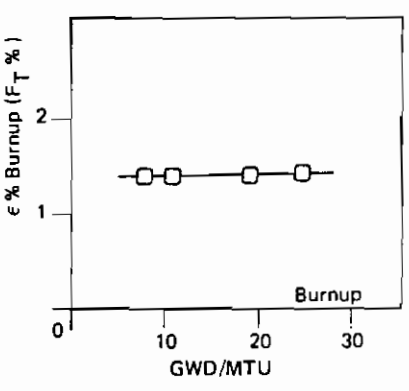

Fig. II.8. Burnup percentage uncertainty against burnup

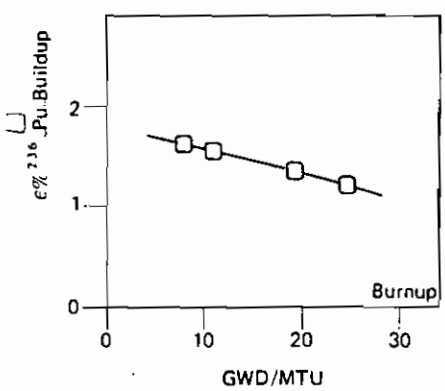

Fig. II.9. ^{236}U buildup percentage uncertainty against burnup

TABLE II.5. Evaluation of the analytical uncertainty of the ^{235}U depletion. (Atoms % of initial heavy atoms)

$$^{235}U\ \text{depletion} = \frac{238.051 \cdot (\text{wt\% } ^{235}U)_{INIT}}{0.03007 \cdot (\text{wt\% } ^{235}U)_{INIT} + 235.044} - \frac{^{235}U}{^{238}U} \frac{100}{\sum_{i=1}^{n} r_i + \frac{^{148}Nd}{^{238}U} \frac{1}{Y}}$$

Schematic equation:

$$^{235}U_D = \frac{K_1 \cdot W_5}{K_2 \cdot W_5 + K_3} - U5 \cdot Z$$

Percentage error:

$$\epsilon^2 = \left\{ F(W5) \frac{dW5}{W5} \right\}^2 + \left\{ F(U5) \frac{dU5}{U5} \right\}^2 + \left\{ F(Z) \frac{dZ}{Z} \right\}^2$$

Error transmission factors against burnup (MWD/MTU) and experimental uncertainties on ^{235}U depletion

BURNUP MWD/MTU	F (W5)	$\frac{dW5}{W5}$	F (U5)	$\frac{dU5}{U5}$	F (Z)	$\frac{dZ}{Z}$	Total ϵ %
7694	3.42	0.6	2.42	0.56	2.42	0.018	2.46
10932	2.57	0.6	1.57	0.59	1.57	0.021	1.80
19039	1.83	0.6	0.83	0.66	0.83	0.031	1.23
24637	1.57	0.6	0.57	0.71	0.57	0.038	1.03

of the analytical uncertainty on ^{235}U depletion showed in Fig. II.10. The error on Z does not play any role in the overall uncertainty buildup.

Next example is the buildup of ^{239}Pu.

The uncertainty on ^{239}Pu buildup is presented in Table II.6. The overall error in ^{239}Pu buildup is practically dominated by the error on concentration ratio

$$\frac{[Pu]_{CONC}}{[U]_{CONC}}$$

as shown in Table II.6.

The burnup dependence of ^{239}Pu buildup error is practically zero, as shown in Fig. II.11.

The example presented in Fig. II.12 concerns the error propagation in the Pu/U which is one of the most important parameters in the ICT (see section II.4).

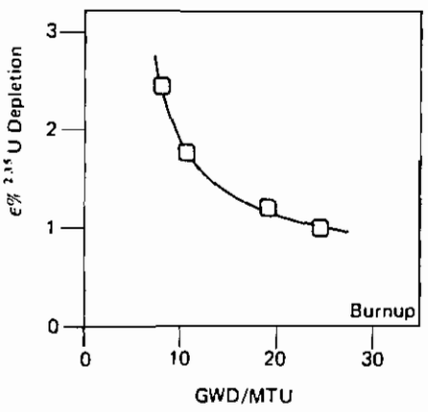

Fig. II.10. ^{235}U depletion percentage uncertainty against burnup

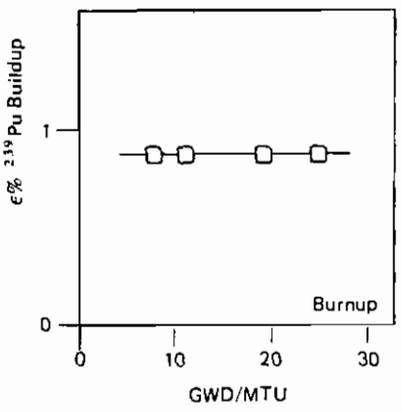

Fig. II.11. ^{239}Pu buildup percentage uncertainty against burnup

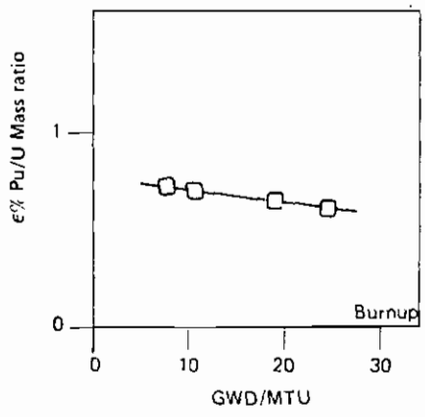

Fig. II.12. Pu/U mass ratio percentage uncertainty against burnup

The analytical expression leading to Pu/U is presented in extended and schematic form in Table II. 7 and an analysis of the transmission of the error shows that the uncertainty on the buildup of ^{239}Pu (Q9 term in the equation) plays a fundamental role, especially in the low burnup range.

TABLE II.6. Evaluation of the analytical uncertainty of the ^{239}Pu buildup. (Atoms % of initial heavy atoms).

$$^{239}Pu \text{ buildup} = \frac{[Pu]_{CONC}}{[U]_{CONC}} \frac{^{239}Pu}{^{238}U} \frac{100}{\sum_{i=1}^{n} r_i + \frac{^{148}Nd}{^{238}U} \frac{1}{Y}}$$

Schematic equation:

$$^{239}P_B = \frac{P}{U} \cdot \frac{P9}{U8} \cdot Z$$

Percentage error:

$$\epsilon^2 = \left\{ F(P) \frac{dP}{P} \right\}^2 + \left\{ F(U) \frac{dU}{U} \right\}^2 + \left\{ F(P9) \frac{dP9}{P9} \right\}^2 + \left\{ F(U8) \frac{dU8}{U8} \right\}^2 + \left\{ F(Z) \frac{dZ}{Z} \right\}^2$$

Error transmission factors against burnup (MWD/MTU) and experimental uncertainties on ^{239}Pu buildup

BURNUP MWD/MTU	F (P)	$\frac{dP}{P}$	F (U)	$\frac{dU}{U}$	F (P9)	$\frac{dP9}{P9}$	F (U8)	$\frac{dU8}{U8}$	F (Z)	$\frac{dZ}{Z}$	Total ϵ %
7694	1.00	0.65	1.00	0.58	1.00	0.07	1.00	0.01	1.00	0.018	0.87
10932	1.00	0.65	1.00	0.58	1.00	0.08	1.00	0.08	1.00	0.021	0.88
19039	1.00	0.65	1.00	0.58	1.00	0.10	1.00	0.10	1.00	0.031	0.88
24637	1.00	0.65	1.00	0.58	1.00	0.11	1.00	0.11	1.00	0.038	0.88

TABLE II.7. Evaluation of the analytical uncertainty of the Pu/U mass ratio.

$$\frac{Pu}{U} \text{ mass ratio} = \frac{\frac{[Pu]_{CONC}}{[U]_{CONC}} \frac{^{238}Pu + ^{239}Pu + ^{240}Pu + ^{241}Pu + ^{242}Pu}{^{238}U} \frac{100}{\sum_{i=1}^{n} r_i + \frac{^{148}Nd}{^{238}U} \frac{1}{Y}}}{1000 - \frac{238.051 \cdot (wt\%\ ^{235}U)_{INIT}}{0.03007 \cdot (wt\%\ ^{235}U)_{INIT} + 235.044} - \frac{100}{\sum_{i=1}^{n} r_i + \frac{^{148}Nd}{^{238}U} \frac{1}{Y}} \left(\frac{^{235}U}{^{238}U} - \frac{^{236}U}{^{238}U} + 1 \right)}$$

Schematic equation:

$$\frac{Pu}{U} = \frac{\frac{P}{U} \frac{P8 + P9 + P0 + P1 + P2}{U8} Z}{K_0 - \frac{K_1 \cdot W_5}{K_2 \cdot W_5 + K_3} - Z \left(\frac{U5}{U8} - \frac{U6}{U8} + 1 \right)} = \frac{Q8 + Q9 + Q0 + Q1 + Q2}{S_1}$$

The transmission factors of the errors of the S_1 elements are negligible, then not considered in the percentage error relationship

Percentage error:

$$\epsilon^2 = \left\{ F(Q8) \frac{dQ8}{Q8} \right\}^2 + \left\{ F(Q9) \frac{dQ9}{Q9} \right\}^2 + \left\{ F(Q0) \frac{dQ0}{Q0} \right\}^2 + \left\{ F(Q1) \frac{dQ1}{Q1} \right\}^2 + \left\{ F(Q2) \frac{dQ2}{Q2} \right\}^2$$

Error transmission factors against burnup (MWD/MTU) and experimental uncertainties on Pu/U mass ratio

BURNUP MWD/MTU	F (Q8)	$\frac{dQ8}{Q8}$	F (Q9)	$\frac{dQ9}{Q9}$	F (Q0)	$\frac{dQ0}{Q0}$	F (Q1)	$\frac{dQ1}{Q1}$	F (Q2)	$\frac{dQ2}{Q2}$	Total ϵ %
7694	0.0016	1.75	0.817	0.87	0.120	0.96	0.057	1.20	0.003	1.91	0.73
10932	0.0028	1.83	0.759	0.88	0.145	0.97	0.085	1.19	0.007	1.75	0.69
19039	0.0084	2.01	0.677	0.88	0.177	0.98	0.121	1.14	0.017	1.33	0.64
24637	0.0127	1.99	0.630	0.88	0.191	0.99	0.142	1.15	0.024	1.10	0.61

The ^{240}Pu uncertainty contributes a little more at higher burnup while the uncertainties on ^{241}Pu and ^{242}Pu play a negligible role.
Also other parameters (such as ^{235}U depletion, ^{238}Pu buildup, etc.) which are considered in the complete expression of Pu/U have no influence on the final error.

In Fig. II.13 the experimental uncertainty on ^{238}U depletion is shown. A marked decrease with the burnup is evidenced.

Two examples of transmission of uncertainty in α-spectrometry measurements are reported now: in Table II.8 the error propagation from raw α-measurements to ^{238}Pu buildup is shown. The first step gives the contribution to the uncertainty of net activity ratio $^{238}Pu/(^{239}Pu + ^{240}Pu)$ due to the subtraction of ^{238}Pu formed from ^{242}Cm decay. The uncertainty in this term $\epsilon(Co)$ is of the order of 4.0% on average (Table (i)) but its transmission factor F(Co) on the net activity ratio A_N becomes significant only at high burnup, as shown in Table (ii). In fact, the highest weight in the uncertainty on A_N (net activity ratio) comes from the measured ratio A_M.
In the following step the ^{238}Pu percentage atoms are calculated from the net activity ratio as shown in Table (iii) with various contributions to the error from activity ratio, decay constanty /3/, etc.

The last step in Table (iv) shows how the errors on the ^{238}Pu buildup are evaluated by showing up the contribution to the uncertainty coming from P8, U8 and the two concentration measurement errors. The burnup dependence is shown in Fig. II.14.

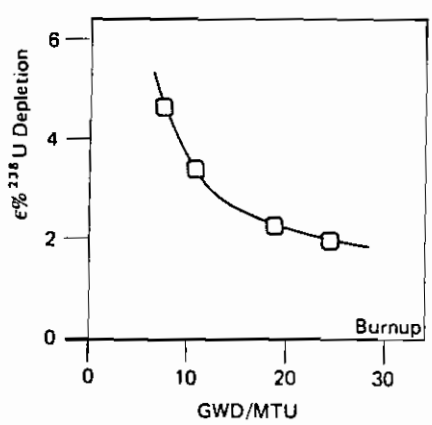

Fig. II.13. ^{238}U depletion percentage uncertainty against burnup

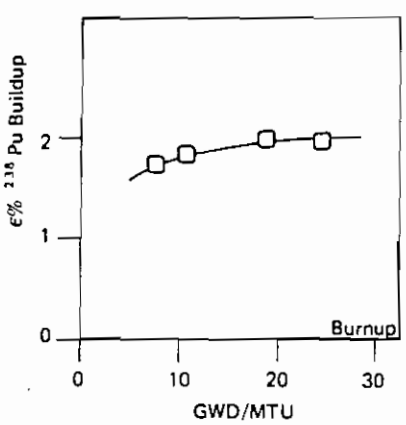

Fig. II.14. ^{238}Pu buildup percentage uncertainty against burnup

TABLE II.8. Evaluation of the analytical uncertainty of the ^{238}Pu buildup. (Atoms % of initial heavy atoms).

$$^{238}Pu\ \text{buildup} = \frac{\left[Pu\right]_{CONC}}{\left[U\right]_{CONC}} \frac{^{238}Pu}{^{238}U} \frac{100}{\sum_{i=1}^{n} r_i + \frac{^{148}Nd}{^{238}U} \frac{1}{Y}}$$

Schematic equation:

$$^{238}P_8 = \frac{P}{U} \frac{P8}{U8} Z \qquad [1]$$

Since ^{238}Pu is measured by α-spectrometry, as activity ratio $\frac{^{238}Pu}{^{239}Pu + ^{240}Pu}$, the ^{238}Pu percentage atoms at shut down time are given by:

$$^{238}Pu = \left[\frac{^{238}Pu}{^{239}Pu + ^{240}Pu}\right]_{NET} \frac{^{239}Pu \cdot \lambda g + ^{240}Pu \cdot \lambda o}{\lambda_8} e^{\lambda_8 \cdot t}$$

Schematic equation:

$$P8 = A_N \frac{P9 + L9 + P0 + L0}{L8} e^{L8 \cdot t} \qquad [2]$$

The net $\frac{^{238}Pu}{^{239}Pu + ^{240}Pu}$ activity ratio is given by:

$$A_N = \left[\frac{^{238}Pu}{^{239}Pu + ^{240}Pu}\right]_{NET} = \left[\frac{^{238}Pu}{^{239}Pu + ^{240}Pu}\right]_{MEAS} - \left[\frac{^{242}Cm}{^{239}Pu + ^{240}Pu}\right]_{MEAS} \cdot \frac{\lambda_8}{\lambda_2} e^{\lambda_2 \cdot t}$$

$\lambda_8, \lambda_9, \lambda_0, \lambda_2$ are the decay constants of ^{238}Pu, ^{239}Pu, ^{240}Pu and ^{242}Cm

Schematic equation:

$$A_N = A_M - C_O \qquad [3]$$

$$\text{where} = C_O = C_M \cdot \frac{L8}{L2} \cdot e^{L2 \cdot t} \qquad [4]$$

Percentage error on C_O (equation 4):

$$\epsilon^2 (C_O) = \left\{F (C_M) \frac{dC_M}{C_M}\right\}^2 + \left\{F (L2) \frac{dL2}{L2}\right\}^2 + \left\{F (L8) \frac{dL8}{L8}\right\}^2$$

Table (i)
Error transmission factors against burnup (MWD/MTU) and experimental uncertainties on C_O

BURNUP MWD/MTU	$F (C_M)$	$\frac{dC_M}{C_M}$	F (L2)	$\frac{dL2}{L2}$	F (L8)	$\frac{dL8}{L8}$	$\epsilon\% (C_O)$
7694	1.00	4.00	7.00	0.06	1.00	0.9	4.12
10932	1.00	4.00	7.00	0.06	1.00	0.9	4.12
19039	1.00	4.00	6.25	0.06	1.00	0.9	4.11
24637	1.00	4.00	6.81	0.06	1.00	0.9	4.12

Percentage error on A_N (equation 3):

$$\epsilon^2 (A_N) = \left\{F (A_M) \frac{dA_M}{A_M}\right\}^2 + \left\{F (C_O) \frac{dC_O}{C_O}\right\}^2$$

Table (ii)
Error transmissions factors against burnup (MWD/MTU) and experimental uncertainties on A_N

BURNUP MWD/MTU	$F (A_M)$	$\frac{dA_M}{A_M}$	$F (C_O)$	$\frac{dC_O}{C_O}$	$\epsilon\% (A_N)$
7694	1.08	1.00	0.08	4.12	1.12
10932	1.13	1.00	0.13	4.12	1.22
19039	1.22	1.00	0.22	4.12	1 46
24637	1.22	1.00	0.22	4.12	1 48

Table II.8. Evaluation of the analytical uncertainty of the ^{238}Pu buildup. (Atoms % of initial heavy atoms). (Cont'd.)

Percentage error on P8 (equation 2):

$$\epsilon^2 (P8) = \left\{ F(A_N)\frac{dA_N}{A_N} \right\}^2 + \left\{ F(P9)\frac{dP9}{P9} \right\}^2 + \left\{ F(L9)\frac{dL9}{L9} \right\}^2 + \left\{ F(P0)\frac{dP0}{P0} \right\}^2 + \left\{ F(L0)\frac{dL0}{L0} \right\}^2 + \left\{ F(L8)\frac{dL8}{L8} \right\}^2$$

Table (iii)
Error transmission factors against burnup (MWD/MTU) and experimental uncertaities on P8

BURNUP MWD/MTU	$F(A_N)$	$\frac{dA_N}{A_N}$	F (P9)	$\frac{dP9}{P9}$	F (L9)	$\frac{dL9}{L9}$	F (P0)	$\frac{dP0}{P0}$	F (L0)	$\frac{dL0}{L0}$	F (L8)	$\frac{dL8}{L8}$	ϵ % (P8)
7694	1.00	1.12	0.65	0.07	0.65	0.4	0.35	0.41	0.35	1 10	1.00	0.9	1.52
10932	1.00	1.22	0.58	0.08	0.58	0.4	0.41	0.42	0.41	1.10	1.00	0.9	1.61
19039	1.00	1.46	0.51	0.10	0.51	0.4	0.49	0.45	0.49	1.10	1.00	0.9	1.81
24637	1.00	1.43	0.47	0.12	0.47	0.4	0.53	0.48	0.53	1.10	1.00	0.9	1.79

Percentage error on $^{238}P_B$ (equation 1):

$$\epsilon^2 = \left\{ F(P)\frac{dP}{P} \right\}^2 + \left\{ F(U)\frac{dU}{U} \right\}^2 + \left\{ F(P8)\frac{dP8}{P8} \right\}^2 + \left\{ F(U8)\frac{dU8}{U8} \right\}^2 + \left\{ F(Z)\frac{dZ}{Z} \right\}^2$$

Table (iv)
Error transmission factors against burnup (MWD/MTU) and experimental uncertainties on ^{238}Pu buildup

BURNUP MWD/MTU	F (P)	$\frac{dP}{P}$	F (U)	$\frac{dU}{U}$	F (P8)	$\frac{dP8}{P8}$	F (U8)	$\frac{dU8}{U8}$	F (Z)	$\frac{dZ}{Z}$	Total ϵ %
7694	1.00	0.65	1.00	0.58	1.00	1.52	1.00	0.01	1.00	0.01B	1.75
10932	1.00	0.65	1.00	0.58	1.00	1.61	1.00	0.01	1.00	0.021	1.83
19039	1.00	0.65	1.00	0.58	1.00	1.81	1.00	0.01	1.00	0.031	2.01
24637	1.00	0.65	1.00	0.58	1.00	1.79	1.00	0.01	1.00	0.038	1.99

Note that considering the large spread of values in Figs. II. 6 and II. 7 the uncertainty on raw data has been considered as constant with the burnup, both for ^{238}Pu and ^{242}Cm.

The second example for the error propagation in α-spectrometry measurements is given in Table II. 9 and concerns the ^{242}Cm buildup, from the measured activity ratio $C_M = {}^{242}Cm/({}^{239}Pu + {}^{240}Pu)$ which gives the highest contribution to the total error. Figure II. 15 gives the burnup dependence of the error on ^{242}Cm buildup.

TABLE II.9. Evaluation of the analytical uncertainty of the ^{242}Cm buildup (Atoms % of initial heavy atoms).

$$^{242}Cm \text{ buildup} = \frac{\left[Pu\right]_{CONC}}{\left[U\right]_{CONC}} \frac{^{242}Cm}{^{238}U} \frac{100}{\sum_{i=1}^{n} r_i + \frac{^{148}Nd}{^{238}U}\frac{1}{Y}}$$

Schematic equation:

$$^{242}C_B = \frac{P}{U}\frac{C2}{U8} Z \qquad [1]$$

Since ^{242}Cm is measured by α spectrometry, as activity ratio $\frac{^{242}Cm}{^{239}Pu + ^{240}Pu}$, the ^{242}Cm percentage atoms at shut down time are given by:

$$^{242}Cm = \frac{^{242}Cm}{^{239}Pu + ^{240}Pu} \cdot \frac{^{239}Pu \cdot \lambda_9 + ^{240}Pu \cdot \lambda_0}{\lambda_2} \cdot e^{\lambda_2 \cdot t}$$

Schematic equation:

$$C2 = C_M \cdot \frac{P9 \cdot L9 + P0 \cdot L0}{L2} \cdot e^{L2 \cdot t} \qquad [2]$$

λ_9, λ_0 and λ_2 are the decay constants of ^{239}Pu, ^{240}Pu and ^{242}Cm

Table II.9. Evaluation of the analytical uncertainty of the ^{242}Cm buildup (Atom % of initial heavy atoms). (Cont'd.)

Percentage error on C2 (equation 2):

$$\epsilon^2(C2) = \left\{F(C_M)\frac{dC_M}{C_M}\right\}^2 + \left\{F(P9)\frac{dP9}{P9}\right\}^2 + \left\{F(L9)\frac{dL9}{L9}\right\}^2 + \left\{F(P0)\frac{dP0}{P0}\right\}^2 + \left\{F(L0)\frac{dL0}{L0}\right\}^2 + \left\{F(L2)\frac{dL2}{L2}\right\}^2$$

Error transmission factors against burnup (MWD/MTU) and experimental uncertainties on C2

BURNUP MWD/MTU	F (C_M)	$\frac{dC_M}{C_M}$	F (P9)	$\frac{dP9}{P9}$	F (L9)	$\frac{dL9}{L9}$	F (P0)	$\frac{dP0}{P0}$	F (L0)	$\frac{dL0}{L0}$	F (L2)	$\frac{dL2}{L2}$	ϵ % (C9)
7694	1.00	4.00	1.35	0.07	1.35	0.40	0.35	0.41	0.35	1.10	7.00	0.06	4.08
10937	1.00	4.00	1.41	0.08	1.41	0.40	0.41	0.42	0.41	1.10	7.00	0.06	4.09
19039	1.00	4.00	1.49	0.10	1.49	0.40	0.49	0.45	0.49	1.10	6.25	0.06	4.10
24637	1.00	4.00	1.53	0.12	1.53	0.40	0.53	0.48	0.53	1.10	6.81	0.06	4.12

Percentage error $^{242}C_B$ (equation 1):

$$\epsilon^2 = \left\{F(P)\frac{dP}{P}\right\}^2 + \left\{F(U)\frac{dU}{U}\right\}^2 + \left\{F(C2)\frac{dC2}{C2}\right\}^2 + \left\{F(U8)\frac{dU8}{U8}\right\}^2 + \left\{F(Z)\frac{dZ}{Z}\right\}^2$$

Error transmission factors against burnup (MWD/MTU) and experimental uncertainties on ^{242}Cm buildup

BURNUP MWD/MTU	F (P)	$\frac{dP}{P}$	F (U)	$\frac{dU}{U}$	F (C2)	$\frac{dC2}{C2}$	F (U8)	$\frac{dU8}{U8}$	F (Z)	$\frac{dZ}{Z}$	Total ϵ %
7694	1.00	0.65	1.00	0.58	1.00	4.08	1.00	0.01	1.00	0.018	4.17
10932	1.00	0.65	1.00	0.58	1.00	4.09	1.00	0.01	1.00	0.021	4.18
19039	1.00	0.65	1.00	0.58	1.00	4.10	1.00	0.01	1.00	0.031	4.19
24637	1.00	0.65	1.00	0.58	1.00	4.17	1.00	0.01	1.00	0.038	4.21

The remaining uncertainty values of the Pu isotopes buildup whose tables of error analysis are not given (Figs. II.16 - II.18) are practically constant with the burnup apart from the error on ^{242}Pu which decreases sharply by almost a factor 2 in the entire exposure range following the net increase in its buildup.

The ^{241}Am error value remains constant at high values around 20% (Fig. II.19).

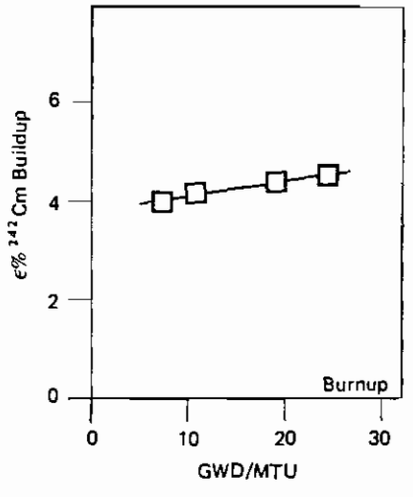

Fig. II.15. ^{242}Cm buildup percentage uncertainty against burnup

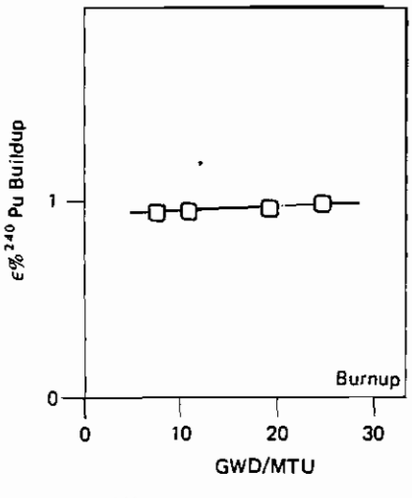

Fig. II.16. ^{240}Pu buildup percentage uncertainty against burnup

The error on ^{244}Cm, Fig. II.20, rapidly decreases from 8.6% to around 2.7% in the range explored.
The complete set of analytical uncertainties are reported in Table II.10 for four different burnup levels.

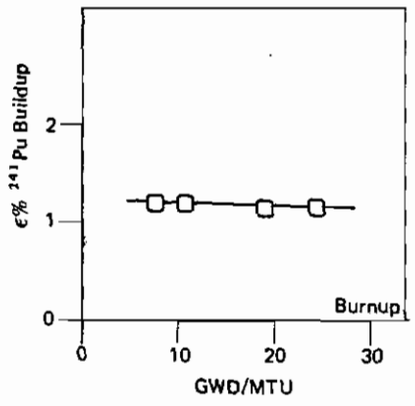

Fig. II.17. ^{241}Pu buildup percentage uncertainty against burnup

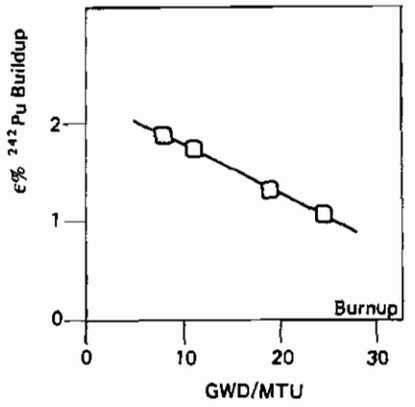

Fig. II.18. ^{242}Pu buildup percentage uncertainty against burnup

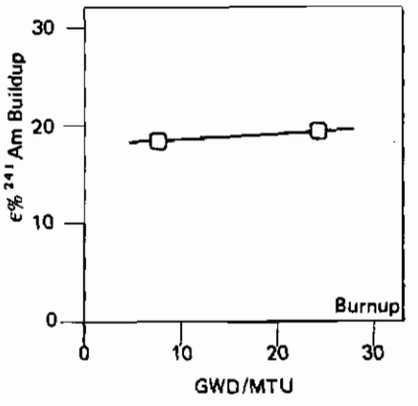

Fig. II.19. ^{241}Am buildup percentage uncertainty against burnup

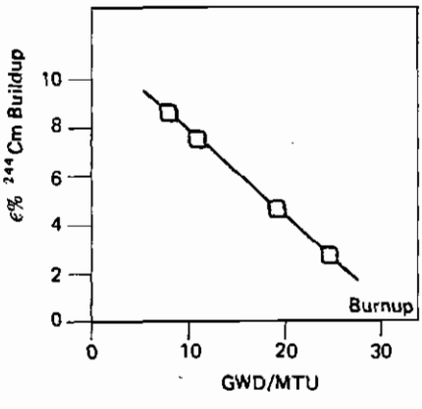

Fig. II.20. ^{244}Cm buildup percentage uncertainty against burnup

TABLE II.10. Percentage analytical uncertainty of derived parameters at different burnup levels.

DERIVED PARAMETERS	Burnup (MWD/MTU)			
	7694	10932	19039	24637
^{235}U Depletion	2.46	1.80	1.23	1.03
^{236}U Buildup	1.64	1.57	1.38	1.24
^{238}U Depletion	4.66	3.43	2.29	2.05
^{238}Pu Buildup	1.75	1.83	2.01	1.99
^{239}Pu Buildup	0.87	0.88	0.88	0.88
^{240}Pu Buildup	0.96	0.97	0.98	0.99
^{241}Pu Buildup	1.20	1.19	1.14	1.15
^{242}Pu Buildup	1.91	1.75	1.33	1.10
^{241}Am Buildup	18.7	–	–	20.00
^{242}Cm Buildup	4.17	4.18	4.19	4.21
^{244}Cm Buildup	8.59	7.53	4.64	2.75
Pu/U Mass ratio	0.73	0.69	0.64	0.61
^{148}Nd Burnup	1.40	1.41	1.42	1.43
^{137}Cs Burnup	–	–	–	1.8

3. Step C: Evaluation of the overall uncertainty

This step concerns the composition of analyticalal errors with uncertainties coming from other sources (cutting, material losses). A typical example of composition of the final error on Pu/U is given in Table II.11. The overall error at 24637 MWD/MTU is evaluated around 0.9%. Similar expressions can be derived for other Pu isotopes. Isotopes of other than Pu element are less sensitive, as previously mentioned, to the cutting uncertainty. The global error on ^{239}Pu buildup is shown in Table II.12, the overall uncertainty for pellets drawn in the outer part of the fuel pins is around 1.1%.

The global error on burnup is shown in Table II.13.

Typical global uncertainties on burnup and buildups at 24637 MWD/MTU derived by combining all sources of error are summarized in Table II.14.

TABLE II.11. Global uncertainty (%) on Pu/U mass ratio at 24637 MWD/MTU

Cutting position (for positions in the extremities)				0.5
Cutting losses				0.5
Chemical				negligible
Analytical: (See Table II.7)	from:	^{238}Pu buildup	–	
		^{239}Pu buildup	0.55	
		^{240}Pu buildup	0.19	
		^{241}Pu buildup	0.16	
		^{242}Pu buildup	–	
		Total analytical	0.61	0.61
			Total	0.93

TABLE II.12. Global uncertainty (%) on ^{239}Pu buildup at 24637 MWD/MTU

Cutting position (for positions in the extremities)				0.5
Cutting losses				0.5
Chemical				negligible
Analytical (See Table II.6)	from:	Pu concentration	0.65	
		U concentration	0.58	
		^{239}Pu atom %	0.12	
		Total analytical	0.88	0.88
			Total	1.13

TABLE II.13. Global uncertainty (%) on burnup at 24637 MWD/MTU

Cutting position (for pellets in extremities)				0.5
Cutting losses				negligible
Chemical				negligible
Analytical: (See Table II.3)	from:	^{148}Nd/^{238}U atom ratio	1.03	
		^{148}Nd fission yield	1.03	
		Total analytical	1.43	1.43
			Total	1.51

TABLE II.14. Typical global percentage uncertainties at 24637 MWD/MTU

Parameter	Analytical uncertainty from Table II.10	Global uncertainty	
		Central pin region (analytical + cutting losses)	Outer pin region (analytical + cutting losses + cutting position)
^{148}Nd Burnup	1.43	1.43	1.51
^{235}U Depletion	1.03	1.03	1.14
^{236}U Buildup	1.24	1.24	1.34
^{238}Pu Buildup	1.99	2.05	2.11
^{239}Pu Buildup	0.88	1.01	1.13
^{240}Pu Buildup	0.99	1.11	1.22
^{241}Pu Buildup	1.15	1.25	1.35
^{242}Pu Buildup	1.10	1.21	1.29
^{241}Am Buildup	20.00	20.00	20.00
^{242}Cm Buildup	4.21	4.21	4.21
^{244}Cm Buildup	2.75	2.75	2.75
Pu/U Mass ratio	0.61	0.79	0.93

Summarizing the procedure followed for the error evaluation, in Table II.1 one can see the uncertainty as evaluated on raw data. In Table II.10 the so-called "analytical uncertainty" is presented, as derived from α, γ and mass spectrometry measurements and finally in Table II.14 global uncertainties which take into account also cutting losses and imprecisions are given.

4. Step D : Comparison with Karlsruhe data

The last step concerning the evaluation of experimental uncertainties was the comparison between the values found by Ispra and Karlsruhe.

As indicators of discrepancy the average percent interlaboratory difference value Δ and the standard deviation of the differences s_d have been currently used:

$$\Delta = \frac{\sum_{i=1}^{n} d_i}{n} = \frac{\sum_{i=1}^{n} 100(X_i^K - X_i^I)/X_i^I}{n}$$

being X_i^I the values measured at Ispra, X_i^K the values measured at Karlsruhe and n the number of determinations.

Thus s_d is defined as:

$$s_d = \sqrt{\frac{\sum_{i=1}^{n} (\Delta - d_i)^2}{n - 1}}$$

In Table II.15 the comparison between the burnup values derived from ^{148}Nd is given. It can be seen that the low average differences and the low standard deviation of the

TABLE II.15. Intercomparison between Ispra and Karlsruhe analytical results. (^{148}Nd burnup - MWD/MTU).

Reactor	Sample	Ispra	Karlsruhe	d (%)
Trino I	L5.4	14,155	14,490	+ 2.37
	L5.9			
	A1.1	8,895	7,814	−12.15(*)
	A1.7			
	M11.7	11,912	12,172	+ 2.18
Trino II	E5.7			
	E11.2			
	E11.4			
	E11.7			
	L11.7	24,023	24,700	+ 2.82
Obrigheim	E3.P4	30,890	30,940	+ 0.16
	G7.P1			
	G7.P3	31,500	31,140	− 1.14
	G14.P3(1)	38,100	36,880	− 3.20
Gundremmingen	B23.B3			
	B23.E5			
	C16.B3			
	C16.E5			

Uncertainty evalueted at 24637 MWD/MTU

ϵ = 1.43%

(*) Outlier (see text)

Observed discrepancy

$\overline{\Delta}$	=	−1.28%	with
s_d	=	5.26%	A 1.1
$\overline{\Delta}$	=	0.53%	without
s_d	=	2.37%	A 1.1

differences give confidence that no appreciable bias was present in the measurements.

The low number of coupled samples in this case is due to the fact that not always in Ispra or in Karlsruhe the ^{148}Nd was measured.

It should be explained at this point that the purpose of the cross check between the two laboratories was not to perform a generic interlaboratory comparison, but rather to draw inferences about the possible bias in buildup or burnup determinations. In parallel the two laboratories obviously have their individual specific channels for minimising their bias. The conclusion drawn on ^{148}Nd burnup is that a standard deviation of the difference (s_d) of about 2% on a parameter whose accuracy was evaluated around 1.4 % is quite satisfactory.

The figures just mentioned are derived from the set of burnup data without considering the A1.1 value which appears to be an outlier, also in Table II.16, where the comparison of burnup values from ^{137}Cs is given. The same anomaly exists for the A1.1 sample in the entire buildup data, so it has been omitted in the following.

The results of the analysis of the ^{137}Cs burnup values given in Table II.16, again indicate a low average difference and standard deviation, but there is some evidence that the data can be split into two groups: for TRINO I Karlsruhe data are systematically lower than the Ispra ones, whilst the contrary happens for TRINO II and GUNDREMMINGEN data.

A detailed analysis of the uncertainty connected with the burnup determination from ^{137}Cs has not been carried out.

TABLE II.16. Intercomparison between Ispra and Karlsruhe analytical results (^{137}Cs burnup - MWD/MTU).

Reactor	Sample	Ispra	Karlsruhe	d(%)
Trino I	L5.4	14.099	13.883	− 1.53
	L5.9	10.478	10.444	− 0.32
	A1.1	8.870	7.716	−13.01(*)
	A1.7	16.146	15.740	− 2.51
	M11.7	12.606	12.035	− 4.53
Trino II	E5.7	24.693	24.683	− 0.04
	E11.2	20.628	21.296	+ 3.24
	E11.4	23.557	23.969	+ 1.75
	E11.7	23.953	25.095	+ 4.76
	L11.7	24.471	24.532	+ 0.25
Obrigheim	E3.P4			
	G7.P1			
	G7.P3			
	G14.P3(1)			
Gundremmingen	B23.B3	21.690	22.100	+ 1.89
	B23.E5	25.380	25.900	+ 2.05
	C16.B3	15.220	15.680	+ 3.02
	C16.E5			

Uncertainty evaluated at 24637 MWD/MTU

$\epsilon = 1.8\%$

(*) Outlier (see text)

Observed discrepancy

$\overline{\Delta} = -0.38\%$ with
$s_d = 4.56\%$ A1.1

$\overline{\Delta} = +0.67\%$ without
$s_d = 2.65\%$ A1.1

To the parameter has been attributed an overall error of 1.8% arising from the combination of 1% uncertainty on fission yield and 1.5% from measurement (see section 1.6.3). But some other systematic errors arising from fission product migration could affect the results, without being easily detected in the interlaboratory comparison.

The paired evaluation of the ^{235}U depletion is shown in Table II.17. Once more a negligible average difference (less than 0.1%) and a s_d of about 2% is again quite satisfactory.
The ^{235}U depletion has, according to Fig. II.10 an average precision ranging from 2.5% down to 1% depending upon the burnup level.
The overall uncertainty quoted for 24637 MWD/MTU is 1.03% according to Table II.14.

TABLE II.17. Intercomparison between Ispra and Karlsruhe analytical results (^{235}U depletion - kg/MTU).

Reactor	Sample	Ispra	Karlsruhe	d (%)
Trino I	L5.4	12.05	12.28	+ 1.91
	L5.9	9.64	9.84	+ 2.07
	A1.1			
	A1.7	13.85	13.67	−1.30
	M11.7	12.56	12.13	−3.42
Trino II	E5.7	19.15	19.03	−0.63
	E11.2	17.00	16.88	−0.70
	E11.4	18.98	18.66	−1.68
	E11.7	19.04	18.87	−0.89
	L11.7	18.98	19.12	+ 0.74
Obrigheim	E3.P4	22.52	22.16	−1.60
	G7.P1	14.79	15.60	+ 5.47
	G7.P3	22.39	22.50	+ 0.49
	G14.P3(1)	23.25	23.89	+ 2.75
Gundremmingen	B23.B3	15.66	15.37	−1.22
	B23.E5	18.62	18.45	−0.91
	C16.B3	12.22	12.14	−0.65
	C16.E5	14.97	14.73	−1.60

Uncertainty evaluated at 24637 MWD/MTU

ϵ = 1.03%

Observed discrepancy

$\overline{\Delta}$ = −0.07%
s_d = 2.12%

TABLE II.18. Intercomparison between Ispra and Karlsruhe analytical results (^{236}U buildup - kg/MTU).

Reactor	Sample	Ispra	Karlsruhe	d (%)
Trino I	L5.4	2.24	2.22	− 0.89
	L5.9	1.91	1.85	− 3.14
	A1.1			
	A1.7	2.47	2.48	+ 0.40
	M11.7	2.52	2.56	+ 1.59
Trino II	E5.7	3.56	3.53	− 0.84
	E11.2	3.24	3.39	+ 4.63
	E11.4	3.53	3.70	+ 4.82
	E11.7	3.62	3.66	+ 1.10
	L11.7	3.45	3.48	+ 0.87
Gundremmingen	B23.B3	2.94	2.95	+ 0.34
	B23.E5	3.25	3.33	+ 2.46
	C16.B3	2.44	2.46	+ 0.82
	C16.E5	2.71	2.77	+ 2.21
Obrigheim	E3.P4	3.83	3.91	+ 2.09
	G7.P1	2.92	2.93	+ 0.34
	G7.P3	3.94	3.98	+ 1.01
	G14.P3(1)	3.89	3.87	− 0.51

Uncertainty evaluated at 24637 MWD/MTU

ϵ = 1.24%

Observed discrepancy

$\overline{\Delta}$ = + 1.02%
s_d = 1.95%

The results of the Ispra/Karlsruhe comparison for ^{236}U buildup are given in Table II.18. The standard deviation of the difference found is 1.95% as compared with an evaluated global uncertainty of 1.24%.

The ^{239}Pu buildup again shows a good agreement: $\overline{\Delta} = 0.13\%$, $s_d = 1.86\%$ as can be seen in Table II.19, to be compared with an average uncertainty of the order of 1%.
But all the Pu isotopes except ^{238}Pu show discrepancies and standard deviation of differences that are always (approximately) the expected values, i.e. the accuracy values show no evidence of systematic bias (Tables II.20 - II.22).

TABLE II.19. Intercomparison between Ispra and Karlsruhe analytical results (^{239}Pu buildup - kg/MTU).

Reactor	Sample	Ispra	Karlsruhe	d (%)
Trino I	L5.4	5.04	4.99	−0.99
	L5.9	4.07	4.16	+2.21
	A1.1			
	A1.7	4.81	4.89	+1.66
	M11.7	4.65	4.52	−2.79
Trino II	E5.7	5.99	5.87	−0.33
	E11.2	5.76	5.75	−0.17
	E11.4	5.86	5.93	+1.19
	E11.7	6.19	5.95	−3.87
	L11.7	6.02	5.97	−0.83
Gundremmingen	B23.B3	5.31	5.43	+2.26
	B23.E5	4.54	4.47	−1.54
	C16.B3	4.68	4.71	+0.64
	C16.E5	4.17	4.15	−0.48
Obrigheim	E3.P4	4.94	4.91	−0.61
	G7.P1	4.26	4.39	+3.05
	G7.P3	4.99	5.04	+1.00
	G14.P3(1)	4.52	4.60	+1.77

Uncertainty evaluated at 24637 MWD/MTU

$\epsilon = 1.01\%$

Observed discrepancy

$\overline{\Delta} = +0.13\%$
$s_d = 1.86\%$

TABLE II.20. Intercomparison between Ispra and Karlsruhe analytical results (^{240}Pu buildup - kg/MTU).

Reactor	Sample	Ispra	Karlsruhe	d (%)
Trino I	L5.4	1.12	1.12	−0.00
	L5.9	0.72	0.75	+4.17
	A1.1			
	A1.7	1.25	1.25	0.00
	M11.7	0.72	0.71	−1.39
Trino II	E5.7	1.78	1.79	+0.56
	E11.2	1.52	1.52	0.00
	E11.4	1.75	1.76	+0.57
	E11.7	1.86	1.79	−3.76
	L11.7	1.82	1.80	−1.10
Obrigheim	E3.P4	2.22	2.24	+0.90
	G7.P1	1.16	1.23	+6.03
	G7.P3	2.27	2.29	+0.88
	G14.P3(1)	2.47	2.52	+2.02
Gundremmingen	B23.B3	1.82	1.88	+3.29
	B23.E5	2.11	2.10	−0.47
	C16.B3	1.16	1.18	+1.72
	C16.E5	1.44	1.44	0.00

Uncertainty evaluated at 24637 MWD/MTU

$\epsilon = 1.11\%$

Observed discrepancy

$\overline{\Delta} = +0.79\%$
$s_d = 2.25\%$

TABLE II.21. Intercomparison between Ispra and Karlsruhe analytical results (^{241}Pu buildup - kg/MTU).

Reactor	Sample	Ispra	Karlsruhe	d (%)
Trino I	L5.4	0.59	0.61	+ 3.39
	L5.9	0.33	0.35	+ 6.06
	A1.1			
	A1.7	0.68	0.68	0.00
	M11.7	0.35	0.34	− 2.85
Trino II	E5.7	1.06	1.05	− 0.94
	E11.2	0.88	0.89	+ 1.13
	E11.4	1.02	1.04	+ 1.96
	E11.7	1.07	1.05	− 1.87
	L11.7	1.05	1.06	+ 0.95
Obrigheim	E3.P4	1.18	1.19	+ 0.85
	G7.P1	0.55	0.59	+ 7.27
	G7.P3	1.20	1.21	+ 0.83
	G14.P3(1)	1.30	1.32	+ 1.51
Gundremmingen	B23.B3	0.87	0.89	+ 2.30
	B23.E5	0.91	0.90	−1.10
	C16.B3	0.54	0.55	+ 1.85
	C16.E5	0.60	0.60	0.00

Uncertainty evaluated at 24637 MWD/MTU

ϵ = 1.25%

Observed discrepancy

$\overline{\Delta}$ = + 1.26%
s_d = 2.58%

TABLE II.22. Intercomparison between Ispra and Karlsruhe analytical results (^{242}Pu buildup - kg/MTU)

Reactor	Sample	Ispra	Karlsruhe	d (%)
Trino I	L5.4			
	L5.9			
	A1.1			
	A1.7			
	M11.7			
Trino II	E5.7	0.255	0.253	− 0.78
	E11.2	0.168	0.176	+ 4.76
	E11.4	0.240	0.247	+ 2.92
	E11.7	0.260	0.255	− 1.92
	L11.7	0.260	0.258	− 0.77
Obrigheim	E3.P4	0.464	0.488	+ 5.17
	G7.P1	0.099	0.112	+ 13.13(*)
	G7.P3	0.478	0.500	+ 4.60
	G14.P3(1)	0.773	0.787	+ 1.81
Gundremmingen	B23.B3	0.215	0.224	+ 4.18
	B23.E5	0.331	0.333	+ 0.60
	C16.B3	0.087	0.088	+ 1.15
	C16.E5	0.151	0.144	− 4.63

Uncertainty evaluated at 24637 MWD/MTU

ϵ = 1.21%

(*) Outlier

Observed discrepancy

$\overline{\Delta}$ = + 2.32% with
s_d = 4.38% G7.P1

$\overline{\Delta}$ = + 1.42% without
s_d = 3.07% G7.P1

In Table II.23 the results are given of the comparison for ^{238}Pu. It is evident that the overall result contains some discrepancy. The standard deviation of the difference is around 12%, whilst the estimated uncertainty is approximately 2%. It should be noted that the TRINO II and GUNDREMMINGEN results are generally in agreement with the evaluated uncertainty, and only the OBRIGHEIM data are strongly divergent. On the other hand we cannot explain these inhomogeneities by the existence of a bias in one of the two laboratories, because the largest discrepancies are in both senses (positive and negative) and of the same order of magnitude (25%).
In conclusion we should mention that the experimental uncer-

tainty of about 2% evaluated for ^{238}Pu is considerably too low, at least for the OBRIGHEIM campaign, and at least for one of the two laboratories. The difficulties pointed out in section I.6.2 in the α-spectrum analysis, and confirmed by the results of the interlaboratory comparison AS-76 already referred to /39,40,41/, are certainly responsible for the great discrepancy between evaluated uncertainty and observed Ispra/Karlsruhe discrepancy.

For the ^{241}Am data, see Table II.24, the paired data are too few and the experimental error is too high, to give a clear statement.

TABLE II.23. Intercomparison between Ispra and Karlsruhe analytical results (^{238}Pu buildup - kg/MTU).

Reactor	Sample	Ispra	Karlsruhe	d (%)
Trino I	L5.4			
	L5.9			
	A1.1			
	A1.7			
	M11.7			
Trino II	E5.7	0.116	0.115	− 0.86
	E11.2	0.080	0.081	+ 1.25
	E11.4	0.109	0.109	0.00
	E11.7	0.120	0.114	− 5.00
	L11.7	0.118	0.114	− 3.39
Obrigheim	E3.P4	0.125	0.103	−17.60
	G7.P1	0.031	0.039	+ 25.80
	G7.P3	0.138	0.145	+ 5.07
	G14.P3(1)	0.190	0.139	−26.80
Gundremmingen	B23.B3	0.080	0.086	+ 7.50
	B23.E5	0.097	0.099	+ 2.06
	C16.B3	0.033	0.033	0.00
	C16.E5	0.041	0.041	0.00

Uncertainty evaluated at 24637 MWD/MTU

ϵ = 2.05%

Observed discrepancy

$\overline{\Delta}$ = − 0.92%
s_d = 12.27%

TABLE II.24. Intercomparison between Ispra and Karlsruhe analytical results (^{241}Am buildup atoms/10^6 i.h.a.) (x 10^{-2})

Reactor	Sample	Ispra	Karlsruhe	d (%)
Trino I	L5.4			
	L5.9			
	A1.1			
	A1.7			
	M11.7			
Trino II	E5.7			
	E11.2			
	E11.4			
	E11.7			
	L11.7			
Obrigheim	E3.P4			
	G7.P1			
	G7.P3			
	G14.P3(1)			
Gundremmingen	B23.B3			
	B23.E5	2.12	1.14	−46.23
	C16.B3	1.00	0.94	− 6.00
	C16.E5	1.43	1.02	−28.70

Uncertainty evaluated at 24637 MWD/MTU

ϵ = 20.00%

Observed discrepancy

$\overline{\Delta}$ = −26.9%
s_d = 20.2%

Nor is there a great deal of paired buildup data available for the ^{242}Cm and ^{244}Cm (Tables II.25 and II.26) but probably sufficient for drawing the conclusion that the quoted experimental uncertainties (about 4% and 3% respectively) are coherent with the interlaboratory discrepancy if one keeps the OBRIGHEIM data out of the comparison.

The standard deviation of the Ispra/Karlsruhe difference for ^{244}Cm (s_d = 12.06%) is considerably higher than the quoted uncertainty (2.75%) but one must remember that the ^{244}Cm error is decreasing rapidly with burnup and the average burnup of the sample is lower than 24637 MWD/MTU especially without OBRIGHEIM data. So an evaluated uncertainty of around 5% might be more representative of the set of data available.

TABLE II.25. Intercomparison between Ispra and Karlsruhe analytical data (^{242}Cm buildup - atoms/10^6 i.h.a.)

Reactor	Sample	Ispra	Karlsruhe	d (%)
Trino I	L5.4 L5.9 A1.1 A1.7 M11.7			
Trino II	E5.7 E11.2 E11.4 E11.7 L11.7	24.3 17.3 23.6 26.2 24.3	25.1 17.8 24.3 26.2 24.2	+ 3.29 + 4.71 + 2.97 0.00 − 0.41
Obrigheim	E3.P4 G7.P1 G7.P3 G14.P3(1)	15.01 14.79 14.54	33.17 27.15 47.03	+ 120.98(*) + 83.57(*) + 223.45(*)
Gundremmingen	B23.B3 B23.E5 C16.B3 C16.E5	9.37 11.29 3.68 5.09	9.22 10.26 3.80 4.82	− 1.60 − 9.12 + 3.26 − 5.30

Uncertainty evaluated at 24637 MWD/MTU

ϵ = 4.21%

(*) Outliers

Observed discrepancy

$\overline{\Delta}$ = + 35.48% with
s_d = 71.74% Obrigheim

$\overline{\Delta}$ = − 0.24% without
s_d = 4.55% Obrigheim

TABLE II.26. Intercomparison between Ispra and Karlsruhe analytical data. (^{244}Cm buildup - atoms/10^6 i.h.a.).

Reactor	Sample	Ispra	Karlsruhe	d (%)
Trino I	L5.4 L5.9 A1.1 A1.7 M11.7			
Trino II	E5.7 E11.2 E11.4 E11.7 L11.7	9.07 4.35 9.03 10.03 9.79	9.31 4.77 8.56 9.29 9.20	+ 2.65 + 9.65 − 5.20 − 7.40 − 6.03
Obrigheim	E3.P4 G7.P1 G7.P3 G14.P3(1)	24.80 1.04 29.73 59.81	22.18 1.97 26.73 45.94	−10.88 + 89.42(*) −10.10 −23.19
Gundremmingen	B23.B3 B23.E5 C16.B3 C16.E5	8.46 15.24 1.44 2.46	8.38 14.14 1.62 2.99	− 1.18 − 7.21 + 12.50 + 21.54

Uncertainty evaluated at 24637 MWD/MTU

ϵ = 2.75%

(*) Outlier

Observed discrepancy

$\overline{\Delta}$ = + 4.97% with
s_d = 27.87% G7.P1

$\overline{\Delta}$ = − 2.07% without
s_d = 12.06% G7.P1

Reported data relevant to ^{242}Cm from OBRIGHEIM obtained at Karlsruhe seem to be largely overestimated as also demonstrated in section III. 3.

Finally, in Table II. 27, the results of the comparison for Pu/U values are given. Having a standard deviation of the difference of about 2. 3% the evaluated overall uncertainty of 0. 8% seems to be only slightly underestimated, but still to remain within acceptable limits.

Table II. 28 provides a summary of the results of the Karlsruhe-Ispra interlaboratory comparison.

TABLE II.27. Intercomparison between Ispra and Karlsruhe analytical results (Pu/U mass ratio)

Reactor	Sample	Ispra	Karlsruhe	d (%)
Trino I	L5.4	6.895	6.857	−0.55
	L5.9	5.179	5.316	+2.64
	A1.1	4.412	4.183	−5.19
	A1.7	6.913	7.016	+1.49
	M11.7	5.601	5.657	+0.99
Trino II	E5.7	9.544	9.511	−0.34
	E11.2	8.668	8.679	+0.13
	E11.4	9.294	9.408	+1.72
	M11.7	9.834	9.490	−3.49
	L11.7	9.604	9.549	−0.57
Obrigheim	E3.P4	9.30	9.31	+0.10
	G7.P1	6.25	6.56	+4.96
	G7.P3	9.47	9.60	+1.37
	G14.P3(1)	9.73	9.85	+1.23
Gundremmingen	B23.B3	8.57	8.80	+2.68
	B23.E5	8.28	8.20	−0.97
	C16.B3	6.65	6.71	+0.90
	C16.E5	6.58	6.54	−0.61

Uncertainty evaluated at 24637 MWD/MTU

ϵ = 0.79%

Observed discrepancy

$\bar{\Delta}$ = +0.36%

s_d = 2.27%

TABLE II.28. Summary of the Ispra-Karlsruhe intercomparison.

Parameter	$\bar{\Delta}$ Ispra-Karlsruhe	S_d % Observed	ϵ % Evaluated	Ispra-Karlsruhe Agreement
^{148}Nd Burnup	− 1.28	2.37	1.43	GOOD
^{137}Cs Burnup	− 0.38	2.65	1.80	GOOD
^{235}U Depletion	− 0.07	2.12	1.03	GOOD
^{236}U Buildup	+ 1.02	1.95	1.24	GOOD
^{238}Pu Buildup	− 0.92	12.27	2.05	ϵ % UNDERESTIMATED
^{239}Pu Buildup	+ 0.13	1.86	1.01	GOOD
^{240}Pu Buildup	+ 0.79	2.25	1.11	GOOD
^{241}Pu Buildup	+ 1.26	2.58	1.25	GOOD
^{242}Pu Buildup	+ 1.42	3.07	1.21	REASONABLE
^{241}Am Buildup	−26.9	20.2	20.00	TOO FEW POINTS
^{242}Cm Buildup	− 0.24	4.55	4.21	GOOD
^{244}Cm Buildup	− 2.07	12.06	2.75	ϵ % UNDERESTIMATED
Pu/U Mass ratio	+ 0.36	2.27	0.79	REASONABLE

5. Conclusions

In order to summarize the content of this section dedicated to the assessment of an overall uncertainty of BM data, the following conclusions can be drawn:

1) The uncertainties in the analytical methodologies are not the only ones present in the rather complex process of destructive assays. We have identified and assessed at least two other possible error sources in the sample cutting position and in the loss of material. These sources can partially affect some of the samples, while some other samples may not be influenced.
This leads to the obvious conclusion that every experimental process should be studied step-by-step in detail in order to evaluate the overall uncertainty connected with the process.
AIthough this conclusion may be obvious, the experimental process modelling may not be so simple.
A further complication, following the modelling, is the statistical treatment of the error data. The additive model used here for simplicity might sometimes be only an approximation of the reality.
Finally, to express the overall uncertainty with only one number without a study of the possible correlations of the error components is as well a simplification of the system.
An effort should be made to assess the correlation components. At present under study is the possibility of expressing the uncertainty by a standard deviation and a correlation matrix, following the suggestions made in /46/.
The sensitivity of the uncertainty of the parameter investigated (burnup and buildup) has been studied and reported throughout this chapter. It is summarized here individually with the aid of Table II. 29. In this table the contribution of the uncertainty of the raw data on final parameters is indicated as a product of $\epsilon_i F_i$, or in other words the product of the raw error times its transmission factor. The table refers only to analytical errors.

Burnup from ^{148}Nd

Two equal components of error are summed up from ^{148}Nd determination and from ^{148}Nd fission yield. The burnup dependence of the error on burnup is weak. The interlaboratory comparison was good.

TABLE II.29. Error sensitivity analysis of ^{148}Nd burnup, ^{235}U and ^{238}U depletion and heavy isotopes buildup at 24637 MWD/MTU

PERCENTAGE EXPERIMENTAL ERROR	0.60	0.71	1.24	0.01	0.12	0.48	0.58	0.67	4.00	2.42	1.97	1.00	0.58	0.65	0.97	1.00	0.04	0.90	0.40	1.10	2.70	1.30	0.90	0.06	0.06	
ROW DATA / DERIVED DATA	INITIAL ENRICH.T $\frac{^{235}U}{U}$ wt%	^{235}U at%	^{236}U at%	^{238}U at%	^{239}Pu at%	^{240}Pu at%	^{241}Pu at%	^{242}Pu at%	$\frac{^{242}Cm}{^{239}Pu+^{240}Pu}$	$\frac{^{244}Cm}{^{239}Pu+^{240}Pu}$	$\frac{^{238}Pu+^{241}Am}{^{239}Pu+^{240}Pu}$	$\frac{^{238}Pu}{^{239}Pu+^{240}Pu}$	U CONCENTRATION	Pu CONCENTRATION	$\frac{^{148}Nd}{^{238}U}$	^{148}Nd FISSION YIELD	(*) Z	$\lambda(^{238}Pu)$	$\lambda(^{239}Pu)$	$\lambda(^{240}Pu)$	$\lambda(^{241}Pu)$	$\lambda(^{242}Pu)$	$\lambda(^{241}Am)$	$\lambda(^{242}Cm)$	$\lambda(^{244}Cm)$	% TOTAL ERROR
BURNUP (Ft %) ^{148}Nd															1.00	1.03										1.43
^{235}U DEPLETION	0.94	0.40		N													N									1.03
^{236}U BUILDUP			1.24	N																						1.24
^{238}U DEPLETION		1.09															1.74									2.05
^{238}Pu BUILDUP				N	0.06	0.25			0.88			1.22	0.58	0.85			N	0.70	0.19	0.58				0.09		2.00
^{239}Pu BUILDUP				N	0.11								0.58	0.65												0.88
^{240}Pu BUILDUP				N		0.48							0.58	0.65			N									1.00
^{241}Pu BUILDUP				N			0.58						0.58	0.85			N				0.49					1.15
^{242}Pu BUILDUP				N				0.67					0.58	0.65			N					N				1.10
^{241}Am BUILDUP				N	0.54	1.28					18.76	5.87	0.58	0.65			N		1.72	1.64			2.43			20.00
^{242}Cm BUILDUP				N	0.18	0.25			4.00				0.58	0.65			N		0.61	0.58				0.41		4.21
^{244}Cm BUILDUP				N	0.18	0.25				2.42			0.58	0.65			N		0.61	0.58					0.41	2.75

N = negligible

$$(*)\ Z = \frac{100}{\sum_{i=1}^{n} r_i + \frac{^{148}Nd}{^{238}U} \cdot \frac{1}{\gamma}}$$

Depletion of ^{235}U

The initial and final ^{235}U percent content have not the same transmission factor. Initial content must be known with a better accuracy than the final one. The burnup dependence of the error is marked. The interlaboratory comparison was good.

Buildup of ^{236}U

Only the error on ^{236}U determination is of any importance. The burnup dependence is sensitive. The interlaboratory comparison was good.

Buildup of ^{238}Pu

The most important parameters with respect to buildup error are:

- the ^{238}Pu ratio measurement
- the decay constant of ^{238}Pu knowledge
- the $^{242}CM/(^{239}Pu + ^{240}Pu)$ ratio measurement
- the U and Pu concentration determination.

The burnup dependence is weak: considering the large spread of the original errors (see Figs. II.6, II.7) and considering also that the dependence on the final error is mainly due to raw data, it has been considered unreasonable to give a burnup dependence on the ^{238}Pu error.

The interlaboratory comparison gave questionable results for Obrigheim data, probably due to a difficult spectrum analysis mainly at high burnups.

Buildup of ^{239}Pu

The Pu and U concentration errors only play a nearly balanced role in the final error. The burnup dependence is weak. The interlaboratory comparison was good.

Buildups of ^{240}Pu, ^{241}Pu, ^{242}Pu

For all these isotopes the uncertainty in buildup is similar: the significant error components are three of approximately the same weight: the U and Pu concentration determination and the mass spectrometric determination of the isotope itself.
The burnup dependence is significant only for ^{242}Pu.
The interlaboratory comparison was good for all of them.

Buildup of ^{241}Am

Only one error component is significant, i.e. uncertainty on the measurement of $(^{238}Pu + ^{241}Am)/(^{239}Pu + ^{240}Pu)$. Too few paired data were available to give a statement on the Ispra-Karlsruhe intercomparison.

Buildup of ^{244}Cm

The only one significant error component is that on $^{244}Cm/(^{239}Pu + ^{240}Pu)$ determination.
The burnup dependence was sensible. The interlaboratory comparison showed that the evaluated error of 2.75% was probably underestimated.

3. Description and Use of the Inverse Code Theory

As said in the introduction one of the aims of the BM program was to provide data for the testing of nuclear codes and collapsed cross-section sets.
However, reactor codes, cross-section libraries and measured isotopic compositions form a "system" whose handling is often particularly complicated. Both the experimental data and collapsed cross-section libraries may contain systematic errors which are frequently not easily detectable.
The approach of one-group cross-section ratios followed here and proposed by R. P. Matsen /47/ aimed to help manage the above-mentioned "system", to detect systematic errors in measured data sets and to help in the adjustment of collapsed few-group cross-section libraries /48/.
It was obviously not the aim of this approach to prepare new cross-section sets, or to give values for the cross-section ratios. For this task more refined tools are available to cross-section evaluators, to reactor physicists and to reactor operators. It is also generally agreed that the cross-section sets generated and evaluated in the main files available (ENDF/B or similar for instance) contain approximations that are largely acceptable (at least for U and Pu isotopes) for reactor physics purposes.
The problem can arise when from these original files each laboratory or plant derives its collapsed cross-section sets, using different codes, originally derived essentially by the same algorithms, but modified according to particular criteria, such as for instance computing capacity, experimental data availability, etc. In addition to those considerations some of the physical complexities already mentioned, such as for instance variation of the group X-sections with spectrum and with burnup, can make the job of preparing suitable X-section sets really complex. The operator has only

the experimental results (e.g. the Bench Mark data) available to verify his codes and X-section sets.
In the event of disagreement between calculated and experimental data, however, it is not always simple or straightforward to discover the reasons for the disagreement, since the nuclear chain itself and the models which describe it are quite complex. In these circumstances a tool like the one described here can be useful by interpreting the experimental data directly through a data fitting in terms of average X-section ratios. In the event of a discrepancy between the expected and evaluated X-section ratios it is obviously compulsory as a first step to re-check the experimental data in order to see whether some bias affecting them could explain the discrepancy. Only in a few cases one could take into consideration the possibility that some spectral parameter could have been poorly evaluated by the burnup codes used. And in any case the algorithm described here should always be used in parallel with conventional reactor burnup codes.

1. General theory

Assuming one-group (effective) cross section ratios, constant with burnup the transmutation equations are of the following general form:

$$\begin{aligned}\frac{dN^i(t)}{dt} = & - \hat{\sigma}_a^i N^i(t)\ \phi(t) \\ & + \hat{\sigma}_c^{i-1} N^{i-1}(t)\ \phi(t) \\ & - \lambda^i N^i(t) \\ & + \Sigma_j \lambda^j N^j(t)\end{aligned} \qquad /1/$$

The first term on the right hand side gives the number of atoms of nuclide i which disappear because of neutron absorption ($\hat{\sigma}_a^i$ is the effective absorption cross-section of nuclide i and ϕ is the total neutron flux at the time t).
The second term gives the atoms of nuclide i, formed by neutron capture in the nuclide (i-1). $\lambda^i N^i(t)$ gives the nuclide i atoms which disappear by natural decay, and $\lambda_j N^j(t)$ gives the number of nuclide i atoms formed through natural decay from other nuclides (β and α decay).

To eliminate the integrated neutron flux $\phi(t)$ the equation for the nuclide i is divided by the transmutation equation for ^{235}U giving:

$$\frac{dN^i}{dN^{25}} = -\frac{\hat{\sigma}_c{}^{i-1}}{\hat{\sigma}_a{}^{25}} \cdot \frac{N^{i-1}}{N^{25}} + \frac{\hat{\sigma}_a{}^i}{\hat{\sigma}_a{}^{25}} \cdot \frac{N^i}{N^{25}} \qquad /2/$$

with obvious notations. With n fuel samples for which we have measured the final isotopic composition, we had a set of n equations.

A least square-fit analysis of the approximated transmutation equations gave the cross-section ratios $\hat{\sigma}_a{}^i/\hat{\sigma}_a{}^{25}$ which can then be compared with those used in theoretical calculations.

Only the $\hat{\sigma}_a{}^{40}$ cross-section was treated differently since in LWRs in the exposure range from 0 to 33 GWD/MTU it has a much higher variation than other cross-sections. Therefore the corresponding ratio derived by the code fitted an empirical curve, which approximates the expected behaviour of the ratio versus burnup:

$$\frac{\hat{\sigma}_a{}^{40}}{\hat{\sigma}_a{}^{25}} = a + b \frac{N^{25}}{No^{25}} \qquad /3/$$

The code THEORY /49/ written at Ispra, solved the set of equations, having in input:

a) measured isotopic atomic ratios of uranium and plutonium nuclides versus ^{235}U atoms, at different burnup levels;
b) measured ratios of final to initial ^{235}U content in the samples;
c) half lives of various isotopes;
d) operation data of the reactor and date of measurements.

The output data were:

- the cross-section ratios;
- the ratios of initial isotopic content to initial ^{235}U (e.g. No^{26}/No^{25});
- the fitting curves of measured isotopic ratios of heavy elements to ^{235}U;
- the burnup values calculated from the evaluated composition of heavy elements.

The uncertainties of the output data were evaluated, using a Monte Carlo procedure. These uncertainties represent the transmission of the error on input data to the output, not the systematic error introduced by the algorithm and the approximations applied in the analysis.

2. Application

The two sets of experimental results obtained in TRINO I and TRINO II campaigns have been analysed by means of the MATSEN algorithm, applying to them the code THEORY. The cross-section ratios as computed with the code are compared in Table II.30 with the corresponding values used by ENEL for TRINO I and TRINO II data. The discrepancies (apart from the two isotopes ^{242}Pu and ^{236}U) are relatively small and determined by both experimental uncertainties and spectrum perturbations.

The two isotopes whose X-section ratios show considerable discrepancies with respect to the ones used by ENEL namely ^{236}U and ^{242}Pu are the last isotopes in the nuclear chains implemented. They are therefore not linked to following isotopes in the fitting and iterative procedure. This fact makes the corresponding cross-section ratios very sensitive to input or model errors as shown in /47/.

Also given in Table II.30 are the ratios N_o^{26}/N_o^{25} computed by THEORY. The code THEORY gives an appreciable initial content of ^{236}U, in disagreement with the input zero value. Further evaluation of "fresh" fuel compositions lead to the conclusion that the values produced by THEORY are reasonable ones. Indeed "fresh" fuel frequently contains a small amount of ^{236}U /50/.

TABLE II.30. TRINO I and TRINO II - Comparison between the cross-section ratios used by ENEL and those computed with THEORY.
(errors are given as one standard deviation, the number of independent measurements is 14).

	Cross Section Ratios of Trino I (2.719 wt%)			Cross Section Ratios of Trino II (3.13 wt%)		
	Theory	Enel	$\frac{\text{Theory-Enel}}{\text{Enel}}$ (%)	Theory	Enel	$\frac{\text{Theory-Enel}}{\text{Enel}}$ (%)
$\hat{\sigma}_a^{28}/\hat{\sigma}_a^{25}$	0.0184 ±0.0006	0.0190	− 3	.0204	.0207	− 1.5
$\hat{\sigma}_c^{28}/\hat{\sigma}_d^{25}$	0.0160 ±0.0004	0.0172	− 7	.0180	.0183	− 1.5
$\hat{\sigma}_a^{49}/\hat{\sigma}_a^{25}$	2.74 ±0.14	2.95	− 6	2.646	2.385	− 8
$\hat{\sigma}_c^{49}/\hat{\sigma}_a^{25}$	1.166 ±0.014	1.105	+ 5.5	1.184	1.092	+ 8
$\hat{\sigma}_a^{41}/\hat{\sigma}_a^{25}$	3.00 ±0.23	2.751	+ 9	3.032	2.732	+ 11
$\hat{\sigma}_c^{41}/\hat{\sigma}_a^{25}$	0.748 ±0.019	0.701	+ 6.5	.775	0.701	+ 10
$\hat{\sigma}_a^{42}/\hat{\sigma}_a^{25}$	1.013 ±0.040	1.022	− 1	1.398	1.110	+ 25
$\hat{\sigma}_c^{25}/\hat{\sigma}_a^{25}$	0.196 ±0.004	0.190	+ 3	.209 (.193)*	0.195	+ 7 (−1)*
$\hat{\sigma}_a^{26}/\hat{\sigma}_a^{25}$	0.290 ±0.054	0.160	+ 80	.294	0.170	+ 70
N_o^{26}/N_o^{25}	0.010 ±0.004	0.0		0.007	0.0	

* values obtained with reduced ^{236}U content.

A quite large discrepancy in the value of $\hat{\sigma}_c^{25}/\hat{\sigma}_a^{25}$ (Table II.30) for the TRINO II case has been found. There is apparently a tendency for the ENEL computed values to underestimate the ^{236}U buildup.

This conclusion is suggested by the underevaluation of TRINO and OBRIGHEIM ^{236}U measured data recalculated by RIBOT and could be due to a poor evaluation of the spectrum averaged ^{235}U value (fission to absorption X-section ratio). The argument will be taken up and expanded at the next section. Another obvious explanation might be a bias in ^{236}U experimental data.

An attempt has then been made to recalculate X-section ratios with THEORY, having artificially reduced by 7% the ^{236}U amount of input for TRINO II. The results are shown also in Table II.30 and the agreement is now quite satisfactory.

In Tables II.31 and II.32 the experimental burnup values from ^{148}Nd for TRINO I and TRINO II samples are compared with the THEORY computed ones, by means of heavy isotope sample content. There is an indication of a slight systematic underevaluation of the burnup by THEORY, at least for TRINO II, which is in any case not dramatically outside the limits of combined errors.

TABLE II.31. TRINO I (2.719 wt%) - Comparison between experimental and THEORY evaluated burnup values

Sample		Burnup (MWD/MTU)		Theory-Experimental / Experimental
		Experimental (from ^{148}Nd)	Theory (heavy isotopes)	
L5	4	14,080	13,515	− 5.3 %
	9	10,070	10,150	+ 0.8 %
J8	1	8,970	8,778	− 2.1 %
	4	14,570	15,280	+ 4.9 %
	7	14,980	15,290	+ 2.0 %
	9	11,000	11,420	+ 3.8 %
A1	1	8,230	8,410	+ 2.2 %
	7	15,290	15,907	+ 4.0 %
	9	11,900	11,907	+ 0.06%

TABLE II.32. TRINO II (3.13 wt%) - Comparison between experimental and THEORY evaluated burnup values

Sample		Burnup (MWD/MTU)		Theory-Experimental / Experimental
		Experimentel (from ^{148}Nd)	Theory (heavy isotopes)	
E5	7	24,220	23,280	−3.9%
	9	19,100	18,612	−2.6%
E11	2	20,380	19,447	−4.6%
	4	23,450	22,775	−2.9%
	5	23,730	23,179	−2.3%
	7	24,010	23,038	−4.0%
	8	23,150	22,523	−2.7%
	9	19,050	18,480	−3.0%
L11	7	24,070	23,204	−3.6%
J9	7	24,950	24,189	−3.1%

Figures II.21, II.22 and II.23 show some of the least-square fitted curves of the relations /2/ together with the measured points, for the TRINO I case.

The experimental points for rod 2 and rod 3, both near a large amount of water and thus in a softer spectrum, do not show a neutron spectrum difference within experimental errors. There is some indication that the neutron spectrum of rod 1 is harder. For the ratios N^{49}/N^{25} two curves could be drawn; one through the points of rod 1 and one through the points of rod 2 and 3. More ^{239}Pu is formed systematically for rod 1. The same effect is strongly expressed for the N^{41}/N^{25} ratios, but much less for the N^{40}/N^{25} and N^{42}/N^{25} ratios.

The explanation of these effects is immediate: the production of ^{239}Pu and ^{241}Pu is determined by capture cross-sections which have important epithermal resonance contributions. This

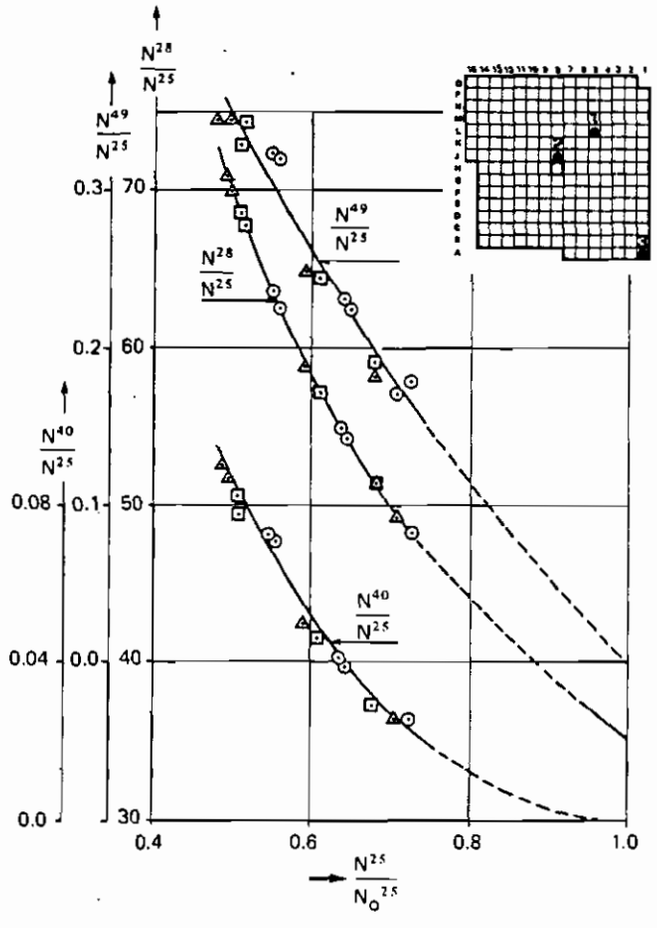

O rod 1 (asymp. spectrum)
□ rod 2 (near central water wall)
△ rod 3 (corner rod)

Fig. II.21. Isotopic ratios versus N^{25}/No^{25} (TRINO I).

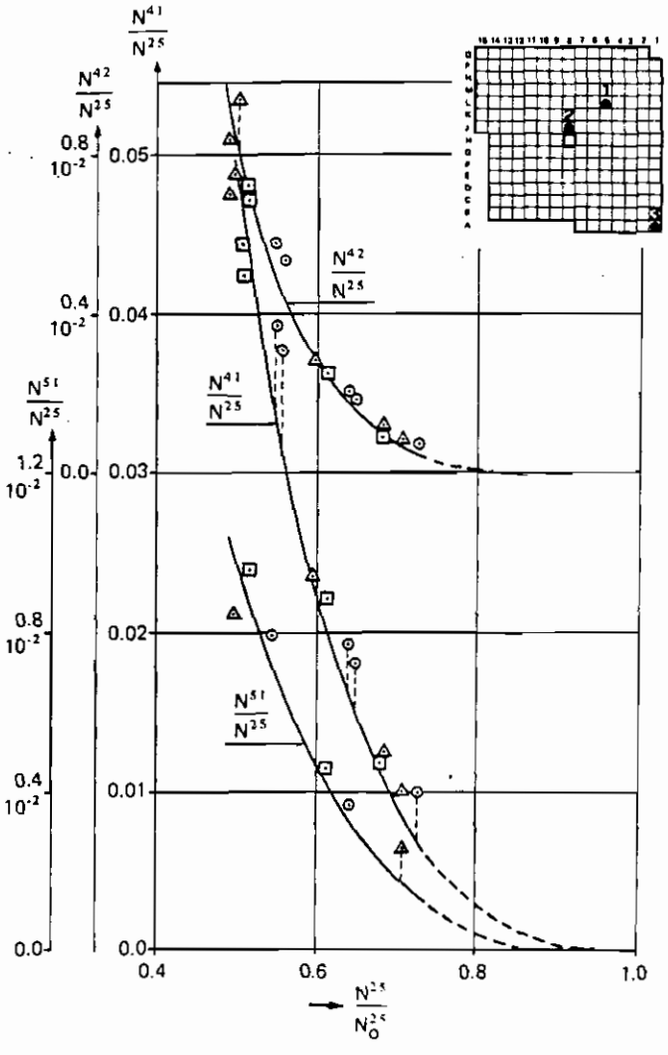

O rod 1 (asymp. spectrum)
□ rod 2 (near central water wall)
△ rod 3 (corner rod)

Fig. II.22. Isotopic ratios versus N^{25}/No^{25} (TRINO I).

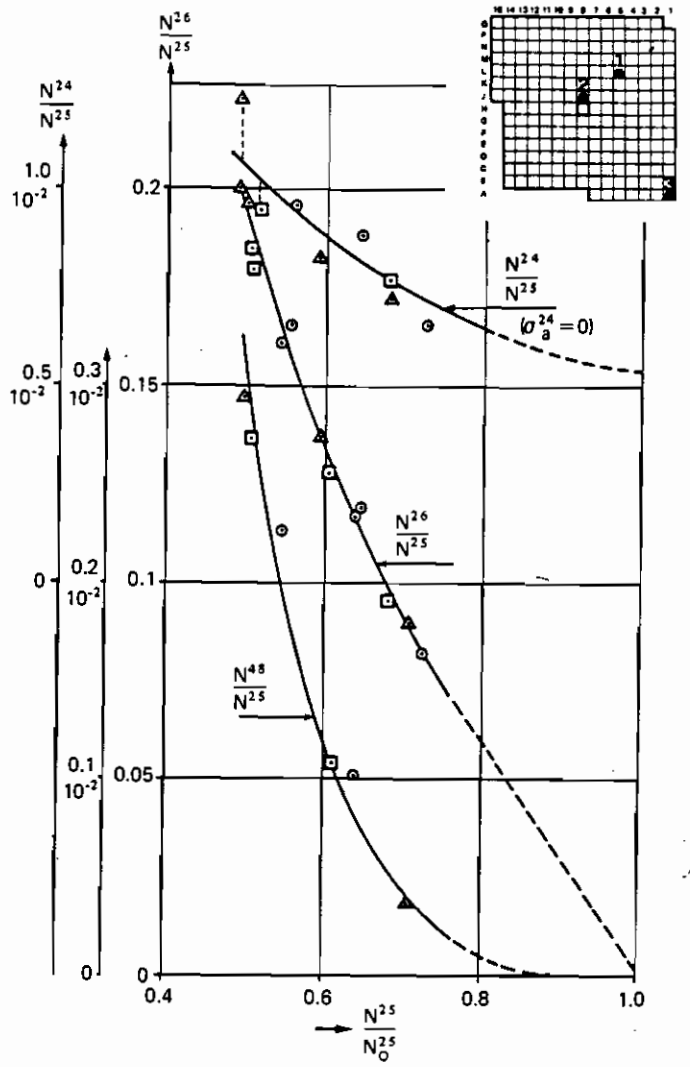

○ rod 1 (asymp. spectrum)
□ rod 2 (near central water wall)
△ rod 3 (corner rod)

Fig. II.23. Isotopic ratios versus N^{25}/No^{25} (TRINO I).

determines a strong spectrum sensitivity in the buildup of the two isotopes. So in the asymptotic position of rod 1 where the spectrum is harder, more Pu is found and detected by the fit. This will be even more evident when the use of isotopic correlation techniques on JRC data is illustrated.

In conclusion, the method developed by Matsen and taken up and revised at the JRC Ispra for the evaluation of cross-section ratios from experimental values certainly suffered from some limitations. For instance to consider the effective cross-section ratios constant with burnup (except $\hat{\sigma}_a^{40}/\hat{\sigma}_a^{25}$) introduces a systematic error which is more or less sizeable according to the different nuclides.

Future development of the code should involve a treatment of at least the $\hat{\sigma}_a^{49}/\hat{\sigma}_a^{25}$ ratio, with attention to its variation with burnup.

Furthermore, the parameters of the last isotopes in the nuclear chains are difficult to handle if they are not linked to a fixed value. This modification should also be carried out. But the code is certainly useful for the detection of errors in the input data as was the case of the evaluation of N_o^{26} for the two experimental sets of TRINO or the systematic discrepancy detected in the N^{26} data for TRINO II.

Another advantage is that this method can be applied successfully to a large range of fuel enrichment (uranium or plutonium fuelling) and reactor spectra, ensuring that the samples analysed have been irradiated in the same spectrum. Otherwise, when irradiated in different spectra, the samples should be fitted separately, giving different effective X-section ratios.

Moreover the code could help to set up collapsed cross-section libraries. If this were introduced as routine in larger codes one could evaluate collapsed cross-sections and check them on experimental values with the help of the code THEORY, as explained in the introduction to this section /48/.

4. Isotopic Correlations

As already mentioned in the introduction the Isotopic Correlation Technique (ICT) may play a fundamental role in the future of Safeguards.

The necessary requirements for this technique to be implemented are:

- development of a certain number of correlations giving accurate answers to certain safeguards questions (burnup, cooling time determination, isotope content, etc.);
- careful assessment of uncertainty levels of the technique;
- limits to its validity.

To answer these points:

- first verified computational methods have to be employed in order to develope usable and rigorous correlations answering to the different questions posed by Safeguards. Thus a selected use of ICT has to be made and a careful choice of correlations has to be performed, following the parameters to be investigated. As we will see in the following it is possible to use correlations which are sensitive to spectrum, or initial fuel enrichment, or fuel cooling time, etc.;
- The second step is to determine always through computational tools the application range of the developed correlations with respect to the parameters to be investigated;
- The third step is to verify the validity of the application through careful comparisons between computed and experimental correlations.

  This last step was one of the main objectives of the BM activity. It is, in fact, clear that only with certified, accurate and traceable (easy to calculate) data, an exercise of comparison with ICs and of implementation of ICs can be performed. It was not the aim of the BM to cover the two preliminary steps: i.e. identification and range of validity

of certain ICs. This task was pursued in another sector of our Institute /51, 52/. But it is evident that, together with the use of ICs for checking the data, the ICs themselves were in a certain sense conversely "checked" by BM data. It is also worthwhile mentioning that all BM values referred to pellets and this could be a limitation of our data sets: it is in fact sometimes difficult to transfer pellet results to batches (constituted by one or more fuel elements). Anyway also in this case the fundamental role of BM data in the assessment of methods remains evident.

The structure of this section will be as follows:

1) use of ICT for a data consistency check;
2) choice of different isotopic correlations for investigations of physical parameters.

1. Data consistency check

The consistency check of the BM data was performed simply by plotting the data on curves representing correlations between experimental values. When the data belonged to the same fuel element and represented the same spectrum, this analysis made it possible to identify points fitting poorly with the remaining ones of the set.

When the samples were from different fuel elements or different reactors, they frequently had to be plotted on separated curves, functions of their initial enrichments, moderating ratios (i.e. spectrum), reactor type, etc. Examples of this first level of interpretation are given in Figs. II.24 - II.26, where the correlations between different heavy elements or fission product ratios are shown.

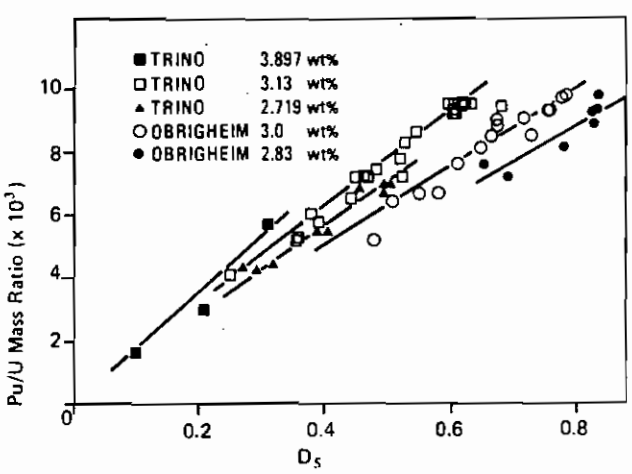

Fig. II.24. Correlation between Pu/U mass ratio and D_5 for all PWR samples analised at JRC

In Fig. II.24 the Pu/U mass ratio is plotted vs the ^{235}U depletion D_5, ($D_5 = (W_o - W^5)/W_o^5$) respectively for TRINO VERCELLESE and OBRIGHEIM fuel samples.

The different enrichments are put clearly in evidence by the curves and only a few perturbed points are badly correlated.

In Fig. II.25 the correlation between $^{235}U/^{238}U$ and $^{240}Pu/^{239}Pu$ is shown again for TRINO and OBRIGHEIM samples. It is obvious how the different spectrum in the two reactors affects the data. There is in fact a tendency to increase the slope with increasing initial enrichment, but the OBRIGHEIM data are systematically lower than those from TRINO, due to the lower moderation ratio of this second reactor (harder spectrum).

In Fig. II.26 for the same two batches of samples the correlation between $^{235}U/^{238}U$ vs D_5 is shown.

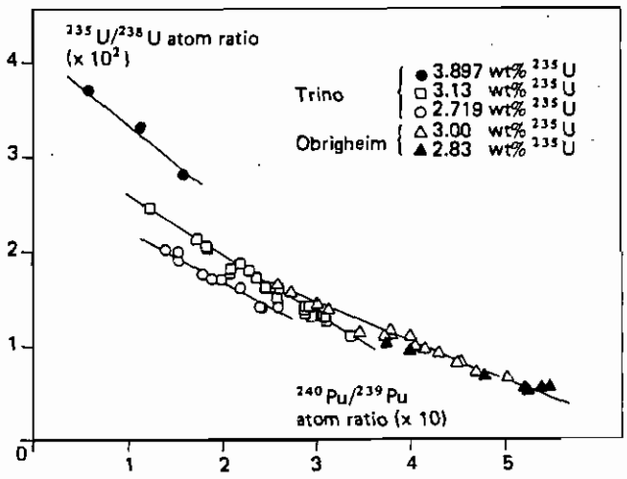

Fig. II.25. Correlation between $^{235}U/^{238}U$ and $^{240}Pu/^{239}Pu$ atomic ratios for all PWR samples analised at JRC

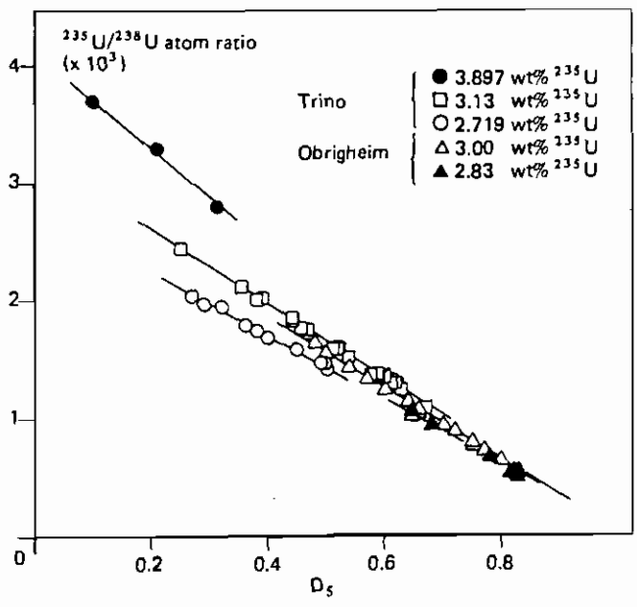

Fig. II.26. Correlation between $^{235}U/^{238}U$ atomic ratio and D_5 for all PWR samples analised at JRC

2. Physical parameters investigation

Spectrum

The above elaboration method has been mostly used for PWRs because the experimental data of PWRs normally refer to samples coming from asymptotic or weakly perturbed positions in the fuel assembly.

The situation with BWRs is slightly different The discussion of the analytical data of BWR samples is sometimes quite difficult due to the complex spectrum structure within the assembly.

Axial and radial spectrum variations determine the fact that the samples of BWR assemblies are normally quite heterogeneous. A few of them have been actually irradiated in the same spectrum (i.e. the effective neutron cross-sections vary from group to group of samples according to their radial and axial position in the bundle).

Both independent and dependent spectrum correlations could then serve to interpret and discuss the experimental data and to obtain information on the physical behaviour of cell parameters.

In Fig. II.27 the Pu/U mass ratio measured on samples of GUNDREMMINGEN BWR fuel element is plotted against the ^{235}U depletion. The different slopes of the curves follow

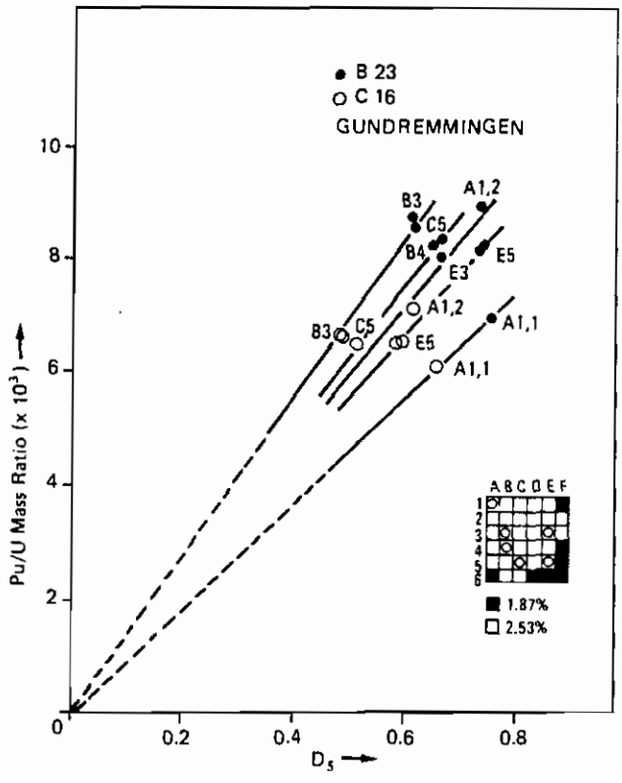

Fig. II.27. Correlation between Pu/U mass ratio and ^{235}U depletion for Gundremmingen BWR samples

the different Pu production rates of the fuel rods according to the spectrum hardening towards inner cluster zones. The sample correlate coherently with their position in the fuel element apart from sample B4 which should perhaps have been closer to the B3 line.

The considerable dispersion of the lines is due to the poor correlation between the ^{239}Pu quantity (around 65% of the total Pu) which is a ^{238}U resonance capture product, and the parameter D_5, linked to the absorption cross-section of ^{235}U which is less dependent upon the spectrum structure. These facts determine the strong dependence of the correlation Pu/U vs D_5 from the spectrum structure in the channel. The spectrum sensitivity of the correlation Pu/U vs D_5 can be applied to show up also minor perturbations due to irradiation in non-asymptotic positions of PWR samples. This is the case of TRINO I and II samples, as shown in Figs. II.28 and II.29 where the two sample batches have been correlated, keeping asymptotic and perturbed samples separated.

The same consideration can be applied to GARIGLIANO BWR fuel samples. In Fig. II.30 the Pu/U results of the first campaign are plotted in correlation with D_5, showing the

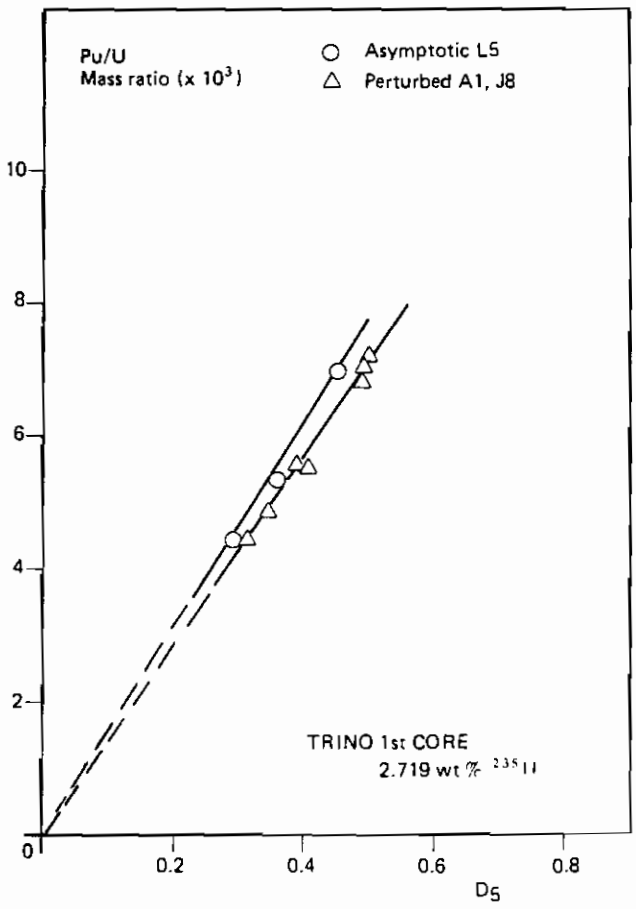

Fig. II.28. Correlation between Pu/U mass ratio and D_5 for asymptotic and perturbed TRINO II samples

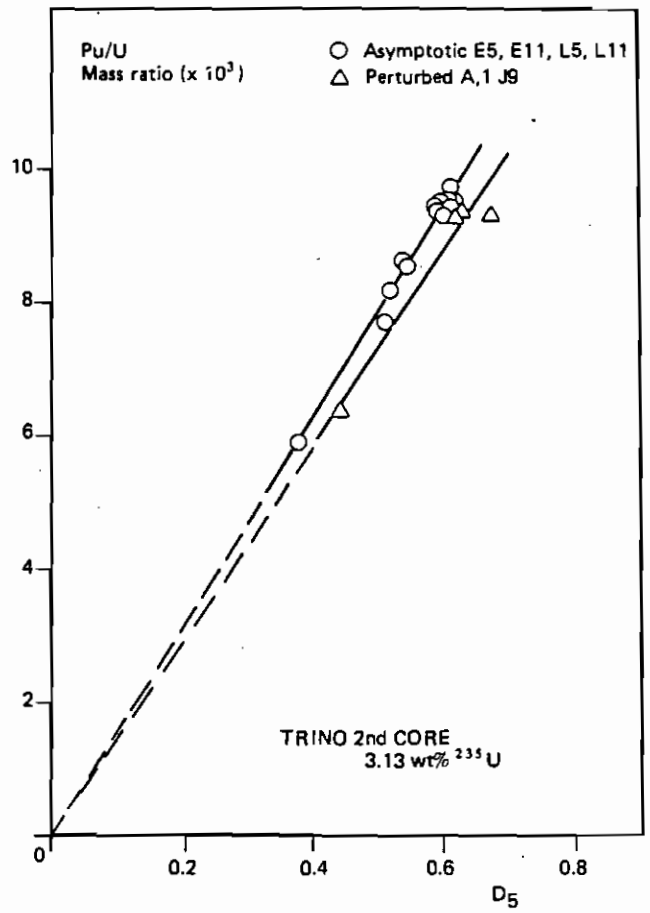

Fig. II.29. Correlation between Pu/U mass ratio and ^{235}U depletion for TRINO II samples

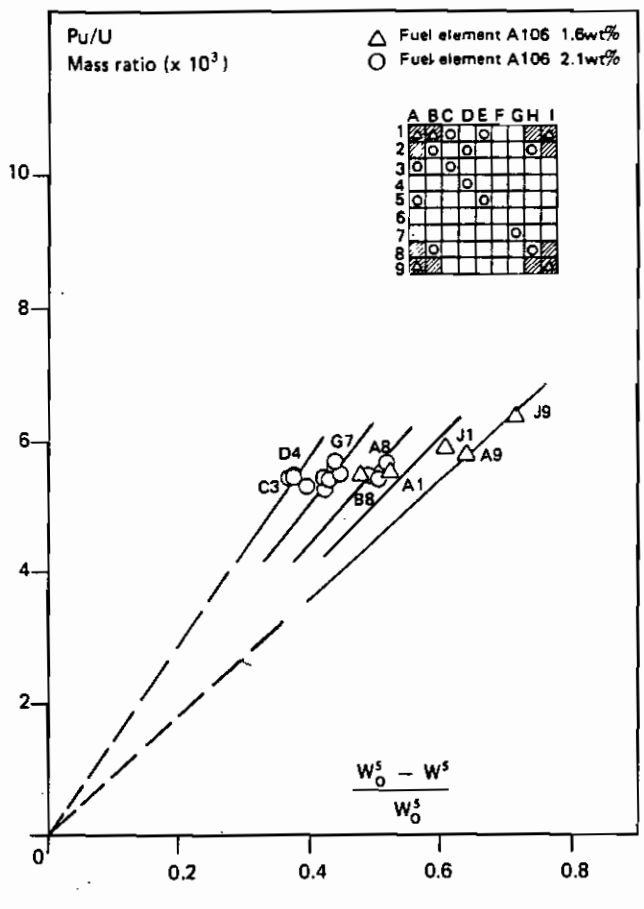

Fig. II.30. Correlation between Pu/u mass ratio and ^{235}U depletion for Garigliano I samples

same radial structure as before indicated for GUNDREMMINGEN data due to the radial spectrum variation. Figure II.31 gives Pu/U axial data from the second GARIGLIANO campaign and the structure of the different lines is now coherent with the axial spectrum variations following increasing void fractions.

In Fig. II.32 the ratio $^{236}U/^{238}U$ vs D_5 is presented for GUNDREMMINGEN and GARIGLIANO. This correlation appears to be less spectrum-dependent than the previous one. In fact the experimental points aggregate on the curve and it is practically impossible to separate them according to their radial position.

Another correlation which appears to be bad spectrum indicator (i.e. weakly spectrum-dependent) is shown in Figs. II.33 and II.34 where the ratio $^{240}Pu/^{239}Pu$ for GUNDREMMINGEN and GARIGLIANO samples is plotted versus the ratio $^{235}U/^{238}U$.

Burnup

One of the most important parameters to be evaluated for Safeguards purposes is the burnup of spent fuel. Even though

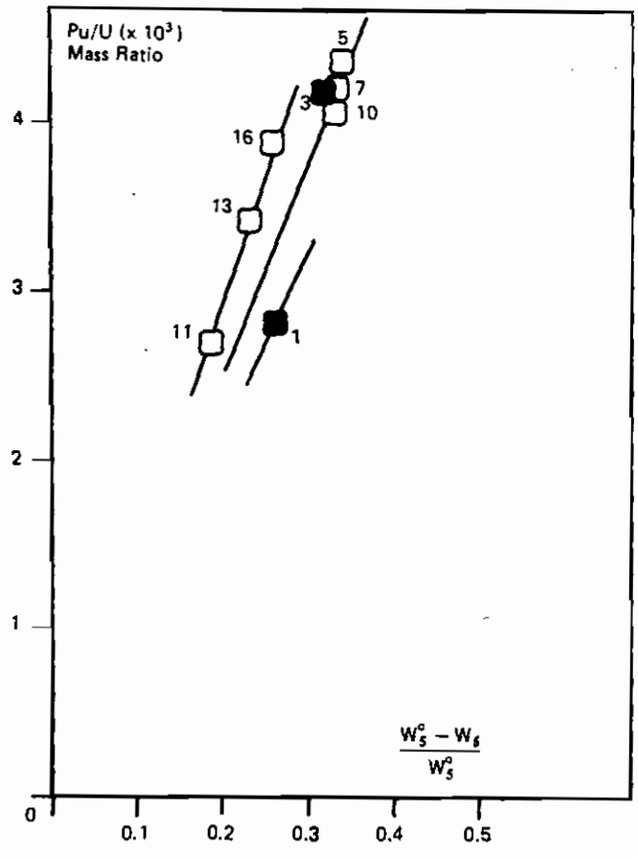

Fig. II.31. Correlation between Pu/u mass ratio and ^{235}U depletion for Garigliano II samples. The cutting position of the samples is indicated (see fig. I.7.)

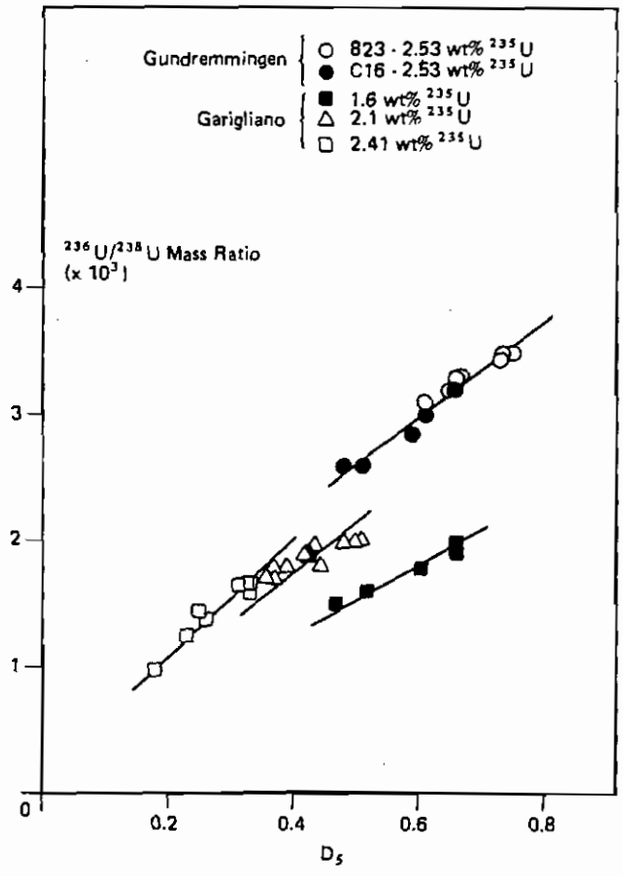

Fig. II.32. Correlation between $^{236}U/^{238}U$ mass ratio and D_5 for all BWR samples analysed at JRC

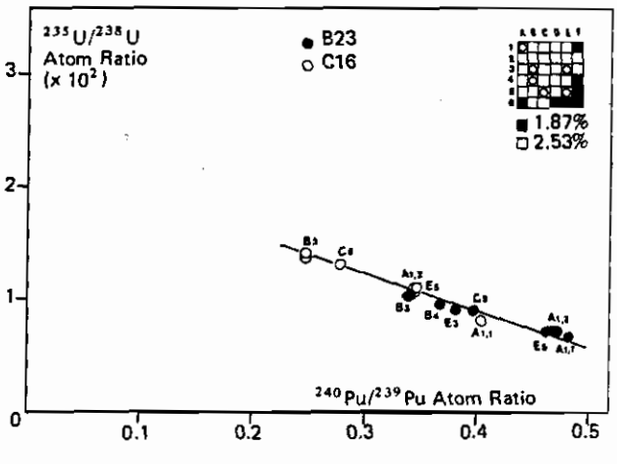

Fig. II.33. Correlation between $^{235}U/^{238}U$ and ^{240}Pu atomic ratios for Gundremmingen samples

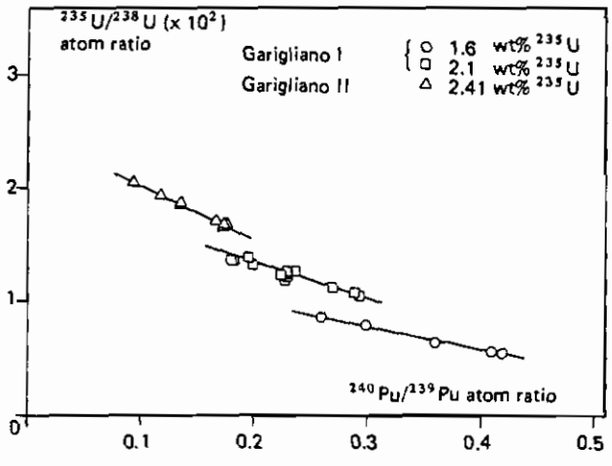

Fig. II.34. Correlation between $^{235}U/^{238}U$ and $^{240}Pu/^{239}Pu$ atomic ratios for Garigliano samples

the burnup is not directly required, it is of fundamental importance for the evaluation of strategic parameters such as Pu content or Pu/U ratios.

It must be stressed once again that concerning the Safeguards aspects of ICT only a few points will be dealt with here, since it was not the direct task of the BM to assess ICT as a Safeguard tool. We were only concerned with this matter indi-

rectly and the purpose of the following discussion is to outline some possible uses and the importance of the BM data in the ICT assessment.

The problem of destructive determination of the burnup of well-identified fuel batches (samples or fuel elements) is in principle almost solved without major uncertainty. From the ^{148}Nd determination, for instance, burnup values with error limits of 1 - 1.5% are attainable (see section II.2). The difficulties arise in the practical aspects. Lengthy sampling and measuring times leading to results that are available only weeks or months after sampling, and the loss of identity of the fuel elements after dissolution with the resulting need to re-evaluate the average burnup.

The use of ICs for non-destructive evaluation of burnup is therefore an interesting study to pursue. The most promising correlations for the determination of burnup are those which make use of fission product activities. Berg et al. /51/ have calculated the dependence of the correlations $^{134}Cs/^{137}Cs$

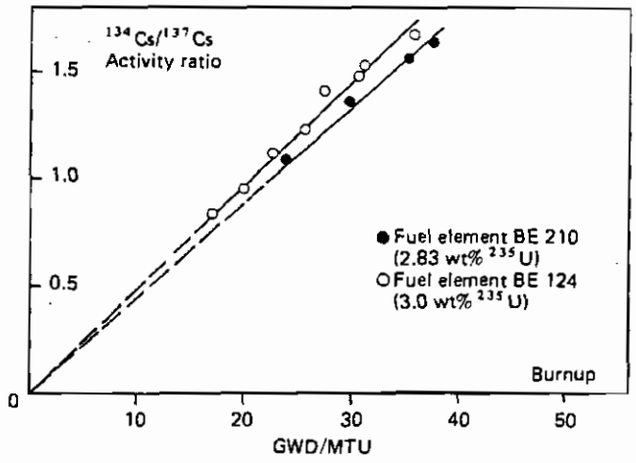

Fig. II.35. Correlation between $^{134}Cs/^{137}Cs$ activity ratio and burnup for Obrigheim samples

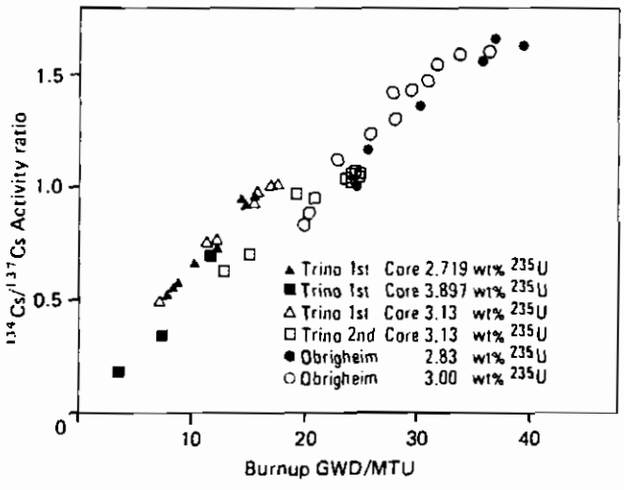

Fig. II.36. Correlation between $^{134}Cs/^{137}Cs$ activity ratio and burnup for all PWR fuel samples analysed at the JRC

ratio vs burnup and $^{154}Eu/^{137}Eu$ vs burnup with different parameters such as moderation ratio (i.e. spectrum) specific power, initial enrichment ratio.

It is obvious (Fig. 8 of the report quoted) that the spectrum variations strongly influence the $^{134}Cs/^{137}Cs$ ratio.

A marked departure from linearity at high burnups is also evident. Experimental evidence for these effects is found in Figs. II.35 - II.38. In Fig. II.35 the correlation is presented for OBRIGHEIM PWR fuel elements. The marked difference in initial enrichments can be seen clearly.

The departure from linearity is not so evident but it can be recognised in Figs. II.36 and II.37 where all JRC data relating to PWRs and BWRs are presented separately.

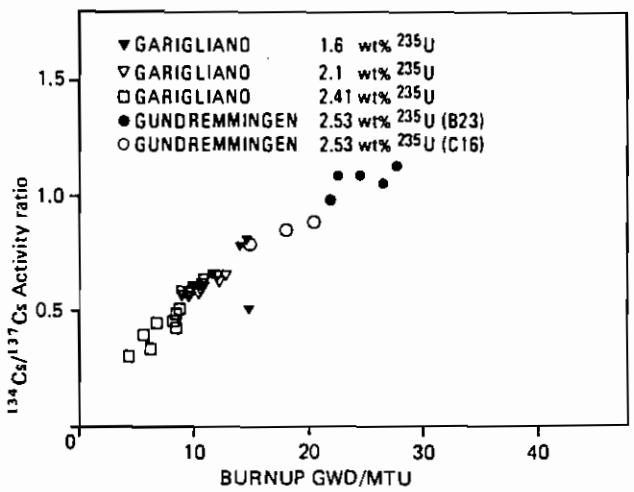

Fig. II.37. Correlation between the activity ratio $^{134}Cs/^{137}Cs$ and burnup for all BWR fuel samples analysed at the JRC

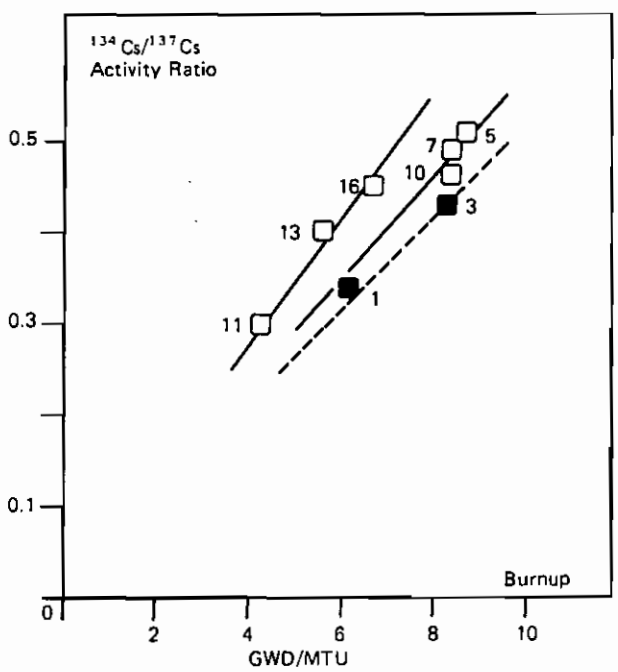

Fig. II.38. Correlation between $^{134}Cs/^{137}Cs$ activity ratio and burnup for Garigliano II fuel samples. The cutting position of the samples is indicated (see fig. I.7.)

The spectrum sensitivity of the correlation is also illustrated in Fig. II.38 where the axial values of a GARIGLIANO rod are plotted. The important epithermal structure of the ^{133}Cs capture cross-section makes in effect the ^{134}Cs production sensitive to spectral conditions.

Less sensitive to spectrum, power density, or power history is the correlation $^{154}Eu/^{137}Cs$ vs burnup, as Foggi calculated and as shown in Fig. II.39 by experimental data.

Very good correlation is also found between burnups derived from ^{148}Nd and ^{137}Cs, as shown in Fig. II.40, where all the JRC data are plotted. A slope of 1.003 is found and an intercept of 0.03 which demonstrate an excellent correlation and linearity of the curve over the entire burnup range. The ^{137}Cs data were destructive data produced atJRC on the same pellets used for all the analysis. Some problems arise in the application of the non-destructive determination of ^{137}Cs due to the absence of normalization terms, to Cs migration, to γ-attenuation, etc.

Recent studies /13, 15, 16/ have been devoted to correlate passive neutron emission of spent fuels with their burnup. As a contribution to these studies the measured uranium, plutonium, curium and americium isotopes buildups reported at reactor shut-down for the fuel pellets analysed were elaborated in order to obtain the spontaneous neutron emission from each isotope at different cooling times.

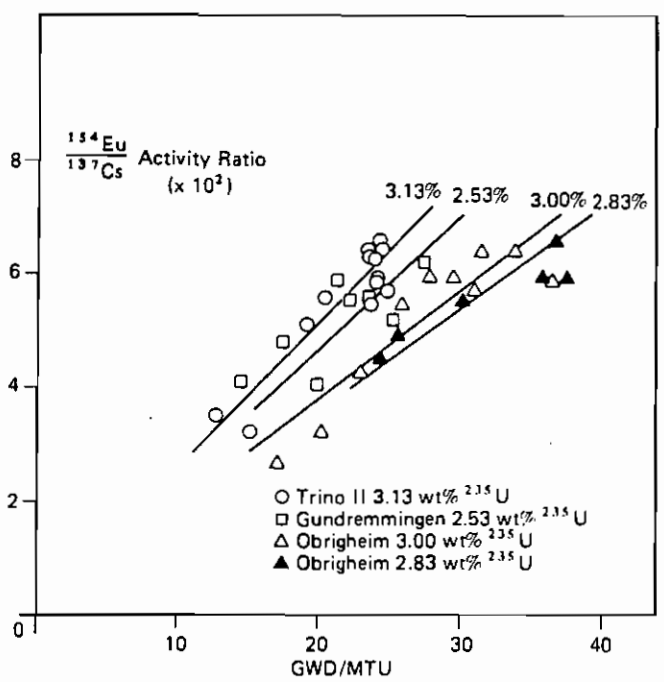

Fig. II.39. Correlation between $^{154}Eu/^{137}Cs$ activity ratio and burnup

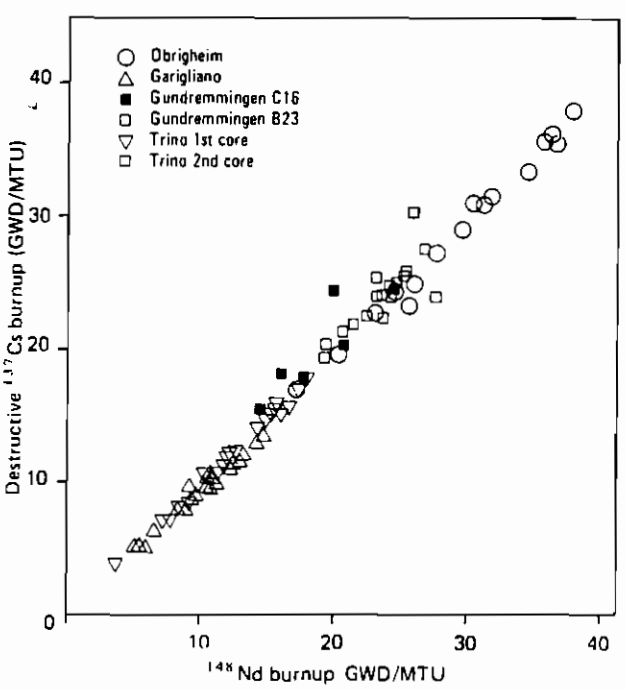

Fig. II.40. Correlation between destructive ^{137}Cs burnup and ^{140}Nd burnup for all samples analysed at the JRC

Table II.33 gives the values of specific spontaneous neutron emission from UO_2 fuel, adopted in this work /53/.
In Fig. II.41 the passive-neutron emission after one year of cooling is shown for all the samples analysed at JRC.

A careful analysis of the results showed up some problems still to be solved before the technique could be applied with great accuracy:

- the correlation is noticeably non-linear over the entire burnup range, due to the isotope evolution during irradiation, which is not at all linear. This conclusion is valid both at low and high burnup, where different isotopes are responsible for the main neutron emission, necessitating the use of interpolation curves of different orders /14-16, 54/;
- the spectral conditions also influence to some extent the correlation, as shown by the difference between BWR and PWR results;
- the fuel irradiation history also affects the correlation at least at short (1-2 years) cooling times, where the emission is dominated by ^{242}Cm. This fact is demonstrated in Figs. II.42 and II.43, where for two different burnups the sharing of neutron emission amongst the various isotopes is shown as a function of cooling times.

In spite of the drawbacks presented by this technique, passive neutron detection for spent fuel burnup evaluation remains particularly attractive in view of the various advantages it presents with respect to γ-detection techniques. This was already pointed out in the general introduction.

TABLE II.33. Specific spontaneous neutron emission in UO_2, PuO_2

Source α and SF	Neutrons/ g. sec		
	n_{SF}	$n_{\alpha,n}$	$n_{tot.}$
^{235}U	5.12×10^{-4}	1.11×10^{-3}	1.62×10^{-3}
^{238}U	1.14×10^{-2}	1.33×10^{-4}	1.15×10^{-2}
^{238}Pu	2.51×10^{3}	1.84×10^{4}	2.09×10^{4}
^{239}Pu	2.20×10^{-2}	4.00×10^{1}	4.02×10^{1}
^{240}Pu	9.14×10^{2}	2.01×10^{2}	1.11×10^{3}
^{241}Pu		1.96	1.96
^{242}Pu	1.68×10^{3}	2.87	1.68×10^{3}
^{242}Am	1.50×10^{2}		
^{241}Am	5.97×10^{-1}	3.64×10^{3}	3.64×10^{3}
^{242}Cm	2.13×10^{7}	4.75×10^{6}	2.60×10^{7}
^{244}Cm	1.11×10^{7}	1.03×10^{5}	1.12×10^{7}

n_{SF} neutrons from spontaneous fissions
$n_{\alpha,n}$ neutrons from (α, n) reactions

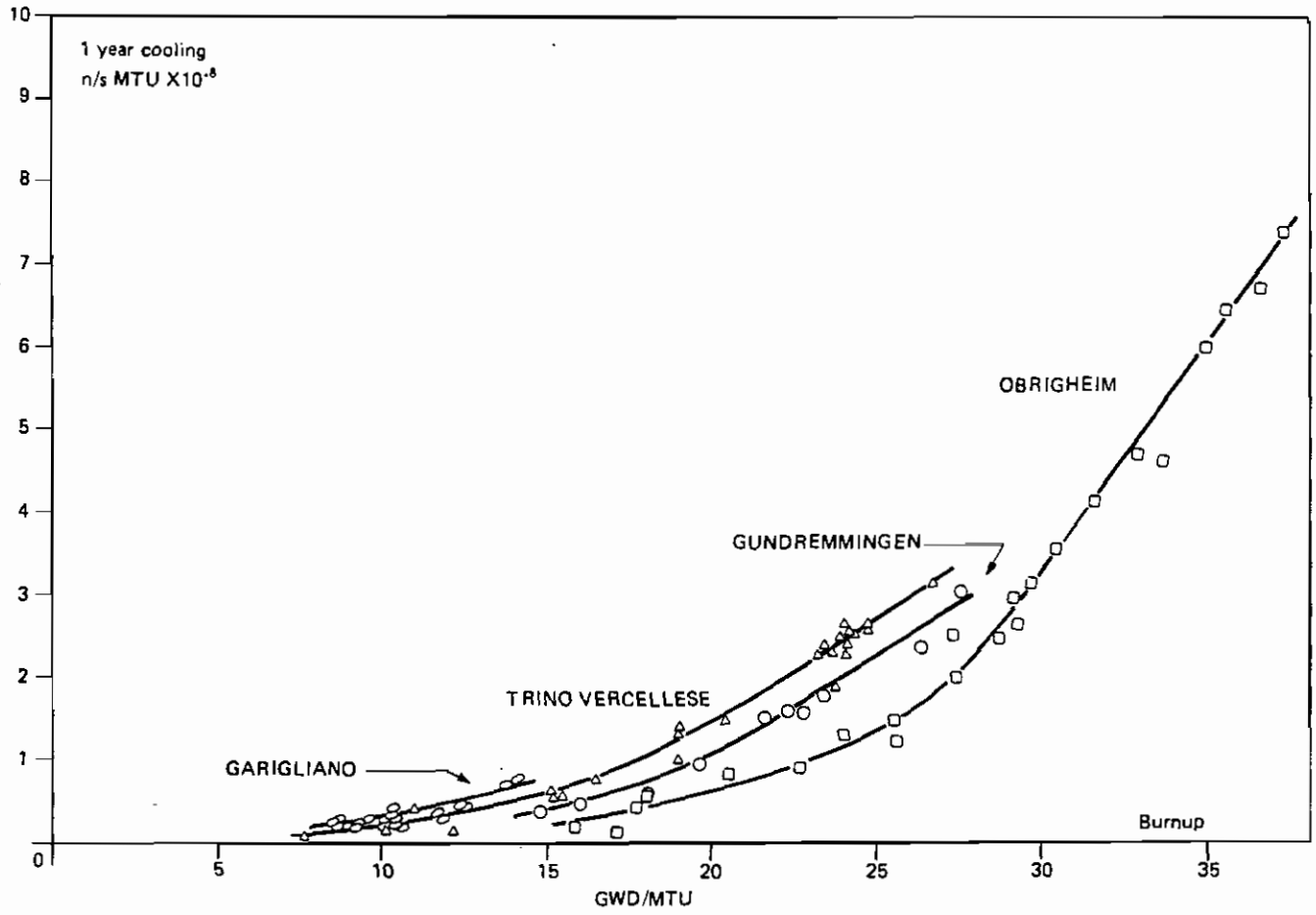

Fig. II.41. Correlation between passive neutron emission and burnup obtained after 1 year of cooling for samples from 4 reactor fuels.

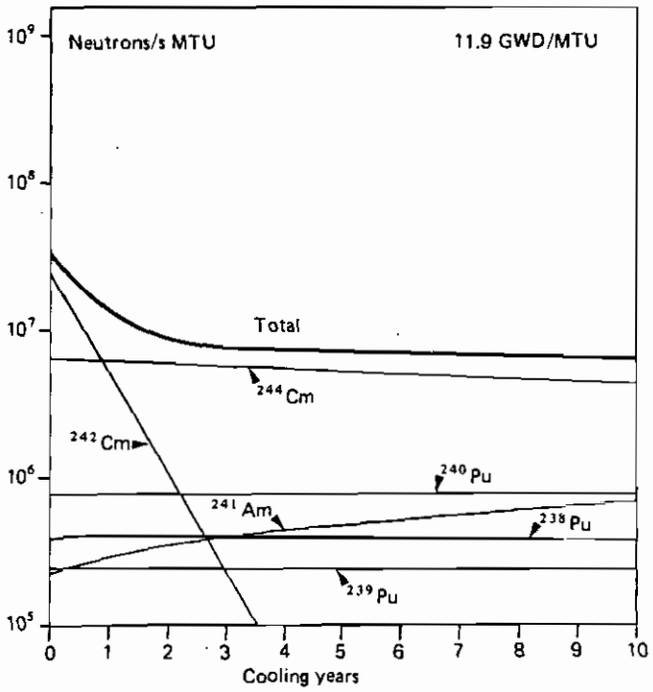

Fig. II.42. Spontaneous neutron emission from different heavy isotopes at a burn up to 11.9 GWD/MTU.The total emission also includes the contribution of the other isotopes listed in Table II.33.

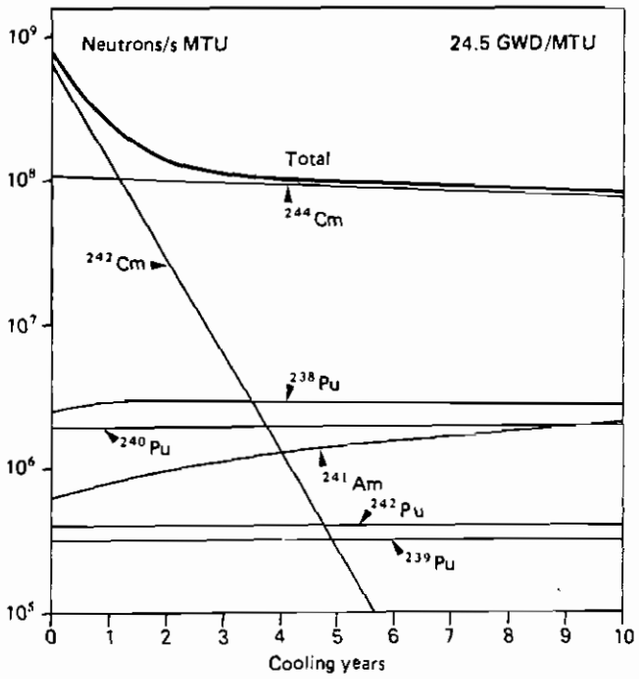

Fig. II.43. Spontaneous neutron emission from different heavy isotopes at a burn up of 24.5 GWD/MTU. The total emission also includes the contribution of the other isotopes listed in Table II.33.

Initial enrichment

Some of the correlations used are sensitive to initial enrichment and can give information on this parameter. The correlation between Pu/U and D_5 already mentioned as a good spectrum indicator is also sensitive to initial enrichment. In Fig. II. 24 the experimental results for three TRINO and two OBRIGHEIM enrichments are shown. The increasing slope of the straight line with increasing initial enrichment (see also ref. 51) has already been pointed out.

Another correlation directly linked with the initial enrichment is $^{235}U/^{238}U$ vs $^{240}Pu/^{239}Pu$ (Fig. II. 25) which extrapolated to zero burnup, should give the initial $^{235}U/^{238}U$ ratio supposed known. The curves interpreted as straight lines give an intercept systematically lower (between 5 and 10%) than the declared ones; the conclusion is that, at least for values covering large burnup ranges, the correlation should possibly be interpreted by higher order curves. For very low burnup batches the curve can be interpreted as a straight line but in any case the extrapolation uncertainty is likely to be higher than acceptable.

Correlations involving Pu and/or U isotopes

Many correlations involving total Pu and/or total U or some of their isotopes have been studied. Some have already been discussed as Pu/U vs burnup or $^{235}U/^{238}U$ vs $^{240}Pu/^{239}Pu$. A few words may also be written on other possible correlations. In Fig. II. 26 the $^{235}U/^{238}U$ vs D_5 plot is shown for all PWR data and the correlation indicates a low spectrum sensitivity but a marked sensitivity to the initial enrichments.

An extrapolation of this correlation should give the initial amount of ^{235}U but the same uncertainties could be introduced as in the case of the $^{235}U/^{238}U$ vs $^{239}Pu/^{240}Pu$ extrapolation.

Nevertheless an attempt to derive the ^{235}U amount for TRINO II batches for extrapolation purposes gave reasonably similar values than those calculated by the code THEORY previously mentioned.

5. Comparison with Calculated Values

Again, in order to characterize at least the Bench Mark data, during the final period of the activity, a comparison between measured and calculated heavy isotope vectors was carried out. The activity was performed jointly with the project of Assessment of Nuclear Transmutation of Actinides /55, 56/ using the codes adopted for this activity to recalculate the BM experimental data.

The codes used were:

- LASER: one dimension, multigroup, burnup, transport cell code /44/;
- RIBOT: a zero dimension multigroup diffusion burnup code /57/.

The comparison exercise will not be described here in detail nor will the characteristics of the two codes be given: extensive information on these aspects can be found in /56, 58/. The aim of this chapter is simply to show how the experimental BM values fit with the calculated ones.

The reactors chosen for this exercise were TRINO VERCELLESE and OBRIGHEIM. The fuel elements analysed are shown in the following table.

Reactor	Fuel Assembly	Average Burnup (MWD/MTU)	^{235}U Enrichment (wt %)
TRINO VERCELLESE (PWR)	509-049	12,400	2.719
	509-032	14,200	3.13
	509-069	21,700	3.13
OBRIGHEIM (PWR)	BE 210	30,100	2.83
	BE 124	29,000	3.0

1. LASER results

The LASER version available at Ispra contained only actinide up to ^{242}Pu. The burnup calculation was very accurate considering small burnup steps (2-3 GWD/MTU each step); the energy group description in the code is detailed, having 50 groups in the fast and epithermal zone with a MUFT format, while in the thermal zone a THERMOS calculation is performed with a structure of 35 groups. LASER calculates accurately the spectrum variation with the burnup and takes into account non-linear effects due to exposure.
The spatial description considers a cell with a maximum number of 14 annular rings, with 5 rings in the fuel region.
The LASER cell geometry is given in Fig. II.44.
Some typical results of the comparison are given in Figs. II.45 and II.46 for TRINO VERCELLESE samples. The ^{239}Pu buildup (Fig. II.45) is correctly calculated and minor discrepancies are due to the spectrum perturbation suffered by some samples and it has already been shown how ^{239}Pu isotope is sensitive to spectrum shifts.
The Pu/U correlation is also shown in Fig. II.46 and again the agreement is excellent taking into account the spectrum

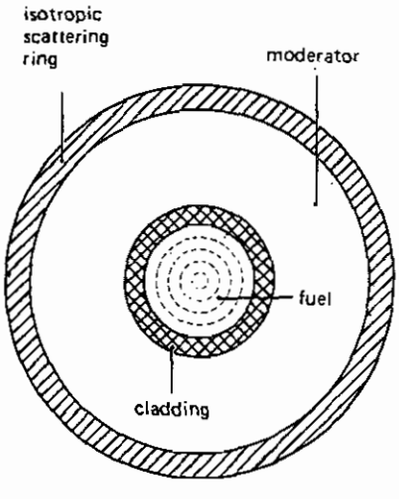

Fig. II.44. LASER cell geometry

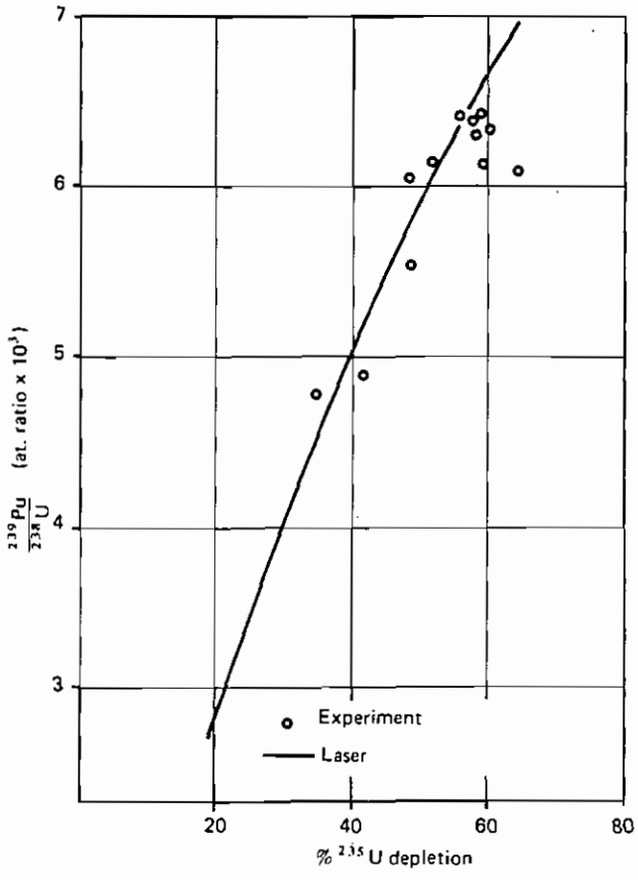

Fig. II.45. Trino Vercellese - ^{239}Pu buildup as a function of ^{235}U depletion.

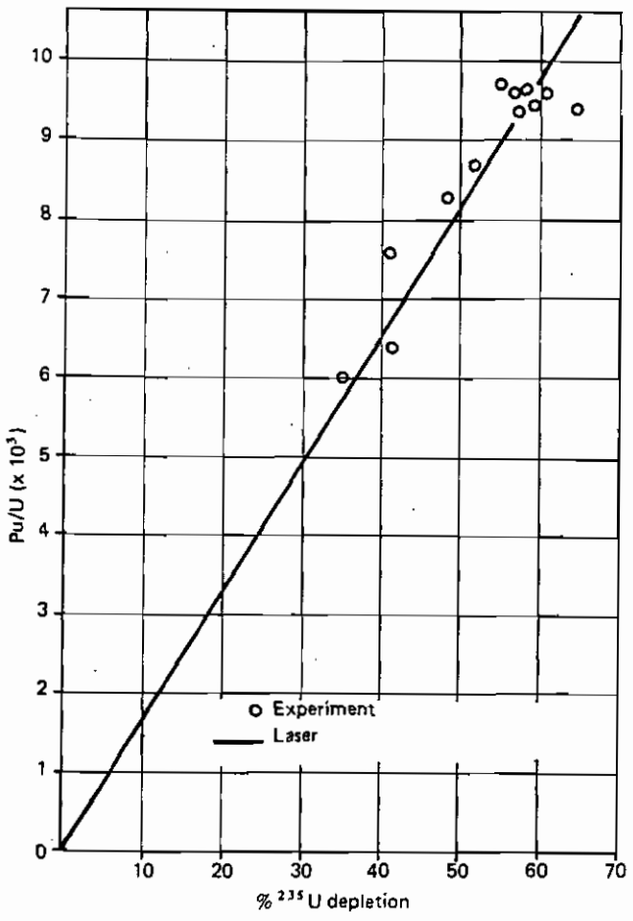

Fig. II.46. Trino Vercellese - Pu/U as a function of ^{235}U depletion.

perturbation. It is worthwhile mentioning here that all the calculations (LASER and RIBOT as well) were performed for the unperturbed cell and not for individual pellets.
So slight discrepancies introduced by the spectrum perturbations, mainly in Pu isotopes, are quite acceptable.

2. RIBOT results

The energy description in RIBOT is much less detailed: macroscopic parameters are calculated in 5 groups and a first order variation with burnup is achieved. An extensive series of comparisons has been performed with RIBOT. They are summarized in the following.
Figures II.47 to II.61 show the comparison between Bench Mark results and calculations performed on TRINO and OBRIGHEIM samples with respect to isotope buildup as a function of D_5 ($D_5 = (^{235}U_o - ^{235}U)/^{235}U_o$).

Burnup vs D_5 (Fig. II.47)

Based upon results obtained for all fuel elements either burn-up or D_5 may be used for comparison purposes. D_5 was chosen because RIBOT-5A was, under the circumstances described here, expected to be better in calculating the ^{235}U depletion than in calculating burnup.

Although the calculation of D_5 is assumed correct, a slight inaccuracy in the ^{235}U fission cross-section cannot be ruled out (see also paragraph 3 of this chapter where the THEORY calculations also suggested a possibly incorrect value of the ^{235}U fission to capture cross-section ratio).

^{236}U buildup

A systematic underestimation is shown in Fig. II.48, and confirmed for all fuel elements, possibly due to an insufficiently well defined ^{236}U capture cross-section. However, the isotopic buildup of ^{236}U is also dependent upon the ^{235}U fission cross-section /59/ and, as noted before, the ^{235}U fission cross-section could be slightly incorrect.

^{238}Pu buildup

As can be seen from Figs. II.49 and II.50 there was a considerable discrepancy between calculated and measured results, for both reactors.

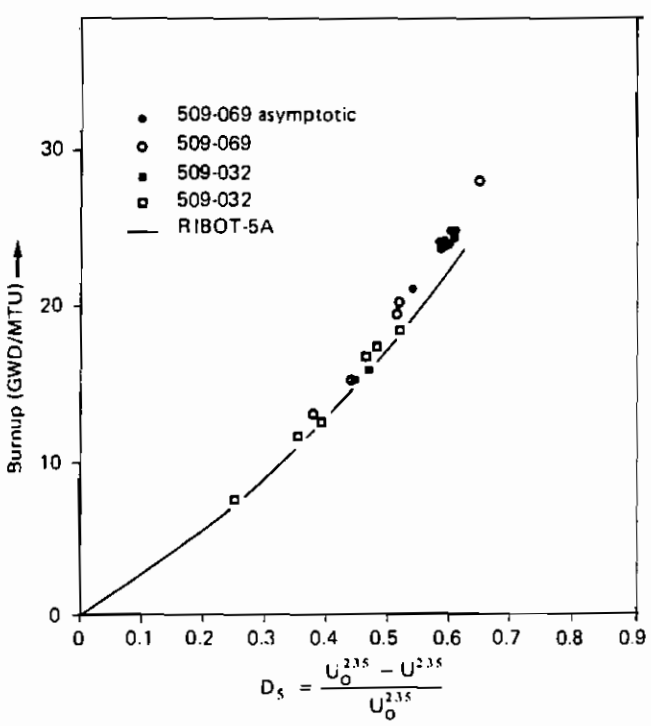

Fig. II.47. Comparison between calculated and experimental results for the Trino Vercellese reactor

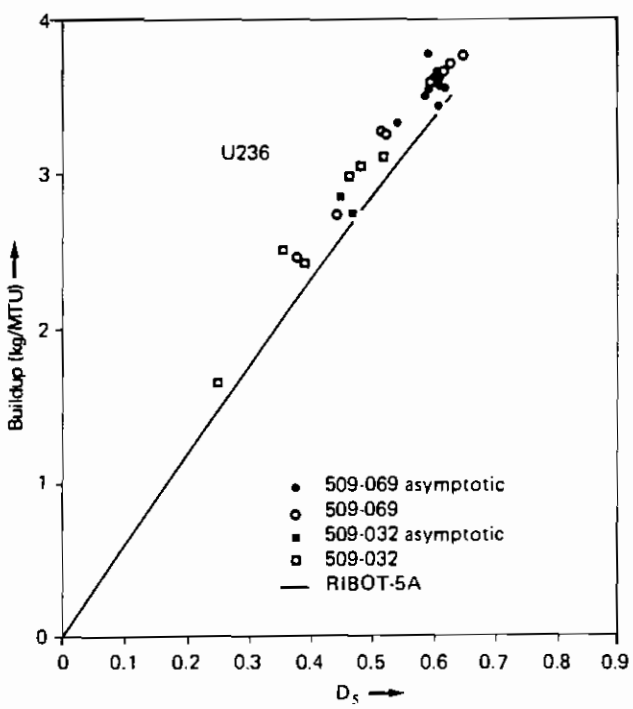

Fig. II.48. Comparison between calculated and experimental results for the Trino Vercellese reactor

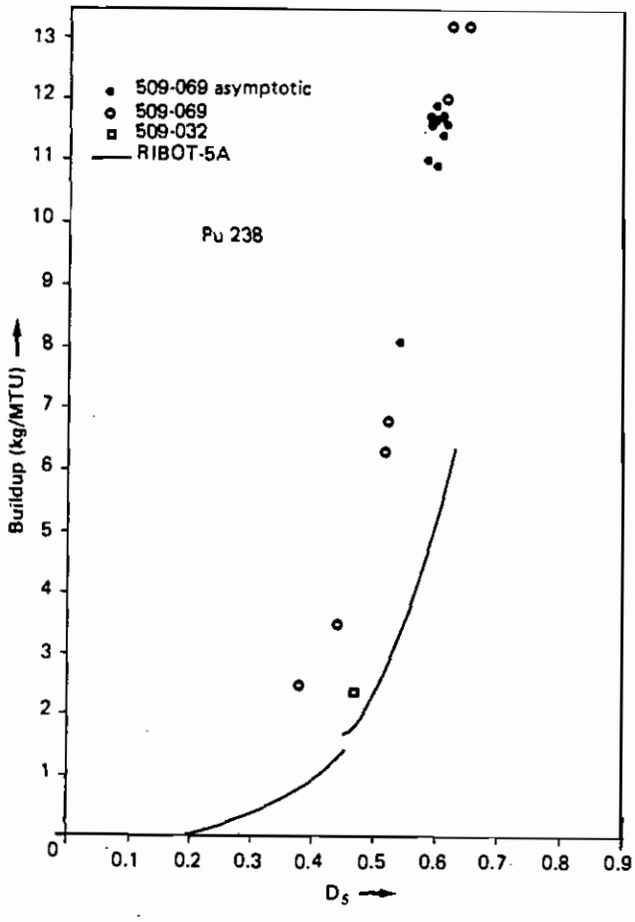

Fig. II.49. Comparison between calculated and experimental results for the Trino Vercellese reactor

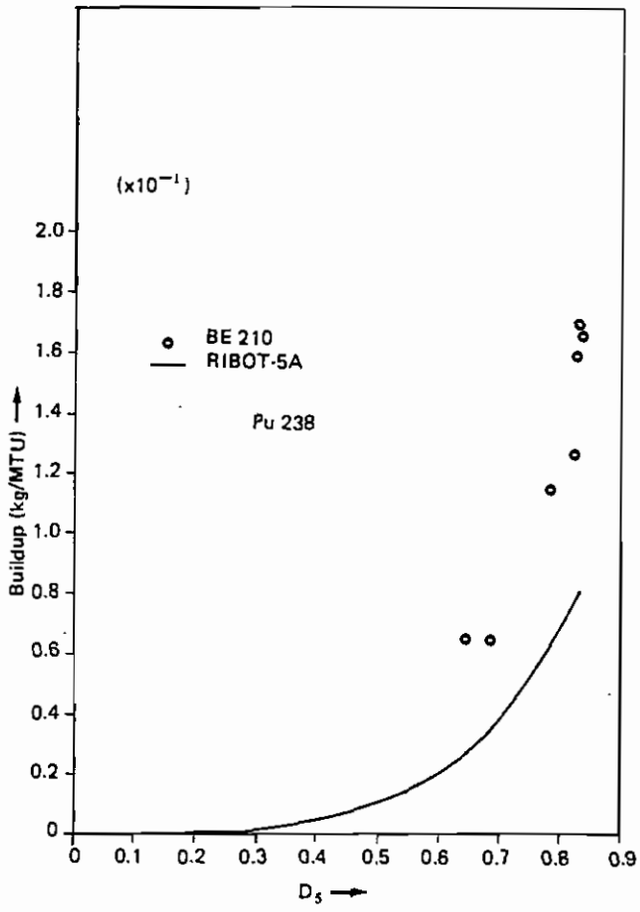

Fig. II.50. Comparison between calculated and experimental results for the Obrigheim reactor

A new value found in recent literature /60/ for ^{237}Np capture cross-section slightly improved the situation: the discrepancy from a factor 2 as shown in Figs. II.49 and II.50 went down to a factor 1.5, leaving other parameters essentially unchanged.

^{239}Pu, ^{240}Pu, ^{241}Pu, ^{242}Pu buildup

For all calculations performed (Figs. II.51 - II.54) the agreement was very good.

^{241}Am buildup

For all calculations performed the agreement was reasonable also remembering the high experimental error connected with the experimental points.

Mass spectrometry was employed specifically because of the difficulty in employing α-spectrometry for ^{241}Am.

Nevertheless a large experimental uncertainty is associated with the points, shown in Fig. II.55, making accurate comparison difficult.

See also chapter II.2 where an analysis of the experimental error was performed, and the discussion of the results in section III where this point is taken up again.

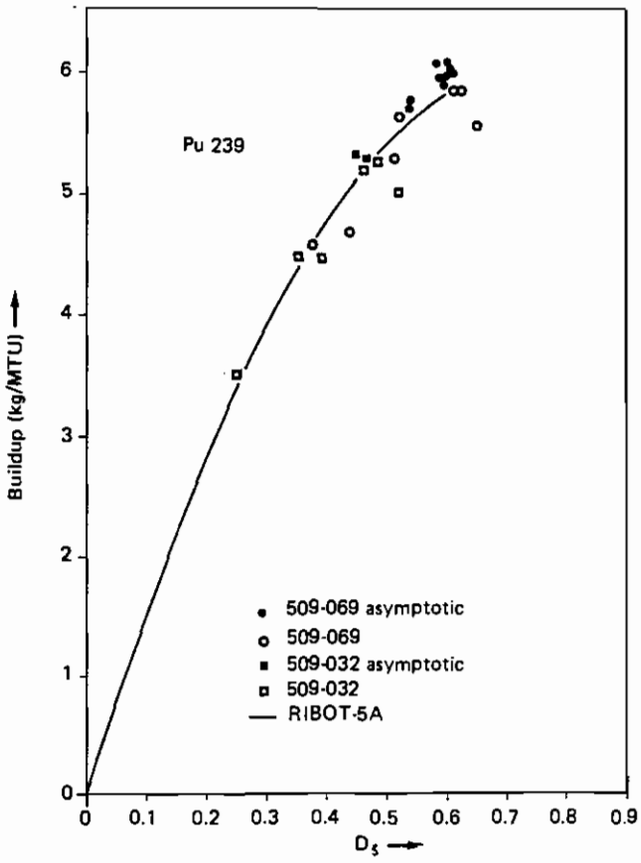

Fig. II.51. Comparison between calculated and experimental results for the Trino Vercellese reactor

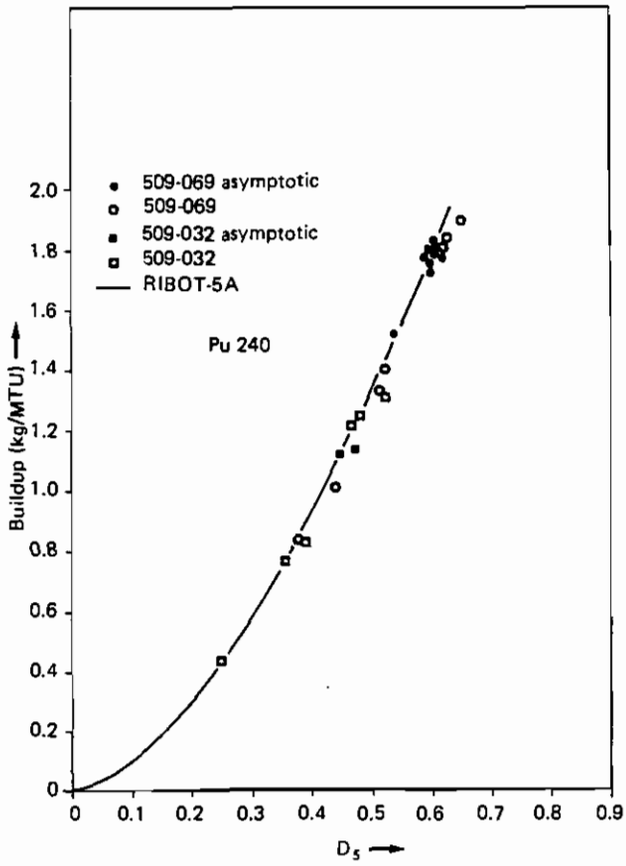

Fig. II.52. Comparison between calculated and experimental results for the Trino Vercellese reactor

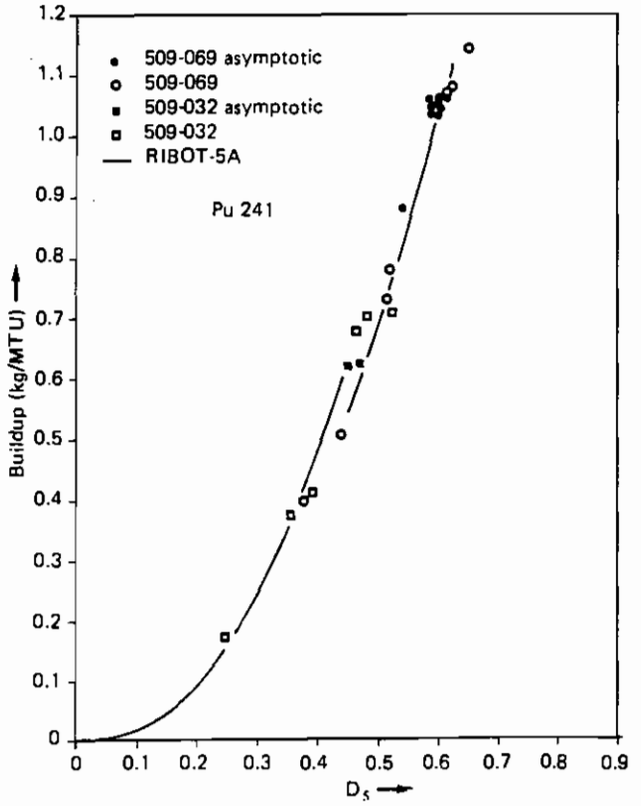

Fig. II.53. Comparison between calculated and experimental results for the Trino Vercellese reactor

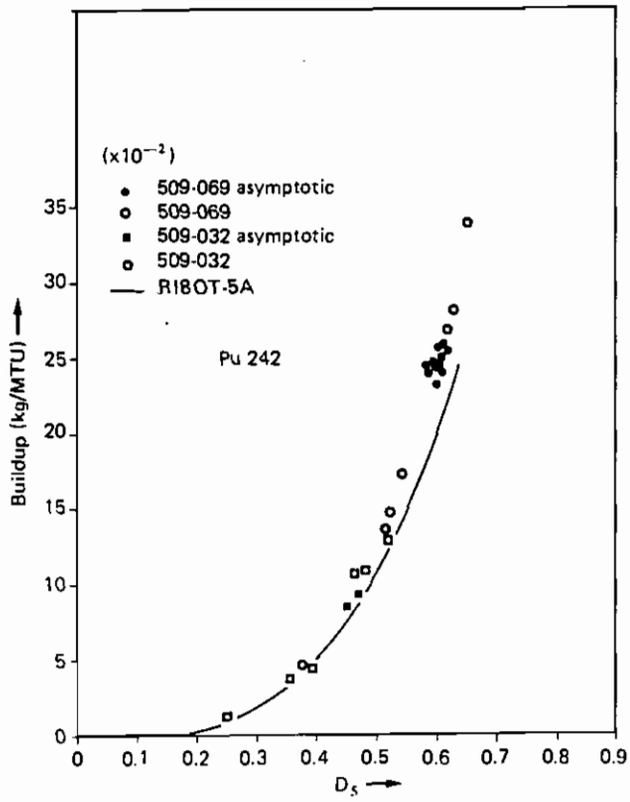

Fig. II.54. Comparison between calculated and experimental results for the Trino Vercellese reactor

^{242m}Am buildup

For all calculations performed the agreement was poor (Fig. II. 56), and the considerable experimental uncertainty associated with the spectrometry measurements performed makes an accurate comparison difficult.

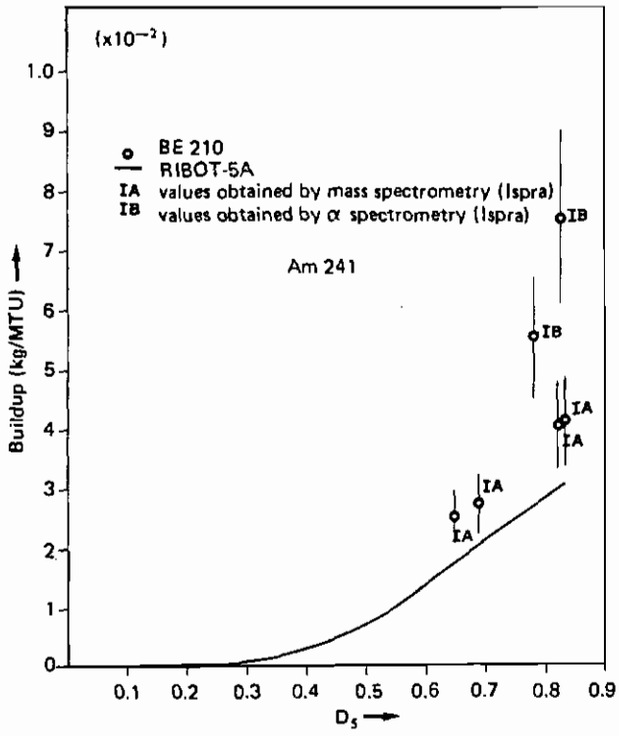

Fig. II.55. Comparison between calculated and experimental results for the Obrigheim reactor

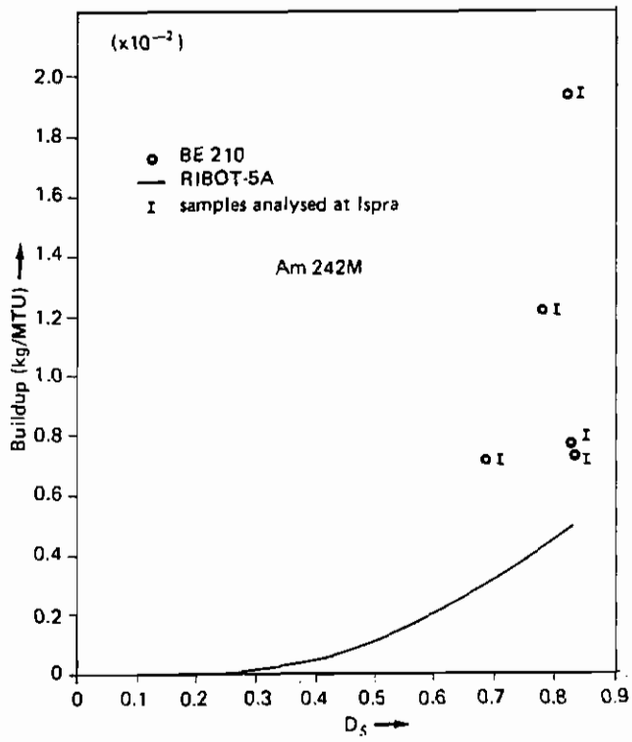

Fig. II.56. Comparison between calculated and experimental results for the Obrigheim reactor

^{243}Am buildup

For all calculations performed (see Figs. II. 57 and II. 58) the agreement was reasonable. The isotopic buildup of ^{243}Am is directly associated with ^{242}Pu and thus unaffected by the uncertainties associated with the other Am isotopes.

^{242}Cm buildup

For all calculations performed the agreement (Fig. II. 59) with α-spectrometry measurements performed at Ispra (I) was good. The two results performed by Karlsruhe (K), at least with respect to the RIBOT-5A calculations, would appear to be incorrect.

The same conclusion was drawn in paragraph 4 of this section dealing with the Ispra-Karlsruhe interlaboratory comparison.

^{244}Cm buildup

For all calculations performed (see Figs. II. 60 and II. 61.) agreement was reasonable. For all fuel elements studied RIBOT-5A overestimated the buildup of ^{244}Cm with respect to the α-spectrometry measurements performed both in Ispra and in Karlsruhe.

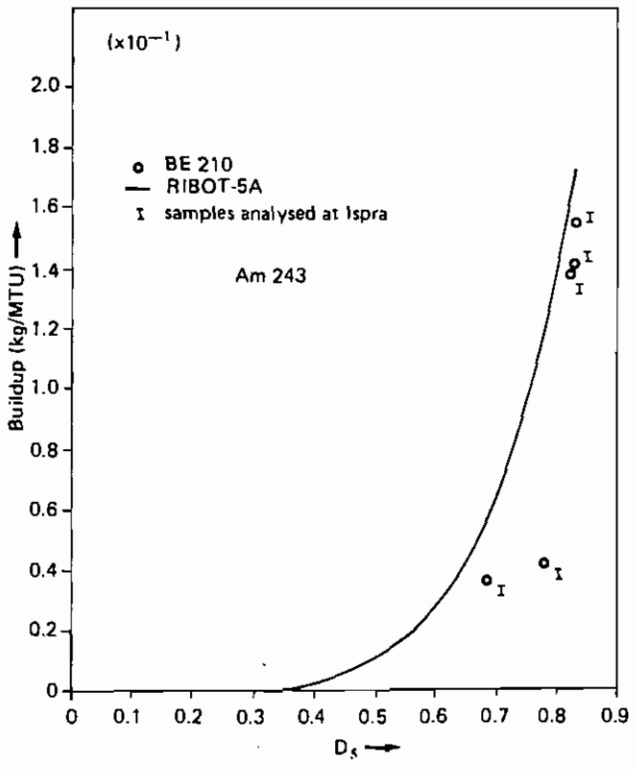

Fig. II.57. Comparison between calculated and experimental results for the Obrigheim reactor

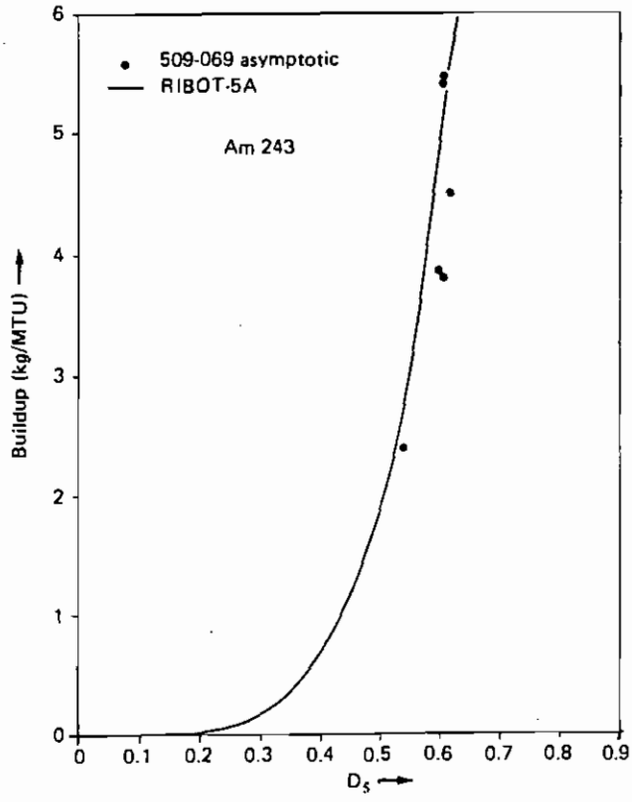

Fig. II.58. Comparison between calculated and experimental results for the Trino Vercellese reactor

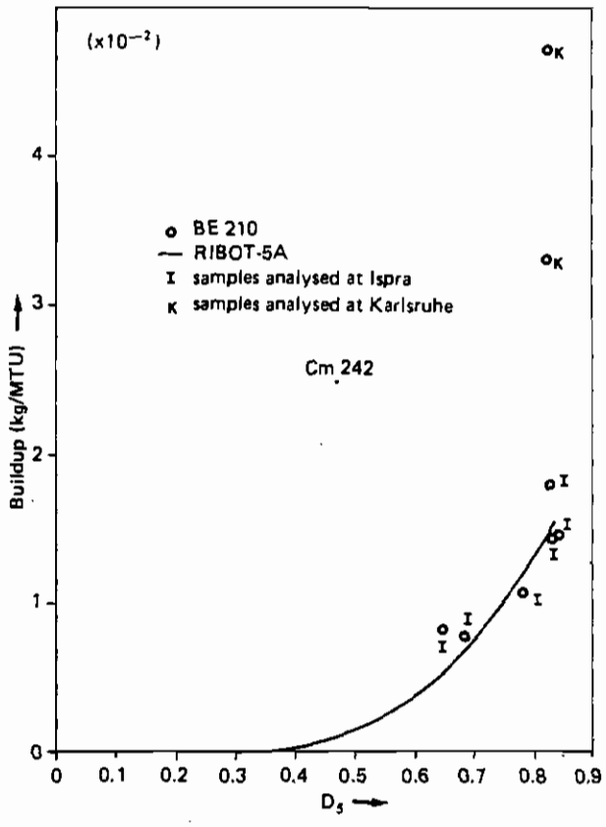

Fig. II.59. Comparison between calculated and experimental results for the Obrigheim reactor

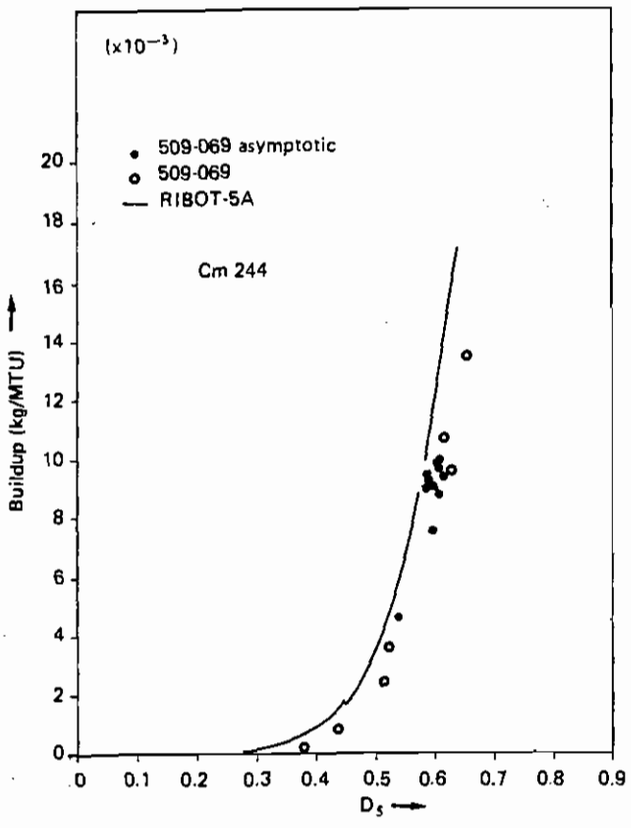

Fig. II.60. Comparison between calculated and experimental results for the Trino Vercellese reactor

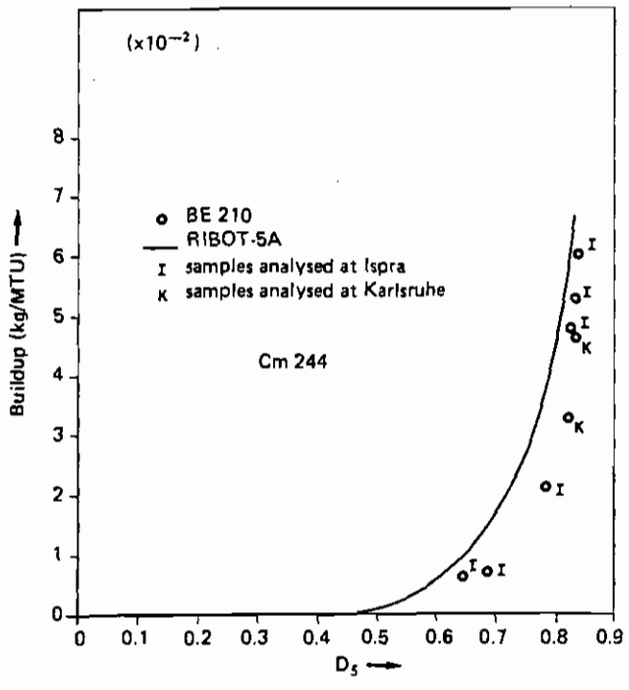

Fig. II.61. Comparison between caluclated and experimental results for the Obrigheim reactor

III. Benchmark Results and Conclusions

1. Results

The purpose of this section is to present most of the results obtained during the development of the BM activity and to draw some general conclusions.
Since the data have been extensively discussed in the preceding chapters, this section will present the tables and the figures considered essential for data recalculation. Some drawings that are not really essential to this purpose (such as radial and axial burnup evolution in the fuel bundles) will also be presented to provide an immediate picture of the physical behaviour of the burnup and buildups in the fuel.
The non-classified information on the reactors and fuel elements have already been given in section I.
The U and Pu isotopic composition, the buildup (or depletion) of heavy isotopes and the burnup of each analysed sample are presented in six sets of tables as follows:

Table Set	Reactor	Fuel Element
A	GARIGLIANO	A106
B	GARIGLIANO	SA13
C	TRINO VERCELLESE	509-049; 509-032;509-104
D	TRINO VERCELLESE	509-069
E	OBRIGHEIM	BE124, BE210
F	GUNDREMMINGEN	B23; C16

Eight tables for each set have been established in the following sequence:

Table 1 U isotopes referred to final ^{238}U atoms

Table 2 Pu isotopes referred to final ^{238}U atoms

Table 3 ^{148}Nd and ^{137}Cs atoms referred to final ^{238}U atoms

Table 4 Am and Cm isotopes referred to final ^{238}U atoms

Table 5 buildup and depletion of U isotopes (Kg/MTU)

Table 6 buildup of Pu isotopes (Kg/MTU) .

Table 7 buildup of Am and Cm isotopes (Kg/MTU)

Table 8 burnup values in percentage (F_T%) and MWD/MTU

The tables presented are the same as already published in the Bench Mark reports/1, 2/. Some data are lacking throughout the set of results because in the issueing of BM reports we left out those data which were not completely certified and traceable.

The reader interested in having all the data can refer to the single reports /21 - 26/.

One last comment: during the preparation of BM reports all the results were reviewed and recalculated from raw data using updated nuclear constants and performing new corrections (to the burnup for ^{147}Nd capture, for instance). This fact explains why some results are slightly different in BM reports with respect to those reported in the original works.

Nuclear data used in the course of the various analytical campaigns can be found in references 1, 2, 21, 22, 23, 24, 25, 26. In Tables III.1 and III.2 we have only reported the half-lives of Pu, Am and Cm isotopes /3/ and the average values of ^{148}Nd and ^{137}Cs fission yield and MeV/fission employed, evaluated by the use of suitable nuclear data /43, 61/ and fission fractions /62/

TABLE III.1. Half lives of Pu, Am and Cm isotopes

Isotopes	Half Life (years)
^{238}Pu	87.8 ± 0.8
^{239}Pu	(2.41 ± 0.01) x 10^4
^{240}Pu	(6.55 ± 0.07) x 10^3
^{241}Pu	14.7 ± 0.4
^{242}Pu	(3.87 ± 0.05) x 10^5
^{241}Am	432 ± 4
^{242m}Am	152 ± 7
^{243}Am	7370 ± 40
^{242}Cm	0.446 ± 0.0003
^{244}Cm	18.11 ± 0.01

TABLE III.2. Average values of ^{148}Nd and ^{137}Cs fission yields and of MeV/fission used for the different reactors

Reactor	Average Fission Yield		Average MeV/fission
	^{148}Nd	^{137}Cs	
Garigliano	$1.733 \cdot 10^{-2}$	$6.359 \cdot 10^{-2}$	204.0
Trino Vercellese	$1.733 \cdot 10^{-2}$	$6.359 \cdot 10^{-2}$	204.0
Obrigheim	$1.734 \cdot 10^{-2}$	$6.376 \cdot 10^{-2}$	207.7
Gundremmingen:			
C16 Assembly	$1.747 \cdot 10^{-2}$	$6.450 \cdot 10^{-2}$	206.8
B23 Assembly	$1.763 \cdot 10^{-2}$	$6.512 \cdot 10^{-2}$	206.8

For most of the fuel elements analysed a set of figures is here also presented, including the axial and/or radial behaviour of some important parameters (burnup, ^{239}Pu buildup) and some particular isotopic compositions with the aim of illustrating singularities. A limited discussion on the experimental data is included when considered necessary to a better understanding of the data.
Numerous references are made to the preliminary sections of this report and to the literature.

1. Garigliano BWR (Garigliano I and Garigliano II)

The standard tables A1 to A8 contain the BM results for the first charge of GARIGLIANO (fuel element A-106).
In Fig. III.1 the radial behaviour (along the diagonal) of the burnup is plotted showing a clear asymmetry due to the insertion of control rod F4 for some periods (see ref. 1, Fig.12).

It is also pointed out in the same figure that the burnup of two low enriched corner pellets is not fitted by the same curve as the high enrichment points.
In Fig. III.2 the ^{239}Pu radial dependence is shown where no evidence of asymmetry is present, in spite of the radial burnup (i.e. integrated flux) shift.

TABLE A1. U isotopes referred to final ^{238}U atoms

Fuel Element	Sample	^{235}U (x 10^{1})	^{236}U (x 10^{2})
A-106 INITIAL ENRICHMENT 1.6 wt% U-235	A 1	0.798	0.165
	9	0.571	0.189
	B 1	0.874	0.146
	J 1	0.649	0.185
	9	0.557	0.197
A-106 INITIAL ENRICHMENT 2.1 wt% U-235	A 3	1.275	0.193
	5	1.222	0.178
	B 2	1.270	0.195
	8	1.083	0.205
	C 1	1.265	0.194
	3	1.390	0.172
	D 2	1.338	0.178
	4	1.373	0.177
	E 1	1.243	0.196
	5	1.376	0.169
	G 7	1.237	0.189
	H 2	1.131	0.201
	8	1.066	0.203

TABLE A2. Pu isotopes referred to final ^{238}U atoms

Fuel Element	Sample	^{238}Pu (x 10^{5})	^{239}Pu (x 10^{3})	^{240}Pu (x 10^{3})	^{241}Pu (x 10^{4})	^{242}Pu (x 10^{5})
A-106 INITIAL ENRICHMENT 1.6 wt% U-235	A 1	1.89	3.824	1.146	4.494	8.835
	9	2.82	3.537	1.461	5.556	16.98
	B 1	1.92	3.960	1.037	4.134	6.931
	J 1	2.99	3.766	1.361	5.688	14.46
	9	3.48	3.844	1.612	6.510	19.91
A-106 INITIAL ENRICHMENT 2.1 wt% U-235	A 3	1.80	4.047	0.957	3.887	5.667
	5	1.68	4.101	0.965	3.959	5.741
	8 2	1.81	3.977	0.907	3.606	5.092
	8	2.09	3.801	1.097	4.136	7.603
	C 1	1.88	4.054	0.948	3.874	5.797
	3	1.33	4.277	0.832	3.444	3.978
	D 2	1.51	4.153	0.834	3.487	4.237
	4	1.75	4.309	0.787	3.401	3.750
	E 1	1.84	4.188	0.964	4.031	5.779
	5	1.79	4.354	0.793	3.503	3.693
	G 7	1.91	4.298	0.971	4.008	5.589
	H 2	2.00	3.942	1.061	4.263	7.135
	8	2.16	3.980	1.169	4.493	8.558

TABLE A3. Atom ratios of ^{148}Nd and ^{137}Cs referred to final ^{238}U

Fuel Element	Sample	^{148}Nd (x 10^4)	^{137}Cs (x 10^4)
A-106 INITIAL ENRICHMENT 1.6 wt% U-235	A 1	1.96	6.92
	9	2.61	9.04
	B 1	1.81	6.29
	J 1	2.38	8.42
	9	2.70	9.18
A-106 INITIAL ENRICHMENT 2.1 wt% U-236	A 3	1.96	6.85
	5	1.97	7.07
	B 2	1.91	6.59
	8	2.26	7.91
	C 1	1.98	6.91
	3	1.70	5.91
	D 2	1.76	6.15
	4	1.64	5.82
	E 1	2.01	6.91
	5	1.66	5.82
	G 7	1.96	6.66
	H 2	2.22	7.55
	8	2.37	7.97

TABLE A4. Am and Cm isotopes referred to final ^{238}U atoms

Fuel Element	Sample	^{241}Am (x 10^5)	^{242}Am (x 10^7)	^{243}Am (x 10^6)	^{242}Cm (x 10^6)	^{244}Cm (x 10^6)
A-106 INITIAL ENRICHMENT 1.6 wt% U-235	A 1	2.09			5.33	1.29
	9	1.62	1.21	6.51	6.80	2.89
	B 1	0.09	1.42	0.73	3.41	0.92
	J 1	0.53		3.50	5.20	2.13
	9	0.20			7.30	3.47
A-106 INITIAL ENRICHMENT 2.1 wt% U-235	A 3	1.68			2.95	1.12
	5	2.90	2.46	2.36	3.41	0.72
	B 2	1.35	1.28	1.47	2.76	1.11
	8	2.71			3.25	1.19
	C 1	0.76			2.92	0.90
	3	1.97			2.14	0.48
	D 2	1.60	0.94	1.16	2.55	0.84
	4	2.45		1.64	2.37	0.98
	E 1	1.69			2.78	0.57
	5	1.63	1.10	1.22	2.02	1.60
	G 7	1.51			2.82	0.74
	H 2	2.25	1.41	2.61	3.96	1.37
	8	2.85			3.32	2.29

TABLE A5. Buildup and depletion of U isotopes ($kg/MTU_{Initial}$)

Fuel Element	Sample	^{235}U (a)	^{236}U	^{238}U (a)
A-106 INITIAL ENRICHMENT 1.6 wt% U-235	A 1	8.32	1.59	9.76
	9	10.51	1.82	11.63
	B 1	7.58	1.41	9.44
	J 1	9.26	1.78	11.17
	9	10.60	1.89	12.63
A-106 INITIAL ENRICHMENT 2.1 wt% U-235	A 3	8.79	1.85	9.38
	5	9.29	1.71	8.87
	B 2	8.83	1.87	8.96
	8	10.62	1.97	9.32
	C 1	8.88	1.86	9.47
	3	7.68	1.65	8.89
	D 2	8.17	1.71	8.66
	4	7.84	1.70	8.47
	E 1	9.10	1.88	9.56
	5	7.81	1.62	8.55
	G 7	9.15	1.81	9.27
	H 2	10.17	1.93	9.62
	8	10.79	1.95	9.99

(a) Depletion

TABLE A6. Buildup of Pu isotopes ($kg/MTU_{Initial}$)

Fuel Element	Sample	^{238}Pu (x 10^6)	^{239}Pu	^{240}Pu	^{241}Pu (x 10^2)	^{242}Pu (x 10^2)
A-106 INITIAL ENRICHMENT 1.6 wt% U-235	A 1	1.84	3.74	1.12	4.43	8.74
	9	2.74	3.45	1.43	5.56	16.7
	B 1	1.87	3.87	1.01	4.07	6.86
	J 1	2.91	3.67	1.33	5.58	14.3
	9	3.38	3.74	1.57	6.40	19.6
A-106 INITIAL ENRICHMENT 2.1 wt% U-235	A 3	1.74	3.94	0.93	3.81	5.58
	5	1.63	3.99	0.94	3.88	5.66
	B 2	1.75	3.87	0.88	3.54	5.02
	8	2.03	3.70	1.07	4.06	7.49
	C 1	1.82	3.94	0.92	3.80	5.71
	3	1.29	4.16	0.81	3.38	3.92
	D 2	1.46	4.04	0.81	3.42	4.17
	4	1.70	4.19	0.77	3.34	3.70
	E 1	1.78	4.07	0.94	3.95	5.69
	5	1.74	4.23	0.77	3.44	3.64
	G 7	1.85	4.18	0.94	3.93	5.50
	H 2	1.94	3.83	1.03	4.18	7.03
	8	2.10	3.87	1.14	4.40	8.43

TABLE A7. Buildup of Am and Cm isotopes (kg/MTU$_{Initial}$)

Fuel Element	Sample	^{241}Am (x 10^2)	^{242}Am (x 10^3)	^{243}Am (x 10^3)	^{242}Cm (x 10^3)	^{244}Cm (x 10^3)
A-106 INITIAL ENRICHMENT 1.6 wt% U-235	A 1	2.06			5.28	1.29
	9	1.59	0.27	15.04	6.72	2.88
	B 1	0.09	0.76	3.95	3.37	0.92
	J 1	0.52		11.25	5.14	2.12
	9	0.20			7.21	3.46
A-106 INITIAL ENRICHMENT 2.1 wt% U-235	A 3	1.64			2.90	1.11
	5	2.85	0.53	5.15	3.37	0.71
	B 2	1.33	0.35	4.02	2.72	1.10
	8	2.66			3.21	1.18
	C 1	0.75			2.88	0.90
	3	1.93			2.11	0.04
	D 2	1.57	0.26	3.24	2.51	0.83
	4	2.41		3.32	2.34	0.97
	E 1	1.65			2.72	0.57
	5	1.60	0.31	3.47	1.99	1.59
	G 7	1.49			2.78	0.73
	H 2	2.21	0.33	6.24	3.90	1.36
	8	2.80			3.27	2.28

TABLE A8. Burnup values F_T % and MWD/MTU obtained from ^{148}Nd and ^{137}Cs

Fuel Element	Sample	F_T %		MWD/MTU	
		^{148}Nd	^{137}Cs	^{148}Nd	^{137}Cs
A-106 INITIAL ENRICHMENT 1.6 wt% U-235	A 1	1.10	1.06	10,590	10,160
	9	1.46	1.38	14,040	13,260
	B 1	1.02	0.96	9,800	9,250
	J 1	1.33	1.28	12,830	12,350
	9	1.51	1.40	14,480	13,460
A-106 INITIAL ENRICHMENT 2.1 wt% U-235	A 3	1.09	1.04	10,510	10,020
	5	1.10	1.07	10,570	10,350
	B 2	1.07	1.00	10,280	9,650
	8	1.26	1.20	12,150	11,560
	C 1	1.11	1.05	10,660	10,100
	3	0.95	0.90	9,140	8,700
	D 2	0.98	0.93	9,440	9,000
	4	0.92	0.88	8,850	8,500
	E 1	1.12	1.05	10,800	10,100
	5	0.93	0.88	8,930	9,730
	G 7	1.10	1.01	10,540	9,730
	H 2	1.24	1.15	11,920	11,050
	8	1.32	1.21	12,700	11,650

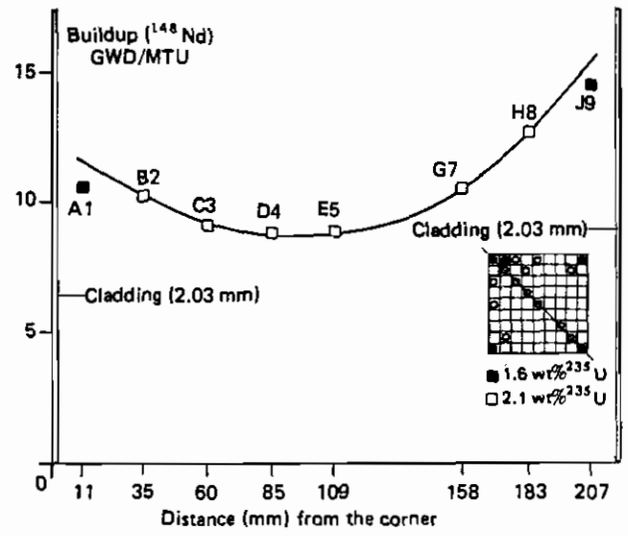

Fig. III.1. Garigliano I - Radial burnup distribution in function of the rod (centre) distance from the corner of the assembly

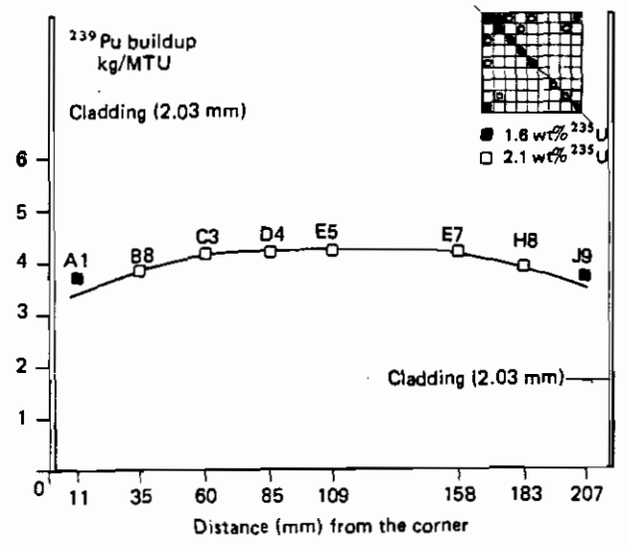

Fig. III.2. Garigliano I - Radial ^{239}Pu buildup distribution in function of the rod (centre) distance from the corner of the assembly

An explanation may be found in the fact that the effect of flux depression on ^{239}Pu formation was compensated by an ^{239}Pu overproduction due to the radial spectrum hardening as a consequence of the control rod insertion. This conclusion is supported by the results shown in Fig. III.3 where the ^{239}Pu/Pu total is plotted showing a net asymmetry, and that the isotopic composition of plutonium is modified along the diagonal.

Fig. III.4 in which the radial ^{240}Pu buildup is shown, gives evidence of the same asymmetric behaviour.

In the second standard table set (table B1 to B8) referring to GARIGLIANO II, some isotopes coming from α-measurement are omitted. This is due to the fact that the low burnup and the long cooling time (10 years) lowered the emission to such a point that it was impossible to detect a meaningful signal.

In Fig. III. 5 the axial behaviour of the burnup (in GWD/MTU) is given for the SA-13 E6 pin. A certain anomaly, beyond experimental error and shown up by points 7 and 10, is possibly due to spectrum perturbation of the zone in which the phase change occured. For qualitative comparison, Fig. III. 6 shows an ENEL evaluation of the normalized axial power distribution averaged over the irradiation cycle 2 of fuel assemblies SA-13, SA-21 and SA-41.

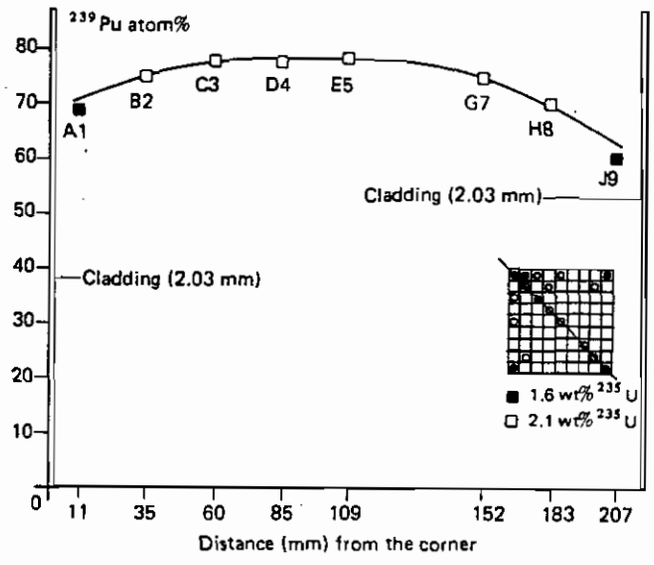

Fig. III.3. Garigliano I - Radial ^{239}Pu (at%) distribution in function of the rod (centre) distance from the corner of the assembly

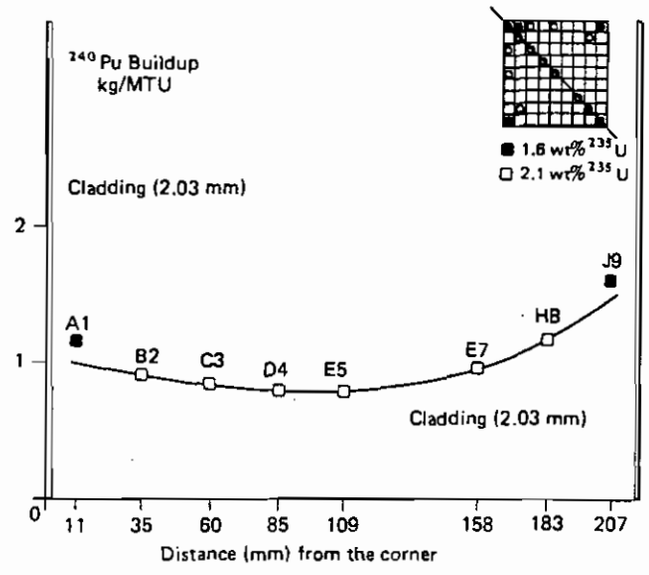

Fig. III.4. Garigliano I - Radial ^{240}Pu buildup distribution in function of the rod (centre) distance from the corner of the assembly

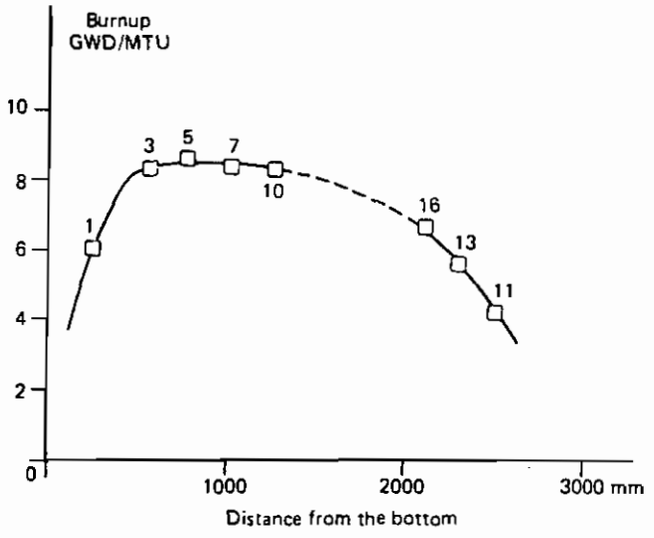

Fig. III.5. Garigliano II - Axial burnup behaviour versus distance from the bottom

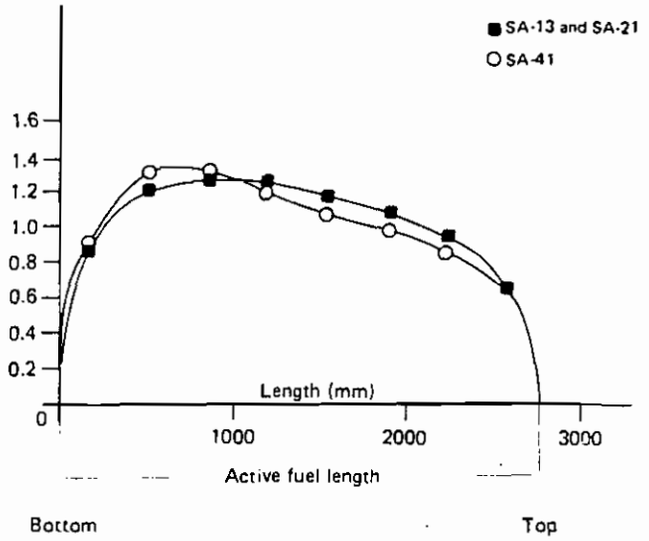

Fig. III.6. Garigliano II - Normalized axial power distribution averaged over the period of residence of fuel assemblies SA-13, SA-21 and SA-41 in the reactor (cycle 2)

TABLE B1. U isotopes referred to final ^{238}U atoms

Fuel Element	Sample	^{235}U ($\times 10^2$)	^{236}U ($\times 10^3$)
SA-13 INITIAL ENRICHMENT 2.41 wt% U-235	E6 1	1.856	1.365
	3	1.721	1.651
	5	1.688	1.649
	7	1.680	1.650
	10	1.680	1.578
	16	1.882	1.438
	13	1.944	1.236
	11	2.054	0.970

TABLE B2. Pu isotopes referred to final ^{238}U atoms

Fuel Element	Sample	^{239}Pu ($\times 10^3$)	^{240}Pu ($\times 10^4$)	^{241}Pu ($\times 10^4$)	^{242}Pu ($\times 10^6$)
SA-13 INITIAL ENRICHMENT 2.41 wt% U-235	E6 1	2.438	3.278	0.946	6.397
	3	3.483	5.806	1.895	16.193
	5	3.578	6.170	2.194	19.743
	7	3.442	5.944	2.148	22.973
	10	3.303	5.804	2.013	18.512
	16	3.352	4.525	1.624	11.086
	13	3.052	3.579	1.182	6.701
	11	2.461	2.281	0.613	2.566

TABLE B3. Atom ratios of ^{148}Nd and ^{137}Cs referred to final ^{238}U

Fuel Element	Sample	^{148}Nd ($\times 10^4$)	^{127}Cs ($\times 10^4$)
SA-13 INITIAL ENRICHMENT 2.41 wt% U-235	E6 1	1.122	3.442
	3	1.544	4.634
	5	1.615	5.871
	7	1.557	5.514
	10	1.001	5.126
	16	1.241	4.561
	13	1.039	3.801
	11	0.782	2.862

TABLE B4. Am and Cm isotopes referred to final ^{238}U atoms

Fuel Element	Sample	^{241}Am ($\times 10^6$)	^{244}Cm ($\times 10^8$)
SA-13 INITIAL ENRICHMENT 2.41 wt% U-235	E6 1	2.81	1.44
	3	11.01	7.24
	5	22.41	12.31
	7	14.82	10.03
	10	5.61	6.72
	16	31.20	6.61
	13	4.76	2.43
	11	–	0.67

TABLE B5. Buildup and depletion of U isotopes ($kg/MTU_{Initial}$)

Fuel Element	Sample	^{235}U (a)	^{236}U	^{238}U (a)
SA-13 INITIAL ENRICHMENT 2.41 wt% U-235	E6 1	6.29	1.31	4.36
	3	7.64	1.58	7.56
	5	8.16	1.58	7.99
	7	8.02	1.58	7.43
	10	8.02	1.57	6.75
	16	6.09	1.38	7.08
	13	5.46	1.19	5.39
	11	4.38	0.93	3.77

(a) Depletion

TABLE B6. Buildup of Pu isotopes ($kg/MTU_{Initial}$)

Fuel Element	Sample	^{239}Pu	^{240}Pu	^{241}Pu	^{242}Pu
SA-13 INITIAL ENRICHMENT 2.41 wt% U-235	E6 1	2.37	0.32	0.093	0.0063
	3	3.38	0.57	0.18	0.016
	5	3.48	0.60	0.21	0.019
	7	3.35	0.58	0.21	0.023
	10	3.21	0.57	0.20	0.018
	16	3.26	0.44	0.159	0.011
	13	2.97	0.35	0.116	0.0066
	11	2.40	0.22	0.060	0.0025

TABLE B7. Buildup of Am and Cm isotopes ($kg/MTU_{Initial}$)

Fuel Element	Sample	^{241}Am ($\times 10^3$)	^{244}Cm ($\times 10^5$)
SA-13 INITIAL ENRICHMENT 2.41 wt% U-235	E6 1	2.76	1.44
	3	10.79	7.18
	5	21.96	12.21
	7	14.5	9.96
	10	5.50	6.67
	16	30.6	6.56
	13	4.67	2.42
	11		0.67

TABLE B8. Burnup values F_T % and MWD/MTU obtained from ^{148}Nd and ^{137}Cs

Fuel Element	Sample	F_T %		MWD/MTU	
		^{148}Nd	^{137}Cs	^{148}Nd	^{137}Cs
SA-13 INITIAL ENRICHMENT 2.41 wt% U-235	E6 1	0.63	0.53	6,038	5,073
	3	0.86	0.71	8,260	6,809
	5	0.90	0.89	8,640	8,601
	7	0.87	0.84	8,325	8,094
	10	0.85	0.79	8,143	7,525
	16	0.69	0.70	6,644	6,688
	13	0.58	0.58	5,578	5,583
	11	0.44	0.44	4,201	4,211

The perturbation appears even more clearly in Fig. III. 7 where the ^{239}Pu buildup is shown since the production of that isotope is much more sensitive to spectrum perturbations. The Pu/U mass ratio vs the axial position is reported in Fig. III. 8 showing the same trend in the region between points 7 and 10.

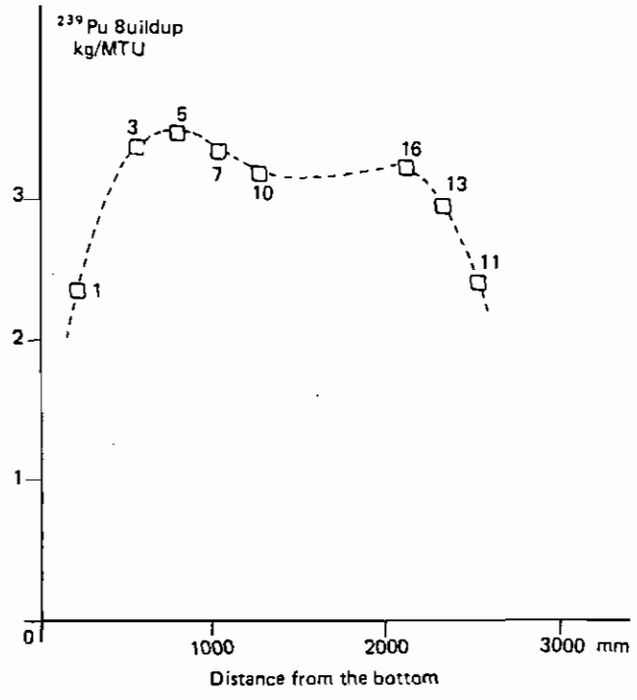

Fig. III.7. Garigliano II - Behaviour of the ^{239}Pu buildup in function of the axial position of the samples

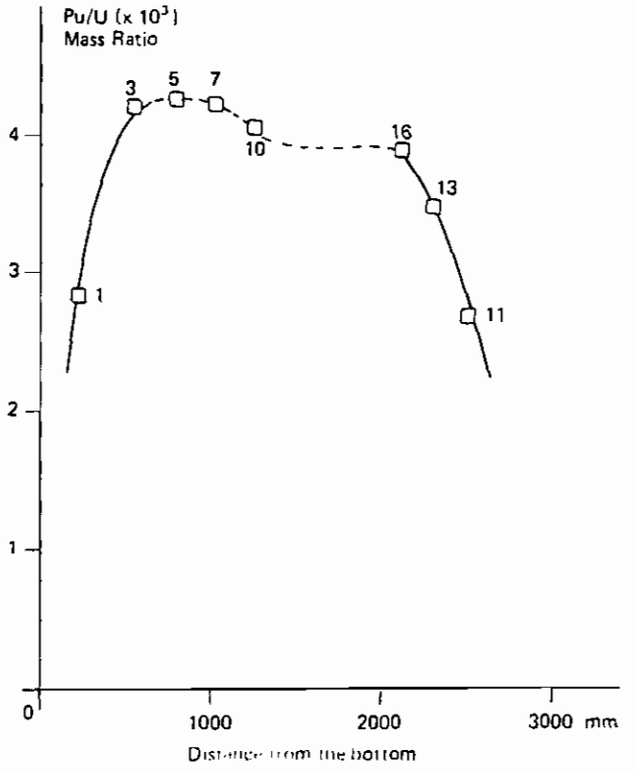

Fig. III.8. Garigliano II - Behaviour of the Pu/U mass ratio in function of the axial position of the samples

2. Trino Vercellese PWR (Trino I and Trino II)

For the results of the campaigns on TRINO VERCELLESE there are no particular problems to be mentioned and they are given in the standard tables (C1 to C8, D1 to D8). Only the axial and radial distributions of burnup and radial distribution of ^{239}Pu buildup for TRINO II samples are presented in Figs. III.9 and III.10.

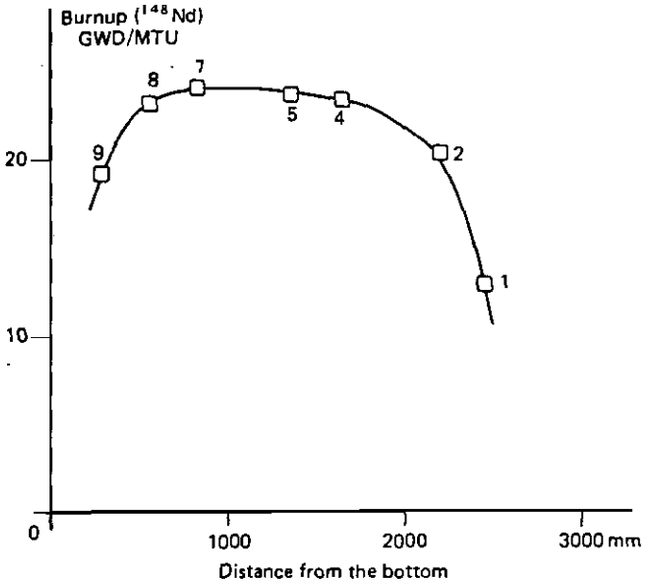

Fig. III.9. TRINO II - Rod E11, axial burnup distribution versus distance from the bottom

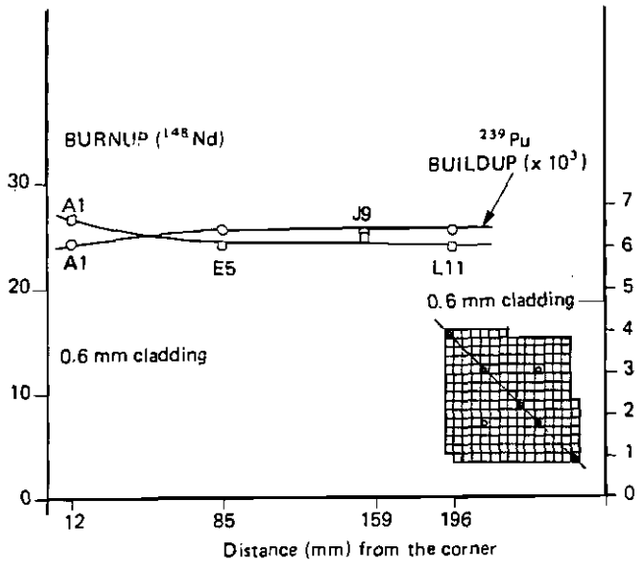

Fig. III.10. TRINO II - Radial burnup distribution at level 7 (814 mm from the bottom) of burnup and ^{239}Pu buildup

TABLE C1. U isotopes referred to final ^{238}U atoms

Fuel Element	Sample	^{235}U (x 10^2)	^{236}U (x 10^2)
509-049 INITIAL ENRICHMENT 2.719 wt% U-235	L5 1	2.068	0.170
	4Δ	1.585	0.255
	9Δ	1.833	0.217
	J8 1	1.945	0.186
	4	1.466	0.263
	7	1.463	0.270
	9	1.748	0.224
	A1 1Δ	1.976	0.183
	7Δ	1.418	0.281
	9	1.698	0.233
509-032 INITIAL ENRICHMENT 3.13 wt% U-235	E11 1	2.451	0.171
	4	1.831	0.299
	7	1.760	0.289
	9	2.129	0.263
	H9 4	1.773	0.315
	7	1.730	0.320
	9	2.020	0.255
	Q15 7	1.593	0.328
509-104 INITIAL ENRICH. 3.897 wt% U-235	M11 7Δ	2.834	0.290
	A12 1	3.700	0.124
	7	3.270	0.204

Δ Values obtained by averaging analytical results from the Ispra and Karlsruhe Laboratories

TABLE C2. Pu isotopes referred to final ^{238}U atoms

Fuel Element	Sample	^{238}Pu (x 10^5)	^{239}Pu (x 10^3)	^{240}Pu (x 10^4)	^{241}Pu (x 10^4)	^{242}Pu (x 10^3)
509-049 INITIAL ENRICHMENT 2.719 wt% U-235	L5 1		3.737	5.311	2.077	1.609
	4Δ	3.16	5.183	11.75	6.166	9.168
	9Δ	1.55	4.319	7.714	3.257	3.716
	J8 1		3.738	5.779	2.334	1.980
	4		4.974	12.05	6.288	10.49
	7	3.24	5.140	12.42	6.477	10.94
	9	1.60	4.373	8.446	3.844	4.503
	A1 1Δ	0.68	3.552	5.371	2.029	1.599
	7Δ	3.67	5.106	13.04	6.947	13.63
	9		4.304	8.690	4.038	4.951
509-032 INITIAL ENRICHMENT 3.13 wt% U-235	E11 1		3.622	4.582	1.764	1.229
	4		5.516	11.66	6.338	8.939
	7		5.484	11.86	6.374	9.816
	9		4.610	8.054	3.814	3.920
	H9 4	2.59	5.423	12.64	6.917	11.11
	7		5.488	13.01	7.106	11.46
	9		4.608	8.605	4.175	4.610
	Q15 7		5.213	13.55	7.193	13.39
509-104 INITIAL ENRICH. 3.897 wt% U-235	M11 7Δ	2.81	4.759	7.440	3.557	3.186
	A12 1		1.528	0.963	0.147	0.046
	7		2.641	3.049	0.383	0.474

Δ Values obtained by averaging analytical results from the Ispra and Karlsruhe Laboratories

TABLE C3. Atom ratios of ^{148}Nd and ^{137}Cs referred to final ^{238}U

Fuel Element	Sample	^{148}Nd (x 10^4)	^{137}Cs (x 10^4)
509-049 INITIAL ENRICHMENT 2.719 wt% U-235	L5 1		5.55
	4Δ	2.65	9.76
	9Δ	1.89	7.26
	J9 1	1.68	5.75
	4	2.74	10.19
	7	2.82	10.07
	9	2.06	7.47
	A1 1Δ	1.54	5.74
	7Δ	2.88	11.14
	9	2.23	8.24
509-032 INITIAL ENRICHMENT 3.13 wt% U-235	E11 1	1.35	5.14
	4	2.87	10.68
	7	2.96	10.82
	9	2.15	7.81
	H9 4	3.09	10.94
	7	3.25	11.95
	9	2.30	8.50
	Q15 7	3.35	12.38
509-104 INITIAL ENRICH. 3.897 wt% U-235	M11 7Δ	2.27	8.49
	A12 1	0.65	2.57
	7	1.43	5.16

Δ Values obtained by averaging analytical results from the Ispra and Karlsruhe Laboratories

TABLE C4. Am and Cm isotopes referred to final ^{238}U

Fuel Element	Sample	^{241}Am (x 10^5)	^{242}Am (x 10^7)	^{243}Am (x 10^6)	^{242}Cm (x 10^6)	^{244}Cm (x 10^5)
509-049 INITIAL ENRICHMENT 2.719 wt% U-235	L5 1					
	4Δ	1.98	4.60	8.87	3.21	2.13
	9Δ	0.49	1.91	2.39	2.34	0.60
	J8 1					
	4					
	7	2.92	3.96	11.53	6.18	1.80
	9	1.21		3.24	1.96	0.78
	A1 1Δ	1.58	1.68	0.91	0.56	0.20
	7Δ	0.65	4.49	11.42	3.91	2.63
	9					
509-032 INITIAL ENRICHMENT 3.13 wt% U-235	E11 1					
	4					
	7					
	9					
	H9 4					
	7					
	9					
	Q15 7					
509-104 INITIAL ENRICH. 3.897 wt% U-235	M11 7Δ	3.31	1.99	2.91	4.48	1.67
	A12 1					
	7					

Δ Values obtained by averaging analytical results from the Ispra and Karlsruhe Laboratories

TABLE C5. Buildup and depletion of U isotopes ($kg/MTU_{Initial}$)

Fuel Element	Sample	^{235}U (a)	^{236}U	^{236}U (a)
509-049 INITIAL ENRICHMENT 2.719 wt% U-235	L5 1	7.46	1.63	6.45
	4Δ	12.26	2.42	12.03
	9Δ	9.82	2.04	8.10
	J8 1	8.64	1.78	6.61
	4	13.27	2.50	11.17
	7	13.31	2.57	11.92
	9	10.55	2.14	8.61
	A1 1Δ	7.95	1.73	6.09
	7Δ	13.64	2.67	12.10
	9	11.03	2.23	9.11
509-032 INITIAL ENRICHMENT 3.13 wt% U-235	E11 1	7.89	1.64	5.28
	4	14.00	2.84	11.84
	7	14.67	2.74	11.62
	9	11.12	2.50	8.93
	H9 4	14.56	2.98	12.82
	7	14.98	3.03	13.38
	9	12.15	2.42	8.78
	Q15 7	16 25	3.11	12.56
509-104 INITIAL ENRICH. 3.897 wt% U-235	M11 7Δ	12.09	2.75	8.96
	A12 1	3.95	1.17	2.37
	7	8.09	1.93	4.69

Δ Values obtained by averaging analytical results from the Ispra and Karlsruhe Laboratories

TABLE C6. Buildup of Pu isotopes ($kg/MTU_{Initial}$)

Fuel Element	Sample	^{238}Pu	^{239}Pu	^{240}Pu	^{241}Pu	^{242}Pu
509-049 INITIAL ENRICHMENT 2.719 wt% U-235	L5 1		3.63	0.51	0.205	0.015
	4Δ	0.030	5.00	1.15	0.612	0.089
	9Δ	0.015	4.18	0.75	0.349	0.036
	J8 1		3.63	0.56	0.230	0.019
	4		4.80	1.17	0.622	0.103
	7	0.031	4.96	1.20	0.643	0.107
	9	0.015	4.23	0.82	0.381	0.044
	A1 1Δ	0.006	3.45	0.52	0.201	0.016
	7Δ	0.035	4.92	1.26	0.691	0.133
	9		4.16	0.84	0.398	0.049
509-032 INITIAL ENRICHMENT 3.13 wt% U-235	E11 1		3.50	0.44	0.173	0.012
	4		5.30	1.12	0.623	0.087
	7		5.27	1.14	0.627	0.095
	9		4.44	0.77	0.375	0.038
	H9 4	0.024	5.20	1.22	0.682	0.108
	7		5.26	1.25	0.698	0.111
	9		4.44	0.83	0.411	0.045
	Q15 7		5.00	1.31	0.708	0.130
509-104 INITIAL ENRICH. 3.897wt% U-235	M11 7Δ	0.026	4.55	0.71	0.348	0.030
	A12 1		1.47	0.09	0.014	0.0004
	7		2.54	0.29	0.081	0.004

Δ Values obtained by averaging analytical results from the Ispra and Karlsruhe Laboratories

TABLE C7. Buildup of Am and Cm isotopes (kg/MTU$_{Initial}$)

Fuel Element	Sample	^{241}Am (x 10^2)	^{242}Am (x 10^4)	^{243}Am (x 10^3)	^{242}Cm (x 10^3)	^{244}Cm (x 10^3)
509-049 INITIAL ENRICHMENT 2.719 wt% U-235	L5 1					
	4Δ	1.93	4.47	8.62	3.13	2.10
	9Δ	0.48	1.87	2.34	2.30	0.59
	J8 1					
	4					
	7	2.84	3.85	11.22	6.03	1.77
	9	1.18		3.16	1.92	0.77
	A1 1Δ	1.55	1.65	0.90	0.55	0.19
	7Δ	0.64	4.36	11.11	3.823	2.59
	9					
509-032 INITIAL ENRICHMENT 3.13 wt% U-235	E11 1					
	4					
	7					
	9					
	H9 4					
	7					
	9					
	Q15 7					
509-104 INITIAL ENRICH. 3.897 wt% U-235	M11 7Δ	3.19	1.92	2.80	4.33	1.63
	A12 1					
	7					

Δ Values obtained by averaging analytical results from the Ispra and Karlsruhe Laboratories

TABLE C8. Burnup values F_T % and MWD/MTU obtained from ^{148}Nd and ^{137}Cs

Fuel Element	Sample	FT %		MWD/MTU	
		^{148}Nd	^{137}Cs	^{148}Nd	^{137}Cs
509-049 INITIAL ENRICHMENT 2.719 wt% U-235	L5 1		0.84		8,080
	4Δ	1.46	1.47	14,080	14,140
	9Δ	1.05	1.10	10,070	10,550
	J8 1	0.93	0.87	8,970	8,370
	4	1.52	1.54	14,570	14,770
	7	1.56	1.52	14,980	14,580
	9	1.14	1.13	11,000	10,850
	A1 1Δ	0.85	0.87	8,230	8,370
	7Δ	1.59	1.68	15,290	16,120
	9	1.24	1.24	11,900	11,960
509-032 INITIAL ENRICHMENT 3.13 wt% U-235	E11 1	0.74	0.77	7,180	7,460
	4	1.58	1.60	15,170	15,390
	7	1.63	1.62	15,690	15,600
	9	1.18	1.17	11,400	11,300
	H9 4	1.70	1.64	16,320	15,770
	7	1.79	1.79	17,180	17,210
	9	1.27	1.28	12,220	12,290
	Q15 7	1.85	1.86	17,730	17,860
509-104 INITIAL ENRICH. 3.897 wt% U-235	M11 7Δ	1.25	1.27	11,920	12,180
	A12 1	0.35	0.38	3,420	3,710
	7	0.78	0.77	7,550	7,440

Δ Values obtained by averaging analytical results from the Ispra and Karlsruhe Laboratories

TABLE D1. U isotopes referred to final ^{238}U atoms

Fuel Element	Sample	^{235}U (x 10^2)	^{236}U (x 10^2)
509-069 INITIAL ENRICHMENT 3.13 wt% U-235	E5 4	1.376	0.374
	7Δ	1.304	0.377
	9	1.609	0.346
	L5 4	1.384	0.369
	7	1.317	0.380
	E11 1	2.055	0.258
	2Δ	1.529	0.352
	4Δ	1.331	0.384
	5	1.309	0.384
	7Δ	1.317	0.386
	8	1.345	0.381
	9	1.589	0.343
	L11 4	1.369	0.399
	7Δ	1.308	0.369
	A1 1	1.844	0.289
	7	1.106	0.399
	J9 4	1.283	0.387
	7	1.254	0.392

Δ Values obtained by averaging analytical results from the Ispra and Karlsruhe Laboratories

TABLE D2. Pu isotopes referred to final ^{238}U atoms

Fuel Element	Sample	^{238}Pu (x 10^4)	^{239}Pu (x 10^3)	^{240}Pu (x 10^3)	^{241}Pu (x 10^3)	^{242}Pu (x 10^4)
509-069 INITIAL ENRICHMENT 3.13 wt% U-235	E5 4	1.23	6.297	1.855	1.114	2.502
	7Δ	1.24	6.413	1.909	1.134	2.689
	9	0.66	5.544	1.393	0.776	1.405
	L5 4	1.15	6.401	1.866	1.151	2.551
	7	1.20	6.316	1.889	1.121	2.619
	E11 1	0.25	4.789	0.879	0.424	0.477
	2Δ	0.86	6.135	1.616	0.944	1.813
	4Δ	1.18	6.312	1.866	1.097	2.583
	5	1.23	6.340	1.884	1.098	2.524
	7Δ	1.24	6.502	1.934	1.134	2.755
	8	1.10	6.383	1.856	1.109	2.470
	9	0.69	6.050	1.511	0.840	1.567
	L11 4	1.14	6.303	1.907	1.128	2.618
	7Δ	1.25	6.417	1.929	1.133	2.760
	A1 1	0.35	4.892	1.069	0.540	0.752
	7	1.45	6.085	2.063	1.242	3.645
	J9 4	1.26	6.153	1.917	1.134	2.831
	7	1.31	6.333	1.993	1.169	3.034

Δ Values obtained by averaging analytical results from the Ispra and Karlsruhe Laboratories

TABLE D3. Atom ratios of ^{148}Nd and ^{137}Cs referred to final ^{238}U

Fuel Element	Sample	^{148}Nd (x 10^4)	^{137}Cs (x 10^4)
509-069 INITIAL ENRICHMENT 3.13 wt% U-235	E5 4	4.49	16.64
	7Δ	4.61	17.35
	9	3.62	13.45
	L5 4	4.55	16.84
	7		17.07
	E11 1		8.92
	2Δ	3.87	14.68
	4Δ	4.47	16.69
	5	4.71	17.09
	7Δ	4.57	17.22
	8	4.41	16.69
	9	3.61	14.08
	L11 4	4.51	16.87
	7Δ	4.58	17.21
	A1 1		10.56
	7	5.06	19.42
	J9 4		17.46
	7	4.75	17.78

Δ Values obtained by averaging analytical results from the Ispra and Karlsruhe Laboratories

TABLE D4. Am and Cm isotopes referred to final ^{238}U atoms

Fuel Element	Sample	^{241}Am (x 10^4)	^{242}Am (x 10^6)	^{243}Am (x 10^5)	^{242}Cm (x 10^5)	^{244}Cm (x 10^6)
509-069 INITIAL ENRICHMENT 3.13 wt% U-235	E5 4	0.82			2.38	9.09
	7Δ	1.03	2.26	4.69	2.62	9.66
	9	0.62			1.43	2.57
	L5 4	0.98			2.68	9.75
	7	1.61			2.57	8.97
	E11 1	0.30			0.52	0.10
	2Δ	0.57	1.44	2.44	1.87	4.76
	4Δ	0.74	1.89	3.97	2.58	9.23
	5	1.74	2.92	5.66	2.67	10.12
	7Δ	1.62	2.84	5.66	2.79	10.19
	8				2.57	7.83
	9				1.79	3.73
	L11 4				2.86	9.23
	7Δ	0.62	2.02	3.94	2.62	10.03
	A1 1	0.14			0.79	0.89
	7				3.18	14.16
	J9 4	0.69			2.69	10.89
	7				3.00	9.94

Δ Values obtained by averaging analytical results from the Ispra and Karlsruhe Laboratories

TABLE D5. Buildup and depletion of U isotopes (kg/$MTU_{Initial}$)

Fuel Element	Sample	^{235}U (a)	^{236}U	^{238}U (a)
509-069 INITIAL ENRICHMENT 3.13 wt% U-235	E5 4	18.39	3.53	19.13
	7Δ	19.23	3.54	19.96
	9	16.16	3.27	15.11
	L5 4	18.33	3.48	19.64
	7	18.99	3.57	21.09
	E11 1	11.84	2.45	9.61
	2Δ	16.94	3.32	16.49
	4Δ	18.82	3.61	18.94
	5	19.03	3.62	19.58
	7Δ	18.96	3.64	19.12
	8	18.68	3.59	18.55
	9	16.33	3.24	14.50
	L11 4	18.48	3.76	18.90
	7Δ	19.02	3.47	20.10
	A1 1	13.87	2.74	11.88
	7	10.95	3.75	20.16
	J9 4	19.29	3.64	20.36
	7	19.55	3.69	19.85

Δ Values obtained by averaging analytical result from the Ispra and Karlsruhe Laboratories

(a) Depletion

TABLE D6. Buildup of Pu isotopes (kg/$MTU_{Initial}$)

Fuel Element	Sample	^{238}Pu	^{239}Pu	^{240}Pu	^{241}Pu	^{242}Pu
509-069 INITIAL ENRICHMENT 3.13 wt% U-235	E5 4	0.117	5.95	1.76	1.05	0.240
	7Δ	0.116	5.98	1.78	1.06	0.254
	9	0.063	5.27	1.33	0.73	0.135
	L5 4	0.110	6.06	1.77	1.06	0.244
	7	0.114	5.97	1.79	1.06	0.250
	E11 1	0.025	4.58	0.84	0.40	0.046
	2Δ	0.081	5.75	1.52	0.88	0.172
	4Δ	0.109	5.89	1.75	1.03	0.244
	5	0.117	6.01	1.79	1.04	0.240
	7Δ	0.117	6.07	1.83	1.06	0.257
	8	0.119	5.91	1.72	1.03	0.232
	9	0.068	5.63	1.41	0.78	0.147
	L11 4	0.116	6.06	1.79	1.05	0.247
	7Δ	0.116	6.00	1.81	1.05	0.259
	A1 1	0.035	4.67	1.02	0.51	0.073
	7	0.132	5.56	1.89	1.14	0.338
	J9 4	0.120	5.82	1.81	1.07	0.270
	7	0.134	5.83	1.84	1.08	0.282

Δ Values obtained by averaging analytical results from the Ispra and Karlsruhe Laboratories

TABLE D7. Buildup of Am and Cm isotopes (kg/MTU$_{Initial}$)

Fuel Element	Sample	^{241}Am (x 10^2)	^{242}Am (x 10^3)	^{243}Am (x 10^2)	^{242}Cm (x 10^2)	^{244}Cm (x 10^3)
509-069 INITIAL ENRICHMENT 3.13 wt% U-235	E5 4	8.22			2.31	8.96
	7Δ	10.31	2.16	4.49	2.51	9.42
	9	5.56			1.39	2.54
	L5 4	10.18			2.52	9.52
	7	15.79			2.48	8.78
	E11 1	3.18			0.51	0.10
	2Δ	5.76	1.41	2.39	1.76	4.67
	4Δ	7.28	1.83	3.84	2.43	9.01
	5	17.05	2.81	5.45	2.57	9.91
	7Δ	15.86	2.73	5.43	2.66	9.90
	8				2.45	7.58
	9				1.73	3.63
	L11 4				2.79	9.15
	7Δ	6.32	2.00	3.80	2.46	9.73
	A1 1	1.63			0.75	0.88
	7				2.99	13.53
	J9 4	6.92			2.55	10.69
	7				2.84	9.66

Δ Values obtained by averaging analytical results from the Ispra and Karlsruhe Laboratories

TABLE D8. Burnup values F_T % and MWD/MTU obtained from ^{148}Nd and ^{137}Cs

Fuel Element	Sample	F_T %		MWD/MTU	
		^{148}Nd	^{137}Cs	^{148}Nd	^{137}Cs
509-069 INITIAL ENRICHMENT 3.13 wt% U-235	E5 4	2.45	2.48	23,550	23,810
	7Δ	2.52	2.58	24,220	24,810
	9	1.99	2.01	19,100	19,330
	L5 4	2.49	2.51	23,900	24,080
	7		2.54		24,420
	E11 1		1.34		12,890
	2Δ	2.12	2.19	20,380	21,060
	4Δ	2.44	2.49	23,450	23,890
	5	2.58	2.55	23,730	24,440
	7Δ	2.50	2.56	24,010	24,620
	8	2.41	2.49	23,150	23,890
	9	1.98	2.10	19,050	20,210
	L11 4	2.46	2.51	23,650	24,120
	7Δ	2.51	2.56	24,070	24,610
	A1 1		1.59		15,260
	7	2.77	2.89	26,550	27,730
	J9 4		2.60		24,970
	7	2.60	2.85	24,950	25,420

Δ Values obtained by averaging analytical results from the Ispra and Karlsruhe Laboratories

3. Obrigheim PWR

Standard tables for OBRIGHEIM results are presented (Tables E1 to E8). On some OBRIGHEIM data hardly any remarks are required. The burnup value of sample G7 P1 obtained at Karlsruhe was about 30% higher than the one from Ispra, as was also pointed out in section II. 2, where the paired comparison Ispra-Karlsruhe was presented.

A calculation made on the asymptotic G7 P1 samples with RIBOT (see section II. 5) also indicated the presence of a possible error of approximately 25% in the burnup of the G7 P1 sample analysed at Karlsruhe. For this reason in Tables E we have only given the values obtained at Ispra for the G7 P1 sample. In Fig. III. 11 the axial distribution of burnup and ^{239}Pu buildup for rod G7 are reported. The ^{241}Am and ^{242}Cm buildup values also presented a rather complex situation. An accurate analysis of the experimental ^{241}Am led to the conclusion that the values could be divided into two sets, A and B. In order to give an idea of the different distribution and of the discrepancy between the A and B sets of data, the ^{241}Am buildup values have been plotted against the burnup and presented in Fig. III. 12.

The first set (A) includes mass spectrometry data obtained at Ispra and α-spectrometry data obtained at Karlsruhe. The second set (B) is composed only of the α-spectrometry data obtained at Ispra.

Considering that the values belonging to A are obtained by two laboratories with differing experimental techniques, a greater degree of confidence may be placed in these values. This indication is also supported by the results obtained with the RIBOT code previously mentioned (see section II. 5, Fig. II. 55, Conclusions on ^{241}Am).

TABLE E1. U isotopes referred to final ^{238}U atoms

Fuel Element	Sample		^{235}U ($\times 10^2$)	^{236}U ($\times 10^2$)
BE 124 INITIAL ENRICHMENT 3.00 wt% U-235	D1	P1	1.438	0.313
		P2	0.998	0.396
		P3	0.742	0.431
	E3	P1	1.337	0.297
		P2	0.897	0.400
		P3	0.653	0.441
		P4Δ	0.814	0.410
		P5	1.258	0.383
	G7	P1	1.607	0.308
		P2	1.146	0.408
		P3Δ	0.804	0.420
		P4	1.077	0.430
		P5	1.064	0.378
	M14	P1	1.639	0.283
		P3	0.936	0.405
		P4	1.088	0.377
BE 210 INITIAL ENRICHMENT 2.83 wt% U-235	G14	P3(1)Δ	0.507	0.414
		P4(1)	0.529	0.422
		P5(1)	0.667	0.388
		P5(2)	0.947	0.353
	K14	P1	1.066	0.341
		P3(1)	0.521	0.413
		P4(1)	0.541	0.408

ΔValues obtained by averaging analytical results from the Ispra and Karlsruhe Laboratories

TABLE E2. Pu isotopes referred to final ^{238}U atoms

Fuel Element	Sample		^{238}Pu ($\times 10^4$)	^{239}Pu ($\times 10^3$)	^{240}Pu ($\times 10^3$)	^{241}Pu ($\times 10^3$)	^{242}Pu ($\times 10^4$)
BE 124 INITIAL ENRICHMENT 3.00 wt% U-235	D1	P1	0.373	4.544	1.373	0.645	1.324
		P2	0.968	4.876	1.972	1.065	3.346
		P3	1.656	5.292	2.480	1.344	5.872
	E3	P1	0.431	4.450	1.408	0.643	1.423
		P2	1.105	4.879	2.097	1.064	3.970
		P3	1.724	5.035	2.537	1.324	6.560
		P4Δ	1.208	5.178	2.337	1.236	4.941
		P5	0.649	4.858	1.688	0.874	2.173
	G7	P1	0.327	4.424	1.204	0.568	1.020
		P2	0.830	4.922	1.889	0.976	2.881
		P3Δ	1.498	5.276	2.391	1.260	5.077
		P4	1.119	5.331	2.135	1.152	3.794
		P5	0.836	5.326	2.031	1.088	3.325
	M14	P1	0.275	4.127	1.076	0.475	0.771
		P3	1.124	5.268	2.180	1.170	3.983
		P4	0.804	5.188	1.939	1.042	3.095
BE 210 INITIAL ENRICHMENT 2.83 wt% U-235	G14	P3(1)Δ	1.750	4.815	2.626	1.371	8.139
		P4(1)	1.684	4.650	2.494	1.262	7.071
		P5(1)	1.197	4.570	2.198	1.136	5.110
		P5(2)	0.682	4.445	1.786	0.893	2.932
	K14	P1	0.686	4.807	1.807	0.936	2.722
		P3(1)	1.789	4.944	2.504	1.362	7.660
		P4(1)	1.326	4.741	2.482	1.266	6.832

Δ Values obtained by averaging analytical results from the Ispra and Karlsruhe Laboratories.

TABLE E3. Atom ratios of ^{148}Nd and ^{137}Cs referred to final ^{238}U

Fuel Element	Sample	^{148}Nd ($\times 10^4$)	^{137}Cs ($\times 10^3$)
BE 124 INITIAL ENRICHMENT 3.00 wt% U-235	D1 P1	4.01	
	P2		1.88
	P3	6.46	2.33
	E3 P1	3.81	1.35
	P2	6.73	
	P3	6.96	2.48
	P4 Δ	5.90	2.15
	P5	4.34	2.36
	G7 P1	3.23	1.77
	P2	4.91	2.59
	P3 Δ	5.99	3.28
	P4	5.29	2.86
	P5	4.91	
	M14 P1	2.94	
	P3	5.60	3.01
	P4	4.73	
BE 210 INITIAL ENRICHMENT 2.83 wt% U-235	G14 P3(1) Δ	7.20	3.94
	P4(1)	6.82	3.70
	P5(1)	5.74	3.20
	P5(2)	4.59	2.55
	K14 P1	4.83	2.39
	P3(1)	7.03	3.75
	P4(1)	6.28	

Δ Values obtained by averaging analytical results from the Ispra and Karlsruhe Laboratories

TABLE E4. Am and Cm isotopes reffered to final ^{238}U atoms

Fuel Element	Sample	^{241}Am ($\times 10^5$)	^{242}Am ($\times 10^4$)	^{243}Am ($\times 10^3$)	^{242}Cm ($\times 10^5$)	^{244}Cm ($\times 10^5$)
BE 124 INITIAL ENRICHMENT 3.00 wt% U-235	D1 P1 K	2.27 A			0.76	0.23
	P2 I					
	P3 I	6.36 B			1.63	3.51
	E3 P1 I	3.02 B			0.46	0.21
	P2 K					1.30
	P3 I	8.97 B			1.76	4.32
	P4 I	7.61 B			1.56	2.55
	P4 K	5.64 B			3.45	2.29
	P5 I	2.45 B			0.73	0.53
	G7 P1 I	1.46 A	0.28	0.85	0.30	0.11
	P1 K					
	P2 I	2.58 A	0.49	3.86	0.89	0.97
	P3 I	18.34 B			1.54	3.06
	P3 K					
	P4 I	14.56 B			1.23	1.70
	P5 K				2.02	1.10
	M14 P1 K	0.69 A				0.11
	P3 I	9.78 B			1.17	1.85
	P4 K				1.45	0.91
BE 210 INITIAL ENRICHMENT 2.83 wt% U-235	G14 P3(1) I	4.30 A	0.72	15.24	1.52	6.19
	P3(1) K				4.91	4.75
	P4(1) I	4.21 A	1.91	13.68	1.49	4.87
	P5(1) I	5.75 B	1.19	4.16	1.21	2.26
	P5(2) I	2.86 A	0.69	3.59	0.79	0.71
	K14 P1 I	2.61 A			0.84	0.67
	P3(1) I	7.84 B	0.75	13.86	1.85	5.41
	P4(1) K				3.44	3.26

I – samples analysed at Ispra

K – samples analysed at Karlsruhe

A – values obtained by mass spectrometry (Ispra)and α spectrometry (Karlsruhe)

B – values obtained by α spectrometry (Ispra)

TABLE E5. Buildup and depletion of U isotopes ($kg/MTU_{Initial}$)

Fuel Element	Sample	^{235}U (a)	^{236}U	^{238}U (a)
BE 124 INITIAL ENRICHMENT 3.00 wt% u-235	D1 P1	16.31	2.99	15.95
	P2			
	P3	23.07	4.06	25.32
	E3 P1	17.25	2.82	12.88
	P2	21.56	3.77	27.85
	P3	23.91	4.12	27.01
	P4	22.34	3.87	23.03
	P5	18.15	3.62	16.59
	G7 P1	14.79	2.92	11.97
	P2	19.24	3.85	19.21
	P3	22.45	3.96	23.63
	P4	19.91	4.05	21.62
	P5	19.91	3.60	19.80
	M14 P1	14.31	2.73	10.91
	P3	21.22	3.81	21.73
	P4	19.67	3.60	18.85
BE 210 INITIAL ENRICHMENT 2.83 wt% U-235	G14 P3(1)	23.57	3.88	29.08
	P4(1)	23.35	3.95	26.36
	P5(1)	22.03	3.66	20.99
	P5(2)	19.36	3.33	16.25
	K14 P1	18.27	3.22	18.86
	P3(1)	23.44	3.86	27.76
	P4(1)	23.26	3.82	24.55

Δ Values obtained by averaging analytical results from the Ispra and Karlsruhe Laboratories

(a) Depletion

TABLE E6. Buildup of Pu isotopes ($kg/MTU_{Initial}$)

Fuel Element	Sample	^{238}Pu	^{239}Pu	^{240}Pu	^{241}Pu	^{242}Pu
BE 124 INITIAL ENRICHMENT 3.00 wt% U-235	D1 P1	0.036	4.35	1.32	0.62	0.128
	P2					
	P3	0.156	5.02	2.36	1.28	0.564
	E3 P1	0.041	4.28	1.36	0.62	0.139
	P2	0.104	4.62	1.99	1.02	0.380
	P3	0.165	4.77	2.41	1.26	0.629
	P4Δ	0.114	4.93	2.23	1.19	0.476
	P5	0.062	4.65	1.62	0.84	0.211
	G7 P1	0.031	4.26	1.16	0.55	0.099
	P2	0.079	4.70	1.81	0.94	0.279
	P3Δ	0.141	5.02	2.28	1.20	0.489
	P4	0.106	5.08	2.04	1.11	0.366
	P5	0.079	5.08	1.95	1.05	0.320
	M14 P1	0.026	3.98	1.04	0.46	0.075
	P3	0.107	5.02	2.08	1.12	0.384
	P4	0.076	4.96	1.86	1.00	0.299
BE 210 INITIAL ENRICHMENT 2.83 wt% U-235	G14 P3(1)Δ	0.165	4.56	2.49	1.31	0.780
	P4(1)	0.159	4.41	2.38	1.21	0.680
	P5(1)	0.114	4.36	2.11	1.09	0.494
	P5(2)	0.065	4.27	1.72	0.86	0.285
	K14 P1					
	P1	0.065	4.60	1.74	0.90	0.264
	P3(1)	0.169	4.69	2.47	1.30	0.735
	P4(1)	0.126	4.51	2.37	1.21	0.658

Δ Values obtained by averaging analytical results from the Ispra and Karlsruhe Laboratories.

TABLE E7. Buildup of Am and Cm isotopes (kg/MTU$_{Initial}$)

Fuel Element	Sample	^{241}Am (x 10^2)	^{242}Am (x 10^4)	^{243}Am (x 10^2)	^{242}Cm (x 10^3)	^{244}Cm (x 10^3)
BE 124 INITIAL ENRICHMENT 3.00 wt% U-235	D1 P1 K	2.19 A			7.40	2.22
	P2 I					
	P3 I	6.08 B			15.65	33.97
	E3 P1 I	2.93 B			4.50	2.04
	P2 K					12.58
	P3 I	9.00 B			14.79	41.62
	P4 I	7.30 B			15.01	24.80
	P4 K	5.41 B			33.17	22.18
	P5 I	2.27 B			7.10	5.13
	G7 P1 I	1.40 A	2.88	0.86	2.94	1.04
	P1 K					
	P2 I	2.48 A	4.94	3.90	8.58	9.49
	P3 I	17.58 B			14.79	29.73
	P3 K				27.15	26.73
	P4 I	13.98 B			11.88	16.52
	P5 K				19.56	10.68
	M14 P1 K	0.67 A				1.04
	P3 I	9.39 B			11.30	17.99
	P4 K				14.07	8.91
BE 210 INITIAL ENRICHMENT 2.83 wt% U-235	G14 P3(1) I	4.10 A	7.29	15.4	15.54	59.81
	P3(1) K				47.03	45.94
	P4(1) I	4.03 A	19.30	13.8	14.36	47.15
	P5(1) I	5.53 B	12.07	4.20	11.70	22.07
	P5(2) I	2.77 A	7.10	3.62	7.56	6.95
	K14 P1 I	2.52 A			8.13	6.53
	P3(1) I	7.49 B	7.57	14.00	17.75	52.59
	P4(1) K				33.10	31.68

I – samples analysed at Ispra

K – samples analysed at Karlsruhe

A – values obtained by mass spectrometry (Ispra) and αspectrometry (Karlsruhe)

B – values obtained by αspectrometry (Ispra)

TABLE E8. Burnup values F_T % and MWD/MTU obtained from ^{148}Nd and ^{137}Cs

Fuel Element	Sample	F_T %		MWD/MTU	
		^{148}Nd	^{137}Cs	^{148}Nd	^{137}Cs
BE 124 INITIAL ENRICHMENT 3.00 wt% U-235	D1 P1	2.20		21,170	
	P2				
	P3	3.51	3.45	33,750	33,160
	E3 P1	2.10	2.03	20,180	19,540
	P2	3.65		35,100	
	P3	3.77	3.66	36,260	35,220
	P4$^{\Delta}$	3.22	3.19	30,920	30,640
	P5	2.38	2.35	22,860	22,570
	G7 P1	1.78	1.76	17,130	16,970
	P2	2.68	2.59	25,830	24,880
	P3$^{\Delta}$	3.26	3.27	31,320	31,400
	P4	2.88	2.85	27,710	27,420
	P5	2.68		25,810	
	M14 P1	1.62		15,600	
	P3	3.05	2.99	29,360	28,800
	P4	2.59		24,900	
BE 210 INITIAL ENRICHMENT 2.83 wt% U-235	G14 P3(1)$^{\Delta}$	3.90	3.92	37,490	37,720
	P4(1)	3.71	3.69	35,640	35,480
	P5(1)	3.14	3.19	30,160	30,660
	P5(2)	2.52	2.54	24,220	24,400
	K14 P1	2.65	2.38	25,450	22,900
	P3(1)	3.81	3.74	36,670	35,990
	P4(1)	3.42		32,900	

$^{\Delta}$ Values obtained by averaging analytical results from the Ispra and Karlsruhe Laboratories

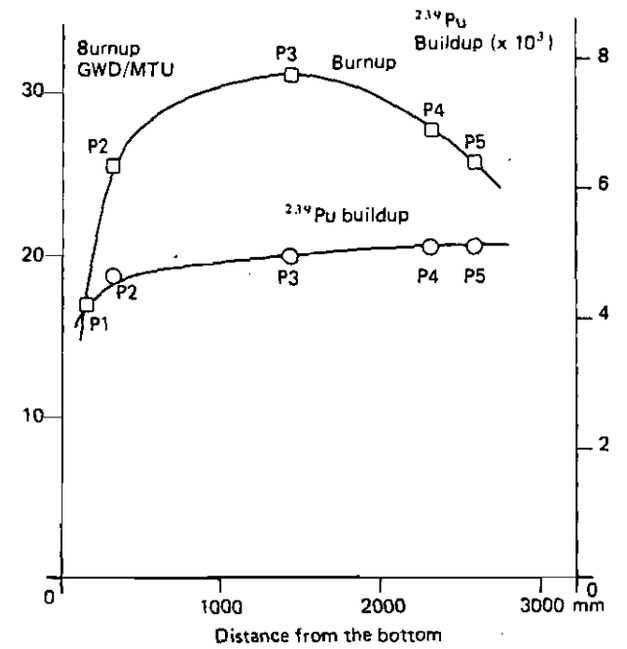

Fig. III.11. Obrigheim - Rod G7, axial distribution versus distance from the of burnup and ^{239}Pu buildup

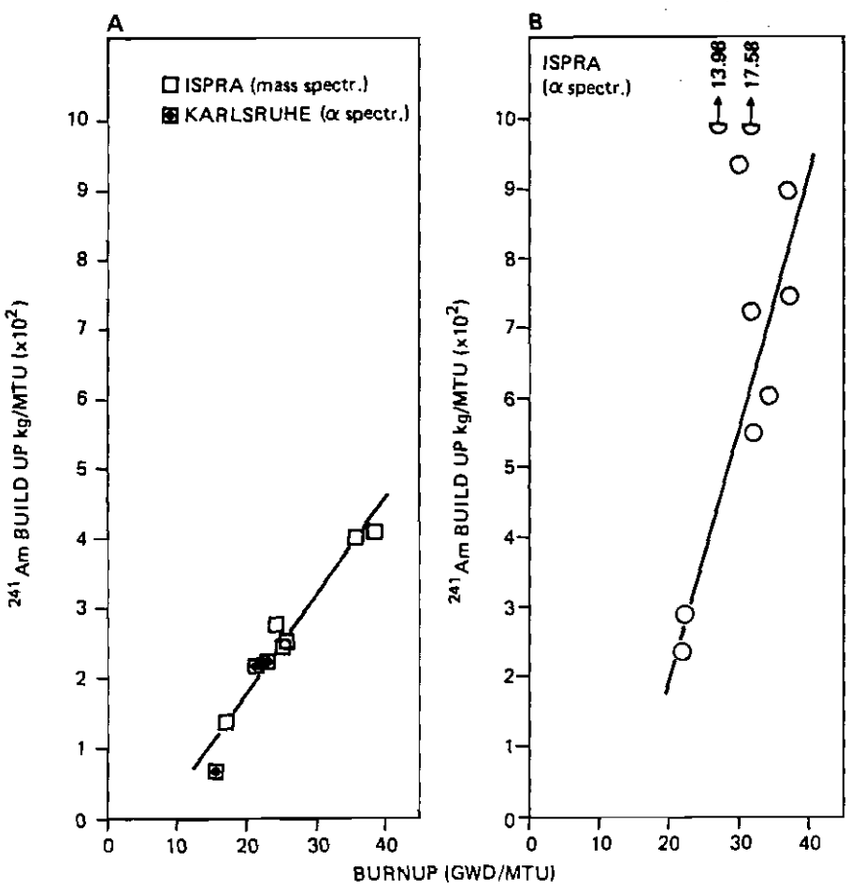

Fig. III.12. Obrigheim - ^{241}Am buildup plotted against burnup

As far as ^{242}Cm is concerned the data obtained at Karlsruhe are systematically higher than those obtained at Ispra (see Fig. III.13). The comparison with the RIBOT code indicates the possible presence of a systematic error in Karlsruhe determinations (section II.5: Conclusions on ^{242}Cm).
Contrary to the procedure in all the standard tables, Tables E4 and E7 show the results obtained at Ispra and Karlsruhe separately so that a critical evaluation of the data can be made. This is because of the indications which emerged from the above-mentioned interlaboratory comparison (see section II.2).

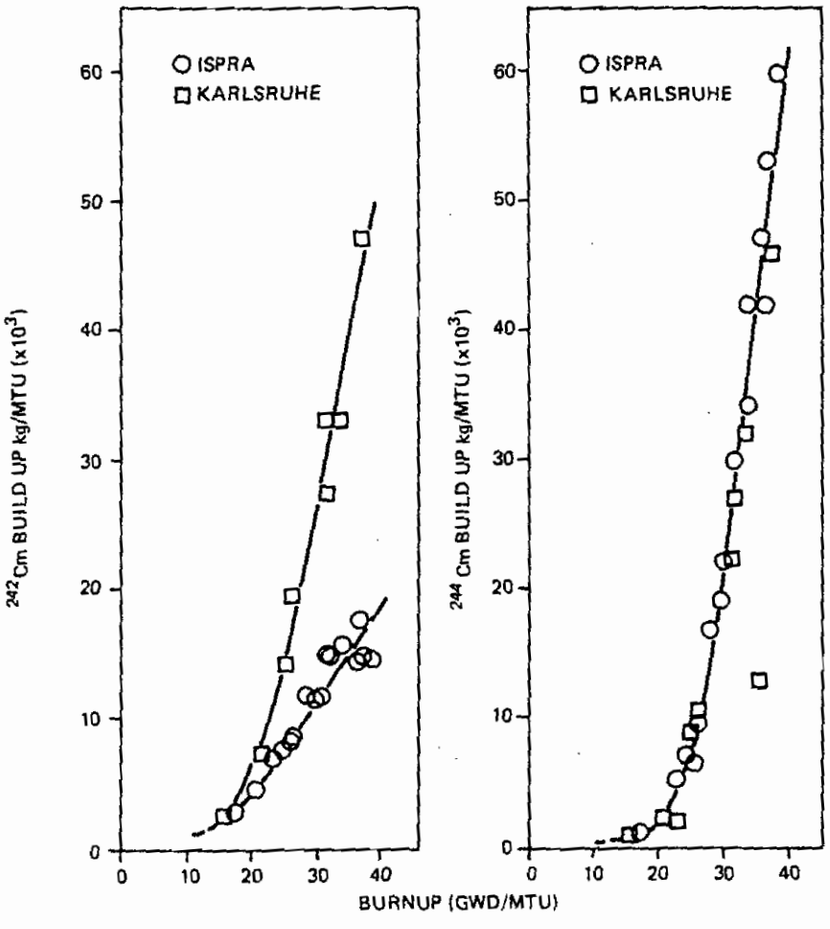

Fig. III.13. *Obrigheim* - Cm isotope buildup plotted against burnup

4. Gundremmingen BWR

The results of GUNDREMMINGEN fuel were also extensively dealt with in references 2 and 21 and in the earlier sections of this report. Since there are no particular remarks to make, only the standard tables are presented (tables F1 to F8).

TABLE F1. U isotopes referred to final ^{238}U atoms

Fuel Element	Sample	^{235}U (x 10^2)	^{236}U (x 10^2)
B 23 INITIAL ENRICHMENT 2.53 wt% U-235	A1 1	0.676	0.346
	2	0.727	0.349
	B 3Δ	1.039	0.311
	4	0.960	0.319
	C 5	0.905	0.332
	E 3	0.914	0.331
	5Δ	0.716	0.348
C 16 INITIAL ENRICHMENT 2.53 wt% U-235	A1 1	0.916	0.323
	2	1.048	0.305
	B 3Δ	1.378	0.257
	C 5	1.306	0.262
	E 5Δ	1.099	0.288

Δ Values obtained by averaging analytical results from the Ispra and Karlsruhe Laboratories

TABLE F2. Pu isotopes referred to final ^{238}U atoms

Fuel Element	Sample	^{238}Pu (x 10^4)	^{239}Pu (x 10^3)	^{240}Pu (x 10^3)	^{241}Pu (x 10^3)	^{242}Pu (x 10^4)
B 23 INITIAL ENRICHMENT 2.53 wt% U-235	A1 1	0.71	3.892	1.881	0.818	3.402
	2	1.13	4.988	2.254	1.185	4.641
	B 3Δ	0.87	5.603	1.921	0.911	2.292
	4	0.97	5.235	1.928	0.899	2.433
	C 5	0.93	5.143	2.042	0.920	2.757
	E 3	0.89	5.018	1.915	0.884	2.532
	5Δ	1.03	4.699	1.199	0.938	3.478
C 16 INITIAL ENRICHMENT 2.53 wt% U-235	A1 1	0.39	3.765	1.523	0.629	1.864
	2	0.49	4.591	1.581	0.788	2.061
	B 3Δ	0.35	4.858	1.205	0.560	0.908
	C 5	0.36	4.592	1.278	0.559	1.021
	E 5Δ	0.43	4.307	1.492	0.617	1.520

Δ Values obtained by averaging analytical results from the Ispra and Karlsruhe Laboratories

TABLE F3. Atom ratios of ^{148}Nd and ^{137}Cs referred to final ^{238}U

Fuel Element	Sample	^{148}Nd (x 10^4)	^{137}Cs (x 10^3)
B 23 INITIAL ENRICHMENT 2.53 wt% U-235	A1 1	4.88	2.12
	2	5.22	1.67
	B 3Δ	4.03	1.54
	4	4.22	1.57
	C 5	4.36	1.78
	E 3	4.58	1.59
	5Δ	4.92	1.83
C 16 INITIAL ENRICHMENT 2.53 wt% U-235	A1 1	3.80	1.46
	2	3.72	1.54
	B 3Δ	2.73	1.07
	C 5	2.96	1.26
	E 5Δ	3.33	1.22

Δ Values obtained by averaging analytical results from the Ispra and Karlsruhe Laboratories

TABLE F4. Am and Cm isotopes referred to final ^{238}U atoms

Fuel Element	Sample	^{241}Am (x 10^4)	^{242}Am (x 10^6)	^{243}Am (x 10^5)	^{242}Cm (x 10^5)	^{244}Cm (x 10^6)
B 23 INITIAL ENRICHMENT 2.53 wt% U-235	A1 1	0.39			1.04	9.04
	2	0.69			1.50	20.25
	B 3Δ	0.29	0.48	2.12	0.99	8.25
	4				0.96	9.58
	C 5	0.11	0.58	3.31	1.09	9.78
	E 3	0.23			0.99	9.38
	5Δ	0.16	0.54	4.38	1.16	14.55
C 16 INITIAL ENRICHMENT 2.53 wt% U-235	A1 1	0.29			0.54	2.66
	2	0.28			0.70	4.56
	B 3Δ	0.09		0.85	0.42	1.52
	C 5	0.11		0.84	0.45	1.77
	E 5Δ	0.12			0.56	2.66

Δ Values obtained by averaging analytical results from the Ispra and Karlsruhe Laboratories

TABLE F5. Buildup and depletion of U isotopes ($kg/MTU_{Initial}$)

Fuel Element	Sample	^{235}U (a)	^{236}U	^{238}U (a)
B 23 INITIAL ENRICHMENT 2.53 wt% U-235	A1 1	18.99	3.26	16.28
	2	18.55	3.26	22.41
	B 3Δ	15.47	2.95	18.48
	4	16.35	2.99	18.39
	C 5	16.74	3.15	19.24
	E 3	16.68	3.13	19.69
	5Δ	18.54	3.29	20.24
C 16 INITIAL ENRICHMENT 2.53 wt% U-235	A1 1	16.71	3.05	13.63
	2	15.49	2.89	15.23
	8 3Δ	12.18	2.45	12.23
	C 5	12.88	2.50	12.89
	E 5Δ	14.85	2.74	13.10

Δ Values obtained by averaging analytical results from the Ispra and Karlsruhe Laboratories

(a) Depletion

TABLE F6. Buildup of Pu isotopes ($kg/MTU_{Initial}$)

Fuel Element	Sample	^{238}Pu	^{239}Pu	^{240}Pu	^{241}Pu	^{242}Pu
B 23 INITIAL ENRICHMENT 2.53 wt% U-235	A1 1	0.068	3.74	1.62	0.79	0.330
	2	0.108	4.80	2.17	1.14	0.449
	B 3Δ	0.083	5.37	1.85	0.88	0.223
	4	0.092	5.03	1.86	0.87	0.236
	C 5	0.089	4.93	1.97	0.89	0.267
	E 3	0.084	4.82	1.85	0.85	0.246
	5Δ	0.098	4.51	2.10	0.90	0.337
C 16 INITIAL ENRICHMENT 2.53 wt% U-235	A1 1	0.036	3.64	1.47	0.61	0.182
	2	0.048	4.42	1.53	0.77	0.201
	8 3Δ	0.033	4.69	1.17	0.55	0.089
	C 5	0.035	4.44	1.24	0.54	0.100
	E 5Δ	0.041	4.16	1.44	0.60	0.150

Δ Values obtained by averaging analytical results from the Ispra and Karlsruhe Laboratories

TABLE F7. Buildup of Am and Cm isotopes ($kg/MTU_{Initial}$)

Fuel Element	Sample	^{241}Am ($\times 10^2$)	^{242}Am ($\times 10^3$)	^{243}Am ($\times 10^2$)	^{242}Cm ($\times 10^3$)	^{244}Cm ($\times 10^3$)
B 23 INITIAL ENRICHMENT 2.53 wt% U-235	A1 1	3.78			10.09	8.87
	2	6.63			14.56	19.77
	B 3Δ	3.14	4.67	2.07	9.45	8.62
	4				9.32	9.39
	C 5	1.05	5.66	3.23	10.07	10.85
	E 3	2.22			9.62	9.17
	5Δ	1.65	5.21	4.27	10.96	15.06
C 16 INITIAL ENRICHMENT 2.53 wt% U-235	A1 1	2.80			5.26	2.61
	2	2.67			6.87	4.48
	B 3Δ	0.98		8.38	3.80	1.57
	C 5	0.32		8.48	3.82	1.94
	E 5Δ	1.24			5.04	2.79

Δ Values obtained by averaging analytical results from the Ispra and Karlsruhe Laboratories

TABLE F8. Burnup values F_T % and MWD/MTU obtained from ^{148}Nd and ^{137}Cs

Fuel Element	Sample	F_T%		MWD/MTU	
		^{148}Nd	^{137}Cs	^{148}Nd	^{137}Cs
B 23 INITIAL ENRICHMENT 2.53 wt% U-235	A1 1	2.78	3.26	25,730	30,120
	2	2.96	2.58	27,400	23,830
	8 3Δ	2.30	2.37	21,240	21,890
	4	2.41	2.42	22,250	22,400
	C 5	2.48	2.74	22,970	25,330
	E 3	2.54	2.39	23,510	22,130
	5Δ	2.72	2.77	25,190	25,640
C 16 INITIAL ENRICHMENT 2.53 wt% U-235	A1 1	2.19	2.28	20,300	21,120
	2	2.15	2.62	19,850	24,230
	B 3Δ	1.56	1.67	14,390	15,450
	C 5	1.71	1.97	15,840	18,200
	E 5Δ	1.89	1.90	17,490	17,600

Δ Values obtained by averaging analytical results from the Ispra and Karlsruhe Laboratories

2. Conclusions

We want to summarize in this chapter the main characteristics of the set of Bench Mark data that are here reported:

- wide range of burnup: the samples measured in the different campaigns covered a burnup range from 3.4 to 37.5 MWD/MTU;
- wide range of LWR types with several enrichments;
- different elaboration procedures or algorithms were employed for the data analysis. The data set in fact was characterized through a careful assessment of the experimental uncertainties, through the comparison with the results obtained by the aid of nuclear codes. "Ad hoc" algorithms such as Isotopic Correlation Technique and the inverse code THEORY were as well employed for the characterisation of the data set.

In some cases a discrepancy found with one method was confirmed and/or explained by other methods. (See for instance the buildup of some heavy isotopes like ^{241}Am and ^{242}Cm.)

- together with analytical results all pertinent mechanical, historical, physico-chemical data are given as well as descriptions of reactors, fuel bundles, fuel pins, control rods, etc. necessary to correctly recalculate the set of Bench Mark data.

The Bench Mark set of spent fuel analytical data is thus considered to be sufficiently wide and characterized to be really useful for recalculation purpose. Consequently, it might serve as a reference for testing nuclear codes and cross-section libraries and for improving Safeguards tools, as pointed out in the introduction.

References

1. S. GUARDINI, G. GUZZI and P. PERONI (Editors), "Bench Mark Report relevant to Trino Vercellese and Garigliano reactors", EUR COM 3609 (1978).
2. S. GUARDINI and G. GUZZI (Editors), "Bench Mark Report relevant to Gundremmingen and Obrigheim reactors", EUR COM 3703 (1979).
3. A. CRICCHIO, "Status and requirements for plutonium, americium and curium nuclear data relevant to plutonium recycling in light water reactors", EUR 5698e (1977).
4. M. DARROUZET and J. PINEL, "A cross section sensitivity study for heavy plutonium isotopes and americium isotopes", EUR COM 3420e,f (1978).
5. H. KÜSTERS and M. LALOVIC, "Transactinium isotope buildup and decay in reactor fuel and related sensitivities to cross section changes", Review paper n. 3 in Proc. of the Advisory Group Meeting on Transactinium Isotope Nuclear Data, Karlsruhe, 3-7 Nov., 1975 .
6. H. KÜSTERS, M. LALOVIC and M. W. WIESE, "Fuel handling reprocessing and waste and related nuclear data aspects", pp. 518-550 of Proc. of the Int. Conf. on Neutron Physics and Nuclear Data, Harwell, Sept. 1978.
7. T.N. DRAGNER, "Experimental techniques for measuring burnup, non destructive techniques: Gamma spectroscopy", IAEA/STR 48 (Oct. 1974).
8. S.T. HSUE, T.W. CRANE, W.L. TALBERT and J.C. LEE, "Non destructive assay methods for irradiated fuels", LA 6923 (Jan. 1978).
9. Advisory Group Meeting on the "Non Destructive Analysis of Irradiated Power Reactor Fuel", IAEA AG 11 (April 1977).
10. H. TSURUTA et al., "Correlation between burnup and fission product ratios obtained from non destructive measurement in a mixed oxide fuel", Proc. of the Symp. on "Isotopic Correlation and its Application to the Nuclear Fuel Cycle", Stresa, 9-11 May, 1978.
11. P. ROUSSET, "Les correlations isotopiques des gaz de fission appliquées à la filière eau ordinaire", Ibid.
12. C. FOGGI and F. FRANQUELLUCCI, "Fission product nuclear data requirements for the calculation of isotopic correlation based on Cs and Eu isotopes in LWR irradiated fuel", Ibid.

13. T.H. HSUE et al., "Passive neutron assay of irradiated nuclear fuel", LA 7645 MS (1978).

14. S. GUARDINI and G. GUZZI, "Neutron emission from spent fuels of pressurized and boiling water reactors by spontaneous fissions and (α, n) reactions", EUR 6315e (1979).

15. J.R. PHILLIPS, J.K. HALBIG, G.E. BOSLER, "Passive neutron measurements and calculations of irradiated PWR fuel assemblies", Proc. 3rd Annual Symp. on Safeguards and Nuclear Mat. Manag., Karlsruhe, 6-8 May, 1981.

16. P.I. FEDOTOV, N.M. KAZARINOV, A.A. VORONKOV, "The use of neutron scanning method for analysis of spent VVER assemblies in safeguards systems", Ibid.

17. S. FINZI, "Introductory speech" to the Symp. on Isotopic Correlations and its Application to the Nuclear Fuel Cycle, Stresa, 9-11 May, 1978.

18. S. SANATANI, "Application of isotopic correlation technique to the nuclear fuel cycle", Ibidem.

19. Panel discussion, Ibidem.

20. S. GUARDINI and G. GUZZI, "The use of isotopic correlation technique as consistency check and elaboration of post-irradiation examination data", Ibidem.

21. A. ARIEMMA et al., "Experimental and theoretical determination of burnup and the heavy isotope content in a fuel assembly, irradiated in the Garigliano BWR", EUR 4638e (1971).

22. A.M. BRESESTI et al., "Post irradiation analysis of Trino Vercellese reactor fuel elements", EUR 4909e (1972).

23. P. BARBERO et al., "Post irradiation examination of the fuel discharged from the Trino Vercellese reactor after the 2nd irradiation cycle", Eur 5605e (1976).

24. P. BARBERO et al., "Post-irradiation analysis of the Gundremmingen BWR spent fuel", EUR 6301e (1979).

25. P. BARBERO et al., "Post-irradiation analysis of the Obrigheim PWR spent fuel", Eur 6589e (1980).

26. S. GUARDINI and G. GUZZI, "Axial post-irradiation analysis of the Garigliano BWR spent fuel", Proc. 3rd ESARDA Symp. on Safeguards and Nucl. Mat. Manag., Karlsruhe, 6-8 May, 1981.

27. Directory of Nuclear Reactors, Vol. VII, page 107, IAEA, Vienna.

28. D.L. DELP, L. FISHER, J.M. MARRIMAN and N.J. STEDWELL, "FLARE - A three-dimensional boiling water reactor simulator", GEAP-4589, July 1964.

29. Directory of Nuclear Reactors, Vol. VII, page 11, IAEA, Vienna

30. A. COSTANTINO, "Report on the operations performed at CCR-EURATOM at Ispra on three irradiated fuel assemblies", ENEL-C3. R1/03/70 (1970).

31. A.M. MONCASSOLI TOSI, P.G. RAMA, "Valutazione dettagliata del livello di irraggiamento e della composizione locale alla prima scarica del combustibile di Trino Vercellese", FIAT report FN-E-117 (1971).

32. M. DE SERAFINI, A.M. MONCASSOLI TOSI, P.G. RAMA, "Trino Vercellese core one post-irradiation analysis: Interpretation of the experimental results and theoretical predictions", FIAT report FN-E-118 (1971).

33. G.M. LEPIE, A.H. MARTIN, "Obrigheim, the KWO nuclear power plant station with a Siemens PWR", Nuclear Engineering, April 1967, 278-285.

34. Kernkraftwerk Obrigheim, EUR 5315d (1974).

35. Directory of Nuclear Reactors, Vol. VII, page 117, IAEA, Vienna.

36. L. KOCH, G. COTTONE und M.W. GEERLINGS, "^{148}Nd Analyse zur Abbrandbestimmung von Kernbrennstoffen", Radiochim. Acta 10, 122 (1968).

37. J.G. VAN RAAPHORST, H. HAREMAKER, "A rapid chemical separation procedure for the determination of burnup of nuclear fuel", Journ. Rad. Chem. 53-1-2 (1979) 71-80.

38. W. BEYRICH and A. CRICCHIO, "The ASET 74 intercomparison experiment on the evaluation of alpha spectra of plutonium", EUR 5208 (1976).

39. W. BEYRICH and G. SPANNAGEL, "The As76 interlaboratory experiment on the alpha spectrometric determination of ^{238}Pu. Part 1", EUR 6400 (1980).

40. G. SPANNAGEL et al., "The As76 interlaboratory experiment on the alpha spectrometric determination of ^{238}Pu. Part 2", EUR 6401 (1980).

41. G. BORTLES et al., "The As76 interlaboratory experiment on the alpha spectrometric determination of ^{238}Pu. Part 3", EUR 4402 (1980).

42. E.A.C. CROUCH and R.K. WEBSTER, "Choice of the optimum quantity and constitution of the tracer used for isotopic dilution analysis", Journ. Chem. Soc. (1963), 118.

43. W.J. MAECK et al., "Discrepancies and comments regarding ^{235}U and ^{239}Pu thermal fission yields and the use of ^{148}Nd as a burnup monitor", ICP-1092 (1976).

44. C.G. PONCELET, "LASER: A depletion programme for lattice calculations based on MUFT and THERMOS", WCAP 6073 (1966).

45. M.E. MEEK and B.F. RIDER, "Compilation of fission products yields", NEDO 12154-1 (1974).

46. W. MANNHART, "A small guide to generating covariances of experimental data", ISSN 0341-6666 (1981).

47. R.P. MATSEN, "The determination of ratios of effective cross sections from measured burnup data for Yankee Rowe", Nucl. Technol., 15, 343 (1972).

48. J. LUFFIN, Z. SZATMARY and J. VANUXEEM, "Adjustment of a burnup code on chemical and isotopic analysis of irradiated fuels", Journ. of Nucl. Energy, Vol. 25, pp. 627-641 (1972).

49. R. DIERCKX, S. GUARDINI, P. PERONI and H. TSURUTA, "Determination of one-group cross section ratios from measured isotopic composition of irradiated nuclear fuel", Energia Nucleare 26, 6 June 1979, 303.

50. R. J. NODVIK et al., "Supplementary report on evaluation of mass spectrometric and radiochemical analysis of Yankee Core 1 spent fuel, including isotopes of elements thorium through curium", NCAP 6086 (1969).

51. R. BERG, C. FOGGI, L. KOCH, R. KRAEMER, F. J. WOODMAN, "Value and use of isotopic correlations in irradiated fuels", Proc. Symp. Practical Applications of R&D in the field of Safeguards - Rome, 7-8 March 1974.

52. R. ERNSTBERGER, R. WELLUM, L. KOCH, "Utilisation des corrélations isotopiques dans la gestion des matériaux nucléaires et des déchets radioactifs", Proc. Symp. Isotopic Correlations and their Application to the Nuclear Fuel Cycle, Stresa, 9-11 May, 1978.

53. A. PROSDOCIMI (JRC Ispra), private communication.

54. L. KOCH, K. KAMMERICHS, S. SCHOOF, "The potential of fission product and transplutonium correlations in the verification of the reprocessing input", Proc. 3rd Annual Symp. on Safeguards and Nucl. Mat. Manag., Karlsruhe, 6-8 May, 1981.

55. Proceedings of the First Technical Meeting on the Nuclear Transmutation of Actinides, Ispra 16-18 April, 1977, EUR 5897 (1977).

56. S. GUARDINI and B. G. R. SMITH, "Actinide recycling in light water reactors: Results of reactor physics calculations", EUR 7426e (1981).

57. P. LOIZZO, "RIBOT 5: A physical model for light water lattice calculations", BNWL 735 (1968).

58. S. GUARDINI, G. OLIVA, B. G. R. SMITH, L. TONDINELLI, "Comparison between measured and calculated by-product actinide buildup within fuel assemblies in a large burnup range", Proc. 2nd Techn. Meeting on the Nuclear Transmutation of Actinides, Ispra, 21-24 April, 1980. EUR 6929 (1980).

59. A. SOLA, "Analytical evaluation of actinide sensitivities", EUR 5763.

60. K. JOSEFOWICZ, "Proc. Symp. on Dosimetry Inst. Nuclear Research", Otwock/Swierk, October 1979.

61. M. E. MEEK and B. F. RIDER, "Computation of fission products yields", NEDO 12154-1 (1974).

62. M. F. JAMES, "Energy release in fission", Journ. Nucl. Energy 23, 517-36 (1969).

European Communities — Commission

EUR 7879 EN — JOINT RESEARCH CENTRE

BENCHMARK: Reference Data on Post Irradiation Analysis
of Light Water Reactor Fuel Samples

Luxembourg: Office for Official Publications of the European Communities

1982 — 164p — 21.0 x 29.7 cm.

EN

This report collects and illustrates the work performed over the past 12 years at the JRC in the field of post-irradiation examinations on light water reactor fuels.
The work was carried out on Garigliano, Trino Vercellese, Obrigheim and Gundremmingen fuel, under the heading "Benchmark Experiments".
The aim of this report is to review the results obtained, to indicate the fields of application for these results, and to provide general information that will make them simple and straightforward to use.
As the aim of the "Benchmark Experiments" activity was to prepare a set of clean reference data, the maximum attention was paid to the characterisation, quality and traceability of the data. As the report shows many different tools were used to check the analytical data, and much complementary information was distributed through *ad hoc* reports to make the recalculation and proper use of the data possible.

The principle users of the Benchmark data should be:
reactor operators, nuclear waste operators and safeguards authorities.

The structure of the report is as follows:
In section I the experimental activity is described in detail.
In section II all the techniques used to certify the analytical data are presented, together with discussions on the evaluated random and systematic uncertainties.
Section III presents the results.

In practice the complete sets of results referring to all JRC measurements are given.